

TERRESTRIAL SEDIMENT DEPOSITION IN RITTERBUSH POND:
IMPLICATIONS FOR HOLOCENE STORM FREQUENCY
IN NORTHERN VERMONT

A Thesis Presented

by

Sarah Linfield Brown

to

The Faculty of the Graduate College

of


The University of Vermont

In Partial Fulfillment of the Requirements
for the Degree of Master of Science
Specializing in Geology


March, 1999

Accepted by the Faculty of the Graduate College, The University of Vermont, in partial fulfillment of the requirements for the degree of Master of Science, specializing in Geology.

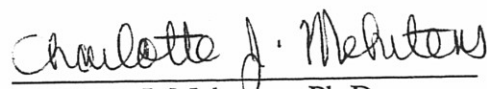
Thesis Examination Committee:



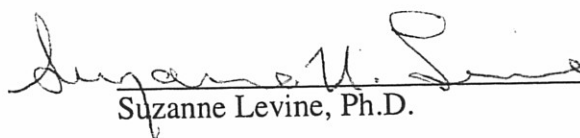
Paul R. Bierman, Ph.D. Advisor



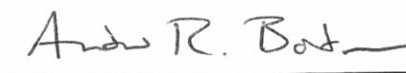
Andrea Lini, Ph.D.



Charlotte J. Mehrtens, Ph.D.



Suzanne Levine, Ph.D. Chairperson



Andrew R. Bodman, Ph.D. Interim Dean,
Graduate College

Date: October 20, 1998

ABSTRACT

This thesis provides a well-dated, high-resolution Holocene record of discrete sedimentation events in a New England lake. Ritterbush Pond is located in Eden, Vermont, within the northern Green Mountains, and is surrounded by a 2.2 km² watershed with steeply sloping, forested hillsides. The lake sediment record consists primarily of organic-rich gyttja that has accumulated since deglaciation (~12,000 ¹⁴C yr BP). Unlike other New England lakes cored to construct pollen and deglacial chronologies, the sediments of Ritterbush Pond record episodic watershed erosion events as distinct layers of sand and silt. These inorganic layers reflect the occurrence of large hydrologic events in northern Vermont during the Holocene. The deposition of terrestrially-derived sediment in mountain lakes, and its potential use as a hydrologic proxy record, had received little prior attention in New England.

I collected and analyzed three continuous (4 to 6 m long) sediment cores, one from the lake center and two closer to the lake margin. I used a variety of analytical techniques to characterize the spatial and temporal distribution of the inorganic layers, and to investigate the mechanisms controlling sediment transport and deposition in the lake. The data produced for each core include records of litho-stratigraphy, organic carbon content (loss-on-ignition), X-radiograph and grayscale density, magnetic susceptibility, and paleomagnetism. Intervals of the cores were also analyzed for grain size, carbon / nitrogen ratios, stable carbon isotopes and percent charcoal. Fourteen radiocarbon dates were obtained on macrofossils and gyttja sampled from the three cores. I matched these cores to an existing, well-dated core (RT-2, 14 ¹⁴C ages) and pollen chronology for Ritterbush Pond (Lin, 1996).

The data support a terrestrial origin for inorganic layers, and suggest episodic, rapid deposition by density currents. The 0.1 to 10 cm-thick sand and silt layers cluster in three intervals, implying an increase in basin-wide hydrologic event frequency prior to 8650 cal yr BP, from 6840 to 6340 cal yr BP and 2620 to 2025 cal yr BP. Charcoal data do not support hillslope-clearing fires as a trigger for layer deposition, nor do pollen data show corresponding vegetation change. The chronology of inorganic sediment layers in Ritterbush Pond cores identifies 52 discrete depositional events, and is reported in both ¹⁴C and calendar yr BP to facilitate comparison with other Holocene records.

Hydrologic event frequency and magnitude, as represented by layer spacing and thickness, has fluctuated throughout the Holocene. The Ritterbush watershed appears to have experienced two different hydrologic regimes. The predominant, quiet regime results in the deposition of layers less than 1 cm thick and alternates with a noisy regime (during the above intervals) where the thickest layers, representing larger events, are clustered. The only layer (1 cm thick) in the last 350 years of the chronology may have been deposited by the largest storm in Vermont's history (1927). This storm appears to represent the smallest magnitude storm necessary to mobilize sediment in the Ritterbush basin, implying that much larger magnitude storms are necessary to deposit the thicker, coarser inorganic layers. Antecedent soil conditions and sediment availability may also influence layer thickness, especially among the thickest layers.

The wider implications of the Ritterbush chronology are still uncertain, due to a lack of similar event records locally and regionally. The Ritterbush record suggests that severe storm events much larger than those historically witnessed, or currently planned for, have occurred in the Ritterbush basin, and perhaps across all of Vermont. The intervals of clustered layers may indicate larger-scale Holocene fluctuations in oceanic and atmospheric circulation patterns that shift northward the flows of tropical air needed to produce extreme amounts of rainfall.

ACKNOWLEDGEMENTS

This thesis was supported by grants from Sigma Xi, the Geological Society of America, and the Vermont Geological Society, and by a Howard Award from the Quaternary Geology and Geomorphology Division of the Geological Society of America. I would like to thank my advisor, Paul Bierman, for inspiration and enthusiasm throughout the development of this thesis. Andrea Lini and Char Mehrtens have provided expertise and encouragement during my research. Additional thanks for field, scientific and/or moral support to: Laura Mallard, P.T. Davis, Dave Shaw, Barry and Sandy Doolan, Christine Massey, Mike Abbott, Stephen and Rebecca Wright, Tracy Rushmer, Brian Atwater, Linfield Brown, Roger Lewis, Kris Bryan, Sara Gran, and Anders Noren.

ACKNOWLEDGEMENTS	ii
TABLE OF CONTENTS	iii
CHAPTER 1 - Introduction	vi
1.1 Background	vii
1.2 Previous Work	5
CHAPTER 2 - Methods	8
2.1 Field Methods	8
2.1.1 Bathymetry and Sediment Probing	8
2.1.2 Coring	9
2.2 Laboratory Methods	9
2.2.1 Core Processing	9
2.2.2 Magnetic Susceptibility	12
2.2.3 Paleomagnetic Measurements	13
2.2.4 X-radiography	16
2.2.5 Loss-on-ignition (LOI)	17
2.2.6 Elemental Analysis (Organic Carbon and Nitrogen)	19
2.2.7 Charcoal Analysis (Nitric Acid Digestion)	21
2.2.8 Stable Carbon Isotope Analysis	22
2.2.9 Grain-Size Analysis	23
2.2.10 Bulk Density	24
2.2.11 Radiocarbon Dating	25
CHAPTER 3 - Data Presentation	28
3.1 Field Data	28
3.1.1 Bathymetry and Sediment Probing	28
3.1.2 Core Location	31
3.2 Laboratory Data	31
3.2.1 Late-Streptocytic Logs	31
3.2.2 Magnetic Susceptibility	34
3.2.3 Paleomagnetic Analysis	37
3.2.4 X-radiography	39

TABLE OF CONTENTS

ACKNOWLEDGEMENTS	ii
TABLE OF CONTENTS	iii
LIST OF TABLES.....	vi
LIST OF FIGURES	vii
CHAPTER 1 - Introduction	1
1.1 <i>Statement of Problem</i>	1
1.2 <i>Overview of Thesis</i>	2
1.3 <i>Ritterbush Pond</i>	4
1.3.1 <i>Physiographic Setting</i>	4
1.3.2 <i>Previous Work</i>	5
CHAPTER 2 - Methods	8
2.1 <i>Field Methods</i>	8
2.1.1 <i>Bathymetry and Sediment Probing</i>	8
2.1.2 <i>Coring</i>	9
2.2 <i>Laboratory Methods</i>	9
2.2.1 <i>Core Processing</i>	9
2.2.2 <i>Magnetic Susceptibility</i>	12
2.2.3 <i>Paleomagnetic Measurements</i>	13
2.2.4 <i>X-radiography</i>	16
2.2.5 <i>Loss-on-Ignition (LOI)</i>	17
2.2.6 <i>Elemental Analysis (Organic Carbon and Nitrogen)</i>	19
2.2.7 <i>Charcoal Analysis (Nitric Acid Digestion)</i>	21
2.2.8 <i>Stable Carbon Isotope Analysis</i>	22
2.2.9 <i>Grain-Size Analysis</i>	23
2.2.10 <i>Bulk Density</i>	24
2.2.11 <i>Radiocarbon Dating</i>	25
CHAPTER 3 - Data Presentation	28
3.1 <i>Field Data</i>	28
3.1.1 <i>Bathymetry and Sediment Probing</i>	28
3.1.2 <i>Core Location</i>	31
3.2 <i>Laboratory Data</i>	31
3.2.1 <i>Litho-Stratigraphic Logs</i>	31
3.2.2 <i>Magnetic Susceptibility</i>	34
3.2.3 <i>Paleomagnetic Analysis</i>	37
3.2.4 <i>X-radiography</i>	39

3.2.5 Loss-on-Ignition.....	41
3.2.6 Elemental Analysis	43
3.2.7 Charcoal Analysis (Nitric Acid Digestion).....	45
3.2.8 Stable Carbon Isotopes.....	45
3.2.9 Grain Size Analysis.....	48
3.2.10 Bulk Density.....	48
3.2.11 Radiocarbon Analysis	51
CHAPTER 4 - Interpretation of Results	55
4.1 <i>Comparison of Data Sets and Methods</i>	55
4.2 <i>Core Correlation</i>	57
4.2.1 Litho-Stratigraphic Correlation.....	60
4.2.2 Time-Stratigraphic Correlation	63
4.2.3 Summary of Spatial and Temporal Distribution.....	63
4.3 <i>Inorganic Layer Emplacement</i>	65
4.3.1 Physical Characteristics.....	68
4.3.2 Organic Matter Source	69
4.3.3 Timing of Layer Deposition.....	69
4.3.4 Emplacement Mechanisms	70
4.3.5 Initiation of Layer Deposition	73
4.4 <i>Age Control on Sedimentation</i>	75
4.4.1 Age Model.....	75
4.4.2 Validity of the Age Model.....	77
4.4.3 Gytija Accumulation Rates.....	81
4.4.4 Event Chronology.....	84
CHAPTER 5 - Discussion	88
5.1 <i>Event Sedimentation in Ritterbush Pond</i>	88
5.1.1 Sedimentation Dynamics of the Ritterbush Watershed	88
5.1.2 Effect of Precipitation Events on Sedimentation	89
5.1.3 The Ritterbush Event Chronology	91
5.2 <i>New England Climate Records</i>	94
5.3 <i>Frequency and Magnitude of Vermont Storms</i>	97
5.3.1 Historic Storms in Vermont and at Ritterbush Pond.....	97
5.3.2 The Potential Magnitude of Large Storm Events	101
5.3.3 The Ritterbush Chronology and Holocene Storm Patterns	107
5.4 <i>Comparison with Regional and Global Events</i>	108
5.4.1 Regional Storm Events.....	108
5.4.2 Global Climatic Events	109
CHAPTER 6 - Conclusions	112
6.1 <i>Summary of Findings</i>	112
6.2 <i>Suggestions for Future Research</i>	114
REFERENCES CITED.....	116

LIST OF TABLES

APPENDIX A: Field Procedures 125

APPENDIX B: Lab Procedures 128

APPENDIX C: Field Data 135

APPENDIX D: Lab Data 137

APPENDIX E: Age Model 153

APPENDIX F: Litho-Stratigraphic Logs 155

Table 3.1 Water Depth, Estimated Sediment Thickness, and Core Section Length..... 30

Table 3.2 Characteristic Litho-Stratigraphy of Cores 2, 3, and 4..... 35

Table 3.3 Accumulation Rates for Ritterbush Pond 32

Table 4.3 Age Model and Accumulation Rate Calculations for Core 2 79

Table 4.4 Modeled Layer Age in Radiocarbon and Calendar Years for Core 2 85

Table 5.1 Rainfall Intensity Estimates for Extreme Events at Ritterbush Pond..... 102

LIST OF TABLES

Table 3.1	Water Depth, Estimated Sediment Thickness, and Core Section Length.....	30
Table 3.2	Characteristic Litho-Stratigraphy of Cores 2, 3, and 4.....	35
Table 3.3	Radiocarbon Dates for Ritterbush Pond	52
Table 4.1	Lateral Variation in Correlated Inorganic Layers.....	62
Table 4.2	Calibrated Radiocarbon Dates for Ritterbush Core Correlation.....	64
Table 4.3	Age Model and Accumulation Rate Calculations for Core 2	79
Table 4.4	Modeled Layer Age in Radiocarbon and Calendar Years for Core 2	85
Table 5.1	Rainfall Intensity Estimates for Extreme Events at Ritterbush Pond.....	102

LIST OF FIGURES

Figure 1.1 Ritterbush Pond Watershed, Eden, VT.	3
Figure 2.1 Reasoner coring device used to retrieve cores at Ritterbush Pond.	10
Figure 2.2 Comparison of Sapphire and Bartington magnetic susceptibility data.	14
Figure 2.3 Replicate analyses for A) LOI, B) TOC, C) total nitrogen, and D) bulk density.	18
Figure 2.4 Smoothing LOI data for Core 2.	20
Figure 3.1 Ritterbush Pond bathymetry and core location.	29
Figure 3.2 Generalized litho-stratigraphic logs for Ritterbush Pond core.	32
Figure 3.3 Photograph of Core 2, Section 3 showing a thick inorganic layer.	33
Figure 3.4 Magnetic susceptibility for Cores 2, 3, and 4.	35
Figure 3.5 Paleomagnetic declination, inclination and intensity for Core 2.	36
Figure 3.6 X-radiograph and grayscale density for a 1 meter section of Core 2.	38
Figure 3.7 Loss-on-ignition for Cores 2, 3, and 4.	40
Figure 3.8 Total organic carbon (TOC) and carbon / nitrogen ratio (C/N) for Core 2.	41
Figure 3.9 Percent charcoal from nitric acid digestion.	43
Figure 3.10 Stable carbon isotope data for two inorganic layers in Core 2.	44
Figure 3.11 Mean grain size data for each cm of the five thickest inorganic layers.	46
Figure 3.12 Gytija bulk density for Core 2.	47
Figure 3.13 Radiocarbon and calibrated ages for Ritterbush Pond cores, correlated to depth in Core 2.	50
Figure 4.1 Comparison of high resolution, whole-core data sets for Core 2.	56
Figure 4.2 Identification of inorganic layer location and thickness by different analytical techniques.	58

Figure 4.3 Comparison of LOI to A) grayscale density, B) TOC and C) magnetic susceptibility	59
Figure 4.4 Correlation of Ritterbush Pond cores using LOI data	61
Figure 4.5 Layer frequency as a function of time since the last event	66
Figure 4.6 Summary data for layer emplacement using Core 2, layer i	67
Figure 4.7 Test of emplacement mechanism for inorganic layers	72
Figure 4.8 Compression of Core 2 for age modeling.	76
Figure 4.9 Age model for Core 2..	78
Figure 4.10 Average bulk density by interval	82
Figure 4.11 Gytija accumulation rates for Core 2.	83
Figure 4.12 Inorganic layer deposition for Core 2	83
Figure 4.13 Layer thickness vs. calendar age.	86
Figure 5.1 Layer thickness as a function of calendar years since the last event	92
Figure 5.2 Extreme value probability distribution of inorganic layer thickness in Ritterbush Pond cores	95
Figure 5.3 Summary of Holocene Climate Proxy (Pollen) Data for the northeastern United States in ¹⁴ C yr BP.	96
Figure 5.4 Seasonal probability of intense precipitation for the northeastern United States, from U.S. Weather Bureau (1959).....	99
Figure 5.5 Rainfall intensity-duration-frequency curves for Burlington and Northfield, Vermont, from U.S. Weather Bureau (1955)	100
Figure 5.6 Intensity-duration relationship for major, debris-flow producing storms in the Appalachians, from Kochel (1990)	104
Figure 5.7 Extreme value distribution of 24-hour annual maximum precipitation data for Burlington (NWS, 1998).....	105

CHAPTER 1 - Introduction

1.1 Statement of Problem

In most New England lakes, the sediment record consists of organic debris (gyttja) deposited as a result of the primary productivity of aquatic organisms living in and around the lake, and sand, silt and plant matter eroded from the surrounding watershed. Traditional Holocene lake research has investigated the chemical, biological, and physical characteristics of the gyttja dominant in New England lake sediment records in order to interpret large scale climatic change since deglaciation (Davis and Jacobsen, 1985; Spear et al., 1994; Winkler, 1985a) and investigate internal lake dynamics (Almquist-Jacobson et al., 1992; Anderson et al., 1992; Davis and Ford, 1982). Excepting deposits correlated with the Younger Dryas (Thompson et al., 1996), the deposition of inorganic, terrestrially-derived sediment in mountain lakes and its potential use as a climate proxy has not received much attention in New England.

My research investigates distinct layers of sand and silt that disrupt the background aquatic sedimentation in Ritterbush Pond, a small lake in northern Vermont. Rare but severe erosional events, such as intense storms and forest fires, may briefly but drastically change the sedimentation dynamics of the watershed. The silt and sand layers provide a datable record of the episodic deposition of terrestrial material in the lake. The changing frequency (tens to thousands of years), and magnitude (0.1 cm- to 10 cm-thick) of inorganic sediment deposition in Ritterbush Pond, implies forcing by local or regional climate patterns.

Most paleoclimate reconstructions for New England suggest a simple three-fold division of post-glacial time: gradual warming after deglaciation, increased moisture in the middle Holocene with temperatures peaking around 6,000 ¹⁴C yr. BP, and cooler

conditions in the past few thousand years (Lin et al., 1995; Spear et al., 1994; Webb et al., 1993). The pollen records show no large or systematic changes within these three periods. Using the distribution and magnitude of the depositional events in Ritterbush Pond, I employ a new approach to resolve changes in climate (storm frequency) as expressed by changes in watershed sedimentation dynamics.

1.2 Overview of Thesis

The objectives of this thesis are to:

- 1) describe the lithology of Holocene sediment cores from Ritterbush Pond, a post-glacial mountain lake in north-central Vermont (Figure 1.1),
- 2) investigate the biogeochemical and physical properties of the sand and silt layers, and determine their spatial and temporal distribution in the cores,
- 3) propose sedimentologic mechanisms for the deposition of the inorganic layers,
- 4) use the inorganic layers to infer a Holocene history of erosion for the lake's drainage basin, and
- 5) compare the inferred hydrologic event chronology with existing Holocene records of local, regional, and global climate change.

I begin with a description of the sampling procedures and analytic techniques used in data collection (Chapter 2), and then present and analyze each data set individually (Chapter 3). I apply and interpret multiple data sets to correlate the cores, determine possible emplacement mechanisms for the inorganic layers, and construct the age model and event chronology (Chapter 4). In Chapter 5, I review and discuss the sedimentation dynamics and hydrologic event chronology of Ritterbush Pond, and compare it to other Holocene climate proxy records. I close with a statement of conclusions and suggestions for future work (Chapter 6).

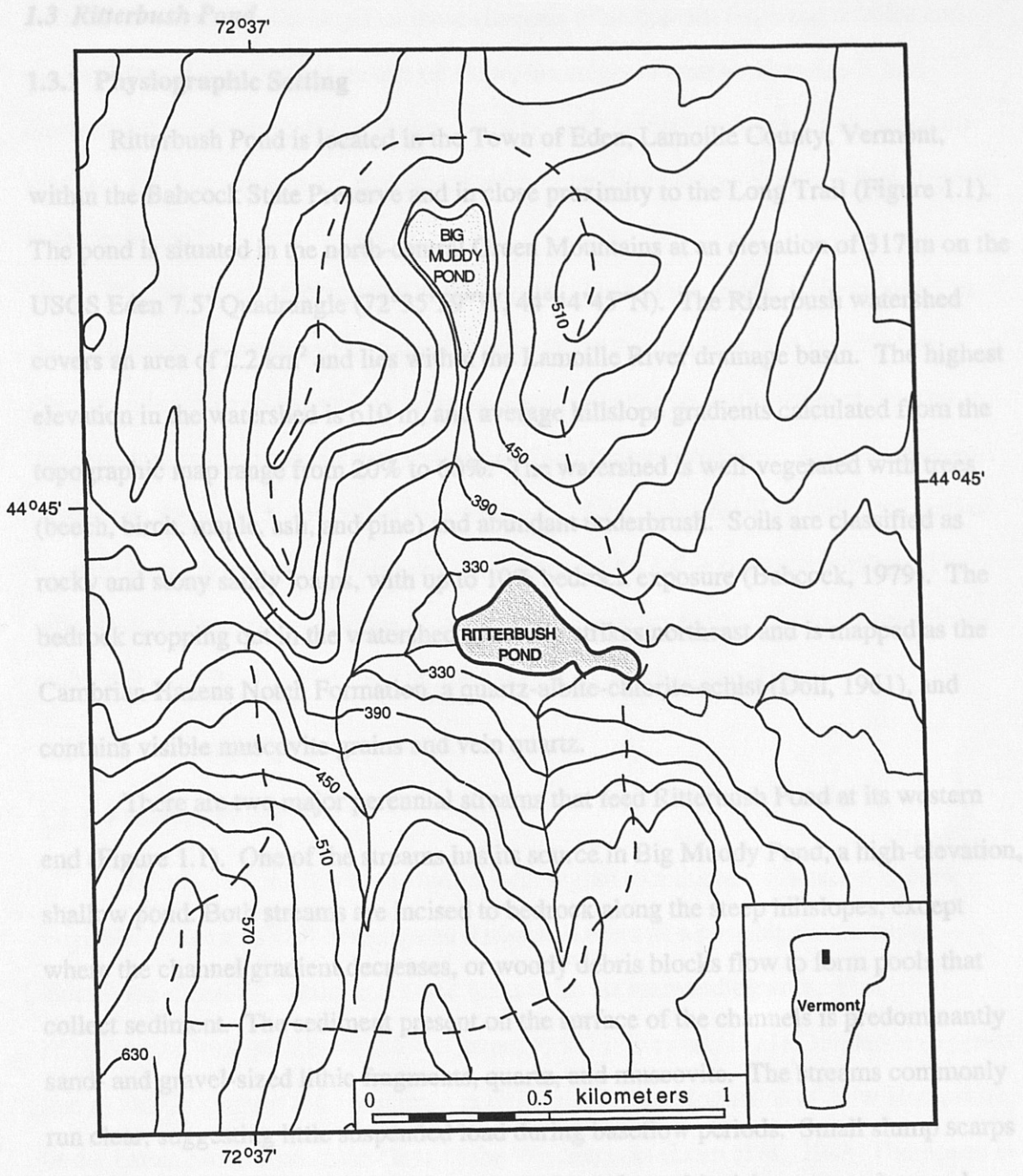


Figure 1.1 Ritterbush Pond Watershed, Eden, VT. Contour interval, 30 meters. Adapted from Eden and Hazens Notch USGS 7.5" topographic quadrangle maps, 1986.

1.3 Ritterbush Pond

1.3.1 Physiographic Setting

Ritterbush Pond is located in the Town of Eden, Lamoille County, Vermont, within the Babcock State Preserve and in close proximity to the Long Trail (Figure 1.1). The pond is situated in the north-central Green Mountains at an elevation of 317 m on the USGS Eden 7.5' Quadrangle (72°35'59"W, 44°44'45"N). The Ritterbush watershed covers an area of 2.2 km² and lies within the Lamoille River drainage basin. The highest elevation in the watershed is 610 m, and average hillslope gradients calculated from the topographic map range from 20% to 60%. The watershed is well-vegetated with trees (beech, birch, maple, ash, and pine) and abundant underbrush. Soils are classified as rocky and stony sandy loams, with up to 10% bedrock exposure (Babcock, 1979). The bedrock cropping out in the watershed generally strikes northeast and is mapped as the Cambrian Hazens Notch Formation, a quartz-albite-chlorite-schist (Doll, 1961), and contains visible muscovite grains and vein quartz.

There are two major perennial streams that feed Ritterbush Pond at its western end (Figure 1.1). One of the streams has its source in Big Muddy Pond, a high-elevation, shallow pond. Both streams are incised to bedrock along the steep hillslopes, except where the channel gradient decreases, or woody debris blocks flow to form pools that collect sediment. The sediment present on the surface of the channels is predominantly sand- and gravel-sized lithic fragments, quartz, and muscovite. The streams commonly run clear, suggesting little suspended load during baseflow periods. Small slump scarps (< 2 m²) were observed at higher elevations where channel incision exposed several meters of hillslope sediments. During a storm in 1997, and following periods of rain in 1997 and 1998, the stream water was brown and contained silt and clay-sized particles.

Several ephemeral channels that were dry in the summer and fall were actively delivering water and sediment to the lake after periods of rain and during spring snow

melt. Even when dry, the larger of these channels often contain fist-sized cobbles and can be followed hundreds of meters up slope; the origin of smaller channels is less discrete, but some originated in slump scarps (<1 m²) on the hillslopes. I observed no evidence for large-scale mass movement, such as landslide scarps or debris flow deposits in the watershed.

The shoreline of Ritterbush Pond is generally shallow, sandy, and vegetated on the southern end, dominated by a marshy area on the western side, and bounded by steeper and rockier slopes to the northeast. On the south and southeastern shores, there are abundant fallen trees and snags with their roots below lake level. At the eastern end of the lake the outlet is controlled by a shallow (0.5 m) bedrock sill on strike with other exposed bedrock outcrops. There does not appear to be active beaver damming. The lake water drains through a series of shallow marshy areas for over 2 km before it joins with Fryingpan Brook to become the White Branch of the Gihon River.

1.3.2 Previous Work

Ritterbush Pond has been studied with regard to mountain glaciation in New England. Wagner (1970) investigated Ritterbush Pond as a possible cirque basin, identifying morainal, kettle, and kame features in the surrounding area. This interpretation was quickly disputed (Connally, 1971; Stewart, 1971). Evidence suggests that mountain glaciers did not remain in either the White Mountains of New Hampshire, or the Green Mountains at the close of the Wisconsinan (Loso et al., 1998; Thompson et al., 1996; Wright et al., 1997).

Sperling (1989) re-examined Wagner's work and cored the western end of the pond (water depth = 9.2 m), interpreting a basal radiocarbon age of $10,730 \pm 200$ ¹⁴C yr BP, at the base of the peaty core, as the age of deglaciation. However, Sperling's (1989)

pollen chronology suggests that the watershed was well-vegetated by that time, leading him to concur with Wagner (1970) that ice remained in the Ritterbush area after the recession of the Laurentide ice sheet. The reported core stratigraphy is not sufficiently detailed for comparison with the cores analyzed for this research, but does show three sand and gravel deposits directly below, and two additional sand deposits one meter above, peat dated at 4210 ± 125 ^{14}C yr BP.

Ritterbush Pond was recently cored in conjunction with pollen and stable isotope research (Lin, 1996; Lini et al., 1995). A pair of overlapping, 2-inch Livingston cores (Cores RT-1 and RT-2) showed distinct variations in organic carbon content as approximated by loss-on-ignition (LOI). Numerous horizons of inorganic sediment (silt and sand) were visually identified within gyttja. Five ^{14}C dates were obtained from gyttja within the cores to construct a pollen chronology and deglacial climate and vegetation history. Lin (1996) hypothesized that the inorganic layers were deposited as a result of sediment resuspended by flood events. Her climate reconstruction, based solely on pollen, does not address the climatic implications of the horizons.

Subsequent examination of Cores RT-1 and RT-2 included stable isotope analysis and nine additional radiocarbon dates. Systematic variations in $\delta^{13}\text{C}$ values with lithology were interpreted as indicating different organic source material for the gyttja (aquatic) and inorganic layers (terrestrial) (Lini et al., 1995). Three pairs of radiocarbon dates that bracket the thickest inorganic layers demonstrate that the terrestrially derived layers were deposited rapidly (Bierman et al., 1997). Bierman et al. (1997) correlate the deposition of inorganic layers in the Ritterbush cores to periods of hillslope erosion recorded by alluvial fans, and suggest a connection between inorganic sedimentation events, hillslope destabilization, and regional climate patterns. The stratigraphic log and loss-on-ignition (LOI) data for Core RT-2, the 14 radiocarbon dates, and the pollen

chronology will be used for comparison with three new Ritterbush Pond cores (Chapter 4).

CHAPTER 2 - Methods

I used a wide variety of methods to investigate sediment cores collected from Ritterbush Pond in order to gain a comprehensive understanding of sediment deposition and distribution in the lake. Most of the methods are routine for lake sediment core retrieval and analysis, and standard procedures required little modification. Additional procedures and equipment were tested and developed as needed. Detailed descriptions of the procedures I used are provided in Appendix A (Field Methods) and Appendix B (Lab Methods). This chapter presents background information on each analytical technique, an overview of the procedure used, and statistical parameters for each data set collected.

2.1 Field Methods

2.1.1 Bathymetry and Sediment Probing

Bathymetry and sediment thickness were measured at Ritterbush Pond in order to estimate sub-aqueous sediment distribution (D. Shaw, unpub. data, 1997) and to help determine locations for coring. Initial bathymetric measurements were made in 1995 (Lin, 1996). I checked and supplemented these measurements in January, 1997. The locations of over 60 holes augered in the ice were surveyed using an electronic total station set to a fixed benchmark on shore. Bathymetry was recorded as the distance from the sediment-water interface to the top of the ice using a weighted (200 g) measuring tape. Magnesium/zirconium core rods were then lowered through the ice and pushed into the sediment. The measured water depth subtracted from the total length of rod lowered provides a minimum estimate of sediment thickness.

2.1.2 Coring

Three cores (Core 2, Core 3, and Core 4) were taken through 30 to 45 cm thick ice in January and March, 1997. All cores were obtained using a modified Reasoner coring device (Reasoner, 1993), a percussion corer fitted with a piston and a core-catcher (Figure 2.1). This device was chosen because it is lightweight, easily transportable, inexpensive to build and maintain, and can be used to obtain a large diameter (7.5 cm) continuous core. The corer is constructed of PVC pipe and has three parts: a core barrel holds the sediment, the core head attaches to the barrel and allows the core to be raised and lowered, and the core driver acts as a hammer to pound the core barrel into the sediment. The head and driver are secured at the ice surface with climbing ropes. The cores were retrieved using a pulley system anchored in the ice to obtain mechanical advantage. In the field, the 6 m-long PVC pipe encasing the core was cut into shorter lengths (1.7 to 3.0 m) for transport back to the University of Vermont (UVM).

2.2 Laboratory Methods

I conducted most analyses at UVM between February 1997 and May 1998. Paleomagnetic analysis equipment was used at the University of Rhode Island. Grain size was measured at Union College in New York. Radiocarbon sample preparation and dating were performed at Lawrence Livermore National Laboratory in California.

2.2.1 Core Processing

In the UVM laboratory, the three cores were cut into a total of eleven segments ranging in length from 1.24 to 1.62 m. I estimate that <1 cm of the core was disturbed by cutting the segments, and the record is therefore considered continuous. During May and

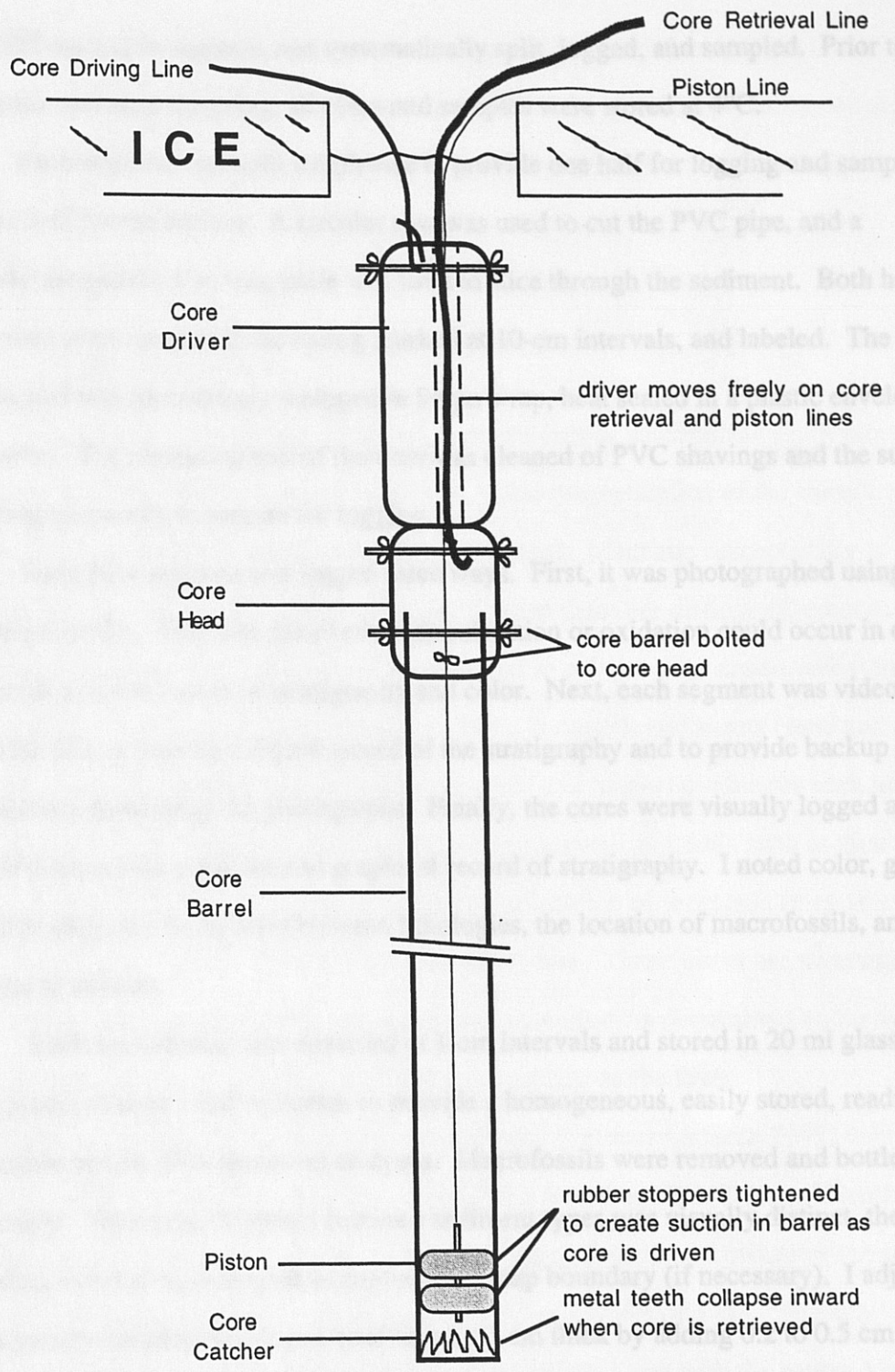


Figure 2.1 Reasoner coring device used to retrieve cores at Ritterbush Pond. A lightweight, PVC percussion corer with piston (Reasoner, 1995). Sketch adapted from J. Robison, unpublished figure, 1998.

June 1997 each core segment was systematically split, logged, and sampled. Prior to processing and after sampling, all cores and samples were stored at 4°C.

Each segment was split lengthwise to provide one half for logging and sampling and one half for the archive. A circular saw was used to cut the PVC pipe, and a specially designed 1.8 m long knife was used to slice through the sediment. Both halves of the core were measured, the casing marked at 10-cm intervals, and labeled. The archive half was immediately wrapped in Saran wrap, heat sealed in a plastic envelope, and stored. The remaining half of the core was cleaned of PVC shavings and the surface was scraped smooth to prepare for logging.

Each core segment was logged three ways. First, it was photographed using color 35 mm print film. This was done before discoloration or oxidation could occur in order to provide a visual record of stratigraphy and color. Next, each segment was video taped with Hi8 film to provide a digital record of the stratigraphy and to provide backup in case of problems developing the photographs. Finally, the cores were visually logged and sketched to provide a written and graphical record of stratigraphy. I noted color, grain size, lithology, the boundaries between lithologies, the location of macrofossils, and other features of interest.

Each section was then dissected at 1-cm intervals and stored in 20 ml glass (Core 2) or plastic (Cores 3 and 4) bottles to provide a homogeneous, easily stored, readily accessible sample for subsequent analyses. Macrofossils were removed and bottled separately. Where the boundary between sediment types was visually distinct, the 1-cm sampling interval was adjusted to capture the sharp boundary (if necessary). I adjusted the interval primarily for silt and sand layers >3 cm thick by adding 0.2 to 0.5 cm to the preceding sample (increasing it from 1 cm to 1.2 to 1.5 cm) and increasing or decreasing the subsequent interval by 0.2 to 0.5 cm respectively. Boundaries less than 0.1 cm off the sampling boundary were incorporated into the appropriate sample without adjustment to

the recorded depth. Sampling intervals range from 0.5 cm to 1.5 cm. Over 1700 sediment and macrofossil samples were collected from the three cores and stored at 4°C. During sampling, subtle changes in sediment type not evident from surface logging were noted on the stratigraphic logs.

2.2.2 Magnetic Susceptibility

Magnetic susceptibility is a relative measurement of susceptibility of a sample to magnetization. The value, reported in SI units, is the magnetization of the sample (gauss) divided by the strength of the magnetic field (oersteds). Magnetic susceptibility is commonly used to identify changes in lithology when there are distinct differences in magnetic mineral content, and is routinely reported as a down core measurement in marine and lake sediment studies (Dearing, 1986). Inorganic sediments (sand and silt) have a higher susceptibility than organic sediments, and magnetic minerals such as magnetite will have higher susceptibility than non-magnetic minerals such as quartz. I use peaks in magnetic susceptibility to identify the location of inorganic (magnetic) layers within the primarily organic (non-magnetic) core. These peaks are superimposed on a background signal from the gyttja and peak magnitude is determined by the type, concentration, and amount of magnetic material making up the layer.

I initially measured whole core susceptibility (February, March 1997) using a Sapphire magnetic susceptibility meter and coil, on loan from P.T. Davis of Bentley College in Massachusetts. The coil generates a magnetic field and measures the response of the material within the coil. The Sapphire coil has a width of 4 cm, and each measurement integrates over approximately 10 cm of the core, with the center 4 cm influencing the measurement most strongly. Susceptibility was recorded at 3-cm increments down each unsplit core. Initial runs included empty PVC pipes (blanks) that

demonstrated linear drift of approximately 10% of the background measurement with time (Figure 2.2A). I compensated for this drift by taking free air measurements before and after each core segment was run to determine the magnitude and direction of the drift and adjust the susceptibility records accordingly by linear interpolation. Susceptibility measurements were repeated three times for each segment, stacked, and compiled to create a master record for each core with a standard deviation of 5%.

I repeated susceptibility measurements in February 1998 using a Bartington Magnetic Susceptibility Meter (MS2) with higher resolution (integration over 4 cm) and an automated core-logging system. Split (half-cores) were run once at 1-cm increments and corrected for slight linear drift (<1%) using free air measurements as detailed above. Repeated runs of core segments showed a standard deviation of 1%.

Comparison of the two techniques used to measure magnetic susceptibility shows a strong positive correlation (Figure 2.2B). The Sapphire data, at 3-cm resolution and on whole-cores, show the same peaks as the Bartington measurements on half-cores almost a year later, implying no degradation of the magnetic signal due to core storage (Figures 2.2C, D). The 1-cm resolution Bartington data are presented in Chapter 3, and subsequently used for comparison with other high-resolution data.

2.2.3 Paleomagnetic Measurements

Paleomagnetic secular variation (PSV) is the short-period, small-amplitude change in the earth's magnetic field and is measured by the natural remanent magnetism (NRM) (declination, inclination, and intensity) of earth materials (Lund, 1993; King et al., 1983). Lake sediments have been shown to be excellent recorders of this signal where the dominant sedimentation mechanism is slow settling of clay-sized particles, allowing detrital magnetite to align with the earth's magnetic field. Rapid deposition,

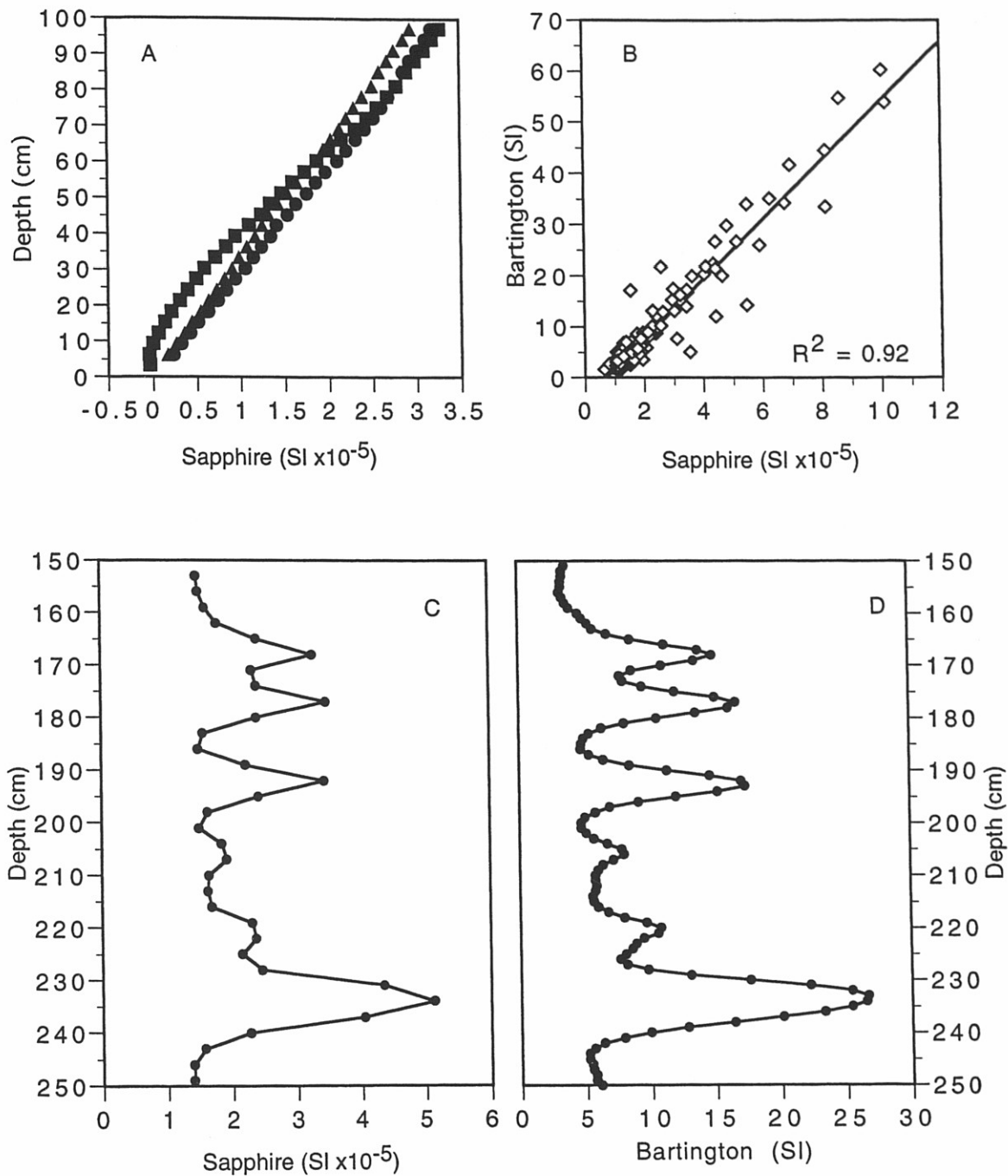


Figure 2.2 Comparison of Sapphire and Bartington magnetic susceptibility data. A) Linear drift of Sapphire signal over 1 m blank core, B) data show good correlation between methods, C) Sapphire, and D) Bartington data over a meter of Core 2 (150 cm to 250 cm), showing higher resolution of Bartington analysis.

reworking of sediment, or bioturbation will obscure the magnetic signal (Verosub, 1977). Reliability criteria, such as the length and continuity of the record, and the stability and reproducibility of the signal, have been established to determine the suitability and robustness of paleomagnetic records for use as PSV records (Thompson, 1985). Secular variation of both declination and inclination has been used to correlate lake sediment records from deglacial and Holocene lakes in New England, North America, and Europe (Lund, 1996; Peck et al., 1996; Ridge et al., 1990).

I performed paleomagnetic analysis on the Ritterbush Pond cores as a potential tool for correlating cores within the lake, and comparing the Ritterbush Pond record with other dated Holocene lake sediment records. I measured NRM for all archived core segments in December 1997, on a cryogenic magnetometer at the Paleomagnetic Laboratory at the University of Rhode Island, under the direction of John King and John Peck. Each core section was demagnetized at 10 mT to remove the unstable portion of the paleomagnetic signal (Zijdeveld, 1964). Declination (degrees), inclination (degrees), and intensity (emu cm^{-3}) measurements were taken at 2-cm increments. The magnetometer integrates over approximately 14 cm for each measurement. Average variations for replicate samples are reported to be as great as 8 degrees in inclination and declination (Peck et al., 1996; King et al., 1983).

The original orientation of each core segment with respect to north, and rotation relative to the adjacent core segments, were not recorded, causing significant shifts in measured declination and inclination within and between cores. Continuous records were compiled for each core by adjusting all values for a core segment by the magnitude of the offset from the adjacent segment. Each core record was then normalized to the mean value for the core to allow for comparison between cores.

2.2.4 X-radiography

The differential absorption of X-rays by sample material produces a graphic image depicting changes in material type. The absorption of X-rays is dependent on the density (packing and water content) and composition (atomic number) of the sample material (Axelsson, 1983). Marine and lake sediment studies often use x-rays of cores to document and interpret sedimentary structures and for the correlation of laminations between cores (Van Weering and Van Iperen, 1984). X-rays are absorbed by inorganic matter (silt and sand), but pass through organic matter (gyttja), resulting in a black and white picture of core stratigraphy. I used X-radiographs to provide a visual image of the un-opened cores, to identify small-scale structures and changes in lithology not visible to the naked eye, and to construct X-ray density profiles based on the scanned, grayscale images.

I was trained to use the X-ray machine, an apparatus primarily used for medical research, at the UVM Radiation Safety Lab in May, 1997. All eleven core segments were X-radiographed in overlapping, 30-cm sections with depth increments (20 cm) marked with lead. The X-rays are projected from a point source above the table, pass through the cores, and expose film inserted beneath the cores. The conical scattering of the X-rays from the point source slightly distorts the resulting image away from the point directly below the X-ray source. I calculated the degree of distortion for each image by measuring the resulting distance on the developed film between the lead markers. Distortion was consistent at 2 cm per 30 cm, and was corrected as a linear function of distance away from the center of the image.

I scanned the X-radiographs from Core 2 in order to obtain images that could be digitally analyzed and reproduced. Using a transparency scanner, each image was imported into *Adobe Photoshop 3.0*, and adjusted, using a linear stretch, for the measured distortion of the image. Scanner parameters, such as intensity and resolution, were kept

constant for all images. The images were compiled in *CANVAS 3.45*, using the graphic logs to accurately match the images, to create a continuous, graphic record for each segment. *NIH image* was used to develop gray-scale (256 levels) density data for the complete record.

2.2.5 Loss-on-ignition (LOI)

Loss-on-ignition (LOI) is measured as a proxy for organic carbon content. Percent LOI is calculated as the percent weight lost when a dried sample is combusted (Berglund, 1986). Combustion of a sediment sample ashes the organic matter and releases CO₂. High loss-on-ignition (LOI) values are associated with organic-rich sediments such as gyttja and peat. Low LOI values indicate inorganic sediments (sand and clay). Loss-on-ignition records are routinely reported in lake and marsh research to characterize lithologic changes in sediment cores with depth (Anderson et al., 1992; Peteet et al., 1990; Thompson et al., 1996). Published LOI records for New England were developed primarily in conjunction with pollen research (Davis and Jacobsen, 1985; Spear, 1989; Spear, 1993). The resolution of these records is rarely better than one sample every 10 cm.

I use LOI to detect down-core trends in organic-matter content, to estimate average carbon content of both gyttja and inorganic layers, and to delineate the boundaries of the inorganic layers. Aliquots from each sample bottle for all three cores were weighed, dried, weighed a second time, combusted at 450°C for 2 hours, and weighed a final time. Prior to weighing, the samples cooled to room temperature in open air for 1 hour (P.T. Davis, written comm., 1997). From these measurements, I calculated percent water loss and percent weight loss (LOI) for each centimeter of all three cores. The precision (1 sigma) of the measurement was quantified at $\pm 0.05\%$ LOI by running replicates of ten samples spanning the range of LOI values (Figure 2.3A).

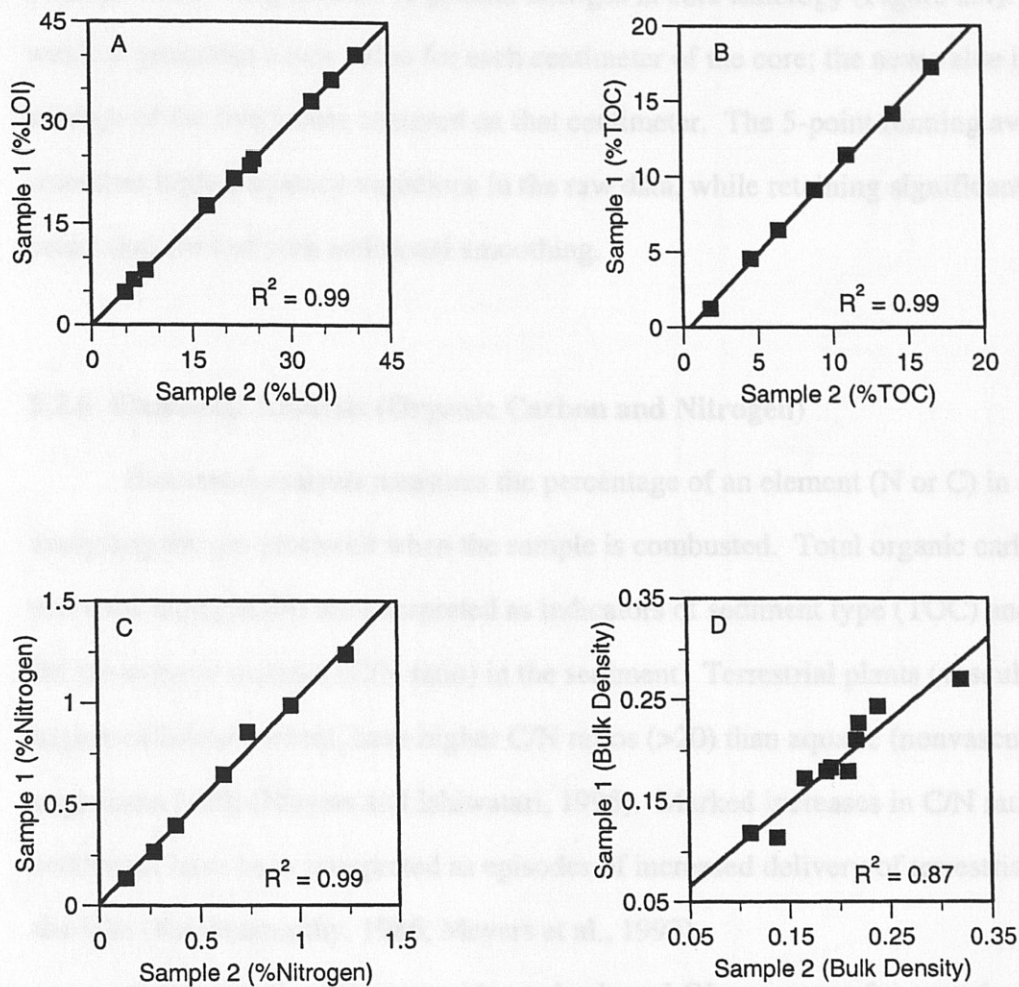


Figure 2.3 Replicate analyses for A) LOI, B) TOC, C) total nitrogen, and D) bulk density.

LOSS ON IGNITION (%)

The centimeter-resolution LOI data are used for comparison with other high-resolution data sets. I have also used a 5-point running average or window to smooth the data for visual interpretation of general changes in core lithology (Figure 2.4). The window generates a new value for each centimeter of the core; the new value is the average of the five values centered on that centimeter. The 5-point running average smoothes high-frequency variations in the raw data, while retaining significant individual peaks that are lost with additional smoothing.

2.2.6 Elemental Analysis (Organic Carbon and Nitrogen)

Elemental analysis measures the percentage of an element (N or C) in a sample by analyzing the gas produced when the sample is combusted. Total organic carbon (TOC) and total nitrogen (N) are interpreted as indicators of sediment type (TOC) and the source for the organic material (C/N ratio) in the sediment. Terrestrial plants (vascular), due to a higher cellulose content, have higher C/N ratios (>20) than aquatic (nonvascular) organisms (<10) (Meyers and Ishiwatari, 1995). Marked increases in C/N ratios in lake sediments have been interpreted as episodes of increased delivery of terrestrial material to the lake (Krishnamurthy, 1986; Meyers et al., 1993).

Total organic carbon provides a check on LOI as a proxy for organic carbon content. Organic molecules are composed of carbon, hydrogen, oxygen, nitrogen, and other minor constituents, with the ratio of elements determined by the type of organic material, and the amount of decomposition that has occurred. Carbon (TOC) generally represents 40% to 60% of the weight of organic material combusted by loss-on-ignition (Bengtsson and Enell, 1986).

I measured total organic carbon and total nitrogen for Core 2 using a CE NA2500 Elemental Analyzer in the Environmental Stable Isotope Laboratory at UVM. An

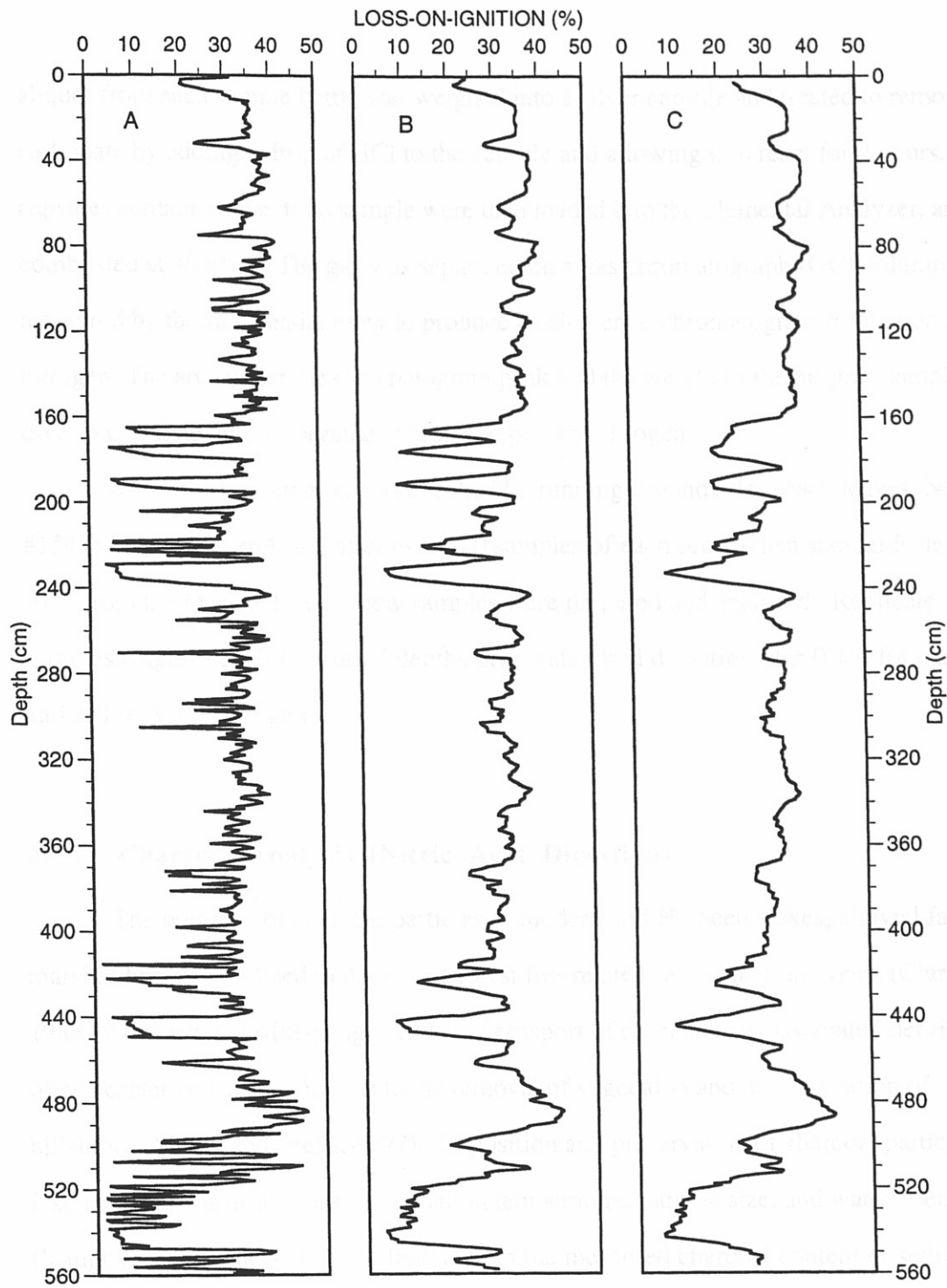


Figure 2.4 Smoothing LOI data for Core 2. A) Raw data, B) 5-point and C) 9-point running averages progressively smooth the data. The 5-point running average maintains resolution while providing enough smoothing to allow for ease of comparison with other records.

aliquot from each sample bottle was weighed into a silver capsule and treated to remove carbonate by adding a drop of HCl to the capsule and allowing it to react for 2 hours. The capsules containing the dried sample were then loaded into the Elemental Analyzer, and combusted at 1020°C. The gas was separated on a gas chromatograph (GC) column and measured by thermal conductivity to produce an elemental chromatogram for carbon and nitrogen. The area under the chromatogram peak and the weight of the original sample were used to calculate percent organic carbon and percent nitrogen.

Drift of the calibration was checked by running 2 standards (peach leaves, NIST #1547) at the start, end, and after every 20 samples of each run. When standards deviated >1% from the expected value, new samples were prepared and analyzed. Replicate samples (Figures 2.3B,C) from 7 depths give a standard deviation of $\pm 0.1\%$ for carbon and $\pm 0.05\%$ for nitrogen.

2.2.7 Charcoal Analysis (Nitric Acid Digestion)

The presence of charcoal particles in modern and Holocene lakes, alluvial fans, and marshes has been utilized to document forest fire-related sedimentation events (Clark, 1988; Whitlock and Millspaugh, 1996). Transport of charcoal and associated debris is often accelerated after a fire due to the removal of vegetation and destabilization of hillslopes (Meyer and Wells, 1997). Deposition and preservation of charcoal particles in lake sediments is influenced by formation temperature, particle size, and water chemistry (Vaughan and Nichols, 1995). Increases in the measured charcoal content of sediments, or the presence of visible charcoal particles, is used to construct local and regional fire-history chronologies (Millspaugh and Whitlock, 1995; Clark, 1988; Winkler, 1985). Visual techniques for charcoal identification require thin section preparation or sieving of samples and investigation under a microscope (Clark, 1988). I used a nitric acid digestion

technique, shown to correlate well with visual identification, to measure percent charcoal in the sediment (Winkler, 1985b).

I analyzed 122 samples from eight intervals in Core 2 to test for association between fire-generated charcoal particles and inorganic layers. Five of the intervals included the thickest inorganic layers in the core. Three intervals were composed entirely of gyttja to provide an estimate of the background fluctuation of charcoal content. Each sample was treated with concentrated nitric acid to oxidize organic material, carbonate, and pyrite, leaving the inorganic material and charcoal particles as residue. Traditionally, this residue is then combusted at 450°C to remove charcoal, and the loss in weight calculated as percent charcoal. My initial tests of this method gave very low and occasionally negative values for charcoal mass, suggesting that my equipment (balance, crucibles) were not accurate enough to measure small weight changes or that there was negligible carbon, charcoal or otherwise, associated with the treated samples. To increase the precision of my measurements, I combusted the residue in the Elemental Analyzer (procedure detailed above and in Appendix B) and recorded TOC as a percentage of the digested sample. This modification produced percent charcoal values comparable to expected values for lake sediments (Winkler, 1985b). Replicate samples were not run.

2.2.8 Stable Carbon Isotope Analysis

Stable carbon isotope composition ($\delta^{13}\text{C}$, relative to PDB standard) of organic matter depends on the CO_2 source, photosynthetic pathway (C3, C4, CAM), and subsequent diagenetic processes (Fogel and Cifuentes, 1993). Fluctuations in the $\delta^{13}\text{C}$ values of lake sediments can be interpreted as changes in organic matter source, lake productivity, and watershed vegetation (Meyers and Ishiwatari, 1995; Winkler, 1994). The organic carbon associated with terrestrial and aquatic sediments in Ritterbush Pond has

been shown to have different stable carbon isotope values (Lini et al, 1995). I use stable carbon isotopes to investigate the degree of mixing between terrestrial and aquatic sediments associated with the deposition of the inorganic layers. Gyttja and macrofossil samples were also analyzed in conjunction with radiocarbon dating (section 2.2.11).

I chose two inorganic layers in Core 2 for $\delta^{13}\text{C}$ analysis, and sampled each centimeter comprising the layer, and one centimeter of gyttja above and below the layer, for a total of 20 samples. Each sample was washed with 1N HCl to remove carbonate, and combusted in quartz tubes with copper and copper oxide at 900°C to produce H_2O , N_2 and CO_2 . The CO_2 was isolated on a vacuum line for mass spectrometric analysis. The mass spectrometer (VG SIRA II) measures the ratio of ^{13}C and ^{12}C necessary to calculate $\delta^{13}\text{C}$ with a standard deviation of 0.1‰.

2.2.9 Grain-Size Analysis

Grain size is routinely measured in paleoecological studies as an aid in interpreting depositional environments (Aaby and Berglund, 1986). Disruption of the low-energy, deep-water environment of a lake by increased stream flow or sediment load is often recorded by an erosional contact or increase in average sediment grain size (Allen and Collinson, 1986). Variations in grain size within a single inorganic deposit can be used to determine the direction of transport and depositional mechanism for the layer (Gorsline, 1984). Turbidity current deposits, for example, tend to thin and fine away from their source (Walker, 1967), and produce a characteristic vertically graded sequence (Bouma, 1962). I use grain-size analysis to confirm estimates of relative grain size made during visual logging, to trace changes in the grain size of an individual inorganic layer, and to verify the graded nature of the thickest layers.

I chose five representative inorganic layers to sample at a 1 cm interval: three layers from Core 2 and one layer each from Cores 3 and 4. I prepared the resulting 50 samples at UVM for analysis by treating them with HCl to remove carbonate, H₂O₂ to remove organic matter, and NaOH to remove biogenic silica. The samples were then analyzed with a Coulter Laser Diffraction Unit (LS 230) at Union College, NY under the direction of Donald Rodbell. Each grain size diffracts the laser at a characteristic angle, allowing the frequency at which each grain size occurs in the sample to be calculated. Replicate samples produced a standard deviation in mean grain size of $\pm 5\%$.

2.2.10 Bulk Density

Bulk density, mass per unit volume, is controlled by the composition (lithology) of the sediment, the amount of pore space between sediment grains, and initial water content (Bendtsen and Enel, 1986). In lake sediment cores, autocompaction, the compaction of sediments under their own weight, results in a decrease of pore space and, when lithology is homogeneous, a systematic increase in density with depth (Baldwin, 1971). To interpret changes in accumulation of sediment through time, the apparent rate of sedimentation (cm yr⁻¹) must be adjusted for down-core changes in density (g cm⁻³) in order to calculate the accumulation rate (g cm⁻² yr⁻¹). In cores containing interlayered lithologies, differential compaction is accounted for by treating each lithology individually. Organic-rich sediments may compact to 20% of their original thickness; sand layers tend to maintain their original density (Baldwin, 1971; Pizzuto and Schwendt, 1997).

I estimated the bulk density of eighteen samples from ten locations in Core 2 to determine changes in density as a function of depth, and to calculate accumulation rates. Representative gyttja samples (1 cm³) were removed from the archive half of the core,

dried overnight, and weighed. I avoided sampling inorganic layers. Replicate samples were analyzed at eight of the ten locations and have an average standard deviation of 7% (Figure 2.3D).

2.2.11 Radiocarbon Dating

Radiocarbon (^{14}C) is produced in the upper atmosphere through the interaction of ^{14}N with cosmic radiation, and incorporated into living organisms through photosynthesis. The exponential decay of ^{14}C , with a half-life of 5730 yr, is used to date organic matter by calculating the time elapsed since the death of the organism(s). Accelerator Mass Spectrometer (AMS) techniques measure the $^{14}\text{C}/^{13}\text{C}$ ratio in a sample, and calculate a radiocarbon age based on the assumptions that 1) the original ^{14}C in the sample was in equilibrium with the atmosphere concentration, and 2) atmospheric ^{14}C concentration has been constant over time (Olsson, 1986; Nelson, 1986). However, both of these assumptions have been shown to be untrue, requiring adjustment of radiocarbon ages to reflect more accurately calendar years (Tyler, 1997). Isotopic fractionation, resulting in disequilibrium of the organic matter with atmospheric ^{14}C , is corrected for by measuring the $\delta^{13}\text{C}$ ($^{13}\text{C}/^{12}\text{C}$) value of the sample (Donahue et al., 1990). Deduced variation in paleo-atmospheric CO_2 is used to calibrate radiocarbon years to an equivalent age in calendar years (Stuiver and Reimer, 1993). I use AMS radiocarbon dates, adjusted for isotopic fractionation and calibrated to calendar years, to confirm the stratigraphic correlation of cores, to provide age control on deposition of inorganic layers, and to calculate sediment accumulation rates for Core 2.

Samples of gyttja and macrofossils, were removed from the refrigerated sample bottles for analysis. In March 1998, I prepared eight samples for AMS dating at Lawrence Livermore National Laboratory, according to standard procedures and under the direction of John Southon. The samples were washed in HCl and NaOH to remove

carbonate and humic acids, and then combusted with CuO in quartz tubes to produce CO₂ gas. The gas was isolated and graphitized on a vacuum line. The graphite was packed into targets for analysis by accelerator mass spectrometry (Nelson et al., 1986).

Additional samples were sent to Lawrence Livermore for preparation and processing in September 1997 (2 samples) and June 1998 (4 samples). For 7 samples, acid/base treated sample material was measured for $\delta^{13}\text{C}$ at UVM. When treated sample was unavailable, $\delta^{13}\text{C}$ was estimated as the average of the measured values, -31‰ for gyttja, and -28‰ for macrofossils.

The agreement of radiocarbon dates of gyttja and macrofossils from the same stratigraphic horizon was tested at Ritterbush Pond (Bierman et al., 1997). A macrofossil was dated at 8450 ± 60 ¹⁴C yr BP, while the surrounding gyttja was dated at 8900 ± 40 ¹⁴C yr BP, resulting in an age difference of 450 years. Bierman et al. (1997) suggest that the young macrofossil age is due to the lake reservoir effect, and/or sinking of the macrofossil through the unconsolidated gyttja. The lake reservoir effect is caused by a low ¹⁴C/¹²C ratio in the dissolved CO₂ used by the aquatic plants comprising the gyttja. The low ¹⁴C/¹²C ratio is attributed to the introduction of old, ¹⁴C depleted carbon from bedrock, basal sediments, or groundwater (Olsson, 1986). Bulk dates of carbonate-free gyttja have been shown to be hundreds of years (400 to 500 yr) older than AMS dates of terrestrial plant fragments (Wohlfarth et al., 1993). Sinking of the macrofossil may contribute to the observed offset, and would vary with the density of the gyttja at the sediment / water interface and the mass of the macrofossil. Sinking is unlikely, however, to achieve independently the entire observed offset. I accounted for the offset documented at Ritterbush Pond by subtracting 450 ¹⁴C yr from all gyttja ages.

Radiocarbon dates were calibrated to calendar years using CALIB rev3.0.3A (Stuiver and Reimer, 1993). I chose to smooth the bi-decadal tree ring records used for calibration with a 40-yr running average, as each 1 cm sample dated represents at least

20-yr of gyttja accumulation (Taylor, 1997). The analysis results in intercepts (where the ^{14}C date crosses the calibration curve) and 68% confidence ranges (where the endpoints of the 1 sigma range cross the calibration curve). Due to the shape of the calibration curve, calibration may result in more than one intercept and/or more than one range for some radiocarbon ages. To determine a single date for use in age modeling, I interpret the calibration based on the predicted values (intercepts) and the statistical significance of the standard deviation (range) of the data set. Where one range is reported, I use the intercept or average of the intercepts; where two ranges are reported, I use a weighted average of intercepts, or weighted average of range midpoints where no intercept is reported (Eden and Page, 1997). My best estimate for each calendar age equivalent of each ^{14}C age is reported to the nearest decade.

3.1 Field Data

3.1.1 Bathymetry and Sediment Probing

The maximum water depth for Ritterbush Pond, measured during the winters of 1997 and 1998, was 13.6 m (Figure 3.1). Bathymetry data collected in 1995, suggest a maximum depth of just over 14 m. During the spring and summer of 1998, the bedrock sill controlling outflow was at 0.5 m to 0.1 m below the water surface. This observed range suggests that the difference in the bathymetric measurements is probably due to natural water level fluctuation.

Sediment probing underestimated actual sediment thickness (Table 3.1). The length of the retrieved cores exceeded the sediment depth predicted by probing by 0.6 to 1.8 m, except in the center of the pond. The underestimate is most likely due to well-compacted, fine-grained inorganic layers that resisted the small diameter, uncased probe rod at depth. Therefore, sediment probing provides only a minimum sediment thickness estimate.

CHAPTER 3 - Data Presentation

This chapter presents and analyzes the data collected by the methods outlined in Chapter 2. For most analyses, the complete data set is graphed and discussed; for some analyses that produced extensive data, representative data are chosen. Individual inorganic layers are identified by core and depth, and by the lettered correlation presented in section 4.2. Complete field data are given in Appendix C. All laboratory data are tabled in Appendix D.

3.1 Field Data

3.1.1 Bathymetry and Sediment Probing

The maximum water depth for Ritterbush Pond, measured during the winters of 1997 and 1998, was 13.6 m (Figure 3.1). Bathymetry data collected in 1995, suggest a maximum depth of just over 14 m. During the spring and summer of 1998, the bedrock sill controlling outflow was at 0.5 m to 0.1 m below the water surface. This observed range suggests that the difference in the bathymetric measurements is probably due to natural water level fluctuation.

Sediment probing underestimated actual sediment thickness (Table 3.1). The length of the retrieved cores exceeded the sediment depth predicted by probing by 0.6 to 1.8 m, except in the center of the pond. The underestimate is most likely due to well-compacted, fine-grained inorganic layers that resisted the small diameter, uncased probe rod at depth. Therefore, sediment probing provides only a minimum sediment thickness estimate.

Table 3.1. Water Depth, Estimated Sediment Thickness, and Core Section Length

	CORE 2	CORE 3	CORE 4
Water Depth (m)	13.5	7.8	12.0
Sediment Thickness (m)	5.7	3.3	4.1
Total Core Length (m)	5.80	4.50	4.75
Section 1 (cm)	(0-133)	(0-119)	(0-159)
Section 2 (cm)	133	119	159
Section 3 (cm)	(133-253)	(119-242)	(159-321)
Section 4 (cm)	130	129	182
Section 5 (cm)	(130-253)	(129-253-382)	(182-325)
Section 6 (cm)	154	154	154

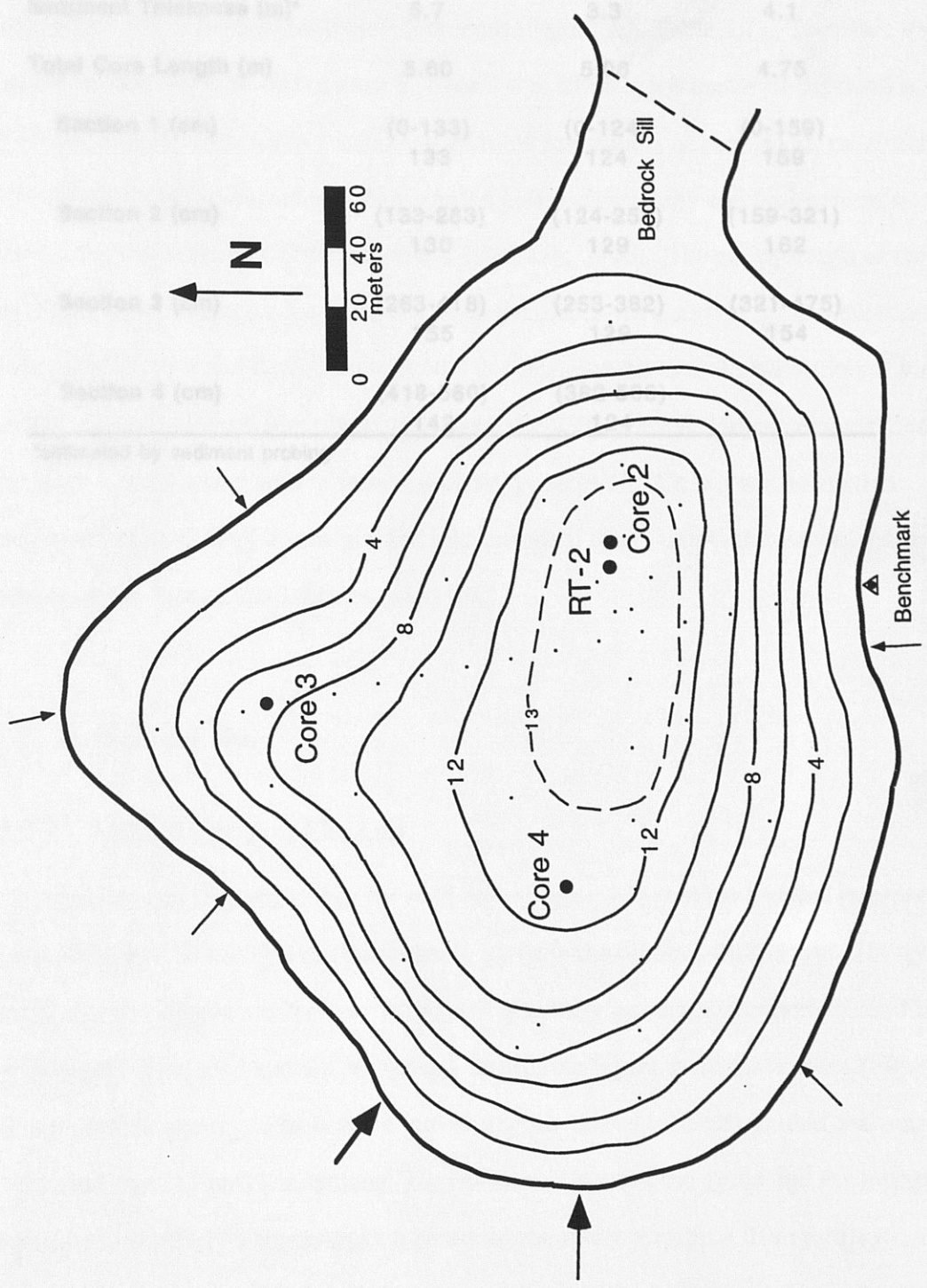


Figure 3.1 Ritterbush Pond bathymetry and core location. Contour interval 2 meters. North is approximated from Eden USGS 7.5" topographic quadrangle. Broad arrows represent perennial stream inflow; smaller arrows denote intermittent streams.

Table 3.1 Water Depth, Estimated Sediment Thickness, and Core Section Length

	CORE 2	CORE 3	CORE 4
Water Depth (m)	13.5	7.8	12.0
Sediment Thickness (m)*	5.7	3.3	4.1
Total Core Length (m)	5.60	5.06	4.75
Section 1 (cm)	(0-133) 133	(0-124) 124	(0-159) 159
Section 2 (cm)	(133-263) 130	(124-253) 129	(159-321) 162
Section 3 (cm)	(263-418) 155	(253-382) 129	(321-475) 154
Section 4 (cm)	(418-560) 142	(382-506) 124	

*estimated by sediment probing

3.1.2 Core Location

Core locations were selected based on bathymetry, estimated sediment thickness, and likely sources for terrestrial sediment input (Figure 3.1, Table 3.1). To obtain the longest, undisturbed, sediment record, Core 2 was taken in the center of the pond at a water depth of 13.5 m. Core 2 is located within a few meters of core RT-2, maximizing the probability of correlation with the existing pollen chronology and fourteen radiocarbon dates for Ritterbush Pond (Bierman et al., 1997; Lin, 1996). The entire length of the core barrel (5.8 m) was driven, but it did not reach the glacial till underlying the lacustrine sediments. Core 3 and Core 4 were located to determine the lateral distribution of inorganic layers. Core 4 (12.0 m) was placed between Core 2 and the two largest streams feeding the lake. Core 4 was driven to refusal and bottomed in till. Core 3 was located in shallower water (7.8 m) on the gentlest lake marginal slope, below the steepest hills bounding the lake. Core 3 did not reach till.

3.2 Laboratory Data

3.2.1 Litho-Stratigraphic Logs

Generalized graphic logs for each core (Figure 3.2) provide a visual reference of core lithology. Black, fine-grained organic gyttja is the dominant lithology. The gyttja is relatively homogenous within each core, and generally increases in coherency and firmness with depth. Fine sand and silt are present as discrete layers in all three cores (Figure 3.3). The inorganic layers can be divided into two types: thick (1-10 cm) graded and non-graded beds, and thin (<1 cm) laminations. The boundary between the gyttja and the inorganic material is generally a sharp contact; however, the lower transition from gyttja to sand or silt in some of the thickest inorganic layers appears gradual. Evidence for bioturbation is present in the upper centimeter of only one inorganic layer. Macrofossils (seeds, leaves,

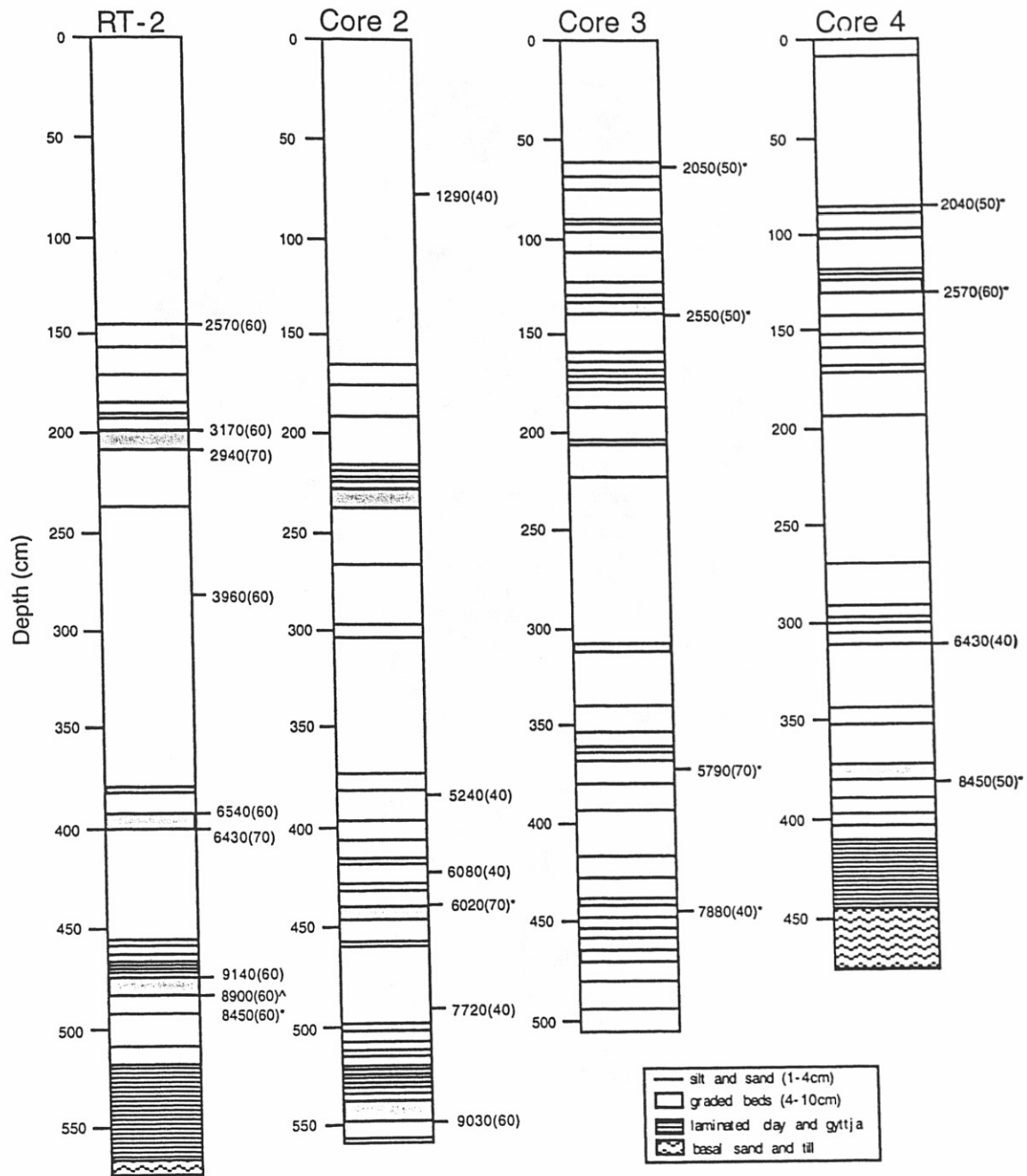


Figure 3.2 Generalized litho-stratigraphic logs for Ritterbush Pond cores. Log for RT-2 is adapted from Lin (1996). Location of inorganic layers within gyttja is shown. All radiocarbon dates are in ^{14}C yr BP (1 standard deviation). Asterisk (*) denotes macrofossil ages; carrot (^) is an average of three replicates on one gyttja sample.

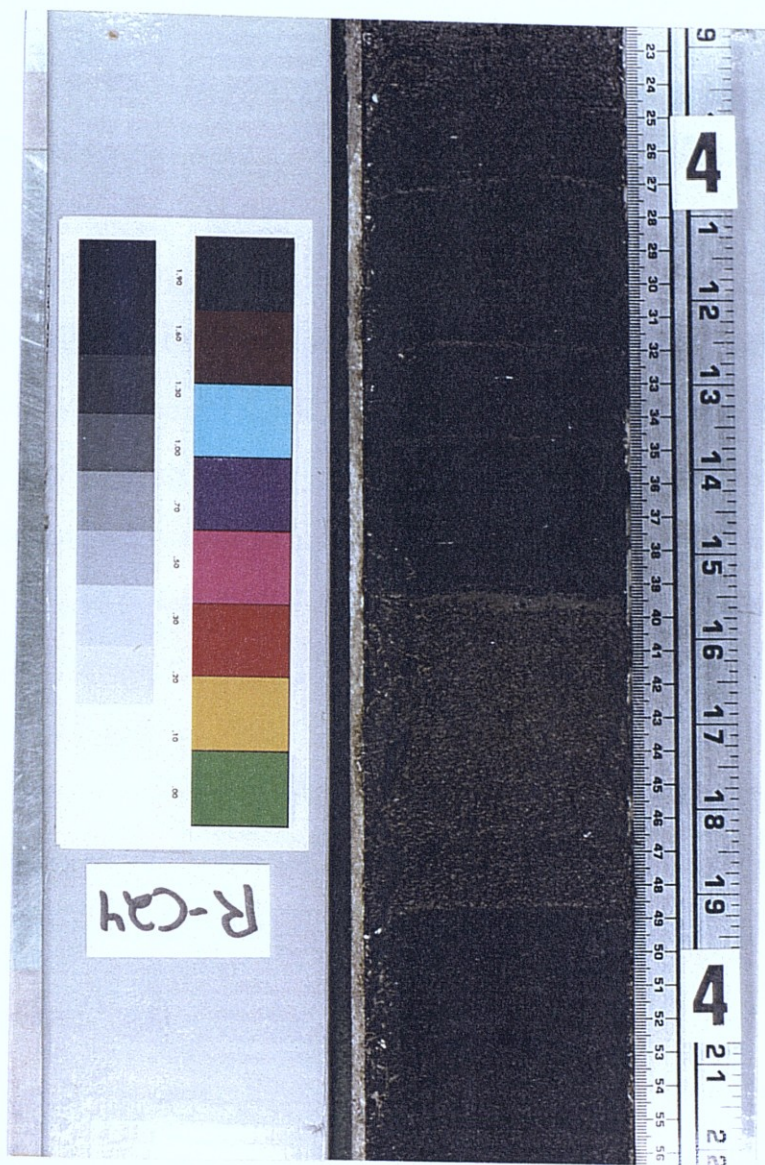


Figure 3.3 Photograph of Core 2, Section 3 showing a thick inorganic layer. The 10-cm thick brown layer has sharp upper and lower contacts with the surrounding black gyttja. Millimeter-scale gray/brown laminations are also visible (depth = 427, 432 and 434.5 cm).

and woody particles) are found above, below, and within the inorganic layers, as well as in the gyttja where visible inorganic layers are absent. The inorganic layers are less frequent in the upper and middle portions of the cores, and appear to cluster within the core. Three clusters of inorganic layers can be identified in each of the cores, and although the number and distribution of the layers varies within each cluster, it is possible to trace visually the thickest graded beds between cores.

The three cores, while sharing general characteristics, exhibit distinct differences in lithology and grain size (Table 3.2) that are a function of water depth and sediment source. Core 3, deposited in the shallowest water and closest to shore, has the coarsest gyttja and inorganic grain size, as well as the highest percentage of macrofossils (wood and leaves) and inorganic material. Core 2, at the center of the pond in the deepest water, shows the finest grain size and the lowest occurrence of inorganic layers and macrofossils. These data suggest that the deposition of gyttja is controlled primarily by the settling of organic and fine, inorganic particles. The coarser grains of the inorganic layers, the visible grading of the thick beds, and the sharp contacts with the gyttja, imply a change in depositional energy and sediment source from the quiet-water settling conditions of the gyttja.

3.2.2 Magnetic Susceptibility

The three cores have background magnetic susceptibility levels (<5 SI) that increase slightly with depth, suggesting a general down-core increase in magnetic mineral content (Figure 3.4). Apparent background levels may be elevated by the close spacing of magnetic peaks and the presence of the aluminum core catcher at the base of the core. This increase could also be due to compaction of the cores and indicate an increasing density with depth, or indicate a dilution of the magnetic signal due to increased gyttja sedimentation rates toward the top of the core. Superimposed on this general trend are

Table 3.2 Characteristic Litho-Stratigraphy of Cores 2, 3, and 4

	INORGANIC MATERIAL										INORGANIC LAYERS		
	GYTTJA			laminations			layers				Number	>3 cm	>6 cm
	color	grain size	color	thickness	grain size	color	thickness	color	thickness	grain size			
CORE 2	black	clayey silt	gray	< 5 mm	silt	brown/ gray	2 to 10 cm	silt/fine sand	23	5	3		
CORE 3	brown	fine silt	gray	< 1 cm	coarse silt	brown	2 to 7 cm	silt/sand	45	10	3		
CORE 4	black/ brown	clayey silt	gray	< 1 cm	silt	brown/ gray	2 to 7 cm	silt/fine sand	21	5	3		

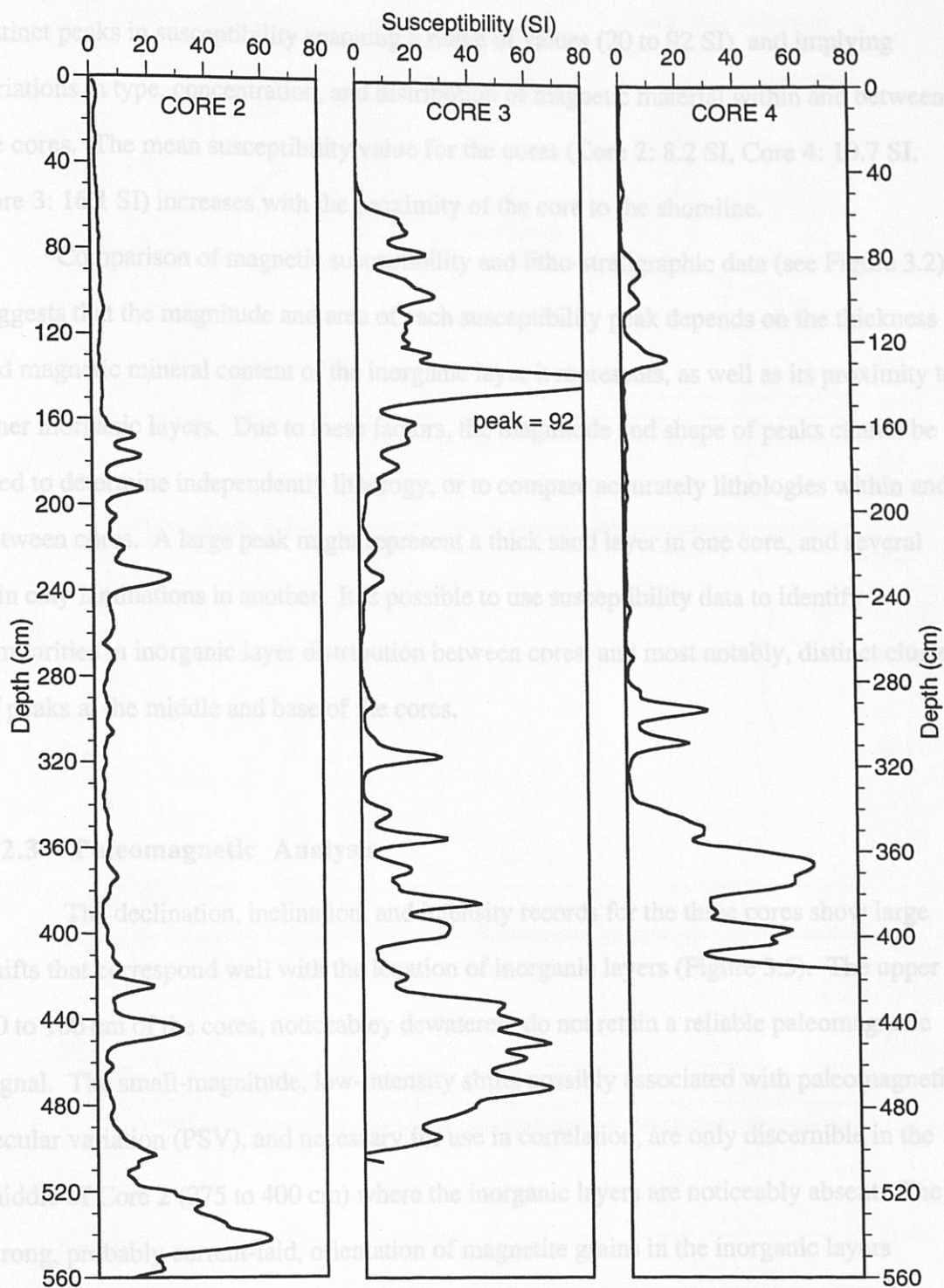


Figure 3.4 Magnetic susceptibility for cores 2, 3, and 4. Gaps in the record indicate section breaks. Peaks of increased susceptibility correspond to inorganic layers. Intervals of low susceptibility are clearly visible in the upper-middle part of each record.

distinct peaks in susceptibility spanning a range of values (20 to 92 SI), and implying variations in type, concentration, and distribution of magnetic material within and between the cores. The mean susceptibility value for the cores (Core 2: 8.2 SI, Core 4: 10.7 SI, Core 3: 16.1 SI) increases with the proximity of the core to the shoreline.

Comparison of magnetic susceptibility and litho-stratigraphic data (see Figure 3.2) suggests that the magnitude and area of each susceptibility peak depends on the thickness and magnetic mineral content of the inorganic layer it represents, as well as its proximity to other inorganic layers. Due to these factors, the magnitude and shape of peaks cannot be used to determine independently lithology, or to compare accurately lithologies within and between cores. A large peak might represent a thick sand layer in one core, and several thin clay laminations in another. It is possible to use susceptibility data to identify similarities in inorganic layer distribution between cores, and most notably, distinct clusters of peaks at the middle and base of the cores.

3.2.3 Paleomagnetic Analysis

The declination, inclination, and intensity records for the three cores show large shifts that correspond well with the location of inorganic layers (Figure 3.5). The upper 90 to 100 cm of the cores, noticeably dewatered, do not retain a reliable paleomagnetic signal. The small-magnitude, low-intensity shifts possibly associated with paleomagnetic secular variation (PSV), and necessary for use in correlation, are only discernible in the middle of Core 2 (275 to 400 cm) where the inorganic layers are noticeably absent. The strong, probably current-laid, orientation of magnetite grains in the inorganic layers decreases the ability of the magnetometer (integrating over 14 cm) to resolve small-scale changes in declination and inclination of the surrounding gyttja. The high number of inorganic layers in Cores 3 and 4 precludes detection of PSV in the records at the

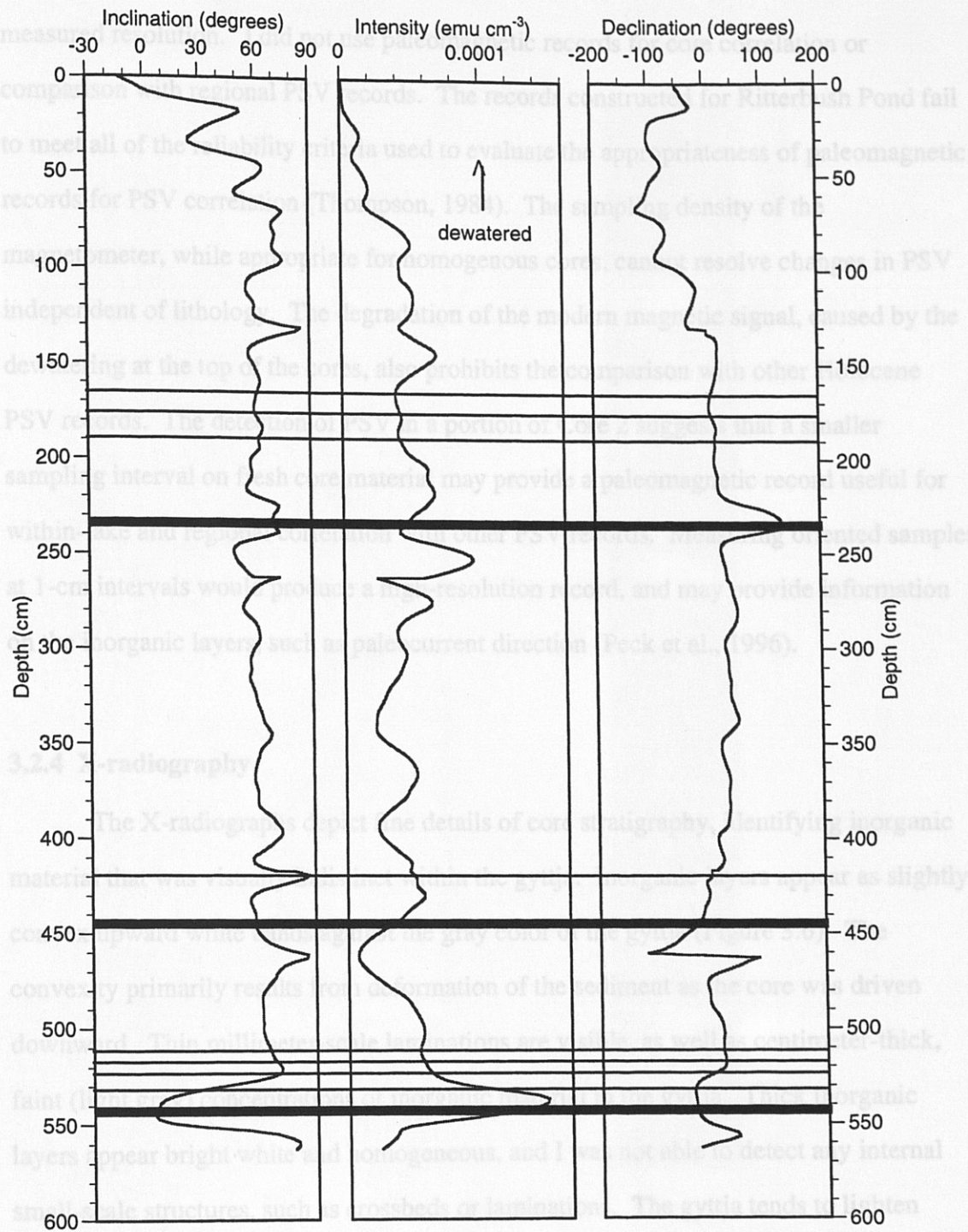


Figure 3.5 Paleomagnetic declination, inclination and intensity for Core 2. Horizontal lines indicate the location of the thickest inorganic layers.

measured resolution. I did not use paleomagnetic records for core correlation or comparison with regional PSV records. The records constructed for Ritterbush Pond fail to meet all of the reliability criteria used to evaluate the appropriateness of paleomagnetic records for PSV correlation (Thompson, 1984). The sampling density of the magnetometer, while appropriate for homogenous cores, cannot resolve changes in PSV independent of lithology. The degradation of the modern magnetic signal, caused by the dewatering at the top of the cores, also prohibits the comparison with other Holocene PSV records. The detection of PSV in a portion of Core 2 suggests that a smaller sampling interval on fresh core material may provide a paleomagnetic record useful for within-lake and regional correlation with other PSV records. Measuring oriented samples at 1-cm intervals would produce a high-resolution record, and may provide information on the inorganic layers, such as paleocurrent direction (Peck et al., 1996).

3.2.4 X-radiography

The X-radiographs depict fine details of core stratigraphy, identifying inorganic material that was visually indistinct within the gyttja. Inorganic layers appear as slightly convex upward white bands against the gray color of the gyttja (Figure 3.6). The convexity primarily results from deformation of the sediment as the core was driven downward. Thin millimeter-scale laminations are visible, as well as centimeter-thick, faint (light gray) concentrations of inorganic material in the gyttja. Thick inorganic layers appear bright white and homogeneous, and I was not able to detect any internal small-scale structures, such as crossbeds or laminations. The gyttja tends to lighten toward the edges of each image, and varies significantly in X-ray density between X-radiographs.

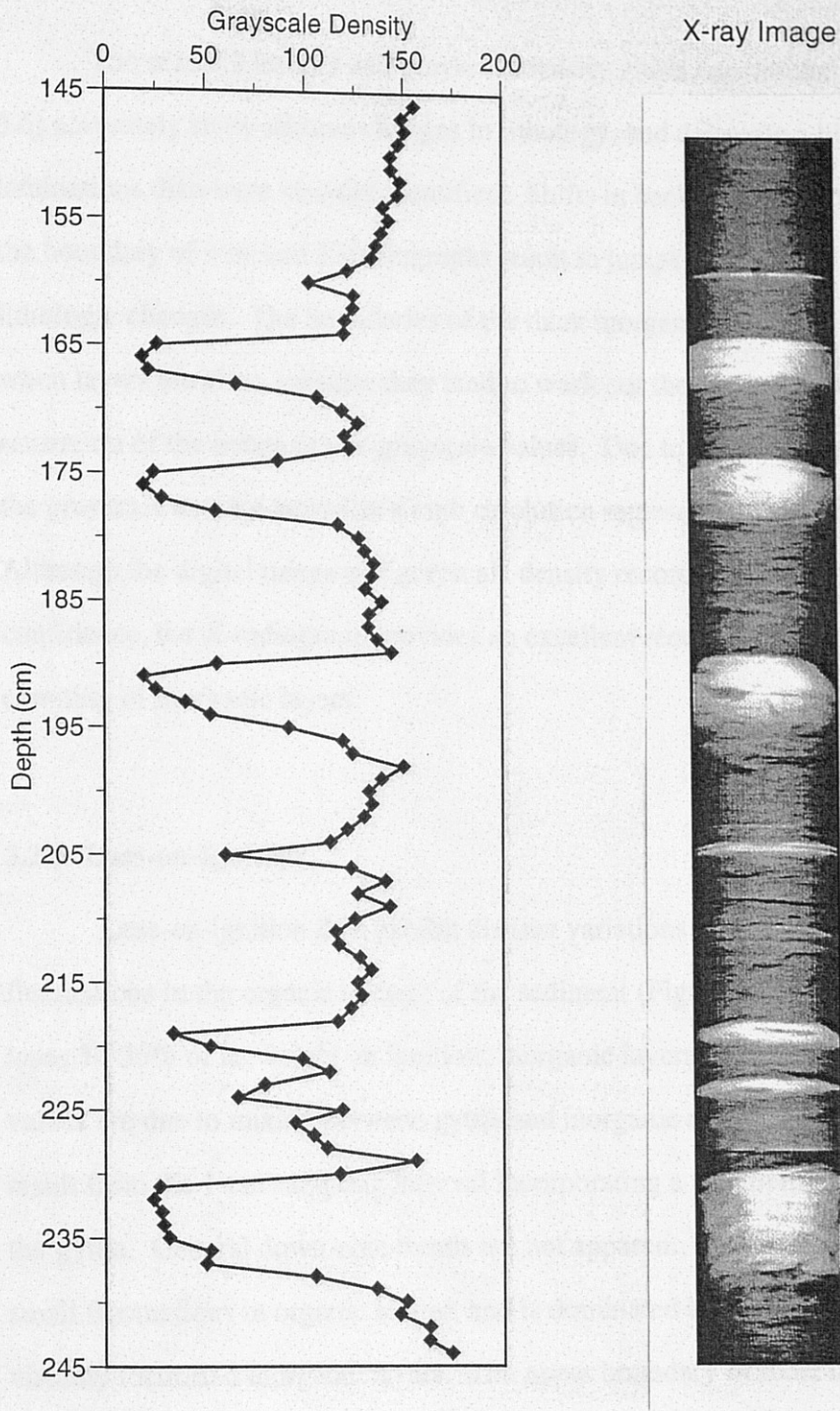


Figure 3.6 X-radiograph and grayscale density for a 1 meter section (145 cm to 245 cm) of Core 2.

The scanned images and grayscale density graph constructed for Core 2 (Figure 3.6) accurately show relative changes in lithology, and delineate a higher number of fine laminations than were visually identified. Shifts in background (gyttja) X-ray density at the boundary of matched X-radiographs result in jumps in grayscale values that mimic lithologic changes. The boundaries of the thick inorganic layers are often indistinct, and when layers are close together they tend to wash out the gyttja separating them, due to the saturation of the image at low grayscale values. Due to these inconsistencies, I do not use the grayscale density record as a high resolution representation of core stratigraphy. Although the digital image and grayscale density record are difficult to manipulate with confidence, the X-radiograph provides an excellent record for visual location and counting of inorganic layers.

3.2.5 Loss-on-Ignition

Loss-on-ignition data exhibit distinct variations with depth, and quantify fluctuations in the organic content of the sediment (Figure 3.7). In all three cores, gyttja loses 30-35% of its weight on ignition; inorganic layers lose only 5-10%. Intermediate values are due to mixing between gyttja and inorganic material during deposition, or result from the 1-cm sampling interval incorporating a <1-cm thick inorganic layer into the gyttja. General down-core trends are not apparent, as the record is sensitive to even small fluctuations in organic matter, and is dominated by peaks that correlate well with visually identified inorganic layers. The upper boundary of most inorganic layers is sharp; the lower boundary of the thickest layers shows a gradual change from gyttja to inorganic values over 1 to 4 cm. The close correlation of peak magnitude and lithology makes LOI records ideal for detecting the location and thickness of inorganic layers.

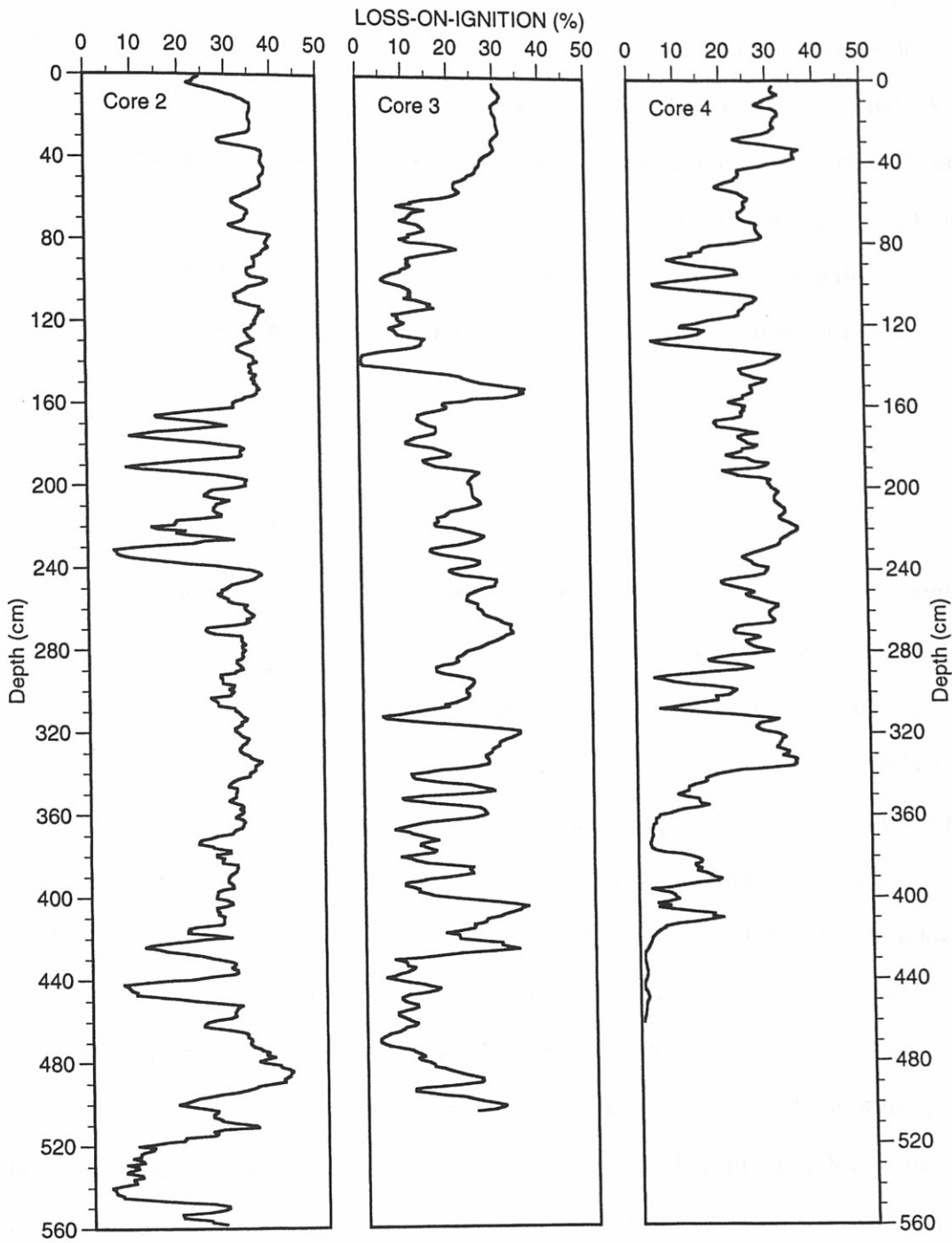


Figure 3.7 Loss-on-ignition for cores 2, 3, and 4. Values <15% indicate significant inorganic layers. Data have been smoothed with a 5-point running average.

Core 2 is characterized by clusters of low LOI values from 160 to 240 cm, 400 to 450 cm, and at the base of the core. Outside of these clusters, LOI values do not drop below 20%, although smaller shifts to low values (25 to 30%) are easily identified. A similar clustering of low values also occurs in Core 4. LOI values of <15% occur from 80 to 140 cm, 280 to 310 cm, and the base of the Core 4. Smaller shifts range in magnitude from 15% to 30%. Core 3 exhibits the most frequent fluctuations in LOI, with values <20% occurring over the entire core length. Shifts of <10% cluster at 60 to 140 cm, and below 320 cm.

3.2.6 Elemental Analysis

Total organic carbon (TOC) values for Core 2 range from 15% to 20% for gyttja and average 5% for inorganic layers (Figure 3.8). The patterns, trends, and relative changes in peak magnitude are nearly identical to LOI records (see above, and section 4.1). To avoid redundancy, I did not measure TOC for Cores 3 and 4, as LOI analysis had already been completed. The LOI values (approximate % organic matter) could be used to estimate percent organic carbon by using a conversion factor obtained from measured values. The conversion calculation for Core 2 ($\% \text{TOC} = 0.53 * \% \text{LOI}$) would provide approximate TOC values, but should be checked with measured values as the carbon content of the organic material will vary slightly between cores.

The highest carbon / nitrogen ratios (16 to 21) generally occur at major inorganic layers in Core 2, while the background ranges widely (9 to 15) (Figure 3.8). If the inorganic layers contained only terrestrial woody plant debris, the C/N values should be >20; if the gyttja was entirely aquatic material, the C/N ratio should be <10 (Meyers and Ishiwatari, 1995). The measured C/N values suggest that mixing between terrestrial and

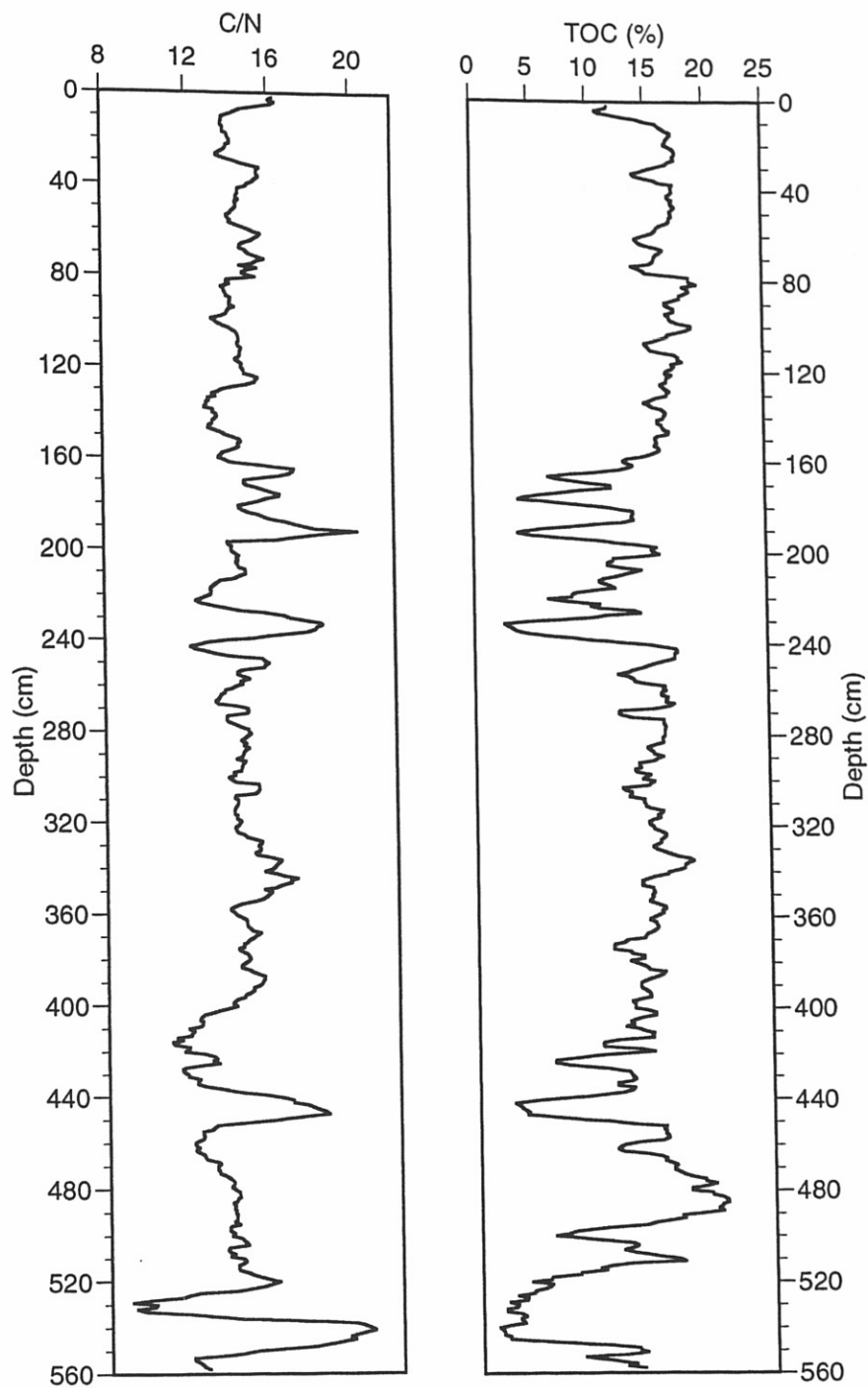


Figure 3.8 Total organic carbon (TOC) and carbon / nitrogen ratio (C/N) for Core 2. Five-point running averages of data show decreases in TOC generally correspond to increases in C/N.

aquatic material occurs in both the inorganic layers and the gyttja. The average C/N ratio of the gyttja still remains lower than the average C/N ratio of the inorganic layers, implying a predominant source for each; the gyttja is dominantly aquatic and the inorganic layers are dominantly terrestrial. One notable exception is at depth 530 cm in Core 2. C/N values drop to 9, the lowest value for the core and typical of nearly pure aquatic material; however, TOC values (5%) suggest an inorganic source. This discrepancy may indicate reworked organic lake sediments within a matrix of terrestrial inorganic material.

3.2.7 Charcoal Analysis (Nitric Acid Digestion)

Charcoal values for samples from the five inorganic layers exhibit little deviation and are lower (<0.5%) than values for the sampled gyttja (Figure 3.9). The three sections of gyttja average $2 \pm 0.8\%$ (1 sigma) charcoal carbon. Values for the samples collected immediately above and below the inorganic layers fall within the range of values observed for the gyttja. Charcoal values appear to depend on the original carbon content of the gyttja. This may be due to incomplete digestion of the organic material by the nitric acid, or to a background abundance of charcoal in the gyttja.

3.2.8 Stable Carbon Isotopes

Two inorganic layers from Core 2, having sharp contacts with gyttja and exhibiting internal grading, show systematic variation in $\delta^{13}\text{C}$ with depth (Figure 3.10). Average gyttja values (-31‰) and inorganic values (-27‰) agree with aquatic and terrestrial values (respectively) previously measured for Ritterbush Pond (Lini et al., 1995). In both layers, down-core changes from gyttja to silt are marked by a jump to less negative (terrestrial) values. The $\delta^{13}\text{C}$ values peak in the upper centimeters of the layers,

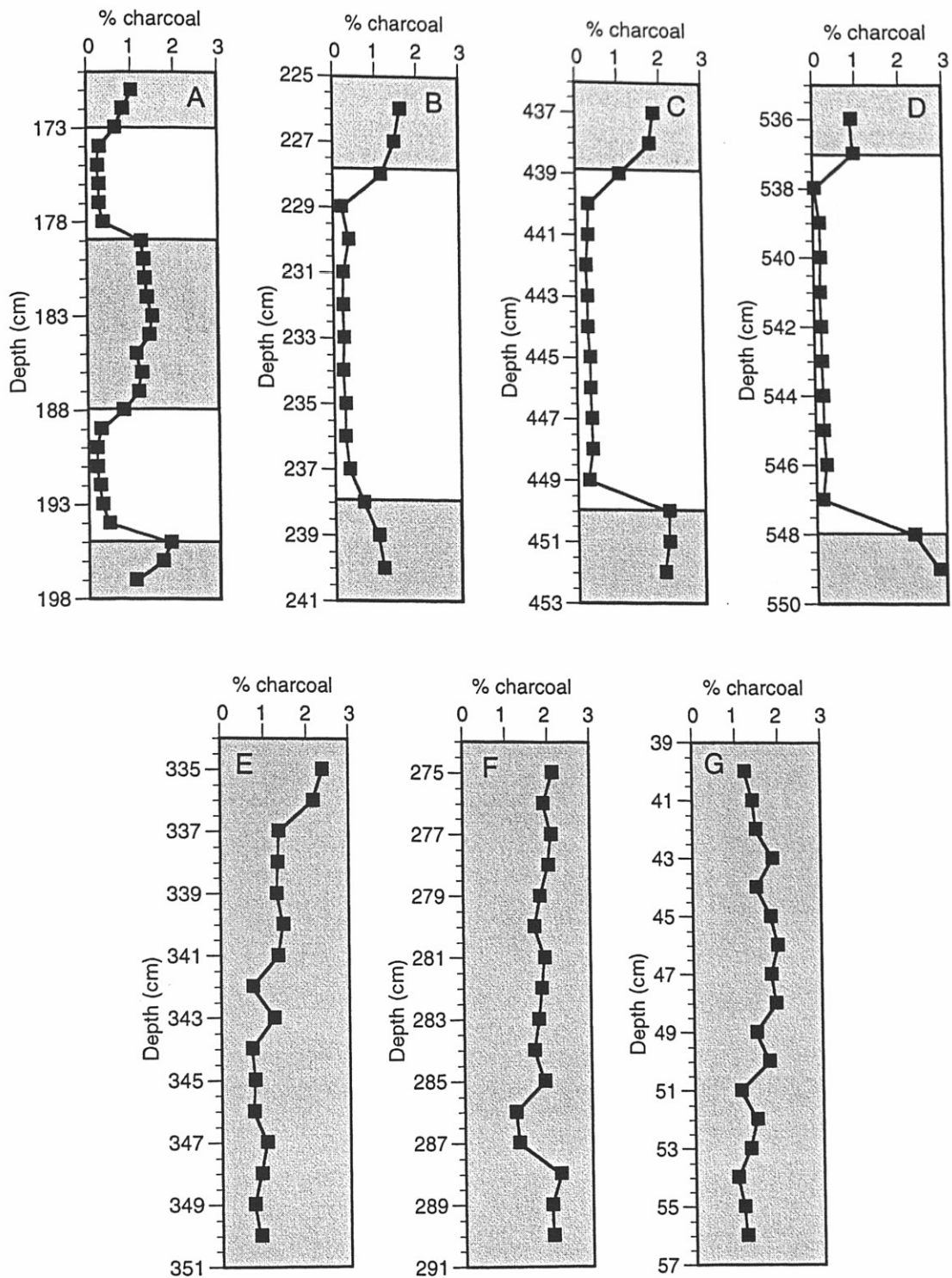


Figure 3.9 Percent charcoal from nitric acid digestion. A-D contain inorganic layers and the surrounding gyttya (shaded). E-G are gyttya only.

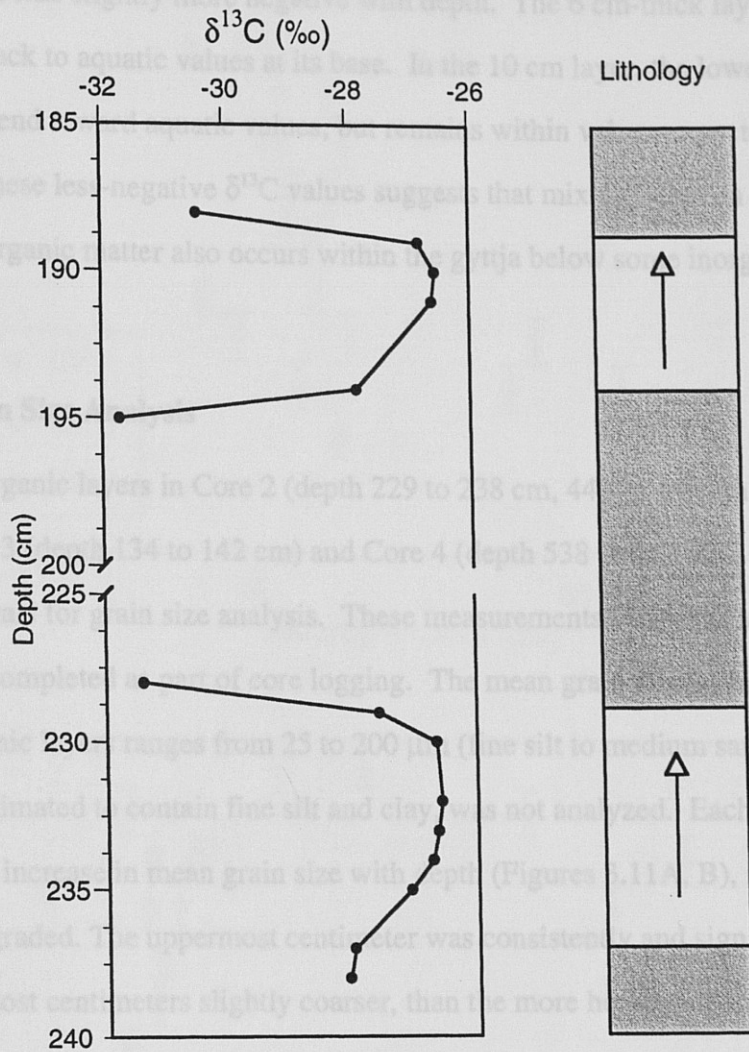


Figure 3.10 Stable carbon isotope data for two inorganic layers in Core 2. Shifts from aquatic ($\delta^{13}\text{C} = -31\text{‰}$) to terrestrial ($\delta^{13}\text{C} = -27\text{‰}$) isotopic values occur at the inorganic layers. Arrows indicate grading of inorganic layers.

and then become slightly more negative with depth. The 6 cm-thick layer shows a sharp transition back to aquatic values at its base. In the 10 cm layer, the lower contact shows a 2 to 3 cm trend toward aquatic values, but remains within values expected for terrestrial material. These less-negative $\delta^{13}\text{C}$ values suggests that mixing between aquatic and terrestrial organic matter also occurs within the gyttja below some inorganic layers.

3.2.9 Grain Size Analysis

Inorganic layers in Core 2 (depth 229 to 238 cm, 440 to 449 cm and 538 to 547 cm), Cores 3 (depth 134 to 142 cm) and Core 4 (depth 538 to 547 cm), were sampled at 1-cm intervals for grain size analysis. These measurements verify the visual estimates of grain size completed as part of core logging. The mean grain size of samples from the five inorganic layers ranges from 25 to 200 μm (fine silt to medium sand). The gyttja, visually estimated to contain fine silt and clay, was not analyzed. Each inorganic layer exhibits an increase in mean grain size with depth (Figures 3.11A, B), indicating that the layers are graded. The uppermost centimeter was consistently and significantly finer, and the lowermost centimeters slightly coarser, than the more homogeneous middle of the layer. The mean grain size of a correlative layer (layer i, see section 4.2) sampled in each of three cores, decreases with distance away from the lake margin (Figure 3.11B). As grain size corresponds to the velocity of transport, this trend suggests deposition by a decelerating current.

3.2.10 Bulk Density

Bulk density of gyttja increases with depth (Figure 3.12). The uppermost sample (depth = 71 cm) had significantly dewatered since the core was logged; there is no evidence for dewatering in other samples. The data generally conform to the expected

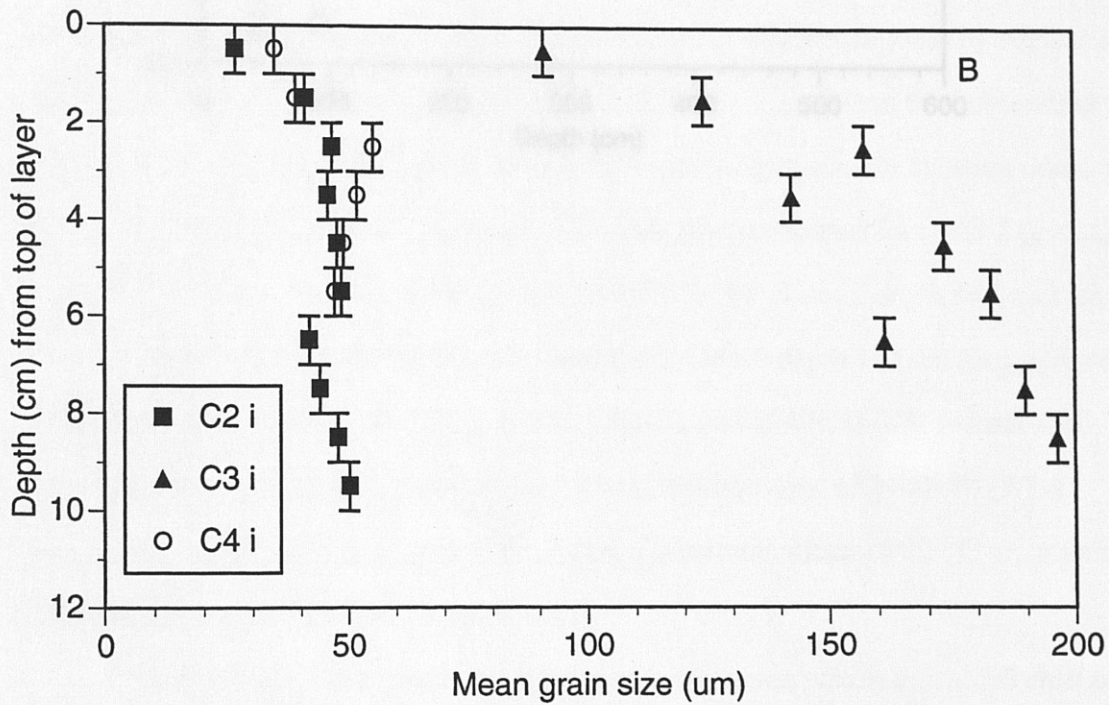
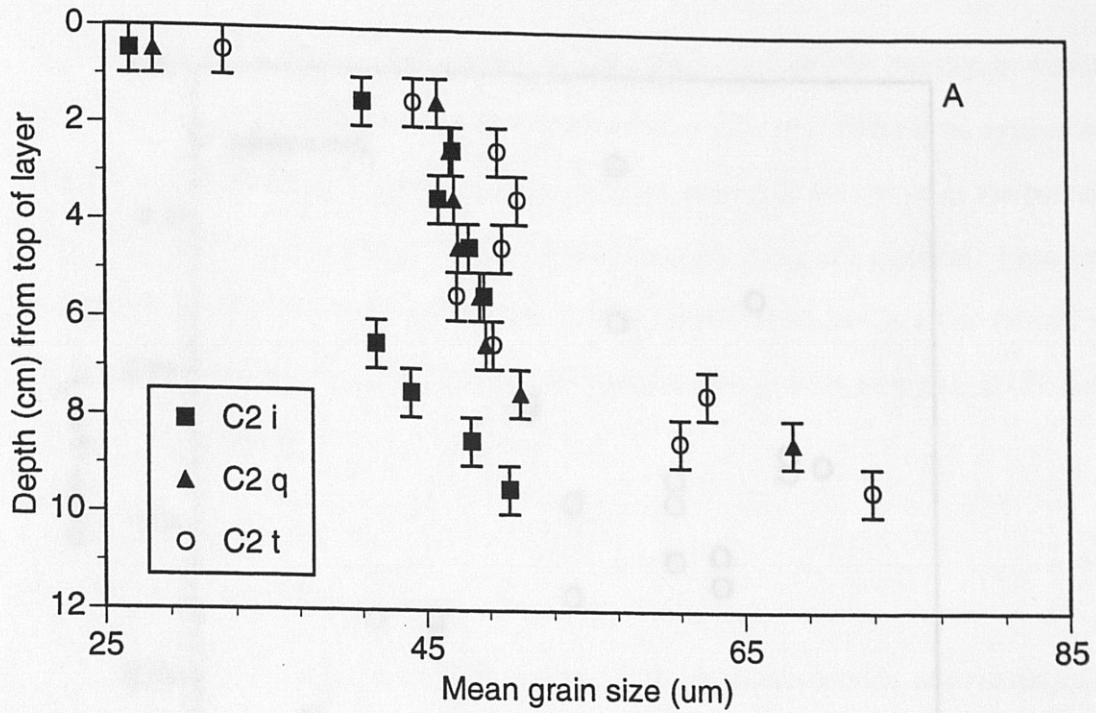


Figure 3.11 Mean grain size data for each cm of the five thickest inorganic layers (6 to 10 cm). A) Three layers (i, q and t) from Core 2 are normally graded, with grain size decreasing toward the top of the layer. B) A single layer (i), correlated between the cores, shows the coarsest grain size in Core 3.

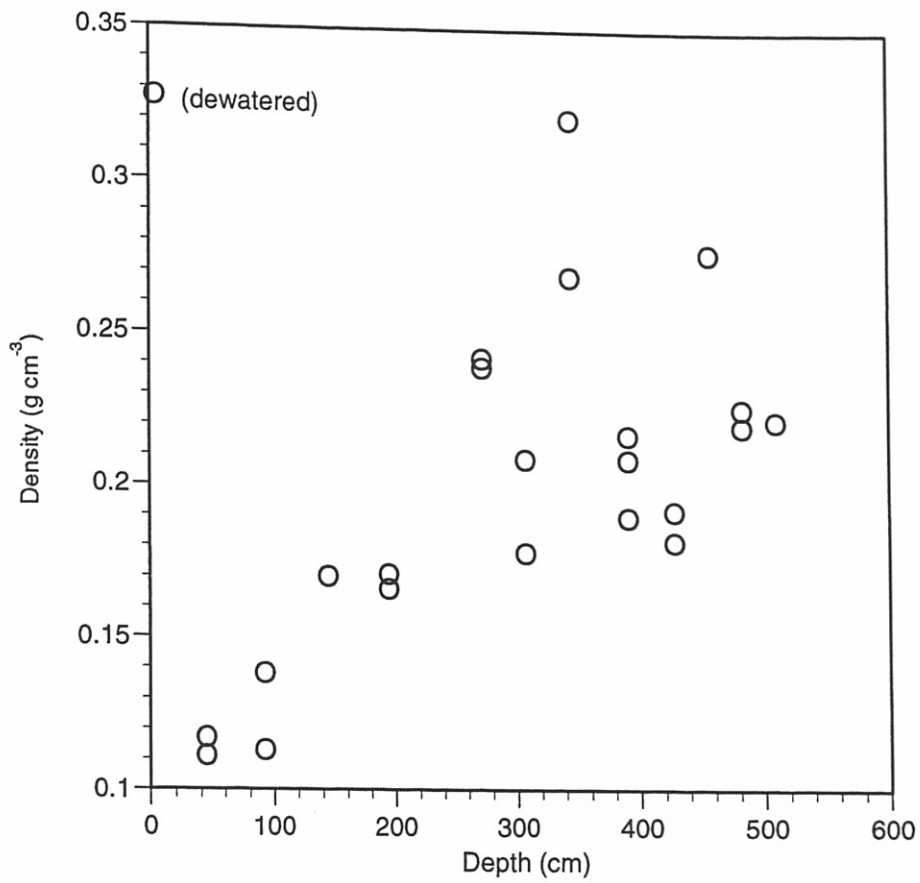


Figure 3.12 Gyttja bulk density for Core 2. Density generally increases with depth.

increase with depth due to autocompaction. The maximum value for density, however, does not occur at the base of the core, but at a depth of 350 cm. There is no evidence to suggest that this high density represents a lithologic change in the gyttja, as the percent organic matter for the measured sample does not suggest inorganic material. I propose that variations in bulk density, in addition to being depth dependent, are also related to the proximity and thickness of inorganic layers that undergo little compaction (Pizzuto and Schwendt, 1997).

3.2.11 Radiocarbon Analysis

Two types of material from the cores, gyttja and macrofossils, were dated using radiocarbon analysis to constrain the timing of deposition of the inorganic layers. I accounted for the gyttja / macrofossil offset measured at Ritterbush Pond by subtracting 450 ^{14}C yr from all gyttja ages (see section 2.2.11, Table 3.3). When this adjustment is applied to other macrofossil / gyttja dates correlated stratigraphically between cores, the offset is systematic within and between cores. Samples correlated from RT-2 (gyttja) and Core 4 (macrofossil) both result in ages of 5980 ^{14}C yr BP (Core 2 depth 448 cm) and 8450 ^{14}C yr BP (Core 2 depth 547 cm). Samples at Core 2 depth 164 cm give ages of 2120 \pm 60 (RT-2, gyttja), 2050 \pm 50 (C3, macrofossil), and 2040 \pm 50 (C4, macrofossil), while samples correlated to Core 2 depth 238 cm result in ages of 2490 \pm 70 (RT-2, gyttja), and 2550 \pm 50 (C3, macrofossil), giving a maximum offset of 80 ^{14}C yr, which is within the analytic uncertainty of the dates.

Calibration of the radiocarbon ages to calendar years results in a small shift of 30 years at the youngest date (Core 2 depth = 164), and a maximum shift of 990 years at the oldest date (Core 2 depth 548) (Figure 3.13). The age-depth model compiled for Core 2, from all samples dated from all four cores, is a decreasing exponential. This exponential

Table 3.3 Radiocarbon Dates for Ritterbush Pond

CAMS#	Core	Depth (cm)	Core 2 depth	material	$\delta^{13}\text{C}$	^{14}C age	^{14}C age	³ adjusted ^{14}C age	⁴ Calibrated Age (calendar yr B.P.)	⁵ best age estimate
33132	RT-2	96	164	gyttja	-31.7	2570 ± 60	2120	2146 (2093)	1993	2090
33135	RT-2	142	228	gyttja	-31.5	3170 ± 60	2720	2855 (2787)	2767	2790
33352	RT-2	154	238	gyttja	-29.5	2940 ± 70	2490	2717 (2707, 2629, 2499)	2475	2610
22993	RT-2	220	300	gyttja	-30.6	3960 ± 60	3510	3843 (3817, 3782, 3732)	3700	3780
33351	RT-2	339	439	gyttja	-32.0	6540 ± 60	6090	7014 (6915)	6871	6920
20195	RT-2	348	448	gyttja	-32.4	6430 ± 70	5980	6884 (6833, 6826, 6799)	6742	6820
32856	RT-2	416	537	gyttja	-32.7	9140 ± 60	8690	9666 (9638)	9533	9640
32854	RT-2	426	547	gyttja	-31.8	8870 ± 60	8420	9469 (9434)	9374	9430
33134	RT-2	426	547	gyttja	-31.8	8950 ± 50	8500	9469 (9467)	9444	9470
33350	RT-2	426	547	gyttja	-31.8	8890 ± 60	8440	9471 (9440)	9385	9440
32855	RT-2	426	547	seed	-28	8450 ± 60	8450	9475 (9442)	9389	9440
46942	C2	77	77	gyttja	-31	1290 ± 40	840	771 (733)	699	730
46943	C2	383	383	gyttja	-31	5240 ± 40	4790	5587 (5578)	5566	5520
46944	C2	424	424	gyttja	-31	6080 ± 40	5630	5540 (5510, 5505)	5473	6410
40775	C2	439.7	439.7	twig	-28	6020 ± 70	6020	6456 (6412)	6394	6870
46945	C2	489	489	gyttja	-31	7720 ± 40	7270	8081 (8060, 8039)	8021	8030
40776	C2	548	548	gyttja	-31	9030 ± 60	8580	8017 (8001)	7981	9510
44693	C3	63.5	164	wood	-26.5	2050 ± 50	2050	9571 (9505)	9459	1990
44695	C3	144	238	wood	-27.6	2550 ± 50	2550	2060 (1990)	1931	2610
44697	C3	375	432	wood	-28	5790 ± 70	5790	2751 (2726)	2709	6630
44699	C3	444	510	bark	-32.0	7880 ± 50	7880	2622 ()	2502	6630
44694	C4	81	164	leaves	-28.0	2040 ± 50	2040	6677 (6626)	6504	8580
44696	C4	132	238	gyttja / leaves	-29.5	2570 ± 60	2570 ⁶	8718 (8582)	8540	1980
44698	C4	311	448	gyttja / leaves	-23.3	6430 ± 40	5980	2042 (1980)	1916	2630
44700	C4	380	547	wood	-30.6	8450 ± 50	8450	2761 (2734)	2709	6820
								2623 ()	2502	9440
								6860 (6833, 6826, 6799)	6774	
								9473 (9442)	9399	

¹ All ages are stratigraphically correlated to depth in Core 2

² measured acid-base-acid washed samples reported to one decimal place. Estimated values are average for all measured samples.

³ ^{14}C ages were adjusted for measured gyttja / macrofossil offset by subtracting 450 ^{14}C years from each gyttja age.

⁴ all adjusted ^{14}C ages calibrated using CALIB rev3.0.3A (Stuiver and Reimer, 1993). A 1 sigma range encloses reported intercepts in ().

⁵ intercept or average of intercepts where 1 range is reported, weighted average of intercepts (or midpoint of range where no intercept is reported) where 2 ranges are reported. Ages rounded to nearest decade

⁶ sample not adjusted for gyttja / macrofossil offset due to ambiguity of material dated and agreement with expected age.

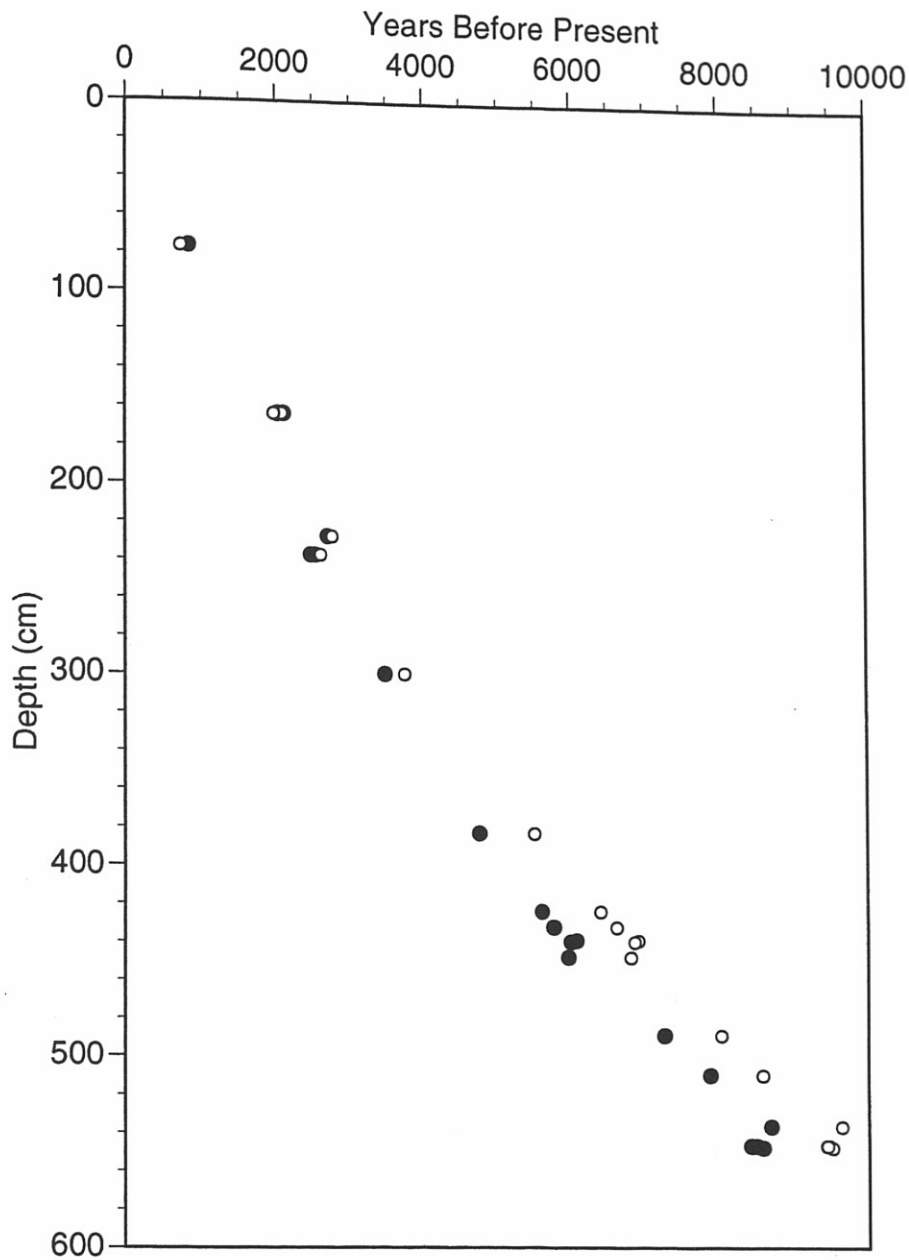


Figure 3.13 Radiocarbon and calibrated ages for Ritterbush Pond cores, correlated to depth in Core 2. Closed circles are uncalibrated radiocarbon ages; open circles are ages converted to calendar years using CALIB rev3.0.3A (Stuiver and Reimer, 1993).

relationship can be used to estimate that the age of sediment at the base of Core 2 (560 cm) is about 10,000 cal yr BP.

I use selected data sets (presented in Chapter 3) to investigate several aspects of inorganic layer deposition in Ritterbush Pond. In the following subsections I: 1) compare the different analytical methods used to determine the best tools for characterization of the inorganic layers, 2) correlate the cores to determine the spatial and temporal variability of the layers, 3) suggest emplacement mechanisms for the inorganic layers, and 4) estimate the age and frequency of inorganic layer deposition.

4.1 Comparison of Data Sets and Methods

Visual stratigraphy, loss-on-ignition, total organic carbon, magnetic susceptibility, x-radiography, and grayscale density were used to identify the location and type of material within the cores. Although the data sets are similar, each method measures a different physical or biochemical property of the sediment at varying resolutions and sensitivities, resulting in slightly different records of inorganic layer location and thickness within the gyttja (Figure 4.1). Visual methods (logs and pictures) rely on distinct color and textural changes for identification of varying lithology. Organic carbon content analysis (LOI and TOC) is a proxy for lithologic variation but detection of small-scale fluctuations is restricted by the sampling interval (1 cm). Magnetic susceptibility analysis is also limited by the resolution of the measurement (4 cm), decreasing the ability of the record to detect small changes in magnetic mineral content. X-radiographs, which depict variations in composition and density, have the highest resolution. The grayscale density data, based on gradation in the X-radiograph density, is also at measured high resolution (72 pixels per inch), and smoothed to 1 value per centimeter for comparison with other data sets.

CHAPTER 4 - Interpretation of Results

I use selected data sets (presented in Chapter 3) to investigate several aspects of inorganic layer deposition in Ritterbush Pond. In the following subsections I: 1) compare the different analytical methods used to determine the best tools for characterization of the inorganic layers, 2) correlate the cores to determine the spatial and temporal variability of the layers, 3) suggest emplacement mechanisms for the inorganic layers, and 4) estimate the age and frequency of inorganic layer deposition.

4.1 Comparison of Data Sets and Methods

Visual stratigraphy, loss-on-ignition, total organic carbon, magnetic susceptibility, x-radiography, and grayscale density were used to identify the location and type of material within the cores. Although the data sets are similar, each method measures a different physical or biochemical property of the sediment at varying resolutions and sensitivities, resulting in slightly different records of inorganic layer location and thickness within the gyttja (Figure 4.1). Visual methods (logs and pictures) rely on distinct color and textural changes for identification of varying lithology. Organic carbon content analysis (LOI and TOC) is a proxy for lithologic variation but detection of small-scale fluctuations is restricted by the sampling interval (1 cm). Magnetic susceptibility analysis is also limited by the resolution of the measurement (4 cm), decreasing the ability of the record to detect small changes in magnetic mineral content. X-radiographs, which depict variations in composition and density, have the highest resolution. The grayscale density data, based on gradation in the X-radiograph density, is also at measured high resolution (72 pixels per inch), and smoothed to 1 value per centimeter for comparison with other data sets.

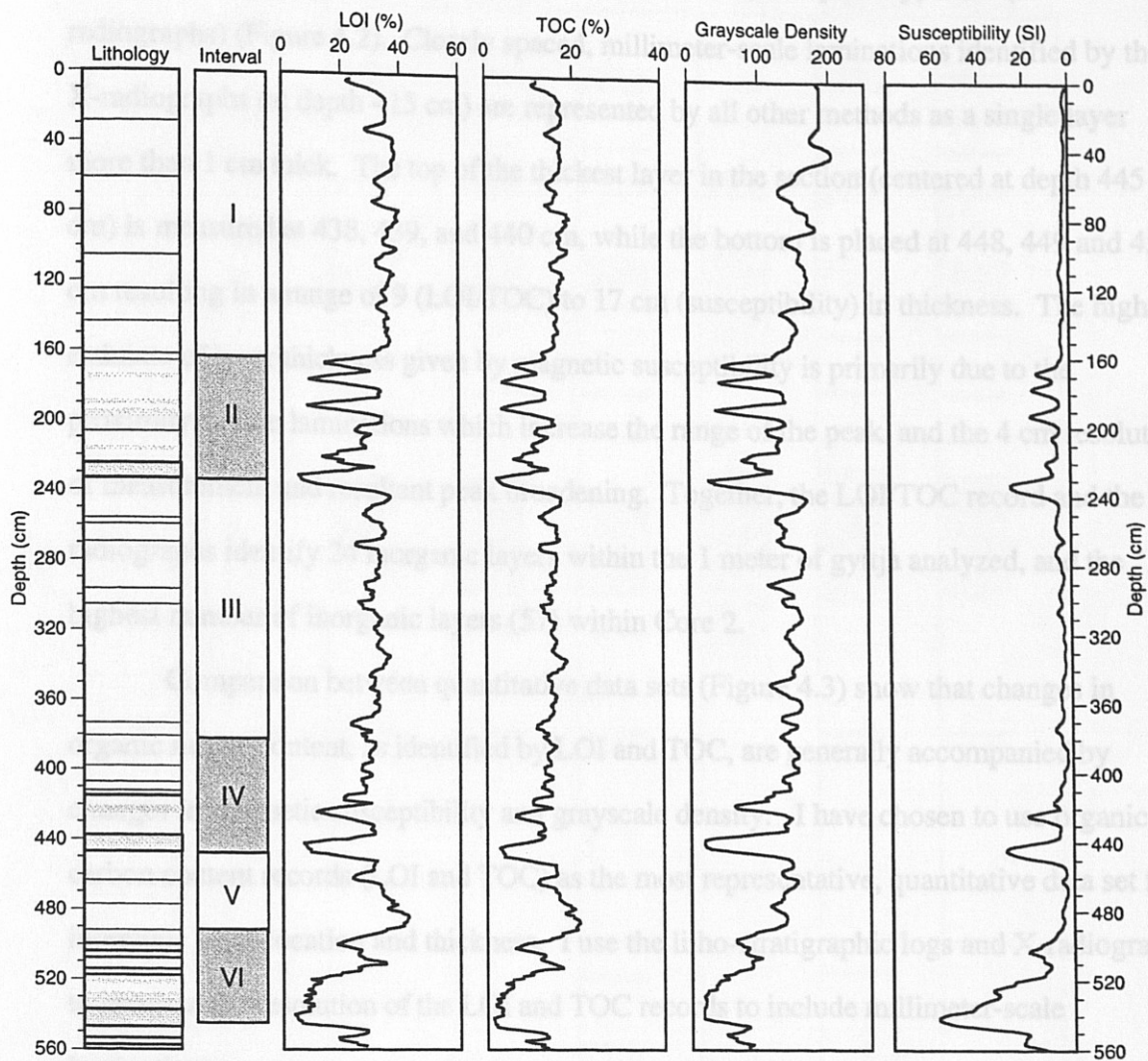


Figure 4.1 Comparison of high-resolution, whole-core data sets for Core 2. Shifts to the left indicate the location of inorganic layers.

Over a representative one meter section of Core 2, the number of layers independently identified by each method varies from 7 (susceptibility) to 24 (X-radiographs) (Figure 4.2). Closely spaced, millimeter-scale laminations identified by the X-radiographs (at depth 415 cm) are represented by all other methods as a single layer more than 1 cm thick. The top of the thickest layer in the section (centered at depth 445 cm) is measured at 438, 439, and 440 cm, while the bottom is placed at 448, 449 and 456 cm resulting in a range of 9 (LOI/TOC) to 17 cm (susceptibility) in thickness. The high estimate of layer thickness given by magnetic susceptibility is primarily due to the proximity of fine laminations which increase the range of the peak, and the 4 cm resolution of measurement and resultant peak broadening. Together, the LOI/TOC record and the X-radiographs identify 24 inorganic layers within the 1 meter of gyttja analyzed, and the highest number of inorganic layers (57) within Core 2.

Comparison between quantitative data sets (Figure 4.3) show that changes in organic matter content, as identified by LOI and TOC, are generally accompanied by changes in magnetic susceptibility and grayscale density. I have chosen to use organic carbon content records (LOI and TOC) as the most representative, quantitative data set for inorganic layer location and thickness. I use the litho-stratigraphic logs and X-radiographs to increase the resolution of the LOI and TOC records to include millimeter-scale laminations.

4.2 Core Correlation

Correlation of the four cores for Ritterbush Pond permits the determination of the lateral extent and lithologic variability of the inorganic deposits. Correlating Cores 2, 3, and 4 with Core RT-2, augments my data set with the existing pollen chronology and 14 radiocarbon dates (Lin, 1996). Together, the core correlation and radiocarbon dates

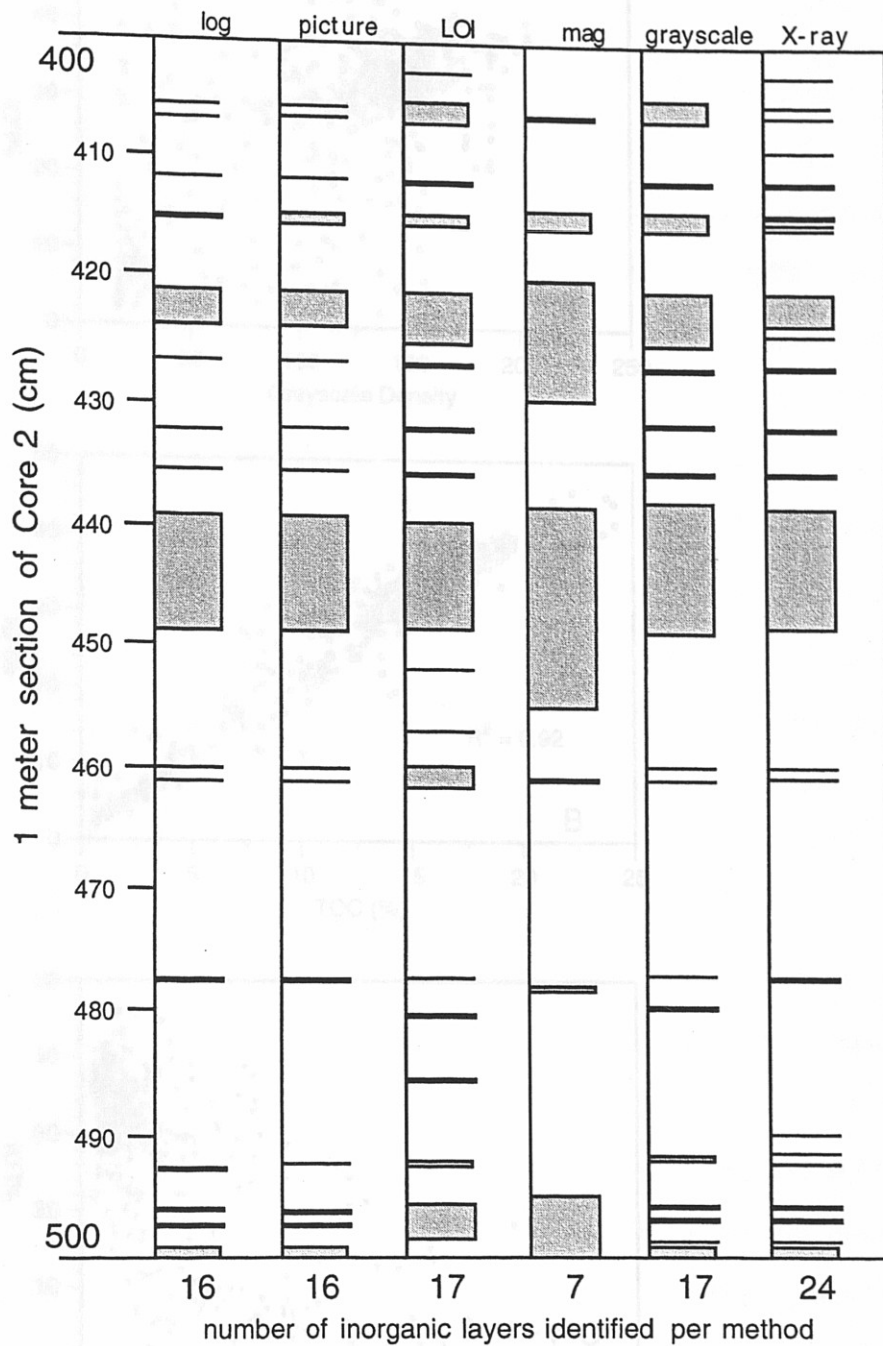


Figure 4.2 Identification of inorganic layer location and thickness by different analytical techniques.

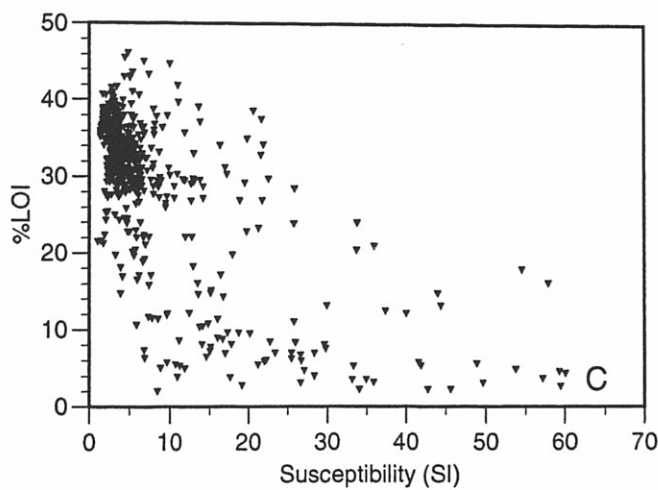
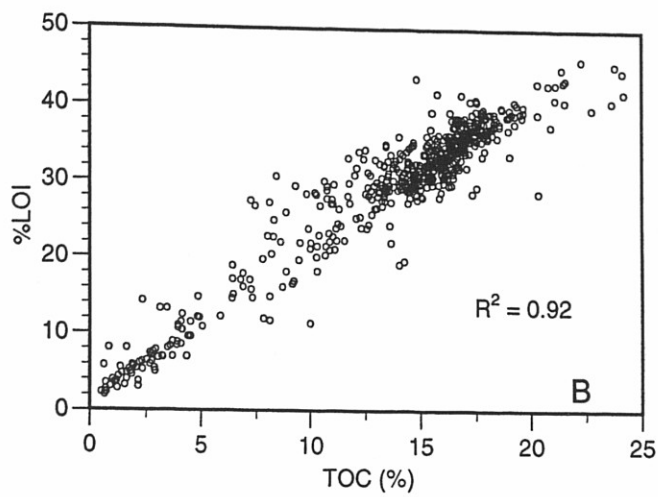
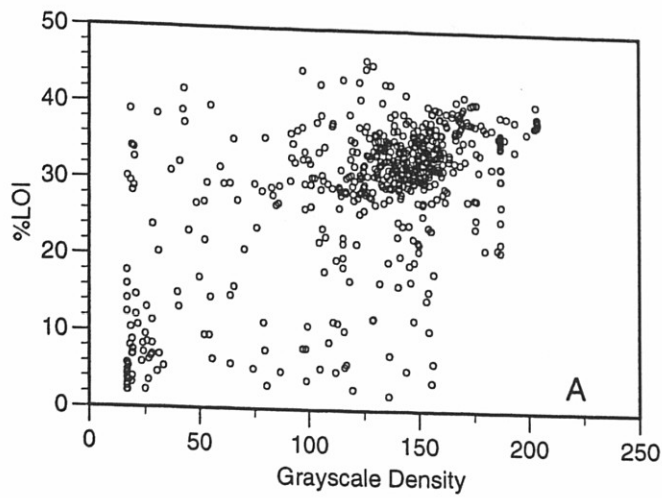


Figure 4.3 Comparison of LOI to A) grayscale density (low and high values appear linear), B) TOC (linear) and C) magnetic susceptibility (exponential).

allow me to investigate the spatial and temporal distribution of the inorganic layers throughout the lake.

4.2.1 Litho-Stratigraphic Correlation

The sensitivity of the LOI data to varying amounts of inorganic material make it an ideal record for correlating inorganic layers between cores. Using the 5-point running average record for Core 2, I assigned a lowercase letter to each significant low LOI value, or negative peak, or in some cases, a single letter to pairs of small peaks (Figure 4.4). The peaks (aa to u) vary in magnitude according to the thickness and number of inorganic layers they represent. I then made a peak-by-peak correlation of Cores 3, 4, and RT-2 using LOI records and litho-stratigraphic logs. The peaks identified in Core 2 account for all significant peaks in the other cores, although one large peak in Core 2, may be represented as two closely spaced, smaller peaks in another core. The best agreement in number, magnitude, and shape of peaks is between Cores 2 and RT-2, due to the proximity of the coring locations in the center of the lake. Cores 4 and RT-2, the only cores to bottom in till, contain an additional peak (v) at their base.

The number, thickness, and grain size of the layers comprising each peak (aa to v) for all four cores were tabulated to assess the lateral variability in layer frequency, size, and lithology (Table 4.1). Peaks l through o in the LOI record for Core RT-2 were not visually represented in the stratigraphic log. In all cores, layers in peaks aa through d were visibly indistinct and contained brown (organic-rich) sand and silt, in contrast to the gray silt and gray/brown sand observed in the rest of the core. Thick graded beds (peaks f, g, i, p, and t) are present in all four cores and show thickness variations of up to 4 cm. The greatest variation of numbers of layers occurs in peak q, where four 1-cm sand layers are identified in Core 3. In Cores 2 and 4 and RT-2, all collected in deeper water, layer q is a single 8 to 9 cm layer.

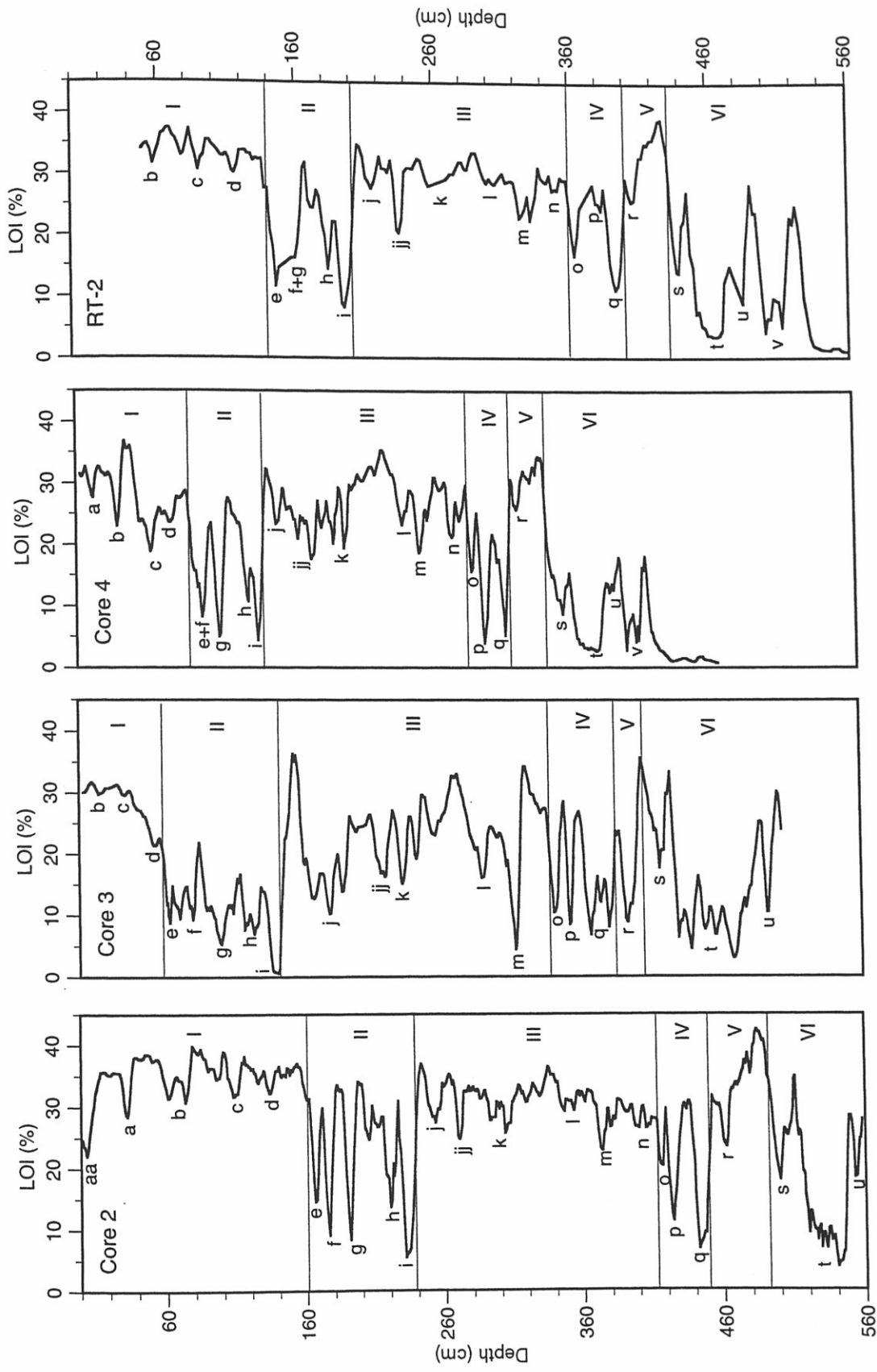


Figure 4.4 Correlation of Ritterbush Pond cores using smoothed (5 pt) LOI data. Lettered peaks indicate stratigraphic correlation between cores. Roman numerals indicate the division of each core into six intervals. RT-2 LOI data from Lin (1996).

Table 4.1 Lateral Variation in Correlated Inorganic Layers

Peak (layer)	RT-2	C2	C3	C4
aa	4 cm br silt	2 cm br sand		
a	2 mm br silt	2 mm br silt		
b	2 mm br silt	2 mm br silt		1 cm br sand
c	2 mm br silt	2 mm br silt		1 cm silt^
d	2 mm br silt	1 cm br silt		
e	5 mm silt 3 cm sand *	2mm silt 2 cm sand *	2 cm br sand 1 cm sand 2 cm sand *	1 cm sand ^
f	5 cm sand *	3.5 cm sand*	7 cm sand * 2, 1 cm sand	4 cm sand *
g	4.5 cm sand	5 cm sand *	6 cm sand * 1 cm sand	6 cm sand *
h	couplet 4, <1cm silt 2, 1 cm sand *	couplet 4, <1cm silt	3, 1cm sand	8 mm silt 2 cm silt
i	10 cm sand *	10 cm sand *	5 mm silt 9 cm sand *	6 cm sand *
j	5, <1 cm silt	2, 2mm silt	8, 1-2 cm sand^	4 mm silt 3 mm silt^
**	1 cm sand	5 mm silt	2, 1 cm sand	2, 1 cm sand^ 4 mm silt
k	5, <1 cm silt	3 mm silt 5 mm silt	1 cm sand^ 5 mm silt	2,1 cm sand ^ 5 mm silt
l		2, <1mm silt	1 cm sand^	8 mm lam
m		2, 2 mm silt 2.5 mm silt	5 cm sand^*	3 cm sand lam 5 mm silt
n		<1mm silt couplet		8 mm silt 1 mm silt
o		8 mm silt		1.5 cm silt^
p	2.5 cm sand *	2 cm sand *	2, 3 cm sand	5 cm sand * 2, 5 mm silt
q	8 cm sand *	9 cm sand *	4, 1 cm sand	3 cm sand *
r	2 mm couplet	2mm couplet	<1 cm sand 5 cm sand^	1 mm couplet
s	1 cm sand	2, 3mm silt 6 cm mix 2, 2mm silt 1 cm sand *	1 cm sand^ 2 cm sand^	3, 4mm silt
t	6, <1 cm silt 9 cm sand *	7, 1-3 cm sand* 9 cm sand *	7,1-4 cm sand* 8 cm sand^	faint lam 8 cm sand *
u		1 cm sand 2 cm sand *	2, 1 cm sand 1 cm sand	1.5 cm sand
v				1 cm silt 3 cm sand *

* graded bed

^ abundant macrofossils

4, 1 cm silt = 4 layers of silt, each 1 cm thick

lam = lamination

mix = inorganic and organic material

br = brown

4.2.2 Time-Stratigraphic Correlation

Fourteen radiocarbon dates from four stratigraphic horizons (peaks e, i, q and t) confirm that the litho-stratigraphic correlation proposed above is a time-stratigraphic correlation (Table 4.2). These four horizons were chosen for dating because of the presence of a thick, graded bed at the base of each peak (i, q, t), and the coincidence of the peak with an interval boundary (e, i, q, t) (Figure 4.4). Two samples from Core 3 (layers q and t) were located significantly above the base of the peak and therefore provide minimum ages for event initiation. Core 2 was sampled 1 cm below the base of the peak t, and gives a maximum age for the event. All the samples for layer e are located above the lowest layer in the peak, and give a minimum estimate of peak initiation age. The best estimates of the peak ages are averages of values from the base or within the lowest layer contained in the peak. The standard deviation of the average values does not exceed the statistical variability associated with the dates.

4.2.3 Summary of Spatial and Temporal Distribution

The variation in thickness and grain size of the inorganic layers within a single core is probably due to changes in sediment source location and availability, and velocity of subaqueous transport. Laminations (<5 mm thick) tend to be finer grained than thicker layers, suggesting lower transport velocity and a smaller magnitude transport event. In Core 2, layers composed of similar grain sizes range from 1 to 10 cm thick. The thicker layers may be due to a larger amount of sediment available for transport or a greater magnitude (duration and intensity) hydrologic event. The variation in layer grain size and thickness between cores, in addition to transport velocity and sediment availability, are also due to distance from sediment source and bathymetry. The deposition of layers in lake-marginal cores but not in the center cores may represent an event that did not

Table 4.2 Calibrated Radiocarbon Dates for Ritterbush Core Correlation

peak	CAMS #	Core	Depth	sample	position in peak	calendar age (yr BP)	age in relation to base of peak	best estimate of peak age ($\pm 1\sigma$)
e	33132	RT-2	96	gyttja	above first of 2 layers	2090	younger	2020 \pm 60
	44693	C3	63.5	wood	above second of 3 layers	1990	younger	
	44694	C4	81	leaves	above the only layer	1980	younger	
i	33352	RT-2	154	gyttja	base	2610	same	2620 \pm 10
	44695	C3	144	wood	base (in layer)	2610	same	
	44696	C4	132	leaves	base (in layer)	2630	same	
q	20194	RT-2	348	gyttja	base	6820	same	6840 \pm 30
	40775	C2	439.7	twig	in the only layer	6870	same	
	44697	C3	375	wood	base of second of 4 layers	6630	younger (minimum)	
	44698	C4	311	gyttja	base	6820	same	
t	32854	RT-2	426	gyttja	base	9440	same	9440*
	40776	C2	548	gyttja	1 cm below base	9510	older (maximum)	
	44699	C3	444	bark	top of the third of 8 layers	8580	younger (minimum)	
	44700	C4	380	wood	base	9440	same	

* no variance

reach the center of the lake. The sediment in layers not identified in a lake-marginal core, but present in the other cores, may have originated on the opposite lake shore. The flat bottom of the lake, where Cores 2 and 4 were collected, is likely to receive more sediment and experience less net erosion than the site of Core 3, located on a steeper slope.

I subdivide Core 2 into six intervals, each noted by a Roman numeral (Figure 4.1), based on the location and clustering of the inorganic layers. These intervals are common to all cores and the depth of the intervals is determined for Cores 3, 4 and RT-2 by the stratigraphic correlation (see Figure 4.4). Even-numbered intervals (II, IV, VI) contain the lowest LOI values, and the thickest inorganic layers, while odd intervals (I, III, V) have higher average LOI values and fewer and thinner inorganic layers. The clustering of the inorganic layers into three, easily-identifiable intervals in each of the cores suggests that frequency of layer deposition is not constant throughout the core (Figure 4.5). The time between events in the even intervals is highly variable, whereas the time between events is shorter in odd intervals.

4.3 Inorganic Layer Emplacement

Layer i, in Core 2, is the interval of the core for which the most (nine) lab analyses have been performed (Figure 4.6). This layer was chosen as representative of the thickest graded beds in the core, and these data are used to constrain the interpretation of possible emplacement mechanisms for this and other inorganic layers.

Figure 4.5 Layer frequency as a function of time since the last event. Even and odd intervals exhibit different trends.

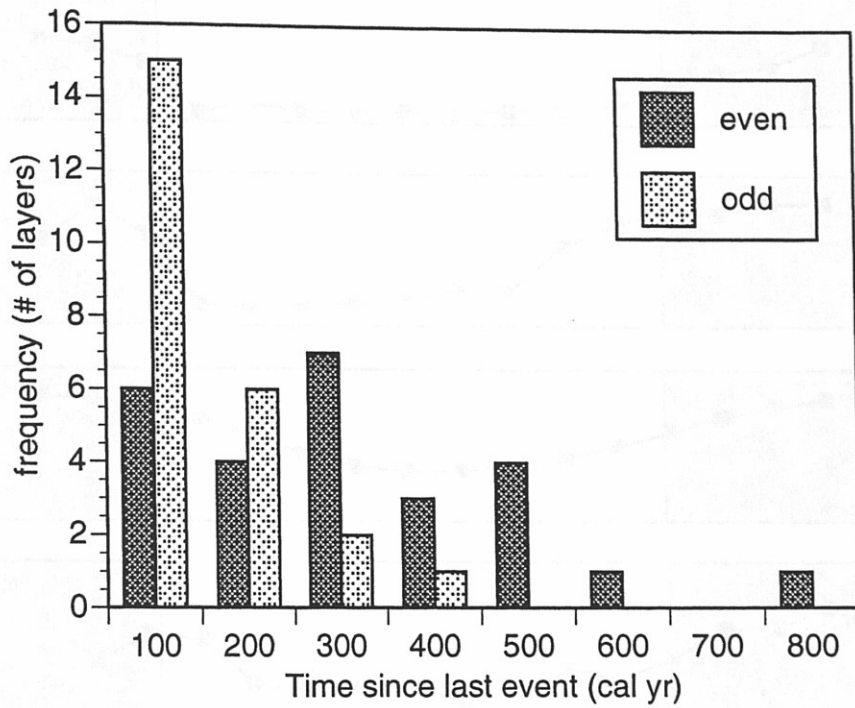


Figure 4.5 Layer frequency as a function of time since the last event. Even and odd intervals exhibit different trends.

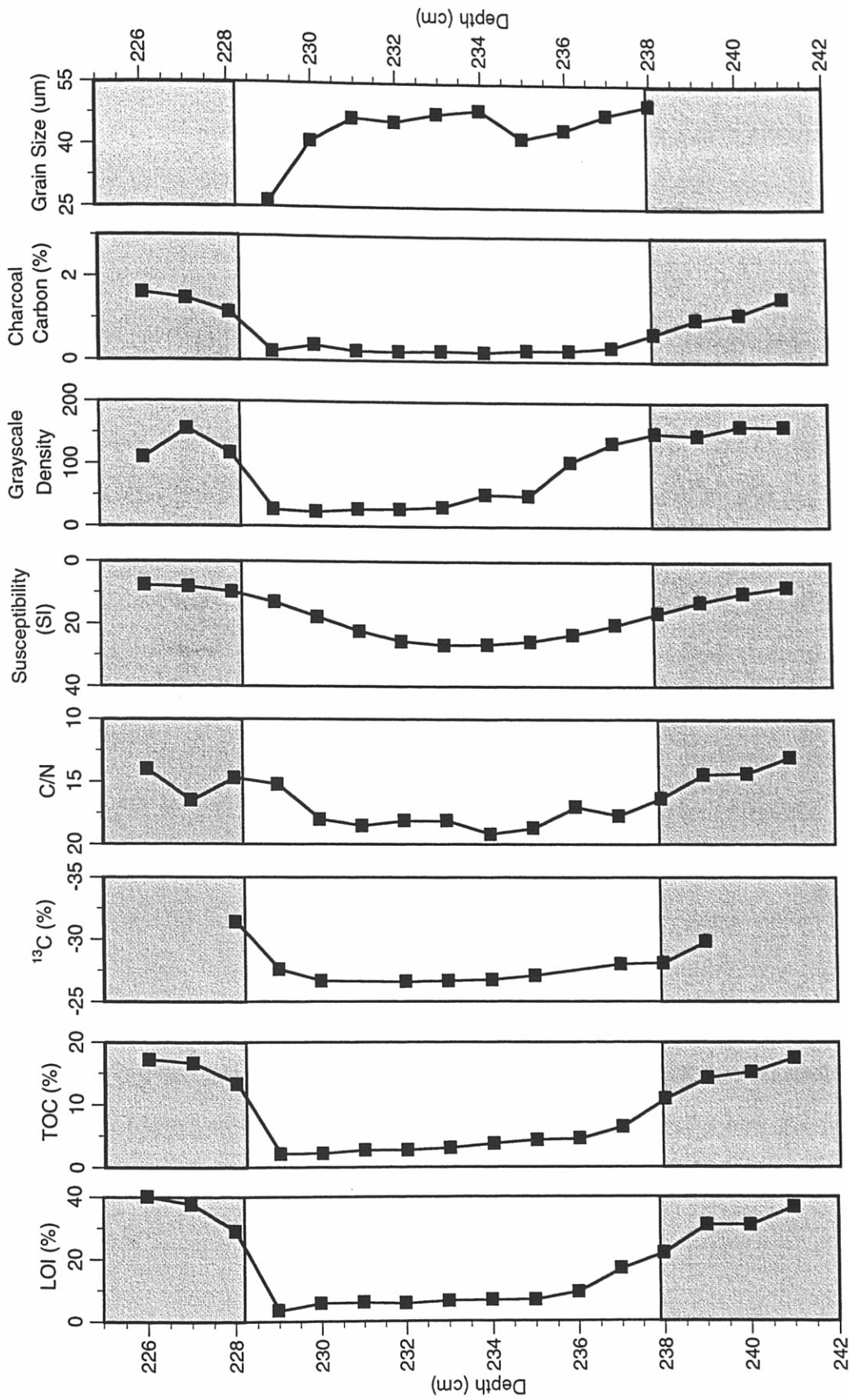


Figure 4.6 Summary data for layer emplacement using Core 2, layer i. Shifts to terrestrial material are to the left; shifts to the right indicate aquatic material (with the exception of the grain size data). Radiocarbon dated gyttja above (2720 ^{14}C ybp) and below (2490 ^{14}C ybp) the inorganic layer exhibit an age inversion (Bierman et al., 1997).

4.3.1 Physical Characteristics

Layer i was visually estimated to extend from depth 228 to 238 cm, with sharp upper and lower boundaries and internal grading. LOI and TOC data show a 2-cm transition from silt to gyttja at the base beginning at depth 238 cm, a well-mixed center 8 cm thick, and an abrupt change back to gyttja at depth 228 cm. This trend is also present in the grayscale density data, although the lower transition from gyttja to silt appears to begin 1 cm higher, and the well-mixed center spans only 7 cm. The magnetic susceptibility data, due to the lower resolution of this record, show a gradual transition at both the top and the bottom, and have a maximum value at depth 233 cm, the center of the layer identified by LOI and TOC. These data suggest that the deposition of inorganic layers involves initial mixing of gyttja and silt followed by deposition of relatively organic-free, homogenous sand and silt, and then a return to gyttja deposition with little to no mixing at the layer top.

Grain size in layer i generally increases with depth, confirming the visual identification of the layer as a graded bed ranging from coarse to fine silt. The upward decrease in grain size is interrupted at depth 234 cm by 3 cm of coarser sediment. The grading continues at depth 231 cm with significantly finer material in the top 1 centimeter. Graded beds are deposited by the suspension settling of particles, the grain size of which is determined by the available sediment and the energy of the water. Grain size in Core 3, taken close to the lake margin, is significantly coarser than in Cores 2 and 4, located closer to the lake center. This decrease in grain size with distance from shore suggests deposition by a decelerating current carrying sediment toward the center of the lake.

4.3.2 Organic Matter Source

Stable carbon isotope values ($\delta^{13}\text{C}$) shift to less negative values with the transition from gyttja to silt, indicating a change from aquatic organic material to terrestrial organic material. This observation is supported by the visual identification of leaves, wood, and other macrofossils within the inorganic layers. The upper transition from silt back to gyttja is sharper than the lower transition, supporting the hypothesis that the deposition of the inorganic layers involves mixing with gyttja at the base, and not at the top. The intermediate values between the average gyttja ($\delta^{13}\text{C} = -31\text{‰}$) values and the average terrestrial ($\delta^{13}\text{C} = -27\text{‰}$) values for Ritterbush Pond could also be due to a third source of organic material such as macrophytes, or previously mixed terrestrial and aquatic material that is incorporated into the base of the layer.

C/N ratios support a terrestrial origin of the organic material in the inorganic layers, with values increasing from 15 to 20 toward depth 234, 1 cm below the center of the layer. The C/N values show a 2 cm transition to higher values at the base, and a jump to lower values 1 cm below the visually-identified top of the layer. The change in source of organic material from aquatic to terrestrial in this layer suggests the delivery of material to the lake from the surrounding hillslopes or lake margins. The data available do not allow me to distinguish between terrestrial and lake marginal (emergent macrophytes) sources for organic material.

4.3.3 Timing of Layer Deposition

Samples previously analyzed (Bierman et al, 1997) in Core RT-2 for radiocarbon include gyttja samples above and below three inorganic layers (i, q and t) that have been correlated to Core 2. Each of the 3 pairs exhibits an inversion in age; the date above the layer is consistently older than the date below the layer. For layer i the offset is 180 cal yr, for layer q it is 100 cal yr, and for layer t the offset is 200 cal yr. As the offset is not

within the analytic uncertainty of the ages (1σ), and is systematic for each of the thickest, graded inorganic layers in the core, it is probably a function of the depositional mechanism for the inorganic layers.

The inversion of ages suggests that there is both erosion and deposition associated with the mechanism emplacing the inorganic layer. Bierman et al. (1997) propose initial scouring of sediments by turbidity currents at the lake margins, followed by deposition of the graded bed and then redeposition of the disturbed sediments on top of the turbidite. At the lake center, where the inversion is observed, the scouring would erode less sediment than at the lake margins; the net movement of the disturbed sediments toward the center of the lake creates the measured offset in age. A similar inversion was observed by Bondevik et al. (1997) in the gyttja above tsunami deposits that was 300-500 ^{14}C yr older than the material below and within the tsunami deposit. The offset was interpreted to be the post-tsunami reworking of older material exposed by tsunami scouring at the edges of the coastal lake basin. Both interpretations of the age offset invoke relatively rapid transport and deposition of allochthonous material by a sedimentation event, which disrupts the slow accumulation of lake-produced gyttja.

4.3.4 Emplacement Mechanisms

Together, the lithologic, organic matter characterization, radiocarbon, and grain size data suggest sedimentation mechanisms for the inorganic layers in Ritterbush Pond. The following criteria must be met by the emplacement mechanism(s): 1) rapid deposition of terrestrial material from suspension, 2) possible gyttja scouring and mixing with inorganic material at the base of the deposit, 3) fining of the deposit toward the center of the lake, and 4) deposition of both fine laminations and thick (>1 cm) layers. Mechanisms associated with event sedimentation in lakes include, but are not limited to: turbidity currents (density currents with a high concentration of dispersed sediment), plumes of

sediment that undergo suspension settling or evolve into density-driven bottom currents, reworking of lake marginal sediment by storm (wind and wave) generated bottom currents, and slumping of lake marginal or hillslope sediments (Gorsline, 1984).

Of these mechanisms, suspension settling would fail to produce significant scouring or mixing at the base of the deposit and sediment slumping not accompanied by suspension sedimentation would be unlikely to produce grading. Density-driven bottom currents and high-concentration turbidity currents are most likely to result in the set of characteristics observed in the thickest inorganic layers. Inorganic, graded beds described in lake sediment studies are often simply called turbidites (Ludlam, 1974). Controversy exists over the common characterization of graded beds and associated sedimentary structures, such as planar laminations, as turbidites (Bouma, 1962), due to abundant evidence that turbidites may exhibit a wide variety of features or none at all (Kuenen and Migliorini, 1950; Kuenen and Menard, 1952; Piper, 1972; Walker, 1967). Deposits conforming to the sequence typical of turbidite deposits may be produced by a variety of mechanisms (Shanmugam, 1997; Nelson, 1982).

One test of turbidity current emplacement employs the linear relationship between coarsest 1% grain size in the layer to layer thickness (Mehrtens, 1988). Turbidite thickness is positively correlated to slope, flow depth, and the grain size distribution of the sediment, which determine the velocity of a turbidite (Sadler, 1982). The velocity of the turbidite at the moment of layer emplacement controls the coarsest grain size that can be deposited; the size of the turbidite at the moment of emplacement controls the thickness of the deposit. The five representative layers analyzed for grain size, however, do not exhibit a clear relationship between the coarsest 1% grain size and the thickness of the layer (Figure 4.7). Combined with the absence of sedimentary structures associated with turbidity current deposition (Bouma, 1962), this lack of a grain size to thickness correlation does not provide sufficient evidence to determine if the inorganic layers

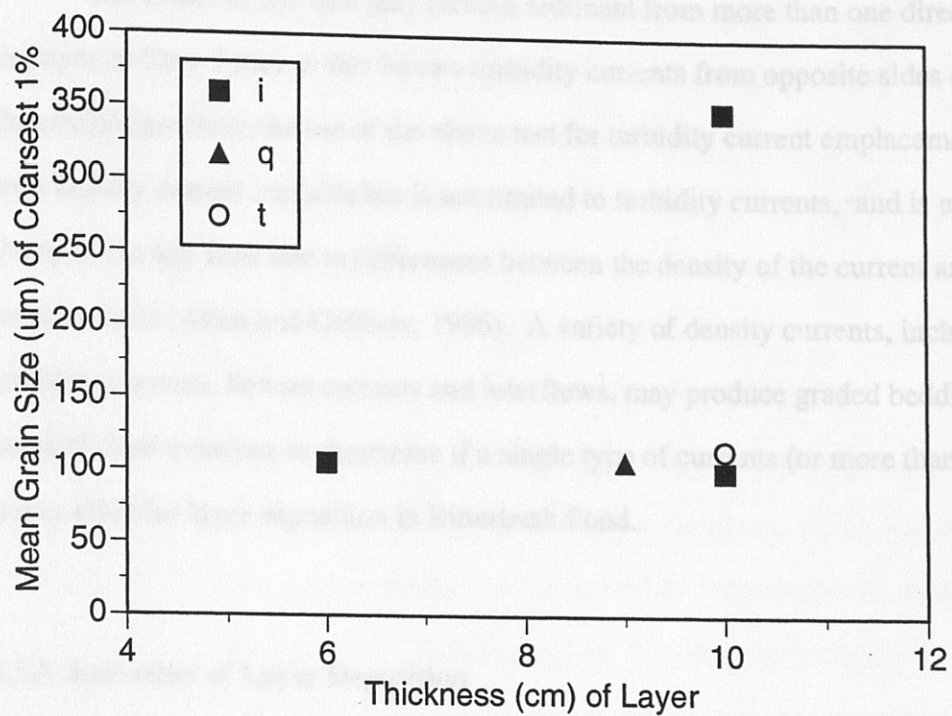


Figure 4.7 Test of emplacement mechanism for inorganic layers. The five thickest inorganic layers do not show a clear relationship between coarsest 1% of grains and layer thickness.

identified in Ritterbush Pond cores were emplaced by turbidity currents (Mehrtens, 1988; Sadler, 1982).

The center of the lake may receive sediment from more than one direction; the 10-cm layer in Core 2 may in fact be two turbidity currents from opposite sides of the lake. This would preclude the use of the above test for turbidity current emplacement. The term density current includes but is not limited to turbidity currents, and is used to characterize any flow due to differences between the density of the current and the ambient fluid (Allen and Collison, 1986). A variety of density currents, including turbidity currents, bottom currents and interflows, may produce graded bedding. There is not sufficient evidence to determine if a single type of currents (or more than one) is responsible for layer deposition in Ritterbush Pond.

4.3.5 Initiation of Layer Deposition

Numerous studies link increased lacustrine sediment deposition with fluctuations in the amount and intensity of rainfall. Recently, lake sediment research linked increased average grain size to storm occurrence (Campbell, 1998) and identified silt and clay layers within gyttja as products of individual storm events (Eden and Page, 1998). The sparse deposition of discontinuous sand layers (not-dated) in Mirror Lake has been attributed to storm-generated waves and currents at the lake margins redistributing sediment (Davis and Ford, 1984). Marshes and lakes in close proximity to the coast record hurricane generated sand layers (Liu and Fearn, 1993, Winkler, written comm., 1998). Nelson (1982) documented turbidite-mimicking sedimentary structures produced by post-storm-surge bottom currents on a marine shelf. Inorganic layer deposition in Ritterbush Pond is most likely initiated by hydrologic events, such as rainstorms and

spring snowmelt, which cause increased hillslope erosion and sediment transport to the lake.

The susceptibility of the hillslopes to erosion may also be increased by forest fires that strip the hillslopes of protective vegetation (Clark, 1988; Meyers et al., 1995). Representative charcoal data for Core 2, layer i and the surrounding gyttja (Figure 4.6) show a decrease in charcoal abundance within the inorganic layer. Although this does not exclude the possibility that fires occurred in the surrounding watershed, or contributed to sediment availability for deposition, it does not support widespread, hillslope-clearing fires as a trigger for inorganic layer deposition.

Inorganic layers in sediment cores from the Puget Sound region (Adams, 1992), the Dead Sea (Ben-Menahem, 1976; Niemi and Ben-Avraham, 1994), and other areas, have been attributed to lake marginal slumps caused by seismic shocks, and used to document the paleoseismic activity of the region. Unlike these tectonically-active regions, Vermont is located in a relatively stable setting, and the largest historic earthquakes have not exceeded Richter magnitude 4.1. Vermont is proximal to several areas (the Adirondack Mountains, the White Mountains, and the Saint-Lawrence Valley) where larger earthquakes (up to magnitude 6.5) have been recorded (Ebel et al., 1995). A detailed study of lake sediment disturbance by earthquakes in the Charlevoix region of the Saint-Lawrence Valley, over 500 km from Ritterbush Pond, showed disturbance was limited to a radius of approximately 100 km from the seismic zone (Ouellet, 1997). Ritterbush Pond is also located more than 100 km away from other active seismic zones, minimizing the possibility that inorganic layer deposition is initiated by shaking associated with large earthquakes.

4.4 Age Control on Sedimentation

4.4.1 Age Model

An average whole-core sedimentation rate (0.58 mm yr^{-1}) can be estimated for Ritterbush Pond by dividing the depth of the oldest sample dated in Core 2 (548 cm) by its age (9440 cal yr BP). However, this rate (see Figure 3.13) does not account for the time discrepancy between the slow background sedimentation of gyttja, and the relatively rapid deposition of the inorganic layers that comprise 12% of the core. In order to portray more accurately changes in gyttja and inorganic layer sedimentation and model the age of individual inorganic layers, I constructed an age model based on the background accumulation of gyttja alone. Using the clustering of the inorganic layers to define six intervals, I systematically removed the inorganic layers from the stratigraphy and used calibrated radiocarbon dates at the top and bottom of each interval to calculate an age for each centimeter of gyttja within the interval (Figure 4.8). I then assigned an age to the location of each removed layer, creating a chronology of inorganic sedimentation events.

Inorganic layers are removed from the stratigraphy based on distinct changes in lithology identified at 1 cm intervals. Using the litho-stratigraphic logs, I noted the depth and thickness of each layer thicker than 5 mm. The model is insensitive to layers <5 mm, although the age of the thin layers can be calculated after age model construction. The TOC data were used to identify any additional 1-cm intervals containing inorganic material (TOC <5%) that was not identified visually. Each centimeter of material identified as containing significant inorganic matter, including centimeters containing several fine laminations, was then removed from the stratigraphy. The removal of the inorganic layers shortens the core by 67 cm. The percent inorganic material removed is calculated for each interval and is higher (18% to 49%) in the intervals where inorganic layers were clustered than in the intervals dominated by gyttja (<1%). Depth for each

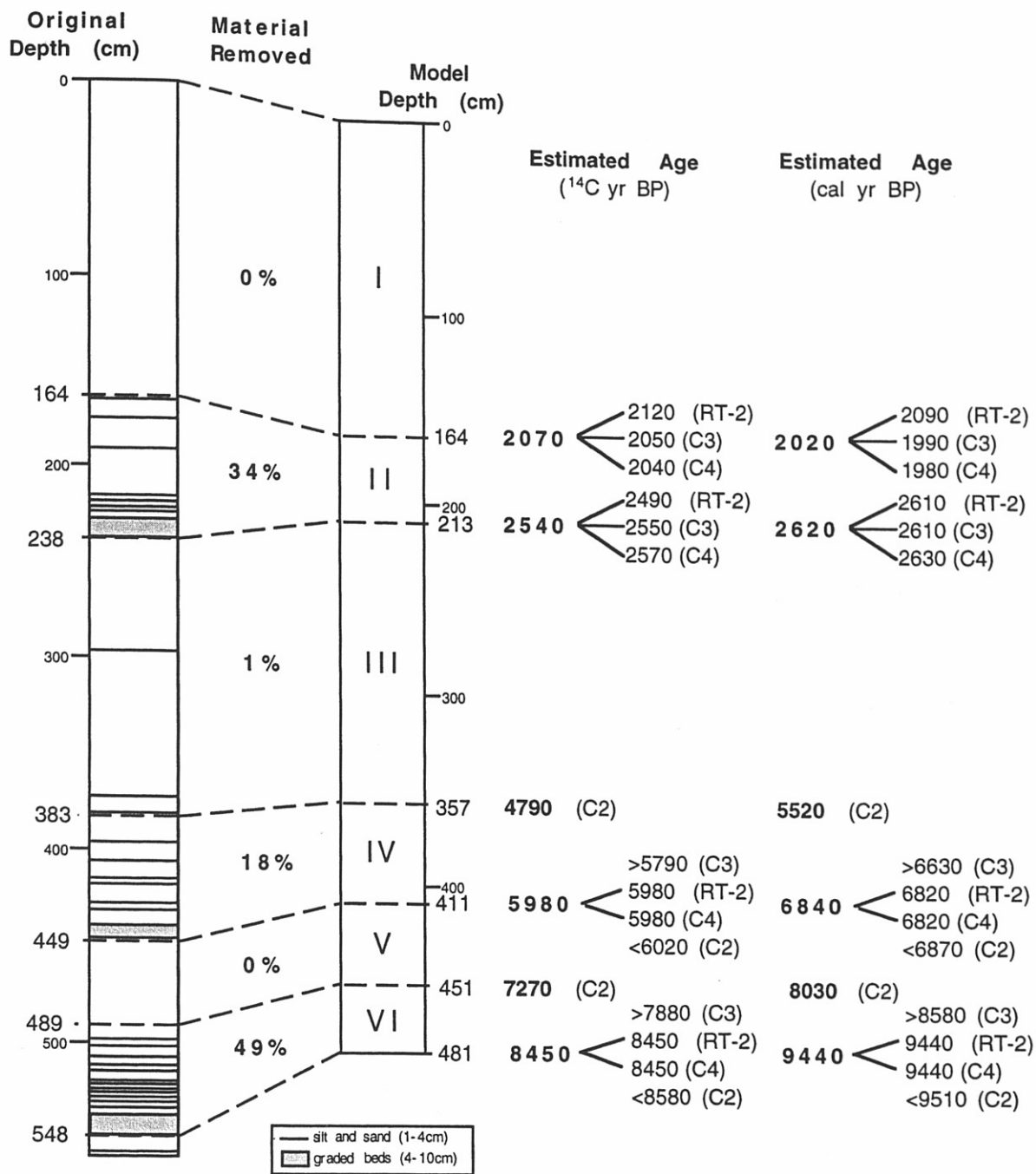


Figure 4.8 Compression of Core 2 for age modeling. Layers representing rapid deposition are removed (12% decrease in length) from the stratigraphy based on identification by logs, pictures, TOC and X-ray data. Ages (¹⁴C and cal yr) bracketing each interval are estimates based on stratigraphically equivalent ages from all cores. Limiting ages (> or <) are not used in estimation.

centimeter of the core is recalculated as model depth to denote the removal of the inorganic horizons.

Dates (both ^{14}C and cal yr BP) from six depths in Core 2 used to construct the age model for Ritterbush Pond. Ages are derived from best estimates where stratigraphically equivalent samples from more than one core have been dated, and from depths dated only in Core 2 (Figure 4.8). A zero age is assigned to the top of the core (depth = 0 cm). Gyttja accumulation is modeled as linear between the upper and lower control points for each interval (Figure 4.9, Table 4.3).

4.4.2 Validity of the Age Model

Radiocarbon dated samples from the middle of intervals I, III and IV were used to check agreement with the modeled age (Figure 4.9). In interval IV, the age offset for model depth 395 cm (Core 2 depth 424 cm), is 80 years. A sample from interval III at model depth 275 cm (Core 2 depth 300 cm) also shows an offset of 80 years, which is within the analytic uncertainty for the dates. A sample was also dated for interval I at core depth 77 cm (730 cal yr BP), model depth 77 cm (947 cal yr BP) giving an offset of 220 years. Using all three ages for interval I, and modeling deposition as exponential (due to the lack of inorganic layers) does not significantly change the ages of the identified layers.

Continuous fine sediment (gyttja) resuspension and redeposition occurring due to seasonal lake turnover and lake marginal erosion, termed sediment focusing, can move sediment toward the lake center (Davis et al., 1984; Hilton, 1985; Lehman, 1975). Sediment focusing may result in the record in higher rates of gyttja accumulation in the lake center than at the lake margins, and thus a higher resolution sedimentation record. The age model I constructed is most likely an overestimation of basin-wide gyttja accumulation

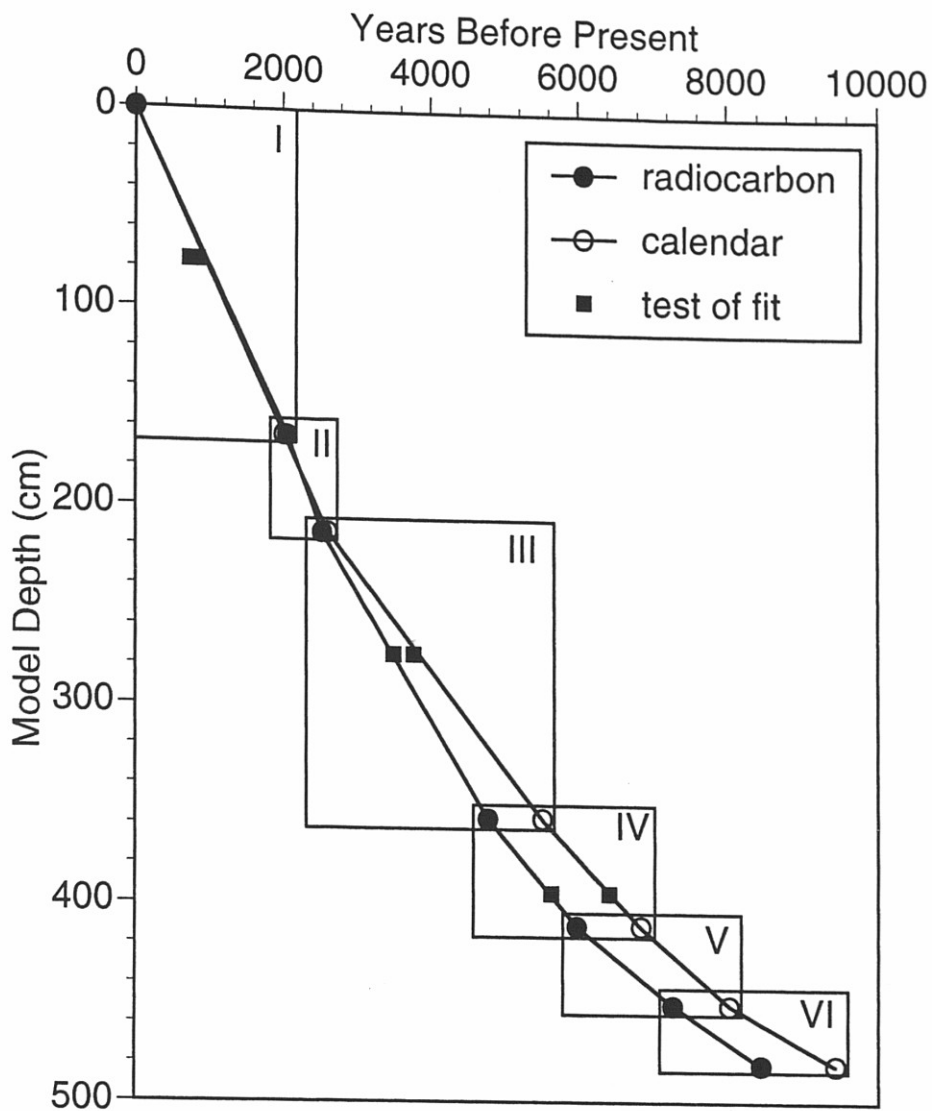


Figure 4.9 Age model for core 2. Accumulation rate is modeled as linear between age control points. Linear modeling was tested by independently dating samples from intervals I, III, and IV (squares).

Table 4.3 Age Model and Accumulation Rate Calculations for Core 2

A: Radiocarbon year calculations

interval	¹⁴ C yr BP	model depth (cm)	slope (yr cm ⁻¹)	linear intercept	sedimentation rate (cm yr ⁻¹)	bulk density (mg cm ⁻²)	accumulation rate (mg cm ⁻² yr ⁻¹)	average TOC (%) of interval	organic carbon (mg cm ⁻² yr ⁻¹)
1	0- 2070	0- 164	12.6	0.0	0.08	137	10.9	0.16	1.78
2	2070- 2540	164- 213	9.6	496.9	0.10	169	17.6	0.13	2.26
3	2540- 4790	213- 357	15.6	-788.1	0.06	225	14.4	0.15	2.23
4	4790- 5980	357- 411	22.0	-3077.2	0.05	196	8.9	0.14	1.20
5	5980- 7270	411- 451	32.3	-7274.8	0.03	250	7.8	0.17	1.34
6	7270- 8450	451- 481	39.3	-10469.3	0.03	222	5.6	0.14	0.77

B: Calendar year calculations

interval	Calendar yr BP	model depth (cm)	slope (yr cm ⁻¹)	linear intercept	sedimentation rate (cm yr ⁻¹)	bulk density (mg cm ⁻²)	accumulation rate (mg cm ⁻² yr ⁻¹)	average TOC (%) of interval	organic carbon (mg cm ⁻² yr ⁻¹)
1	0- 2020	0- 164	12.3	0.0	0.08	137	11.1	0.16	1.82
2	2020- 2620	164- 213	12.2	11.8	0.08	169	13.8	0.13	1.77
3	2620- 5520	213- 357	20.1	-1669.6	0.05	225	11.2	0.15	1.73
4	5520- 6840	357- 411	24.4	-3206.7	0.04	196	8.0	0.14	1.08
5	6840- 8030	411- 451	29.8	-5387.3	0.03	250	8.4	0.17	1.45
6	8030- 9440	451- 481	47.0	-13167.0	0.02	222	4.7	0.14	0.65

note: The linear model is depth = slope * age + linear intercept

rates, but if the rate of gyttja sediment focusing is steady, my model should portray accurately relative rate changes during the Holocene.

The deposition of inorganic layers in Ritterbush Pond is due to episodic sediment focusing events which are likely to disturb the temporal sequence of gyttja accumulation, as illustrated by the age inversion observed above the thickest graded layers (see section 4.3.3). Gyttja erosion and redeposition occurs during the emplacement of the thickest layers. Scouring at the base of the layer may decrease the estimated time since the preceding event; redeposition above the layer will increase the estimated time until the subsequent event. Since thick layers are more likely to generate greater erosion than thin layers, the amount of erosion and deposition will not be equal for each event. The close spacing of layers of varying thickness may result in both overestimates (thin on top of thick) and underestimates (thick on top of thin) of time since the last event. The magnitude of the disturbance of the gyttja stratigraphy can be estimated by the offset observed between the modeled and measured radiocarbon ages. The offset of 80 cal years is equivalent to 4 to 5 cm of gyttja, but within the analytic uncertainty of the dates. In addition, the removal of material visually identified as an inorganic layer during the creation of the age model, will also remove any gyttja mixed into the layer during transport from the lake margins. As I cannot quantify the sediment disturbance associated with each event, and because the age model has been demonstrated to be reasonably accurate, I use layer spacing as a proxy for time between events.

4.4.3 Gyttja Accumulation Rates

The average sedimentation rate calculated for each interval with the age model is used to estimate gyttja accumulation rates and changes in lake primary productivity. I use an average bulk density (Figure 4.10) for each interval to account for compaction and convert sedimentation rate (cm yr^{-1}) to gyttja accumulation rate ($\text{mg cm}^{-2} \text{yr}^{-1}$) (Figure 4.11, Table 4.3). I estimate the fraction of organic carbon in the gyttja by multiplying the accumulation rate by the average TOC (%) for the interval. The average TOC values were calculated after the removal of the inorganic layers from the stratigraphy, and represent the average organic carbon in the remaining sediment. Since the stable carbon isotope and C/N ratios indicate a primarily aquatic source for the organic carbon in the gyttja, I use the estimation of organic carbon accumulation rate as a proxy for changes in primary productivity in the lake. The calculated accumulation rate may also be influenced by down-core changes in decomposition of the organic material.

Gyttja accumulation rate, calculated for 1000 yr intervals, appears to generally increase from 9000 to 4000 cal yr BP, when the rate levels off at $11 \text{ mg cm}^{-2} \text{yr}^{-1}$. Superimposed on this trend are increases at 2000 to 3000 cal yr BP and 7000 to 8000 cal yr BP. These increased values coincide with clusters of inorganic layers and may be increased by episodic sediment focusing of gyttja due to event deposition, or increased primary productivity due to nutrient enrichment by the influx of terrestrial material (Figure 4.12).

Organic carbon shows an irregular increase in accumulation rate but also levels off ($1.7 \text{ mg cm}^{-2} \text{yr}^{-1}$) at 4000 cal yr BP, with peaks at 5000 to 6000 cal yr BP and 7000 to 8000 cal yr BP. The coincidence of the increase in both gyttja and organic carbon accumulation from 7000 to 8000 cal yr BP suggests that inorganic layer deposition may have been accompanied by gyttja sediment focusing. The absence of an increase in

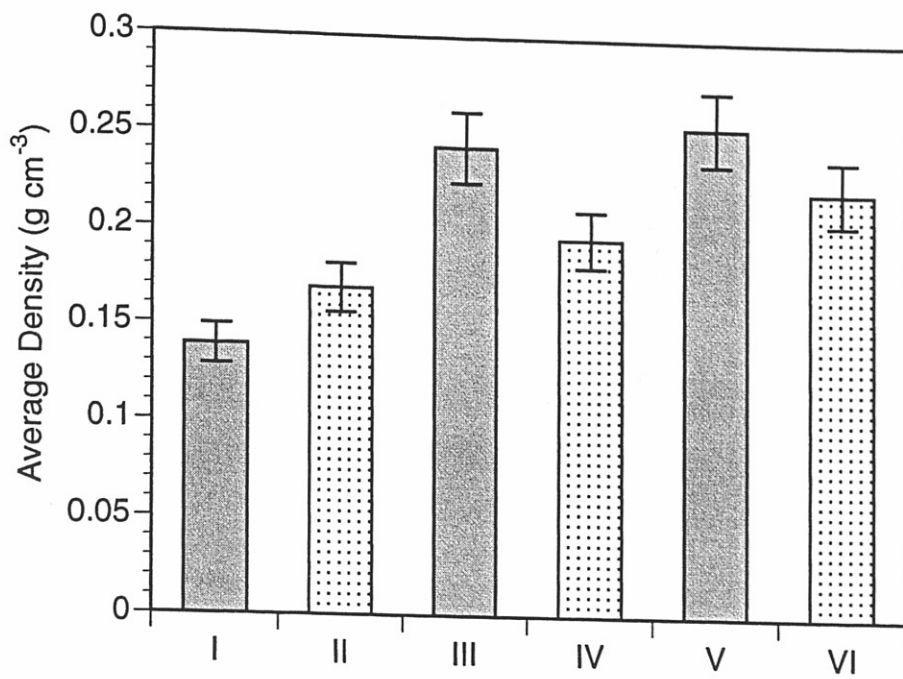


Figure 4.10 Average bulk density and standard deviation (1σ) for each interval. Even intervals, dominated by inorganic layers, show less increase in density with depth.

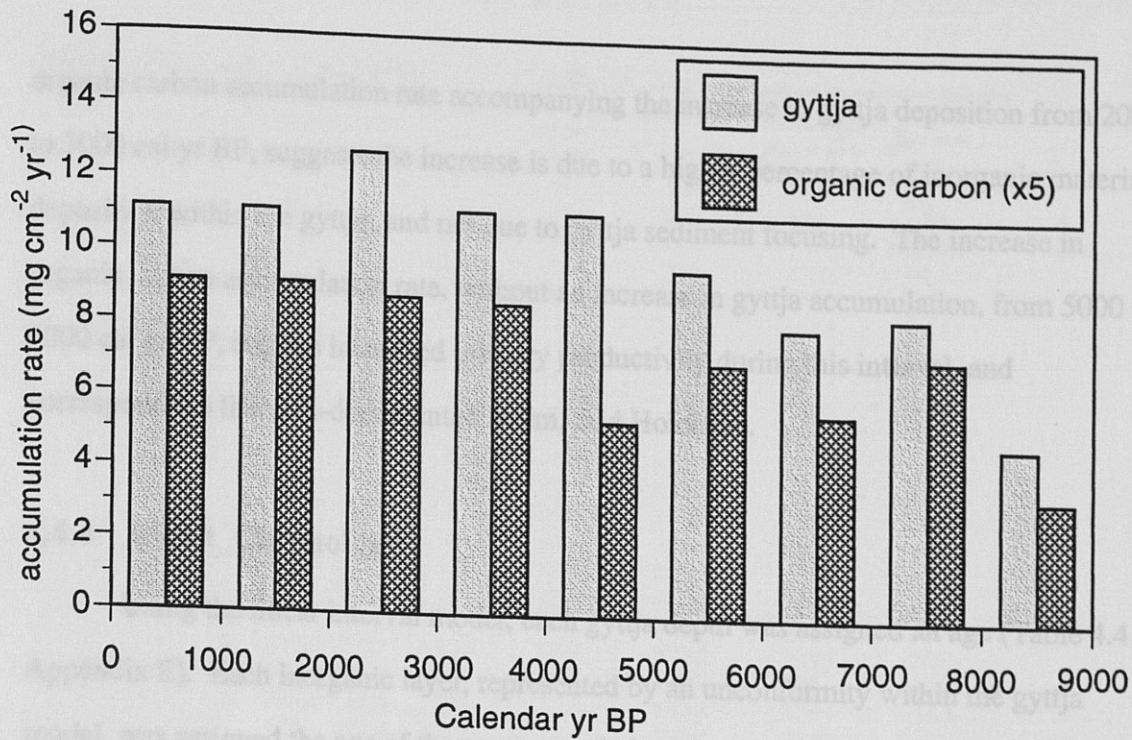


Figure 4.11 Gyttja and organic carbon accumulation rates for Core 2. Calendar year intervals (1000 yr) show increasing rates of gyttja and organic carbon accumulation prior to 4000 cal yr BP.

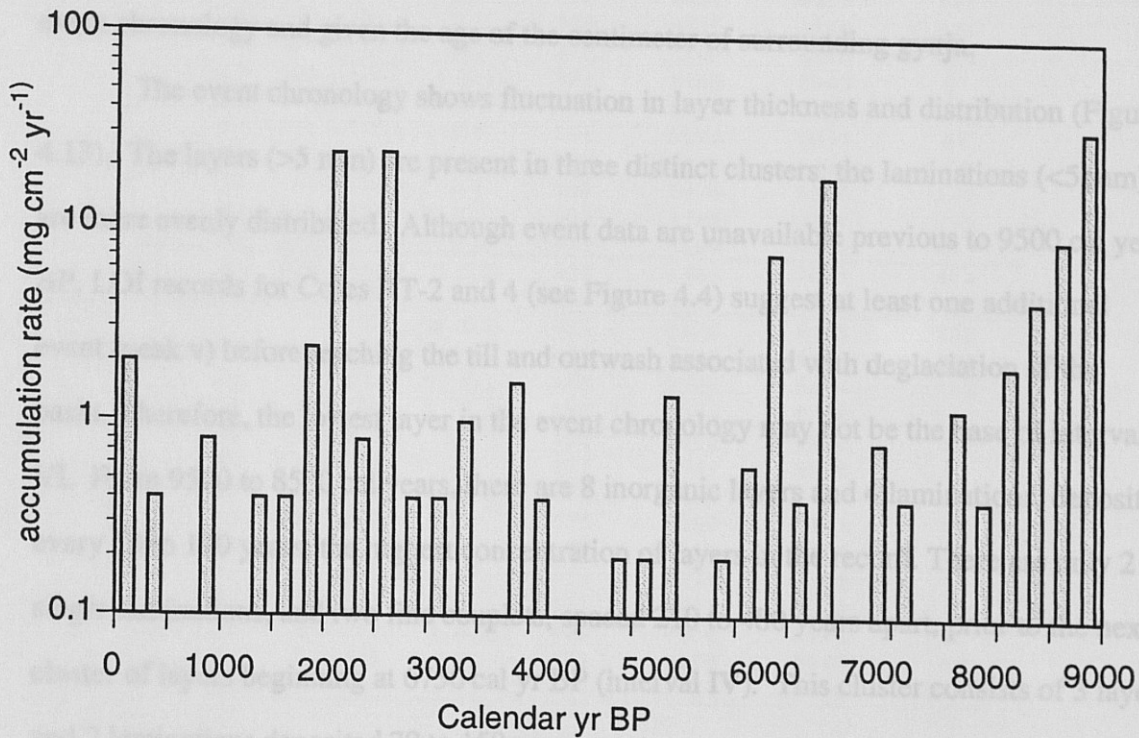


Figure 4.12 Inorganic layer accumulation rates for Core 2. Calendar year intervals (250 yr) show 3 clusters of layer deposition at 2000 to 3000, 6000 to 7000, and prior to 8500 cal yr BP.

organic carbon accumulation rate accompanying the increase in gyttja deposition from 2000 to 3000 cal yr BP, suggests the increase is due to a higher percentage of inorganic material deposition within the gyttja, and not due to gyttja sediment focusing. The increase in organic carbon accumulation rate, without an increase in gyttja accumulation, from 5000 to 6000 cal yr BP, implies increased primary productivity during this interval, and corresponds to the well-documented warm, mid Holocene.

4.4.4 Event Chronology

Using the linear interval model, each gyttja depth was assigned an age (Table 4.4, Appendix E). Each inorganic layer, represented by an unconformity within the gyttja model, was assigned the age of the centimeter below the unconformity, a maximum age for the depositional event. Millimeter-scale laminations identified by litho-stratigraphic logs and X-radiographs, but not originally removed from the stratigraphy, are included in the event chronology and given the age of the centimeter of surrounding gyttja.

The event chronology shows fluctuation in layer thickness and distribution (Figure 4.13). The layers (>5 mm) are present in three distinct clusters; the laminations (<5 mm) are more evenly distributed. Although event data are unavailable previous to 9500 cal years BP, LOI records for Cores RT-2 and 4 (see Figure 4.4) suggest at least one additional event (peak v) before reaching the till and outwash associated with deglaciation of the basin. Therefore, the lowest layer in the event chronology may not be the base of interval VI. From 9500 to 8500 cal years, there are 8 inorganic layers and 4 laminations, deposited every 50 to 190 years, the highest concentration of layers in the record. There are only 2 single laminations, and two fine couplets, spaced 210 to 480 years apart, prior to the next cluster of layers beginning at 6750 cal yr BP (interval IV). This cluster consists of 3 layers and 2 laminations deposited 70 to 150 years apart.

Table 4.4 Modeled Layer Age in Radiocarbon and Calendar Years for Core 2

Interval	peak ¹	layer ²	depth (cm)	thickness (cm)	equivalent gyttja depth	model age (¹⁴ C yr BP)	model age (cal yr BP)	time since last event (cal yr)	
I	aa	1	4-5	1	5	63	62	319	
	a	2	30.8-31.0	0.2	31	391	381	382	
		3	61.0-61.2	0.2	62	781	763	160	
	b	4	74.6-74.8	0.2	75	945	923	356	
	c	5	103.8-104.0	0.2	104	1310	1279	259	
		6	124.7-124.9	0.2	125	1575	1538	221	
	d	7	142-143	1	143	1802	1759	209	
II	e	8	159.0-159.2	0.2	160	2016	1968	57	
		9	164-167	3	165	2081	2025	73	
	f	10	173-177	4	171	2139	2098	134	
	g	11	188-193	5	182	2244	2232	122	
	h	12	203-204	c (0.2)	192	2340	2354	159	
		13	217-219	2	205	2465	2513	24	
		14	221-222	1	207	2484	2537	25	
	i	15	224.0-224.2	0.2	209	2503	2562	58	
		16	228-237	9	213	2540	2620	333	
	III	j	17	254.5-254.7	0.2	230	2800	2953	81
18			258.5-258.7	0.2	234	2862	3034	241	
jj		19	270.5-271.0	0.5	246	3050	3275	523	
k		20	296.0-296.3	0.3	272	3455	3798	60	
		21	305.0-305.5	0.5	280	3502	3858	181	
l		22	309.4-309.5	0.1	284	3642	4039	201	
		23	319.0-319.1	0.1	294	3798	4240	723	
		24	355.0-355.1	0.1	330	4360	4963	61	
m		25	358.0-358.1	0.1	333	4407	5024	261	
		26	371.8-372.0	0.2	346	4610	5285	40	
		27	373.0-373.2	0.2	348	4641	5325	141	
		28	380.0-380.3	0.3	355	4750	5466	404	
IV	n	29	397.8-397.9	0.1	372	5107	5870	220	
		30	406.2-406.7	c (0.1)	381	5305	6090	97	
	31	411.3-411.4	0.1	385	5393	6187	147		
	o	32	415.2-416.0	0.8	391	5525	6334	97	
		33	420-423	3	395	5613	6431	74	
	p	34	426.5-426.6	0.1	398	5679	6505	122	
		35	431.8-431.9	0.1	403	5789	6627	213	
		36	439.5-449.0	9.5	411	5980	6840	441	
V	r	37	461.1-461.8	c (0.2)	423	6388	7281	414	
		38	477.5-477.7	0.2	439	6905	7695	476	
VI	s	39	492-493	c (0.3)	454	7373	8171	282	
		40	497.4-497.6	0.2	460	7609	8453	141	
		41	501-502	1	463	7727	8594	188	
		42	506-508	2	467	7884	8782	141	
		43	511.5-511.6	0.1	468	8002	8923	47	
		44	512.6-512.7	0.1	471	8041	8970	47	
		t	45	513-514	1	472	8080	9017	94
			46	516.0-516.1	0.1	473	8159	9111	47
			47	517.5-520.0	2.5	475	8198	9158	47
			48	521-522	1	476	8238	9205	47
	50	49	523-525	2	477	8277	9252	47	
		50	526-532	c (1.5)	478	8316	9299	94	
		51	533-535	2	479	8395	9393	47	
		52	537-547	10	481	8434	9440	235 ³	

¹ as identified in Core 2

² layers identified by litho-stratigraphic logs, X-radiographs and TOC

³ estimated from lithostratigraphic logs and accumulation rate of interval VI

c = couplet, layer thickness in ()

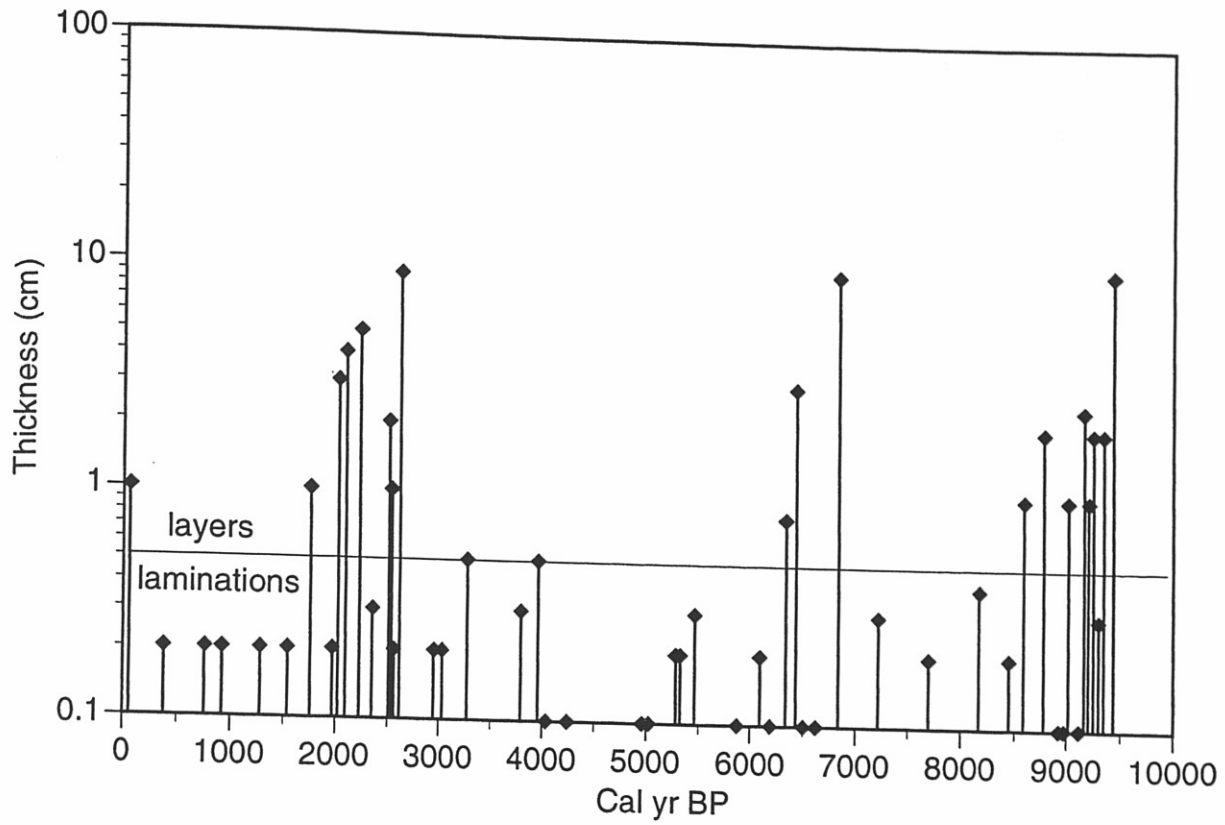


Figure 4.13 Layer thickness vs. calendar age. Solid line at 0.5 cm divides layers from laminations.

From 6250 to 2750 cal yr BP (interval III), 14 laminations and one couplet occur 40 to 720 years apart. The next cluster of layers, from 2750 to 2000 cal yr BP (interval II), contains 6 layers, 2 laminations, and 2 couplets that were deposited 20 to 160 years apart. The frequency of deposition decreases again in interval I, where only one layer and 6 laminations were identified, ranging 160 - 380 years apart. The youngest individual layer identified, estimated at 62 cal yr BP, is a diffuse centimeter of macrofossil rich sand, and is the only evidence of event deposition in the last 300 years. In even intervals where the inorganic layers cluster, the thickest layer is consistently at the base of the interval. Subsequent layers decrease in thickness in each of the intervals.

CHAPTER 5 - Discussion

The chronology of inorganic sediment layers in Ritterbush Pond is a record of both the frequency and magnitude of hydrologic events, and provides a detailed erosional history for the watershed. This chapter summarizes the geomorphic and hydrologic controls on sediment transport to Ritterbush Pond and investigates using the Ritterbush record as a proxy for storm frequency during the Holocene. I then use historic storm records to determine the types of events capable of depositing an inorganic layer in the lake, and compare the Ritterbush event chronology to other global climate records for the Holocene.

5.1 Event Sedimentation in Ritterbush Pond

5.1.1 Sedimentation Dynamics of the Ritterbush Watershed

The Ritterbush Pond cores provide a detailed record of discrete sedimentation events. The sand and silt layers are terrestrially-derived sediment, transported from the lake margins toward the lake center, probably by density currents. The transport of sediment to the lake is most likely caused by episodic increases in stream flow, which erode stream channels, stream banks, and lake margins (see section 4.3.5). However, similar inorganic layers have not been found in sediment cores from Sterling Pond (Bierman et al., 1997) or Richmond Pond, both located in Vermont's Green Mountains. Nor do other New England lakes, extensively cored for de-glacial and pollen research, exhibit recurrent episodes of terrestrial sediment deposition during the last 9000 ^{14}C years (Davis et al., 1984; Thompson et al., 1996).

The physical characteristics of the Ritterbush Pond watershed strongly influence the sensitivity of the hillslopes and stream channels to erosion. Similar to other Vermont

lakes, the watershed is forested, relatively small (<3 km²), and has significant bedrock outcrops. In contrast to the other cored ponds, Ritterbush Pond has steep hillslopes on all sides. Although the vegetation in the watershed limits hillslope erosion and mass movement during moderate hydrologic events, the steep slopes increase the velocity of runoff once the ground is saturated (Dunne and Leopold, 1978; Ritter et al., 1993). During severe hydrologic events, high-velocity saturation overland flow results in short periods of intense stream discharge, maximizing the potential for channel scouring and bank erosion. Streams draining watersheds with lower relief, such as Sterling Pond, are likely to have less-peaked hydrographs, decreasing runoff rates and thus sediment transport potential during intense precipitation events.

Once sediments reach Ritterbush Pond, their preservation potential is enhanced by lake bathymetry. Unlike the gentle, shallow bathymetry of Richmond Pond, Ritterbush Pond has a deeper, bowl-shaped basin. The movement of sediment stored at the shallow lake margins, where streams lose competence and build deltas, toward the deep flat center of the lake, is facilitated by steep inner lake slopes conducive to sediment resuspension and density-current transport. Additionally, the steep lake slopes minimize the removal of material from the lake center once it has been deposited. Shallower basins with lower outlets may experience resuspension and transport of fine-grained sediment from the lake during periods of high discharge.

5.1.2 Effect of Precipitation Events on Sedimentation

The deposition of terrestrial material in Ritterbush Pond occurred episodically throughout the Holocene, suggesting temporary changes in the erosion dynamics of the watershed. Increases in runoff and streamflow, the primary cause of layer deposition, are due to hydrologic events such as rainstorms and spring snowmelt. Very large and damaging floods have been generated by snowmelt alone, and rain on melting snow,

from March to May in New England (Ludlam, 1996). However, the Ritterbush watershed is less likely to experience such flooding, even if the entire snowpack were to melt rapidly, due to the small size of the drainage basin. Additionally, the range of hillslope gradient, elevation and aspect within the Ritterbush watershed, would result in varying rates of snowmelt, and stagger water release from the snowpack (Dunne and Leopold, 1978). Furthermore, hydrologic events occurring during the winter and early spring are probably less likely to result in layer deposition due thick ice cover on the lake.

Precipitation events cause sediment deposition in Ritterbush Pond due to increased sediment erosion from hillslopes and transport to the lake by streams. Precipitation percolates through the thin, moderately well-drained soils, and moves as subsurface stormflow along the bedrock or impervious till substrate to stream channels (Babcock, 1979; Fetter, 1994). Once the soils are saturated, downslope transport of runoff occurs even more rapidly as saturation overland flow, which reaches the stream channels up to 100 times faster than subsurface stormflow (Dunne and Leopold, 1978). The resulting rise in stream discharge increases shear stress and flow velocity at the base and sides of the channel, resulting in a greater volume of material moved by bedload transport, and an increase in the grain size of the particles in the suspended load (Ritter et al., 1995). In the Ritterbush watershed, increased stream flow may result in the scouring of sediment from channel bottoms, and especially where streams run over bedrock or well-consolidated till, the erosion of channel banks by lateral channel migration. The volume and grain size of sediment transported to Ritterbush Pond should generally increase with increasing storm runoff and the resulting stream discharge.

Storm events may also influence sediment deposition in Ritterbush Pond by increasing wave and current activity at the lake margins. Although the basin is small, wind-generated waves may resuspend sediment stored at the lake margins; wind-generated currents, and increased inflow from streams, may alter lake circulation patterns

and transport lake marginal material toward the center of the lake (Horne and Goldman, 1994). Sediment-laden streamflow may cause oversteepening and failure of the delta slopes. Regardless of the exact source for sediment, or the specific mode of transport to the lake, the deposition of each inorganic layer is probably driven by a discrete hydrologic event.

5.1.3 The Ritterbush Event Chronology

If each inorganic layer in Ritterbush Pond represents a erosional event in the watershed, event frequency and magnitude, has fluctuated during the Holocene. Layer frequency, the time between depositional events as calculated by the age model, may be used to estimate the recurrence intervals of hydrologic events large enough to cause layer deposition (see section 4.4.2). The average event recurrence interval for odd intervals is 270 ± 170 cal yr BP, and the average event recurrence for the even intervals is 130 ± 100 cal yr BP. The more frequent event recurrence during the even-numbered intervals suggests periodic changes in the frequency of the largest hydrologic events during the Holocene.

Layer thickness, however, is an uncertain proxy for storm magnitude. In even intervals, layer thickness appears to increase with time since the preceding event, for all events > 2 cm thick (Figure 5.1). This correspondence suggests that layer thickness and/or storm magnitude may depend on the time elapsed between events. In odd intervals, where all layers are thin, and in parts of even intervals where layers are < 2 cm thick, layers exhibit a wide range of recurrence intervals, suggesting that for thin layers, thickness may better indicate the magnitude of the storm event. Accordingly, I conclude that 1) layers > 2 cm thick probably indicate storm events larger than layers < 2 cm thick, but are not necessarily correlative to storm magnitude, and 2) layers ranging from 0.1 to 2 cm thick may represent a range in storm magnitudes.

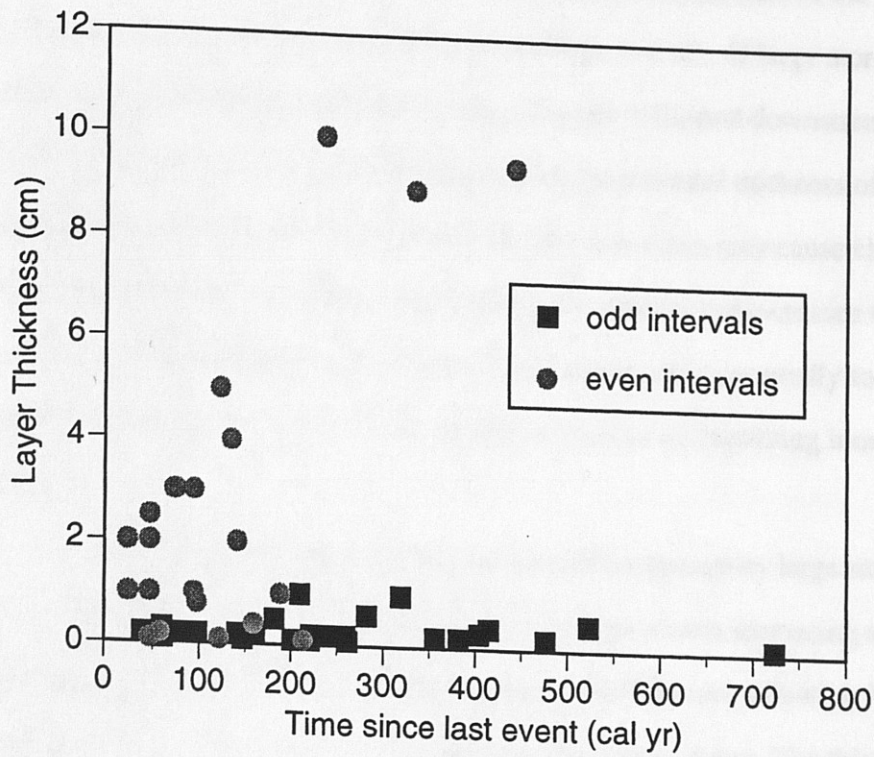


Figure 5.1 Layer thickness as a function of calendar years since the last event. In even intervals, layer thickness increases with time since last event for layers thicker than 1 cm. Thinner layers, occurring in both odd and even intervals, do not exhibit dependence on time since last event.

In the even intervals, the thickest layer occurs at the base of the interval, and subsequent layers decrease in thickness (see Figure 4.13). If large storms occur frequently, sediment stored in the stream channels is flushed downstream. The reduced availability of easily mobilized sediment limits the potential thickness of successive inorganic deposits in the lake. Conversely, the first storm may cause channel bank collapse or hillslope failure that exposes new surfaces to erosion, and increases the sensitivity of the watershed to subsequent storm events. Successive storms, normally too small to cause significant sediment transport, would then be capable of depositing inorganic layers in the lake.

The removal of easily eroded sediment from storage by large storm events seems more probable than the lingering effects of previous storms increasing sediment yield. The elapsed time between events is always greater than 50 years, allowing for slope stabilization and the regrowth of vegetation after a large storm. The thickest layer at the base of each even interval is thus an accurate reflection of the erosion and sedimentation potential of a larger-than-average storm, when abundant sediment is available. The second event in a pair of closely spaced events, may be of greater magnitude, but because less sediment is available, may deposit a thinner layer. Therefore, while the spacing of the layers may be used to estimate storm frequency (assuming negligible erosion and redeposition of gyttja during layer deposition) and the occurrence of thicker layers in even intervals suggests larger storm events, the relative thickness of layers within even intervals may not be an accurate proxy for magnitude of the storm event.

The magnitude of floods, large storm events, and the annual maximum series of 24-hour precipitation totals often fit an extreme-value probability distribution (Hershfield and Kohler, 1960; Dunne and Leopold, 1978). If the thickness of the inorganic layers corresponds to storm magnitude, and is not dependent on sediment availability, then the occurrence of such layers should conform to the extreme-value distribution. The

probability distribution of layers less than 0.5 cm thick fit an extreme value distribution, suggesting that thickness reflects storm magnitude (Figure 5.2). Thicker layers also show correspondence, but with a steeper linear fit that is discontinuous between layers less than 5 cm, and layers greater than 8 cm thick. The discontinuity of the linear fit implies dependence on a factor other than storm magnitude, such as sediment availability, for layers greater than 0.5 cm. Interestingly, the distinct break in slope between thin layers and thick layers corresponds well with the layer thickness occurring in odd and even intervals. Layers thicker than 1 cm occur only within even intervals, possibly indicating a change in factors controlling layer deposition (including storm magnitude, storm frequency and sediment availability) during even-numbered intervals.

5.2 *New England Climate Records*

The three even intervals (II, IV, VI), representing an increased frequency of large storm events in Ritterbush Pond, last 500 to 1,000 calendar years. The lack of large events during the thousands of years separating these intervals suggests that the frequency of layer deposition may be influenced by fluctuations in regional climate. In the northeastern United States, general trends in average precipitation, temperature, and vegetation since deglaciation have been reconstructed using specific pollen abundance as a climate proxy record (Jackson and Whitehead, 1991; Lin, 1996; Spear et al., 1994). Although the exact timing varies, all proxy records suggest a gradual rise in temperature following deglaciation, maximum warmth in the mid-Holocene (the hypsithermal), and cooling toward present climate conditions (Figure 5.3). The wettest period of the Holocene, as interpreted from lake-level curves (Webb, et al., 1993), occurred from 8000 to 6000 ^{14}C yr BP. The pollen chronology for Ritterbush Pond suggests warm, moist conditions

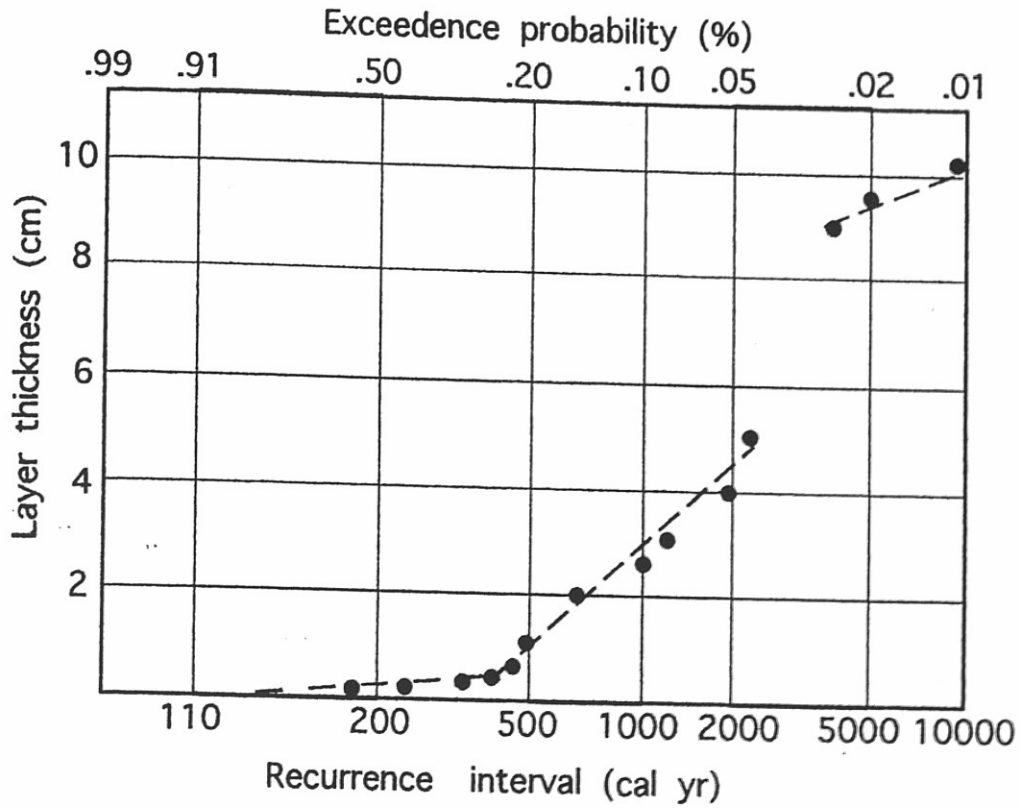


Figure 5.2 Extreme value probability distribution of inorganic layer thickness in Ritterbush Pond cores. When more than one layer of the same thickness occurs, the highest probability is graphed. Thin layers (<0.5 cm) conform to the extreme value distribution; thick layers fit a discontinuous linear distribution.

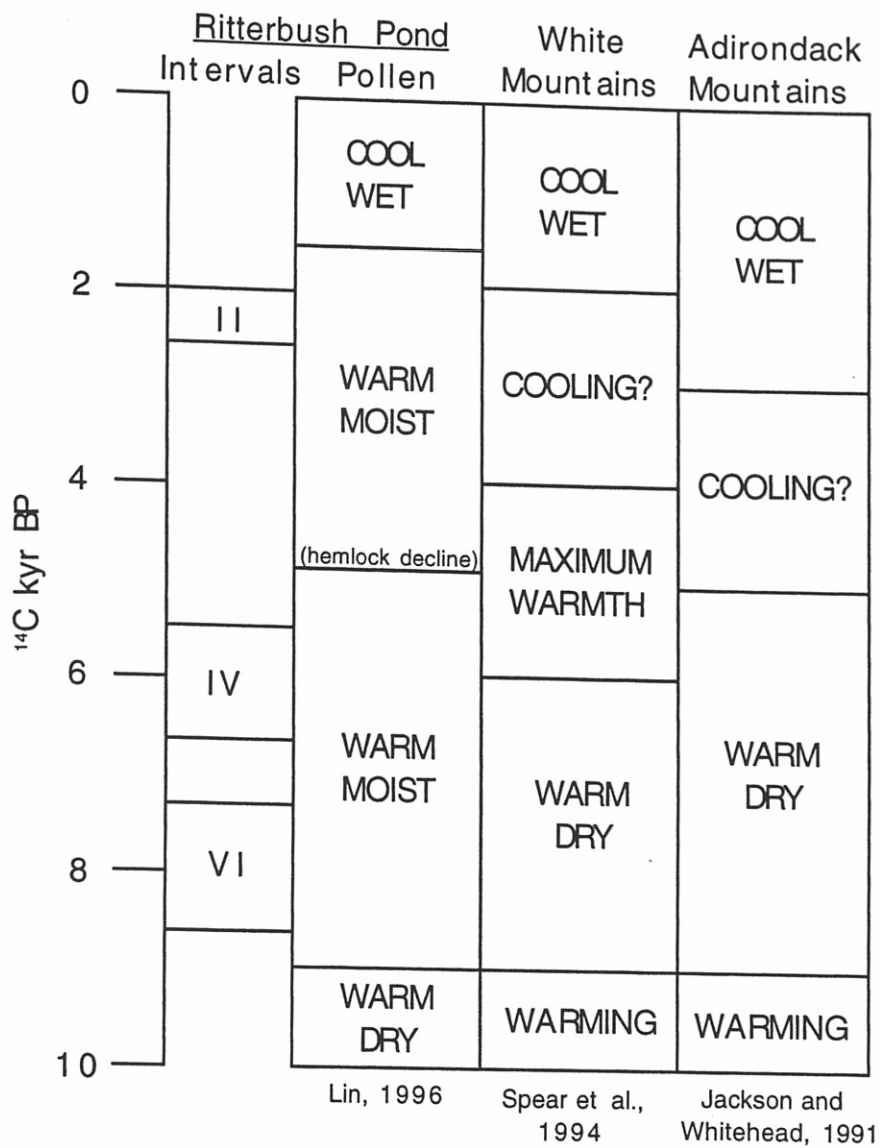


Figure 5.3 Summary of Holocene Climate Proxy (Pollen) Data for the northeastern United States in ¹⁴C yr BP.

from 9000 to 1600 ^{14}C yr BP, spanning all three intervals of increased inorganic layer deposition.

The lack of correspondence between intervals of increased layer deposition with any particular regional climate regime suggests that the increase in storm activity is not necessarily caused, or accompanied, by changes in average climate conditions, primarily mean annual precipitation, that control watershed vegetation. If the increased frequency of layer deposition indicates a prolonged period (up to 1000 years) of increased precipitation, then this change should be, but is not, reflected by a shift in vegetation. A single storm event, however, is unlikely to impact the watershed sufficiently to cause vegetation changes significant enough to be detected by pollen analysis. Clusters of inorganic layers most likely represent clusters of extreme hydrologic events not detected by the pollen data.

5.3 Frequency and Magnitude of Vermont Storms

Extreme storms causing layer deposition in Ritterbush Pond, whether local or regional events, will remain undetected by climate proxy records that integrate over long time periods and wide areas. However, 200 years of written and anecdotal history provide a regional record of storm magnitude and frequency that is a potential analog for pre-historic and Holocene storm activity at Ritterbush Pond.

5.3.1 Historic Storms in Vermont and at Ritterbush Pond

Large or intense rain storms in Vermont fall into two basic categories: low-pressure, or frontal, storm systems that interact with tropical air, and localized thunderstorms (NOAA, 1982). These storms result in different duration, intensities, and distributions of precipitation. Thunderstorms tend to be of shorter duration and localized, while frontal systems last longer and cover wider areas (NOAA, 1982). In Vermont,

intense, shorter thunderstorms have a higher probability of occurring earlier in the summer than longer-lived but low-intensity frontal storms (Figure 5.4). Intensity-frequency-duration curves for Burlington and Northfield (located in central Vermont) quantify the higher intensity of shorter storms (Figure 5.5). Studies of regional and spatial distribution of storms suggest that it is not possible to determine the type of storm (frontal or thunderstorm) using only precipitation data from a single weather station (Hershfield and Wilson, 1960). The regional extent of any storm can only be determined by comparison with similar records from other locations. Although the type of storm event represented by an inorganic layer can not be determined, the Ritterbush Pond record has the potential to record both localized thunderstorms and regional frontal storm systems.

The largest rainstorm in Vermont's recorded history occurred in November 1927, due to the collision of a frontal system with tropical air. The entire state received between 5 and 9 inches of rain over two days (Ludlam, 1996). Isohyetal maps for the storm estimate that the Ritterbush watershed received approximately 7 inches of rain over 2 days (Kinnison, 1930). The 1927 flood was preceded by 3 rainstorms, each just over a week apart, making average rainfall during October 150% higher than normal (Ludlam, 1996). The second largest state-wide storm occurred in 1938, when a what was a Class 3 hurricane tracked diagonally southeast to northwest across Vermont, dropping more than 3 inches of rain in the south in 24-hours, and resulting in five-day totals of 5 to 8 inches across the state (Coch, 1995; Ludlam, 1996). Saturation of the soils by heavy rains prior to the hurricane favored increased runoff and resulted in widespread flooding throughout the state (Ludlam, 1996).

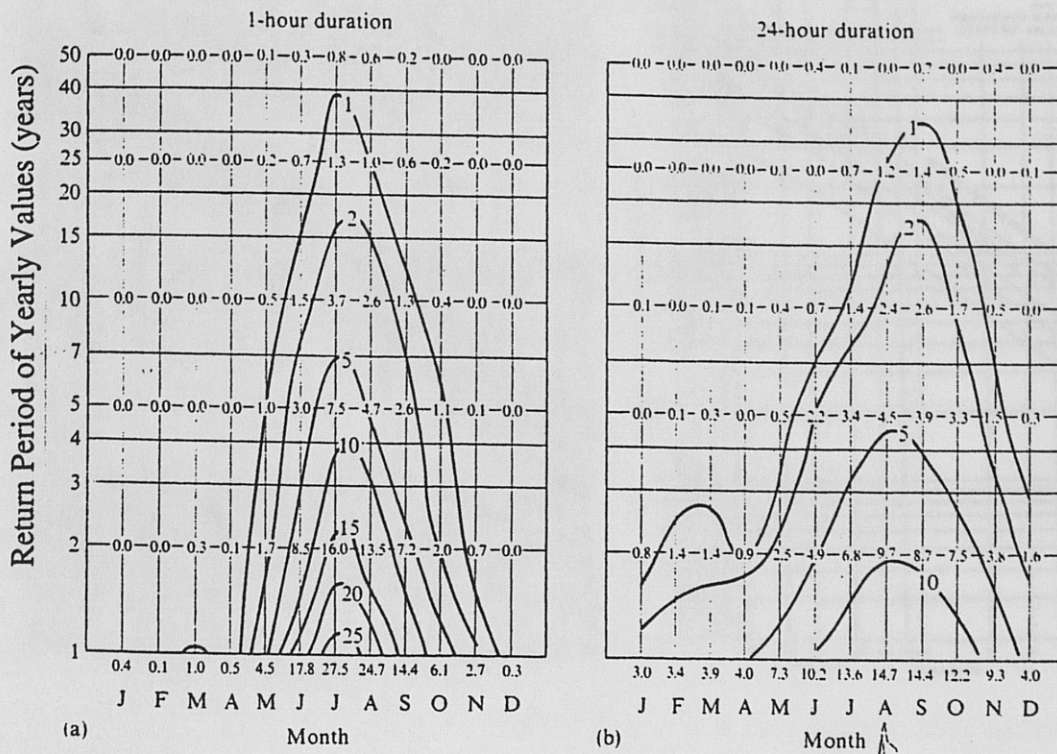


Figure 5.4 Seasonal probability of intense precipitation for the northeastern United States, from U.S. Weather Bureau (1959). Contours indicate the percent probability for each month of obtaining precipitation equal to or exceeding each return period value. Intense 1-hour storms are most likely to occur in July, while intense 24-hour rainfall has the highest probability of occurring in September.

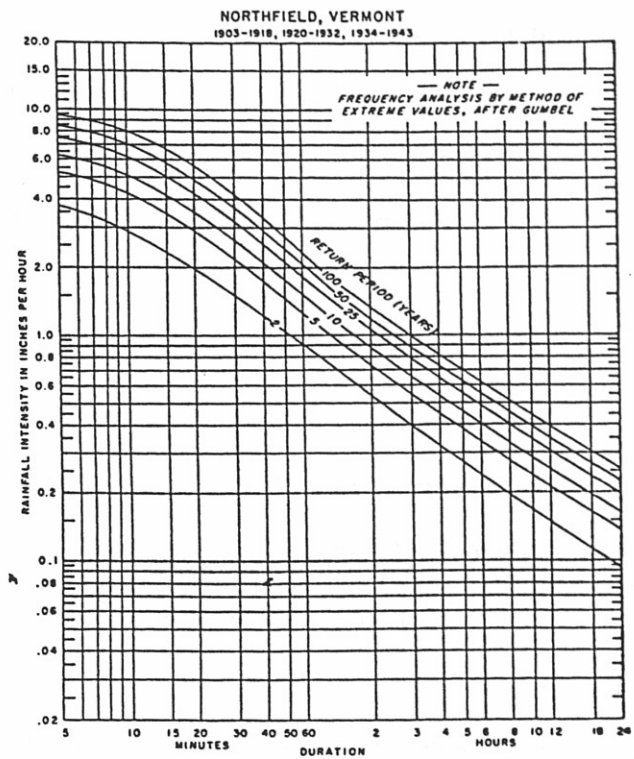
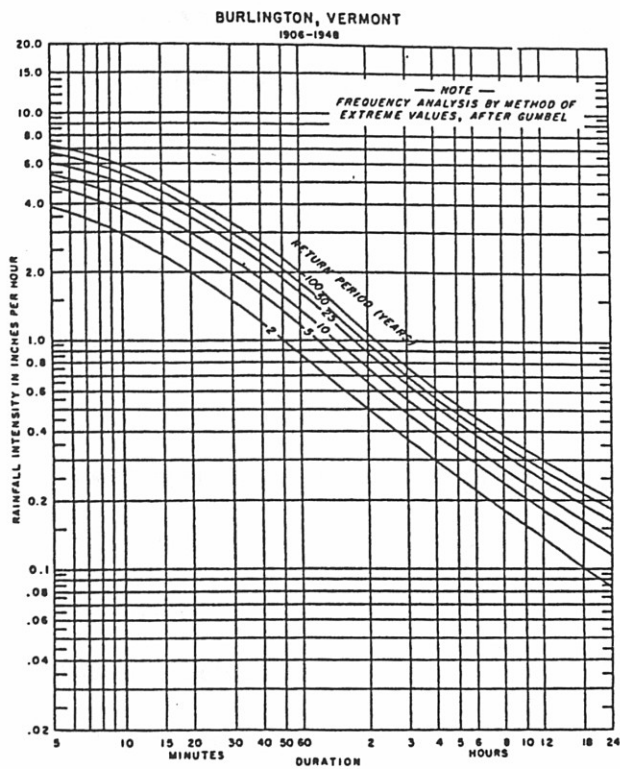


Figure 5.5 Rainfall intensity-duration-frequency curves for Burlington and Northfield, Vermont, from U.S. Weather Bureau (1955). For all return periods, short-duration rainfall events have higher rainfall intensity than long-duration events. Comparing rainfall intensity values for Burlington and Northfield (approx 1000 ft higher in elevation) suggests a dependence of rainfall amount on elevation.

In Ritterbush Pond, only one inorganic layer was deposited in the last 350 years. This layer consists of 1 cm of indistinct, disturbed, organic-rich sand. The age model suggests this layer was deposited about 1935 AD. I estimate that this diffuse sand layer, located in the liquid upper 10 cm of the core would probably correspond to less than 0.5 cm of sand if compressed, placing it among the events where magnitude does correlate to layer thickness in both even and odd intervals. Considering the uncertainty associated with this age, the deposition could represent either the 1927 or 1938 storm. If the largest state-wide storms recorded in 200 years produced only 1 cm of sand, then the deposition of 10 cm of sand suggests a storm of much greater magnitude than witnessed historically.

5.3.3 The Potential Magnitude of Large Storm Events

Based on historic precipitation records and a combination of physical storm system modeling and estimation of meteorological parameters, the National Weather Service (NWS) has made regional estimates of the probable maximum precipitation (PMP) for a six hour period (US Weather Bureau, 1956). The PMP for all of northern Vermont is estimated between 18 and 20 inches (US Weather Bureau, 1961). These estimates are used to indicate the order of magnitude of extremely rare rainfalls. The PMP for Ritterbush Pond is estimated at 19 inches in 6 hours, almost three times the amount that resulted from the 1927 storm over 2 days (Table 5.1).

In 1969, Hurricane Camille hit central Virginia, causing massive hillslope failure, flooding, and general devastation (Williams and Guy, 1973). The PMP estimate for this region is 26 to 30 inches in 6 hours (US Weather Bureau, 1960). Camille delivered 24 inches in 8 hours (Williams and Guy, 1973), suggesting that the PMP is a reasonable estimate of extreme precipitation. Catastrophic rainfall events are required to produce significant debris-flows in the Appalachians (Kochel, 1990), but as the duration

Table 5.1 Rainfall Intensity Estimates for Extreme Events at Ritterbush Pond

Estimate	Return Period	Intensity	Normalized Intensity		Source (Rationale)
			Intensity	(cm hr ⁻¹)	
1927	107 yr	7 in / 48 hr	0.4		Kinnison, 1939 (isohyetal map)
24-hour max	100 yr	6.2 in / 24 hr	0.7		Burlington *1.35
PMP	N/A	19 in / 6 hr	8		U.S. Weather Bureau, 1961 (isohyetal map)
1-hour max	100 yr	4.2 in / 1 hr	10.7		Burlington *2

* Burlington data (NWS, 1998) adjusted (section 5.3.3) for elevation (24-hour max) and intensity (1-hour max) according to Dunne and Leopold (1978).

of a storm increases, the intensity of rainfall required decreases (Figure 5.6). Although there is little evidence of recent debris flows or mass movement in the Ritterbush basin, potentially the PMP storm would drop enough precipitation to destabilize steep slopes (Kochel, 1990).

The longest daily precipitation record for Vermont begins in 1893 and is from Burlington, located on Lake Champlain, approximately 50 km to the southwest of Ritterbush Pond. The 24-hour annual maximum data for Burlington have an extreme value probability distribution (Figure 5.7). The highest value, 4.49 inches, was recorded during the 1927 storm, and represents the 107-year storm event. The 1938 storm does not appear in this record. The second and third largest values are attributed to localized, intense thunderstorms in the Burlington area. The correspondence of the annual maximum series to the extreme value distribution implies that the 1927 storm is within the expected values given the current weather patterns; although a rare event, the 1927 storm is consistent with the past century of weather observations.

Using the isoheytal maps for the 1927 storm, an estimate can be made of the minimum magnitude storm needed to initiate sediment deposition in Ritterbush Pond. The precipitation estimate for Ritterbush Pond during the 2-day 1927 storm is 7 inches (Kinnison, 1939). Given the same antecedent soil conditions (saturated) and sediment availability, 7 inches of rain over 2 days on saturated ground is capable of depositing a thin inorganic layer in the lake. The 1927 storm is just sufficient to generate slope failure according to the data compiled by Kochel (1990) (Figure 5.6).

Precipitation data are not available for Ritterbush Pond, but Burlington data can be used to estimate precipitation for the Ritterbush watershed. Burlington data underestimate the magnitude of precipitation events at Ritterbush Pond. Mean annual precipitation

Figure 5.6 Intensity-duration relationships for major debris-flow producing storms in the Appalachians, from Kochel (1990). Estimates of maximum intensity storms at Ritterbush Pond (Table 3.1) are plotted with asterisks and all estimates fall just within the envelope projected to generate slope failure on steep, forested hillsides.

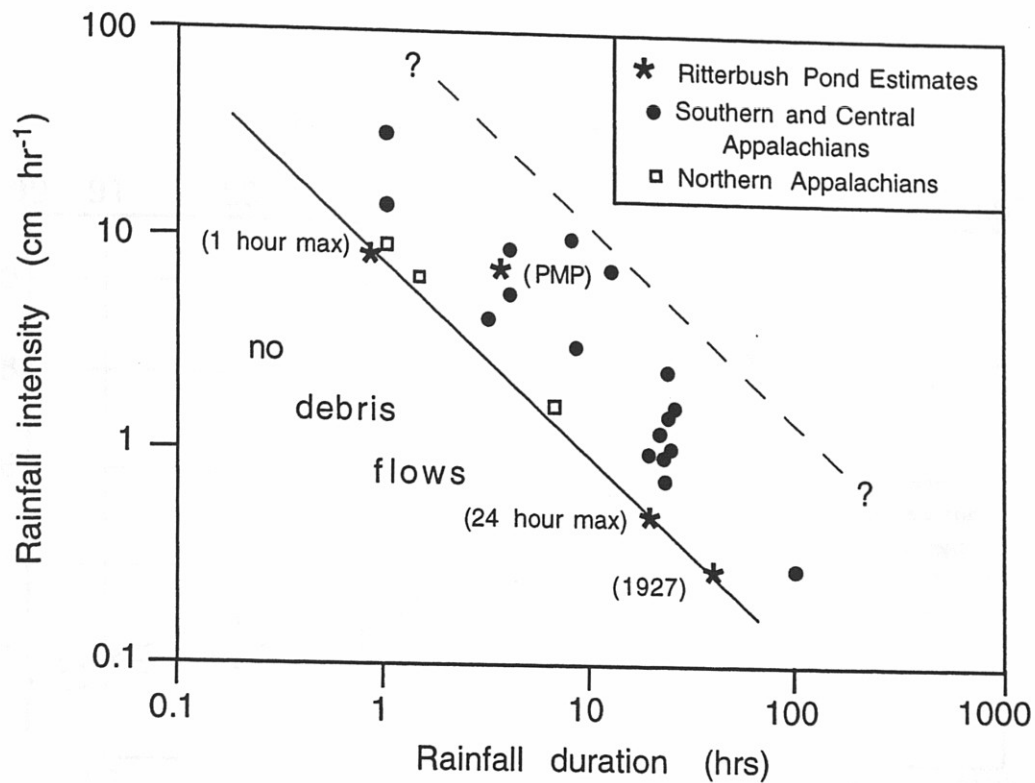


Figure 5.6 Intensity-duration relationship for major, debris-flow producing storms in the Appalachians, from Kocheil (1990). Estimates of maximum intensity storms at Ritterbush Pond (Table 5.1) are plotted with asterisks and all estimates fall just within the envelope projected to generate slope failure on steep, forested hillsides.

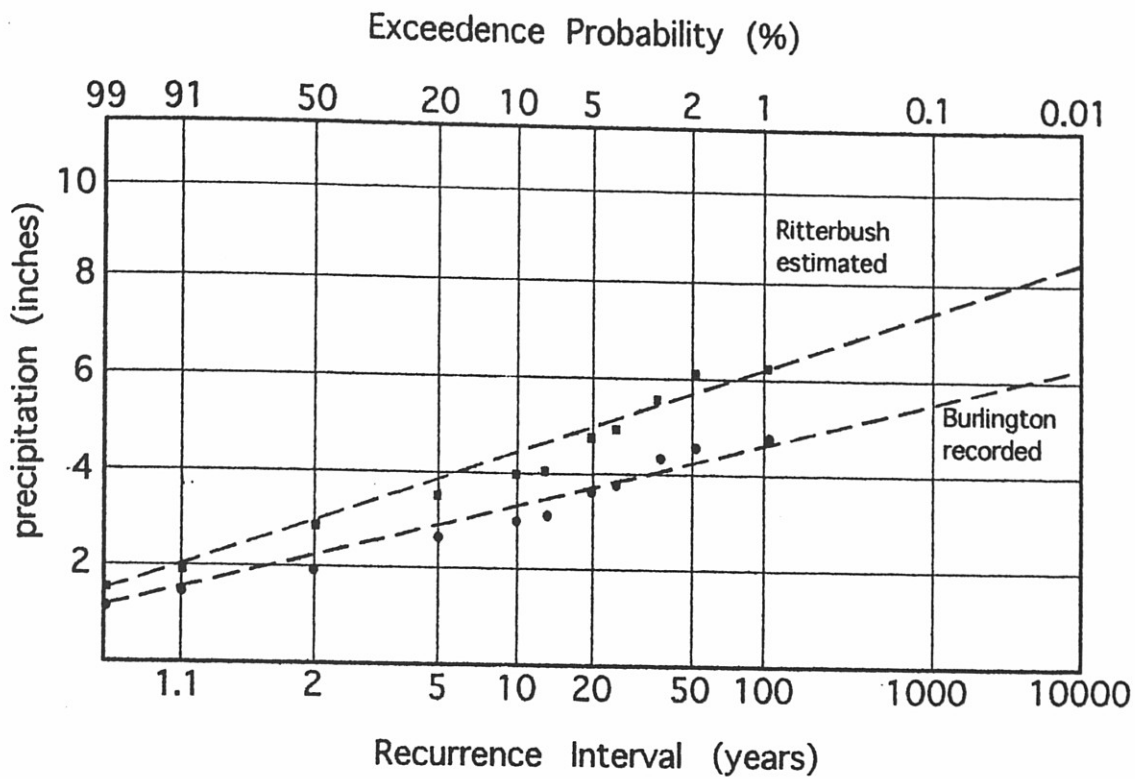


Figure 5.7 Extreme value distribution of 24-hour annual maximum precipitation data for Burlington (NWS, 1998). Burlington data are scaled by 35% to estimate Ritterbush Pond precipitation.

data from northeastern Vermont are positively correlated to elevation (Eq. 1) (NWS, 1998; Dunne and Leopold, 1978),

$$y = 0.0093x + 33.7 \quad (1)$$

where y = precipitation (inches)
 x = elevation (ft)

suggesting that Ritterbush Pond (1430 ft) receives 140% the precipitation of Burlington (320 ft). The isoheytal maps from the 1927 storm show maximum values along the axis of the Green Mountains (Kinnison, 1930); and Ritterbush Pond (7 in) received 130% of Burlington rainfall (5.5 in) during the 1927 storm. Therefore, for regional precipitation events, Ritterbush Pond probably receives 30% to 40% more precipitation on average than Burlington. By scaling the Burlington data by 35%, the magnitude of the 100 year, 24-hour storm is estimated for Ritterbush Pond as 7.2 inches (Figure 5.7).

Since localized, intense storms may also cause layer deposition in Ritterbush Pond, it would be useful to estimate their potential magnitude as well. When short duration precipitation data are unavailable for a specific location, Dunne and Leopold (1978) suggest that an estimate of maximum event magnitude can be made by doubling the recorded value from a nearby station. For example, in a small (<20 mi²), forested watershed in Ohio, the rainfall resulting from a short duration thunderstorm was carefully quantified (McGuinness and Harrold, 1965). Several gauges within the watershed recorded almost 4.5 inches in one hour, but the storm was not even recorded by the regional long-term weather station. The US Weather Bureau estimates for the region that the 1-hour, 100-yr storm event would produce approximately 2 inches of rain, less than half the maximum recorded during the event. Following the method and using Burlington precipitation data, doubling the 1-hour, 100-year storm event maximum of 2.1 inches (NWS, 1998) results in an estimate of 4.2 inches for the 100-year, 1-hour precipitation event at Ritterbush Pond. Each of the four estimates (1-hour, 6-hour, 24-hour and 48-hour) of the 100-year precipitation event (Table 5.1) for Ritterbush Pond plot within the envelope suggesting slope failure (Figure 5.6).

It is interesting to note, that the PMP event, had it occurred even once during the last 10,000 years (thus making it the 24-hour, 10,000-year event) would be inconsistent with the extreme value distribution (Figure 5.7), which estimates the 10,000 year storm would drop only 8.7 inches of precipitation at Ritterbush Pond. This may indicate that the conditions needed to produce the PMP are independent of average weather patterns. Thus, the PMP may be used as a maximum estimate of potential storm magnitude (19 inches in six hours), and the 1927 storm a minimum magnitude (7 inches in 2 days), needed to trigger the deposition of inorganic sediment layers in Ritterbush Pond.

5.3.3 The Ritterbush Chronology and Holocene Storm Patterns

The distinct characteristics of the even and odd intervals of the Ritterbush chronology suggest fluctuation between two sets of conditions, or regimes, that control storm frequency in the watershed. The odd intervals record storms of magnitude similar to the largest in Vermont's history; the events are usually separated by more than 200 years. This quiet regime includes interval III, during the warm Holocene hypsithermal, and interval I, containing the historic storm record. The even intervals constitute the noisy regime and record more frequent storms, often separated by as little as 50 years. Although it is more difficult to determine relative storm magnitude for the noisy regime, each event probably represents a storm equal to or larger than the 1927 storm, and smaller than the PMP event.

In Vermont, storm generation is controlled by the patterns of weather systems that have been highly variable during historic times (NOAA, 1982). The Ritterbush record may represent large storms that impact extensive areas (Vermont or New England) or an increase in localized thunderstorms. If the increase in storm activity during the noisy (even) intervals is due to larger scale changes in weather patterns then, 1) similar storm-generated erosion events might have occurred in other parts of New England, and 2) the

fluctuation in regime may represent shifting atmospheric or oceanic circulation that perturbs storm patterns over a wide area. Abrupt shifts in ocean circulation patterns are thought to have caused significant changes in climate, such as the Younger Dryas cooling event, at the close of the last glaciation (Broecker, 1997).

5.4 Comparison with Regional and Global Events

If the Ritterbush chronology reflects storm frequency and magnitude during the Holocene, two types of data can be used to assess the record in terms of changes in regional and global climate. First, individual layers in the chronology can be compared with other dated events linked to storms and/or climate change. Second, the fluctuation from noisy to quiet regime may be reflected by longer-term shifts in regional or global Holocene climate records. Acknowledging that the uncertainty of these comparisons increases with distance from the Ritterbush basin, I will evaluate the potential that the Ritterbush chronology reflects regional and global climatic events.

5.4.1 Regional Storm Events

A possible geomorphic record of storm events exists for alluvial fan sedimentation in the Huntington Valley, Vermont, 60 km southwest of Ritterbush Pond. The basal ages of the fans represent initiation of aggradation at approximately 8530, 7835, 2500, and 1900 ^{14}C yr BP (Bierman et al., 1997; Zehfuss, 1996; Church, 1997). The oldest ages occur within Ritterbush interval IV (10 cm and 2 cm layers, respectively), and the 2500 ^{14}C yr date corresponds with the base of interval II (9 cm layer). Given the uncertainty of both the fan and inorganic layer ages, the 1900 ^{14}C yr date falls at the end of interval II (1 cm layer). These four alluvial fans record decreased rates of aggradation during intervals III and IV, and a strong increase in aggradation associated with historic settlement. The coincidence of

alluvial fan initiation and two of the thickest layers in Ritterbush Pond suggests that the fans may be responding to the same large storm events.

5.4.2 Global Climatic Events

Episodic, inorganic sediment deposition has recently received increased attention as a climate proxy. Changes in the frequency, grain size, and thickness of inorganic deposits in lake sediments have been used in Chile (Lamy et al., 1998), Ecuador (Rodbell, 1997), Switzerland (Moscarriello et al., 1998), and Scotland (Cooper and Sullivan, 1998), to interpret changes in local sedimentation dynamics and for comparison with global climate records. Layers of inorganic sediment have been used to determine the frequency of monsoons in the South China Sea (Huang et al., 1997) and storms in Canada (Campbell, 1998) and New Zealand (Eden and Page, 1998). These records of storm frequency, with average recurrence intervals ranging from 6 to 1500 years, have all been explained by regional and global climate patterns, such as ENSO events, and changes in atmospheric and oceanic circulation.

A Holocene lake sediment core from coastal Alabama was interpreted to record Class 4 and 5 hurricane recurrence at 600 year intervals over the last 3200 ^{14}C yr (Liu and Fearn, 1993). The base of the 9-m sediment record was not dated, but the hurricane deposits were restricted to the upper 3.2 m of the core. Liu and Fearn (1993) suggest that tropical storm patterns different from today may have dominated during the mid-Holocene. In the Ritterbush Pond chronology, the mid-Holocene (interval III) also exhibits a lack of storm layers. A 7,000 cal yr flood frequency record from the upper Mississippi River also suggests a decrease in flood frequency and size during the mid-Holocene (Knox, 1993). The earlier portion of the record suggests that large floods may also have occurred prior to 6500 cal yr BP, correlative to interval IV of the Ritterbush Pond record.

Ice rafted debris (IRD) events, identified by Bond et al. (1997), are attributed to ocean surface cooling events in the North Atlantic and occur at 1400, 2800, 4200, 5900, 8100 and 9400 cal yr BP. Ritterbush Pond records individual layer deposition within ± 70 years for all but the earliest two events. The intervals of increased storm frequency, however, appear to fall between IRD events. The 8100 cal yr IRD event is hypothesized to correspond to a widespread drying event at 8200 cal yr identified in the GISP2 Greenland ice core (Alley et al., 1997). The layer deposited in Ritterbush Pond at 8170 cal yr BP is a couplet of 0.3 mm silt laminations, and is not a large event in the basin. The 8200 cal yr BP event is the most discrete Holocene event in the GISP2 core. Other smaller scale variations in the ice core record do not correspond to individual layers, or to the noisy intervals (Alley et al., 1997).

Other well documented Holocene climatic events, such as the Younger Dryas (approximately 12,000 cal yr BP), the Mediaeval Warm Period (810 to 750 cal yr BP) and the Little Ice Age (350 to 250 cal yr BP), fit models of climate fluctuation based on century-scale periodicity, although the origin of the apparent global cyclicity has not been identified (Campbell et al., 1998; Bond et al., 1997). The Younger Dryas may be represented at Ritterbush Pond by layer v, not included in the event chronology, but identified in Core RT-2 and Core 4. One layer was deposited during the Mediaeval Warm Period and one during the Little Ice Age, suggesting that storm frequency in Ritterbush probably has little correlation to these global climate events.

Regional and global-scale generalizations of climate change emphasize average conditions, such as temperature, rather than individual meteorologic events, such as storms and floods. The regional variation in hydrologic response to climate change makes it difficult to compare a single storm frequency record, where the relative magnitude of events is difficult to determine, to global trends. The compilation of a regional storm frequency record for the Holocene, that may be more easily compared to global records of climate

change, requires the development of additional storm-generated erosion records for the northeastern United States.

6.1 Summary of Findings

I conclude the following regarding terrestrial sediment deposition in Ritterbush Pond during the Holocene.

1. Inorganic layers (0.1 to 10 cm) of fine sand and silt represent rapid deposition of terrestrial material in Ritterbush Pond. The thickest of these layers cluster in three time intervals: prior to 8560 cal yr BP, from 6840 to 6340 cal yr BP, and from 2620 to 2025 cal yr BP.
2. Layer deposition is probably due to density currents reworking lake marginal sediments and transporting sediment delivered by streams toward the center of the lake. Correlation and apparent continuity of the layers between four cores suggests that transport events are large enough to deposit material throughout the basin.
3. The event chronology estimates the ages of 52 depositional events in Ritterbush Pond since 9440 cal yr BP. The thickest layers occur at 9440 (8450), 6830 (5980) and 2620 (2540) calendar (^{14}C) yr BP and probably represent the largest erosional events in the basin during the Holocene.
4. Gytja and organic carbon accumulation rates follow general regional climate trends. Accumulation rates increase as the climate warms until the mid-Holocene (hypsihermal), probably reflecting increasing primary productivity within the lake. As the climate becomes cooler and wetter toward the present, accumulation rates remain steady.
5. The most likely mechanism for inorganic layer deposition is large hydrologic events. The thickness of the inorganic layers is controlled by event magnitude and sediment availability. The apparent temporal spacing of the inorganic layers is

CHAPTER 6 - Conclusions

6.1 *Summary of Findings*

I conclude the following regarding terrestrial sediment deposition in Ritterbush Pond during the Holocene.

1. Inorganic layers (0.1 to 10 cm) of fine sand and silt represent rapid deposition of terrestrial material in Ritterbush Pond. The thickest of these layers cluster in three time intervals: prior to 8560 cal yr BP, from 6840 to 6340 cal yr BP, and from 2620 to 2025 cal yr BP.
2. Layer deposition is probably due to density currents reworking lake marginal sediments and transporting sediment delivered by streams toward the center of the lake. Correlation and apparent continuity of the layers between four cores suggests that transport events are large enough to deposit material throughout the basin.
3. The event chronology estimates the ages of 52 depositional events in Ritterbush Pond since 9440 cal yr BP. The thickest layers occur at 9440 (8450), 6830 (5980) and 2620 (2540) calendar (^{14}C) yr BP and probably represent the largest erosional events in the basin during the Holocene.
4. Gyttja and organic carbon accumulation rates follow general regional climate trends. Accumulation rates increase as the climate warms until the mid-Holocene (hypsothermal), probably reflecting increasing primary productivity within the lake. As the climate becomes cooler and wetter toward the present, accumulation rates remain steady.
5. The most likely mechanism for inorganic layer deposition is large hydrologic events. The thickness of the inorganic layers is controlled by event magnitude and sediment availability. The apparent temporal spacing of the inorganic layers is

influenced by event frequency and may also vary with the amount of gyttja erosion and redeposition associated with layer emplacement.

6. The storm size necessary to initiate layer deposition in Ritterbush Pond may be estimated using historical data. The minimum size event needed to trigger layer deposition is probably similar in size to the largest storm in Vermont's 100-yr precipitation record (1927). Seven inches of rain fell over a two-day period, and may be represented as the only <1 cm-layer in the last 350 years of the Ritterbush Pond record. The maximum probable rainfall (PMP) estimated for New England by the U.S. Weather Bureau is 19 inches of rain in 6 hours, which should destabilize the hillslopes at Ritterbush and result in significant terrestrial sediment deposition in the lake.
7. The Ritterbush watershed appears to have experienced two different hydrologic regimes during the Holocene. The predominant, quiet regime results in the deposition of inorganic layers ≤ 1 cm thick, such as the one apparently deposited by the 1927 storm. The noisy regime interrupts the quiet one with clusters of inorganic layers >1 cm thick, probably representing more frequent, larger storms prior to 8650 cal yr BP, from 6840 to 6430 cal yr BP, and from 2620 to 2024 cal yr BP.
8. Events extreme enough to deposit 10 cm of sand in Ritterbush Pond could be due to large, regional storm systems that initiate similar erosion in other watersheds, or intense localized thunderstorms that only affect the Ritterbush area. An alluvial fan in north-central Vermont records deposition correlative to the noisy regime (intervals II, VI) at Ritterbush Pond (Bierman et al., 1997), suggesting a regional increase in storms.
9. The change at Ritterbush Pond from a noisy to a quiet hydrologic regime, as represented by the clusters of inorganic layers, may indicate larger-scale fluctuations in oceanic and atmospheric circulation that shift regional storm patterns. A lack of similar high-resolution regional and global climate proxy records makes it difficult to assess the validity of this hypothesis.

6.2 *Suggestions for Future Research*

The data collected for this thesis were evaluated for use in answering specific questions regarding sediment deposition in Ritterbush Pond. The quality and applicability of the resulting data varied among analytical techniques. Basic analysis of some data sets provided sufficient information, but suggested that detailed investigation, beyond the scope of this thesis, would add more insight into sedimentation dynamics. I suggest the following methods or investigations for future research on Ritterbush Pond or lakes with similar inorganic layers:

1. Collecting surface cores that preserve the sediment / water interface and the upper, liquid half-meter of the sediment would increase the chance of preserving a detailed historic record. The upper meter of the core could also be used to investigate sedimentation dynamics. For example, recent sedimentation rates could be measured using ^{210}Pb and/or high-resolution (gamma-ray) density measurements.
2. Detailed measurement of the stable carbon and nitrogen isotope values, in the upper portion of the cores, may facilitate understanding the effects of the mixing of different types (aquatic and terrestrial) of organic matter, and subsequent decomposition and diagenesis, on the values measured for the gyttja and inorganic layers deeper in the core.
3. High-resolution paleomagnetic analysis may provide declination and inclination signals comparable to regional records for the Holocene. This would require removing oriented samples from the core at 1-cm intervals and performing extensive analyses, but has the potential to provide continuous age correlation for the cores. Paleomagnetic signals can also record the orientation of magnetic minerals, suggesting paleocurrent directions for inorganic layer deposition, and the amount and type of magnetic minerals present, providing a diagnostic test for source sediments with distinct magnetic signals.

4. Of the analytical techniques used, I would select the following to investigate cores with lithology similar to Ritterbush Pond cores.
- a) For detecting layers prior to opening the core, I would use magnetic susceptibility for low-resolution field identification and/or X-radiographs for high-resolution lab identification.
 - b) To characterize lithology and sedimentology of the layers and the gyttja, I recommend graphically logging and sampling the core.
 - c) For quantification of changes in lithology and organic matter source, I would perform elemental analysis (TOC and C/N). LOI provides comparable information only on organic carbon content.
5. Additional techniques that may detect changes of interest, but were not tested in this thesis include a) gamma-ray density analysis to provide a high-resolution density record for use in calculating accumulation rates, and b) detailed grain size analysis of the inorganic fraction of the gyttja to detect periods of high-flow (larger grains) not recorded by inorganic layer deposition.
6. Modeling of the spatial distribution of the layers within the lake (requiring additional cores) would allow for quantification of the amount of sediment deposited in the lake by a single event. Using hydrologic parameters, a) the streamflow needed to transport the sediment and b) the rainfall needed to produce the streamflow, could be calculated to estimate the size of event needed to deposit each layer.
7. In order to determine the extent of the hydrologic events initiating deposition in Ritterbush Pond, similar event records for the northeastern US need to be developed. The regional correspondence of the intervals of event deposition would suggest large-scale storm systems, or a regional increase in localized storms. With additional records, an investigation of the relationship between regional storm frequency and global climate would be more feasible.

REFERENCES CITED

- Aaby, B., and Berglund, B.E., 1986, Characterization of peat and lake deposits, in B.E. Berglund, ed., *Handbook of Holocene Palaeoecology and Palaeohydrology*: New York, Wiley and Sons, p.231-246.
- Adams, J., 1992, Paleoseismology: A search for ancient earthquakes in Puget Sound: *Science*, v. 258, p. 1592-1593.
- Allen, P.A., and Collinson, J.D., 1986, Lakes, in H.G. Reading, ed., *Sedimentary Environments and Facies*: Oxford, Blackwell Scientific Publications, p.63 - 72.
- Alley, R.B., Mayewski, P.A., Sowers, T., Stuiver, M., Taylor, K.C., and Clark, P.U., 1997, Holocene climatic instability: A prominent, widespread event 8200 yr ago: *Geology*, v. 25, p. 483-486.
- Almquist-Jacobson, H., Almendinger, J.E., and Hobbie, S., 1992, Influence of terrestrial vegetation on sediment-forming processes in kettle lakes of west- central Minnesota: *Quaternary Research* v. 38, p. 103 - 116.
- Anderson, R. S., Jacobson, G.L.Jr, Davis, R.B., and Stuckenrath, R., 1992, Gould Pond, Maine: late glacial transitions from marine to upland environments: *Boreas*, v. 21, p. 361 - 371.
- Axelsson, V., 1983, The use of X-ray radiographic methods in studying sedimentary properties and rates of sediment accumulation: *Hydrobiologia*, v. 103, p. 65-69.
- Babcock R.D., 1979, Soil survey of Lamoille County, Vermont: US Department of Agriculture p. 16 - 43, sheet no.5.
- Baldwin, B., 1971, Ways of deciphering compacted sediments: *Journal of Sedimentary Petrology*, v. 41, p. 293-301.
- Bengtsson, L., and Enell, M., 1986, Chemical analysis, in B.E. Berglund, ed., *Handbook of Holocene Palaeoecology and Palaeohydrology*: New York, Wiley and Sons, p. 423-454.
- Ben-Menahem, A., 1976, Dating of historical earthquakes by mud profiles of lake-bottom sediments: *Nature*, v. 262, p. 200-202.
- Bierman, P., Lini, A., Zehfuss, P, Church, A, Davis, P.T., Southon, J., and Baldwin, L., 1997, Postglacial ponds and alluvial fans: Recorders of Holocene landscape history: *GSA Today*, v. 7, p. 1-8.
- Bond, G., Showers, W., Cheseby, M., Lotti, R., Almasi, P., deMenocal, P., Priore, P., Cullen, H., Hajdas, I., and Bonani, G., 1997, A pervasive millennial-scale cycle in north Atlantic Holocene and glacial climates: *Science*, v. 278, p. 1257-1266.

- Bondevik, S., Svendsen, J.I., Johnse, G., Mangerud, J., and Kaland, P.E., 1997, The Storegga tsunami along the Norwegian coast, its age and runup: *Boreas*, v. 26, p. 29-53.
- Bouma, A.H., 1962, *Sedimentology of some flysch deposits*: Amsterdam, Elsevier Press, 168 p.
- Broecker, W.S., 1997, Thermohaline circulation, the Achilles Heel of our climate system: Will man-made CO₂ Upset the Current Balance?: *Science*, v. 278, p. 1582-1588.
- Campbell, C., 1998, Late Holocene lake sedimentology and climate change in Southern Alberta, Canada: *Quaternary Research*, v. 49, p. 96-101.
- Campbell, I.D., Campbell, C., Apps, M.J., Rutter, N.R., and Bush, A.B.G., 1998, Late Holocene ~1500 yr climatic periodicities and their implications: *Geology*, v. 26, p. 471-473.
- Church, A.E., 1997, Fan deposits in northwestern Vermont: Depositional activity and aggradation rates over the last 9500 years: University of Vermont Masters Thesis 113p.
- Clark, J.S., 1988, Stratigraphic analysis on petrographic thin sections: Application to fire history in northwest Minnesota: *Quaternary Research*, v. 30, p. 81 - 91.
- Coch, N.K., 1995, Hurricane hazards along the northeastern Atlantic coast of the United States: *Journal of Coastal Research Special Issue No. 12: Coastal Hazards*, p. 115-147.
- Connally, G., 1971, Discussion: Pleistocene mountain glaciation in northern Vermont. *Geological Society of America Bulletin*, v. 82, p. 1763-1766
- Cooper, M.C., and O'Sullivan, P.E., 1998, The laminated sediments of Loch Ness, Scotland: Preliminary report on the construction of a chronology of sedimentation and its potential use in assessing Holocene climatic variability: *Palaeogeography, Palaeoclimatology, Palaeoecology*, v. 140, p. 23-31.
- Davis, M.B., and Ford, M., 1982, Sediment Focusing in Mirror Lake, New Hampshire: *Limnology and Oceanography*, v. 27, p. 137-150
- Davis, M.B., Moeller, R.E., and Ford, J., 1984, Sediment focusing and pollen influx, in E.Y Haworth and J.W.G. Lund, eds., *Lake Sediments and Environmental History*, University of Minnesota Press, Minneapolis, p. 261-294.
- Davis, R. B., and Jacobson, G.L.Jr, 1985, Late glacial and early Holocene landscapes in northern New England and adjacent areas of Canada: *Quaternary Research*, v. 23, p. 341-368.
- Dearing, J.A., 1986 Core Correlation and total sediment influx in B.E. Berglund, ed., *Handbook of Holocene Palaeoecology and Palaeohydrology*: New York, Wiley and Sons, p.247-265.

- Delcourt, P.A., and Delcourt, H.R., 1984, Late Quaternary paleoclimates and biotic responses in eastern North America and the western North Atlantic Ocean: *Palaeogeology, Palaeoclimatology, Palaeoecology*, v. 48, p. 263-284.
- Doll, C., 1961, Centennial Map of Vermont: Vermont Geological Survey.
- Donahue, D.J., Linick, T.W., and Jill, A.J.T., 1990, Isotope-ratio and background corrections for Accelerator Mass Spectrometry radiocarbon measurements: *Radiocarbon*, v. 32, p. 135-142.
- Dunne, T., and Leopold, L.B., 1978, *Water in Environmental Planning*: New York, W.H. Freeman and Company, p.33-71.
- Ebel, J.E., Bedell, R., and Urzua, A., 1995, A report of the seismic vulnerability of the state of Vermont: Vermont Emergency Management Agency.
- Eden, D.N., and Page, M.J., 1998, Paleoclimatic implications of a strom erosion record from late Holocene lake sediments, North Island, New Zealand: *Palaeogeography, Palaeoclimatology, Palaeoecology*, v. 139, p. 37-58.
- Fetter, C.W., 1994, *Applied Hydrogeology*: New York, Macmillan College Publishing Company, p 47-70.
- Fogel, M.L., and Cifuentes, L.A., 1993, Isotope fractionation during primary production in Engel, M.H., and Macko, S.A., eds., *Organic Geochemistry*: New York, Plenum Press, p. 73-81.
- Gorsline, D.S., 1984, A review of fine-grained sediment origins, characteristics, transport and deposition, in Stow, D.A.V. and Piper, D.J.W., eds., *Fine-Grained Sediments: Deep-Water Processes and Facies*, Geological Society Special Publication No 15, Oxford, Blackwell Scientific Publications, p. 17-34.
- Hershfield, D.M., and Kohler, M.A., 1960, An empirical appraisal of the Gumbel extreme-value procedure: *Journal of Geophysical Research*, v. 65, p. 1737-1746.
- Hershfield, D.M., and Wilson, W.T., 1960, A comparison of extreme rainfall depths form tropical and nontropical storms: *Journal of Geophysical Research*, v. 65, p. 959-982.
- Hilton, J., 1985, A conceptual framework for predicting the occurrence of sediment focusing and sediment redistribution in small lakes: *Limnology and Oceanography*, v. 30, p. 1131-1143.
- Horne, A.J., and Goldman, C.R., 1994, *Limnology*: New York, McGraw-Hill, Inc., p 14-25.
- Huang, C.Y., Liew, P.M., Zhao, M., Chang, T.C., Kuo, C.M., Chen, M.T., Wang, C.H. and Zheng, L.F., 1997, Deep sea and lake records of the Southeast Asian paleomonsoons for the last 25 thousand years: *Earth and Planetary Science Letters*, v. 146, p. 59-72.
- Jackson, S.T., and Whitehead, D.R., 1991, Holocene vegetation patterns in the Adirondack Mountains: *Ecology*, v. 72, p. 641-653.

- King, J.W., Banerjee, S.K., Marvin, J., and Lund, S., 1983, Use of small-amplitude paleomagnetic fluctuations for correlation and dating of continental climatic changes: *Paleogeography, Paleoclimatology, Paleoecology*, v. 42, p. 167 - 183.
- Kinnison, H.B., 1930, The New England Flood of November, 1927, US Water Supply Paper 636.
- Knox, J.C., 1993, Large increases in flood magnitude in response to modest changes in climate: *Nature*, v. 361., p. 430-432.
- Kochel, R.C., 1990, Humid Fans of the Appalachian Mountains in Rachocki and Church eds., *Alluvial Fans: A Field Approach*, Wiley and Sons, Ltd., p. 109-129.
- Krishnamurthy, R.V., Bahattacharya, S.K., Kusumgar, S., 1986, Paleoclimatic changes deduced from $^{13}\text{C}/^{12}\text{C}$ and C/N ratios of Karewa lake sediments, India: *Nature*, v. 323, p. 150-152.
- Kuenen, P.H., and Menard, H.W., 1952, Turbidity currents, graded and non-graded deposits: *Journal of Sedimentary Petrology*, v. 22, p. 83-96.
- Kuenen, P. H., and Migliorini, C.I., 1950, Turbidity currents as a cause of graded bedding: *The Journal of Geology*, v. 58, p. 91 - 127.
- Kull, C.A., and Magilligan, F.J., 1994, Controls over landslides distribution in the White Mountains, New Hampshire: *Physical Geography*, v. 15, p. 325-341.
- Lamy, F., Hebbeln, D. and Wefer, G., 1998, Late Quaternary precessional cycles of terrigenous sediment input off the Norte Chico, Chile and palaeoclimatic implications: *Palaeogeography, Palaeoclimatology, Palaeoecology*, v.141, p. 233-251.
- Lehman, J. T., 1975, Reconstructing the rate of accumulation of lake sediment: The effect of sediment focusing: *Quaternary Research* v. 5, p. 541-550.
- Lini, A., 1997, Isotopic records in lake sediments as indicators for landscape and biotic response to Holocene climate change: *GSA Abstracts with Programs*, v. 29, p A-171.
- Lini, A., Bierman, P.R., Lin, L., and Davis, P.T., 1995, Stable carbon isotopes in post-glacial lake sediments: A technique for timing the onset of primary productivity and verifying AMS ^{14}C dates: *GSA Abstracts with Programs* v. 27, p. A-58.
- Lin, L., 1996, Environmental changes inferred from pollen analysis and ^{14}C ages of pond sediments, Green Mountains, Vermont: University of Vermont Masters Thesis 125p.
- Lin, L., Bierman, P.R., Lini, A., and Spear, R.W., 1995, New AMS ^{14}C ages and pollen analyses constrain timing of deglaciation and history of revegetation in northern New England: *GSA Abstracts with Programs*, v. 27, p. A-58.
- Liu, K., and Fearn, M.L., 1993, Lake-sediment record of late Holocene hurricane activities from coastal Alabama: *Geology*, v. 21, p. 793 - 796.

- Loso, M.G., Schwartz, H.K., Wright, S.F., and Bierman, P.R., 1998, Composition, morphology, and genesis of a moraine-like feature in the Miller Brook valley, Vermont: *Northeastern Geology*.
- Ludlam, D., 1996, *The Vermont Weather Book*, Montpelier Vermont, the Vermont Historical Society, 302p.
- Ludlam, S.D., 1974, Fayetteville Green Lake, New York: The role of turbidity currents in lake sedimentation: *Limnology and Oceanography*, v. 19, p. 656-664.
- Lund, S.P., 1993, Paleomagnetic secular variation: Trends in *Geophysical Research*, v.2 p. 423-438.
- Lund, S.P., 1996, A comparison of Holocene paleomagnetic secular variation records from North America: *Journal of Geophysical Research*, v. 101, p. 8007-8024.
- McGuinness, J.L., and Harrold, L.L., 1965, Role of storm surveys in small watershed research: *Water Resources Research*, v. 1, p. 3-28.
- Mehrtens, C.J., 1988, Bioclastic Turbidites in the Trenton Limestone: Significance and Criteria for Recognition in Brian Keith eds., *The Trenton Group of Eastern North America: Deposition, Diagenesis and Petroleum*, AAPG Study #29, p. 87-112.
- Meyer, G.A., and Wells, S.G., 1997, Fire-related sedimentation events on alluvial fans, Yellowstone National Park, USA: *Journal of Sedimentary Research*, v. 67, p. 776-791.
- Meyers, P. A., and Ishiwatari, R., 1995, Organic matter accumulation records in lake sediments in A. Lerman, and Gat, J., eds., *Physics and Chemistry of Lakes*: New York, Springer - Verlag p. 279 - 290.
- Meyers, P.A., Takamura, K., Horie, S., 1993, A reinterpretation of late Quaternary sediment chronology of Lake Biwa, Japan, from correlation with marine glacial-interglacial cycles: *Quaternary Research*, v. 39, pg. 154-162.
- Middleton, G. V., 1966, Experiments on density and turbidity currents: *Canadian Journal of Earth Sciences*, v. 1, p. 477-505.
- Millspough, S.H., and Whitlock, C., 1995, A 750-year fire history based on lake sediment records in central Yellowstone National Park, USA: *The Holocene*, v. 5, p. 283-292.
- Moscariello, A., Schneider, A.M., and Filippi, M.L., 1998, Late glacial and early Holocene palaeoenvironmental changes in Geneva Bay: *Palaeogeography, Palaeoclimatology, Palaeoecology*, v. 140, p. 51-73.
- Nelson, C.H., 1982, Modern shallow-water graded sand layers from storm surges, Bering shelf: A mimic of Bouma sequences and turbidite systems: *Journal of Sedimentary Petrology*, v. 52, p. 537-545.
- Nelson, D.E., Vogel, J.S., Southon, J.S., and Brown, T.A., 1986, Accelerator radiocarbon dating at SFU: *Radiocarbon*, v. 28, p. 215-222.

- Niemi, T.M., and Ben-Avraham, Z., 1994, Evidence for Jerico earthquakes from slumped sediments of the Jordan River delta in the Dead Sea: *Geology*, v. 22, p. 395-398.
- NOAA (national Oceanic and Atmospheric Administration), 1982, *Climate of Vermont: Climatography of the United States No. 60*.
- NWS (National Weather Service), 1998, 24-hour annual maximum data, unpublished.
- Olsson, I.U., 1986, Radiometric dating, in Stow, D.A.V. and Piper, D.J.W., eds., *Fine-Grained Sediments*, Geological Society Special Publication No 15, Oxford, Blackwell Scientific Publications, p. 273-297.
- Ouellet, M., 1997, Lake sediments and Holocene seismic hazard assessment within the St. Lawrence Valley, Quebec: *GSA Bulletin*, v. 109, p. 631-642.
- Peck, J.A., King, J.W., Colman, S.M., and Kravchinsky, V.A., 1996, An 84-kyr paleomagnetic record from the sediments of Lake Baikal, Siberia: *Journal of Geophysical Research*, v. 101, p. 11365-11385.
- Pestiaux, P., Van de Mersch, I., Berger, A., and Duplessy, J.C., 1988, Paleoclimate variability at frequencies ranging from 1 cycle per 10000 yers to 1 cycle per 1000 years: Evidence for non-linear behaviour of the climate systems: *Climatic Change*, v. 12, p. 9-37.
- Peteet, D. M., Vogel, J.S., Nelson, D.E., Southon, J.R., Nickman, R.J., and Heusser, L.E., 1990, Younger dryas climatic reversal in northeastern USA? AMS ages for an old problem: *Quaternary Research*, v. 33, p. 219 - 230.
- Piper, D.J.W., 1972, Turbidite origin of some laminated mudstones: *Geology Magazine*, v. 109, p. 115 - 126.
- Pizzuto, J.E., Schwendt, A.E, 1997, Mathematical modeling of autocompaction of a Holocene transgressive valley-fill deposit, Wolfe Glade, Delaware: *Geology*, v.25, p. 57-60.
- Reasoner, M. A., 1993, Equipment and procedure improvements for a lightweight, inexpensive, percussion core sampling system: *Journal of Paleolimnology* v. 8, p. 273 - 281.
- Ridge, J.C., Brennan, W.J., Muller, E.H., 1990, The use of paleomagnetic declination to test correlation of late Wisconsinan glaciolacustrine sediments in central New York: *Geological Society of America Bulletin*, v. 102, p. 26-44.
- Ritter, D.F., Kochel, R.C., and Miller, J.R., 1995, *Process Geomorphology*: Boston, Wm. C. Brown Publishers, p 137-190.
- Rodbell, D.T., 1997, Sedimentology and paleoclimatological significance of a laminated lacustrine sediment core from a glacial lake in southern ecuador: *GSA Abstracts with Programs*, v. 29, p. A-34.
- Sadler, P.M., 1982, Bed-thickness and grain size of turbidites: *Journal of Sedimentology*, v. 37, p. 746-761.

- Shanmugan, G., The Bouma Sequence and the turbidite mind set: *Earth-Science Reviews*, v. 42, p. 201-229.
- Spear, R. W., 1989, Late-Quaternary History of High Elevation Vegetation in the White Mountains of New Hampshire: *Ecological Monographs*: v. 59, p. 125 - 151.
- Spear, R. W., 1993, The palynological record of Late Quaternary arctic tree-line in northwest Canada: *Review of Paleobotany and Palynology*, v. 79, p. 99 - 111.
- Spear, R. Davis, M.B., and Shane, L.C., 1994, Late Quaternary history of low- and mid-elevation vegetation in the White Mountains of New Hampshire: *Ecological Monographs*, v. 64, p. 85-109.
- Sperling, J. A., Wehrle, M.E., and Newman, W.S., 1989, Mountain Glaciation at Ritterbush Pond and Miller Brook, Northern Vermont, Reexamined: *Northeastern Geology* v. 11, p. 106 - 111.
- Stewart, D.P., 1971, Discussion: Pleistocene mountain glaciation in northern Vermont. *Geological Society of America Bulletin*, v. 82, p. 1759-1760.
- Stuiver, M., 1974, Climate versus changes in ^{13}C content of the organic component of lake sediments during the late Quaternary: *Quaternary Research* v. 5, p. 251-262.
- Stuiver, M., and Reimer, P., 1993, Extended ^{14}C database and revised CALIB 3.0 ^{14}C age calibration program: *Radiocarbon*, v. 35, p. 215-230.
- Thompson, R., 1984, A global review of paleomagnetic results for wet lake sediments, in E.Y Haworth and J.W.G. Lund, eds., *Lake Sediments and Environmental History*, University of Minnesota Press, Minneapolis, p. 145-164.
- Thompson, W.B., Folwer, B.K., Flanagan, S.M., and Dorian, C.C., 1996, Recession of the late Wisconsinan ice sheet from the northwestern White Mountains, New Hampshire in M.R. Van Baalen, eds., *Guidebook to Field Trips in Northern New Hampshire and Adjacent Regions of Maine and Vermont*: Harvard Printing and Publications p. 203 - 234.
- Tyler, R.E., 1997, Radiocarbon dating in Aiken and Tyler, eds., *Chronometric Dating in Archaeology*: New York, Plenum Press, p. 65-96.
- US Weather Bureau, 1955, Rainfall intensity-duration-frequency curves for selected stations in the United States, Alaska, Hawaiian Islands and Puerto Rico: Technical Paper 25.
- US Weather Bureau, 1956, Seasonal variation of the probably maximum precipitation east of the 105th meridian for areas from 10 to 1000 sq miles and duration of 6, 12, 24 and 48 hours: *Hydrometeorological Report* 33.
- US Weather Bureau, 1959, Rainfall intensity-frequency regime: Part IV, Northeastern United States: Technical Paper 29.

- US Weather Bureau, 1961, Rainfall frequency atlas of the United States: Technical Paper 40.
- Van Weering, T.C.E., and Van Iperen, J., 1984, Fine-grained sediments of the Zaire deep-sea fan, southern Atlantic Ocean in Stow, D.A.V. and Piper, D.J.W., eds., *Fine-Grained Sediments: Deep-Water Processes and Facies*, Geological Society Special Publication No 15, Oxford, Blackwell Scientific Publications, p. 95-114.
- Vaughan, A., and Nichols, G., 1995, Controls on the deposition of charcoal: Implications for sedimentary accumulations of fusain: *Journal of Sedimentary Research*, v. A65, p. 129-135.
- Verosub, K.L., 1977, Depositional and post-depositional processes in the magnetization of sediments: *Reviews in Geophysics and Space Science*, v. 15, p. 129-143.
- Wagner, W.P., 1970, Pleistocene Mountain Glaciation, Northern Vermont: *Geological Society of America Bulletin*, v. 81, p. 2465-2470.
- Walker, R.G., 1967, Turbidite sedimentary structures and their relationship to proximal and distal depositional environments: *Journal of Sedimentary Petrology*, v. 36, p. 25-43.
- Webb, T., Bartlein, P.J., Harrison, S.P., and Anderson, K.J., 1993, Vegetation, lake-levels, and climate in eastern North America for the past 18000 years, in Wright H.E., et al., eds., *Global climates since the last glacial maximum*: Minneapolis, University of Minnesota, p. 415-467.
- Whitlock, C., and Millspaugh, S.H., 1996, Testing the assumptions of fire-history studies: an examination of modern charcoal accumulation in Yellowstone National Park, USA: *The Holocene*, v. 6, p. 7-15.
- Williams, G.P., and Guy, H.P., 1973, Erosional and Depositional Aspects of Hurricane Camille in Virginia, 1969: Geological Survey Professional Paper 804, Washington, US Government Printing Office.
- Winkler, M.G., 1985a, A 12,000 - year history of vegetation and climate for Cape Cod, MA: *Quaternary Research* v. 23, p. 305 - ??.
- Winkler, M.G., 1985b, Charcoal analysis for paleoenvironmental interpretation: A chemical assay: *Quaternary Research*, v. 23, p. 313 - 326.
- Winkler, M.G., 1994, Sensing plant community and climate change by charcoal-carbon isotope analysis: *Ecoscience*, v. 1, pg. 340-345.
- Wohlfarth, B., Bjorck, S., Possnert, G., Lemdahl, G., Brunnberg, L., Ising, J., Olsson, S. and Svensson, N.O., 1993, AMS dating Swedish varved clays of the last glacial/interglacial transition and the potential/difficulties of calibrating Late Weichselian 'absolute' chronologies: *Boreas*, v. 22, p. 113-128.

- Wright, S.F., Whalen, T.N., Zehfuss, P.H., and Bierman, P.R., 1997, Late Pleistocene-Holocene history: Huntington River and Miller Brook Valleys, northern, Vermont, in Grover, T.W. et al., eds., Guidebook to field trips in Vermont and adjacent New Hampshire and New York: Castleton State College, p. C41-30.
- Zehfuss, P.H., 1996, Alluvial fans in Vermont as recorders of changes in sedimentation rates due to reforestation: University of Vermont Senior Thesis, 71 p.
- Zijerveld, J.D.A., 1967, Demagnetization of rocks: Analysis of results in Collinson D.W. et al., eds., Methods in Paleomagnetism: Amsterdam, The Netherlands, Elsevier Scientific Publishing Company, p. 254-286.

APPENDIX A: Field Procedures

SURVEYING

Materials

Pentax electronic total station
tripod
triple prism
prism rod
flags (for marking hole locations)

Procedure

1. Set up tripod and total station so that total station is centered and level over the benchmark. The benchmark is a steel post on the south shore of the lake 2 m to the east of a wooden dock and boat launch. This is the first access to the pond from the main trail.
2. Zero set North as far corner of cabin across the pond, set bench coordinates at (1000, 1000). This is a project North, not true North.
3. Survey desired locations, recording northing, easting, and hole or core number.

BATHYMETRY and SEDIMENT PROBING

Materials

hand auger (with extra blades, alan key and blade sharpener)
30 meter measuring tape with weight
magnesium/zirconium rods
probe point
propane torch

Procedure

Bathymetry

1. Auger hole in ice
2. Lower measuring tape slowly. When it stops, note depth to top of ice
3. Survey location of hole (or mark for later surveying).

Sediment Thickness

1. Attach probe point to the female end of a rod.
2. Lower lengths of rod, screwing each on securely. (Many need to use the propane torch to remove ice from threads; propane must be kept warm to work)
3. Keep track of how many rods are lowered (and their length)
4. Keep the rods as close to vertical as possible!
5. Once in the sediment, push rods using full body weight. Do not push too quickly or too hard; the rods will bow out in the water since they are not cased.
6. When there is no longer any net motion downward, measure down from the end of the last rod to the top of the ice and subtract from the rod length lowered to determine total rod length.
7. Record water depth and total rod length.
8. Pull rods back out, again counting each rod to check measurement.
9. Separate the rods as they come out. If the joints are iced over, use the propane torch.
10. Survey in location of hole (or mark for later surveying).

CORING

Materials

Reasoner Corer

1. Core barrel - attachment holes drilled, core catcher/piston installed
 2. Core head - pull rope, bolts and wingnuts
 3. Core driver (pig) - filled with sand or rocks, pull rope
- Piston - wire cable, frummer clamps, vise grips, wrenches, wire cutters and deadman (with webbing and keeper string) (rod to set the piston if needed)
- Pulley system - 6 carabeaners, 6 pulleys and 2 jumars and deadman (with webbing and keeper string)
- Permanent marker, paper and cloth towels, end caps, duct tape, ice auger, gloves

Preparation

Core barrel

1. Obtain desired length of PVC pipe with 3.5" (9 cm) outer diameter. The pistons are designed for an 8 cm inner diameter pipe. A ten foot length of 3" PVC potable with bell and flange ends has been used successfully. Schedule 40 PVC is thicker walled, with an ID of 7.5 cm, which makes setting the piston extremely difficult and is not recommended.
2. Fit core barrel into core head and drill 1/4" holes to attach with bolts in field; mark core barrel where it meets the core head and opposite the black arrow.
3. Mark core barrel in 0.5 m intervals from the bottom up; draw a continuous line down the length of the barrel to allow for realignment once it has been cut. Add arrowheads pointing up (top up) to the continuous line.

Core catcher installation

1. Trace the pattern onto sheet aluminum and cut out; do not use the pattern!
2. Bend the teeth slightly inward to check that they will close properly
3. Insert the catcher, teeth first, into the bottom of the barrel and fold back to the outside of the barrel (cutting with snips where necessary) to secure.
4. Drill 1/4" holes through both layers of sheeting and core barrel
5. Place rivets in holes and pop rivet the core catcher in place
6. Wrap exposed sheeting thoroughly in duct tape

Setting the piston

1. Make sure piston cable is securely fastened to piston (with a frummer) and that all components of the piston are properly attached and tightened.
2. Grease the rubber stoppers lightly with silicon grease.
3. Loosen the nuts on either side of both of the stoppers (need two wrenches)
4. Tighten the lower stopper first, until it fits snugly (almost too tight)
5. Thread the piston cable through the barrel and repeat step 4 for the upper stopper
6. Set the piston such that the lower stopper is flush with the end of the core barrel.

note: if the core catcher is already installed, the piston will need to be pushed down from the top of the barrel.

Comments

This corer is designed for deep water. The length of the head, driver and barrel. A metal core catcher, would be used. aluminum sheeting. The 3/4" diameter endcaps would be used (tightly) even without a core catcher.

Coring Procedure

Preparation

1. Auger an oversized hole (three auger holes) for core. Measure and record water depth.
2. Auger two holes for deadmen: one close to core hole for piston, one 40 ft away for pulley. Deadmen should be set in these holes and tied off to sleds, toolboxes, etc.
3. Check that piston is set tightly and core catcher installed (if desired).
4. Attach the core head with bolts and wignuts.
5. From the bottom of the barrel, measure up the water depth and mark (with tape or marker) both the piston cable and core head rope (1st mark)
6. A second mark should be made on the core head rope to determine when to stop driving the core. This mark should be at most the water depth plus the length of the core barrel, minus 20cm for the length of the piston and the overlap of the head and barrel.
7. Using a hand pump or waterbottles, fill barrel at least half full with water to weigh down the piston and keep it from being buoyed up.
8. Tape piston and rope together to check for slippage while setting the core barrel.
9. Survey in location of hole (or mark for later surveying).

Setting and driving the core

1. Lower core barrel down hole several meters, but not so the lower end touches the lake bottom.
2. Feed piston cable and head rope through center of the driver. Put driver in hole and hold it just below ice.
3. Keep all lines separate!
4. Lower to the FIRST mark (sediment water interface). Check for slippage. If there was no slippage remove tape and proceed. If there was slippage, pull up core and start over.
5. Clamp off piston cable with vice grips to deadman.
6. Carefully lower driver and set core into the sediment with several gentle drops.
7. Drive core in short frequent drops until 2nd mark is reached, the core ceases to move, or a double bounce is consistently felt.

Retrieving the core

1. Pull out driver and remove from piston cable and head rope.
2. Set up pulley system on head rope (see diagram), starting with 4 pulleys.
3. Loosen piston cable.
4. Pull on head rope. If there is a lot of resistance, add pulleys for mechanical advantage OR put tension on the rope wait 10-15 minutes until trying to pull.
5. When the first mark is reached, pull up quickly through water column.
6. Catch under core with hand and endcap. If there is a core catcher and the endcap will not fit, quickly wipe the end clean and wrap with duct tape.
7. Cut piston cable OR saw top of barrel containing piston and cap top.
8. Cut core into <1.5 m lengths using PVC saw. Have endcaps and towels ready.
9. Cap and tape each section, and label with core name and section number.
9. If cores are at risk for freezing, wrap with webbing to hang from deadman in water until ready to transport out.

Comments

This corer is designed for deep water; can be modified for shallow water by decreasing the length of the head, driver and barrel. A tripod would be very helpful with core retrieval. A reusable, metal core catcher, would be easier, and probably more efficient, than the corecatchers cut from aluminum sheeting. The 3 3/4" endcaps do not fit over the end with the core catcher, larger diameter endcaps would be useful if a corecatcher is used. The piston works well (if it is set tightly) even without a core catcher, although the lowest 10 cm of material may be lost.

Procedure

Cleaning

1. Scrape the surface of the core clean with a spatula, being careful to scrape across the core and clean the spatula well with DI water to minimize contamination.
2. Remove any obvious pieces of sediment from the core.
3. Place the core in the core rack.

APPENDIX B: Lab Procedures

CORE PROCESSING

Splitting

Materials

splitting rack (2 x 4's on plywood with saw guide and shims)
circular saw, blade set to 1/4"
safety glasses, ear protection
long (splitting) knife, exacto knife and duct tape
meter stick or tape measure, permanent marker
plastic wrap, roll plastic and heat sealer
paper towels, DI water

Procedure

1. Mark the core for splitting by wrapping a 8.5" by 11" piece of paper (creased in half) around one end of the core and marking where the ends meet and at the crease. These two marks should be on a diameter of the core.
2. Make sure both halves of the core will be labeled after splitting
3. Place core in splitter with one of the cutting marks facing up. Shim in place.
4. Set the circular saw against the guard and be sure the mark lines up in the sight
5. Cut down one side of the core. Stop and readjust blade if it does not go all the way through the PVC or if it goes too deep.
6. Run a piece of duct tape over the cut to hold it together while cutting the other side
7. Remove the shims, flip the core over and line up the second mark. Cut down the side.
8. Take core out of splitter being careful to hold it together.
9. Cut through endcaps and duct tape with the exacto knife.
10. Rotate the core so that the duct tape is on the bottom and the open cut on the top. Split the core by gently sliding the knife into the sediment.
11. Rotate the core so that the knife is horizontal and lift the knife (and half of the core) up and off of the lower half of the core.
12. Slice the duct tape holding the two halves together and clean an edge of the PVC.
13. Using the ruler, mark both halves of the core at 10 cm intervals.
14. Wrap one half of the core in 2 layers of plastic wrap.
15. Seal in a plastic bag, being sure the core name, section, up direction, depth and length are noted on the outside.
16. Refrigerate at 4°C.

CORE PROCESSING

Logging

Materials

spatulas (scraping and sampling), paper towels, DI water
metersticks (at least 2)
labels for core name, section and meter depth
core rack (gray 2 x 4's on white pressboard)
photo stand with daylight bulbs, Kodak color chart
camera and 35mm film
video camera and Hi8 film
graph paper, colored pencils, small ruler
grain size card, hand lens

Procedure

Cleaning

1. Scrape the surface of the core clean with a spatula, being careful to scrape across the core and clean the spatula well with DI water to minimize contamination.
2. Remove any obvious pieces of shredded PVC.
3. Place the core in the core rack on the photo stand.

Photo and Video Log

1. Place camera on photo stand. Mark where the frame of the camera falls on the stand.
2. Starting from the top, line up a section of the core (about 25-30 cm) within the frame.
3. Place a ruler directly next to the core at the appropriate cm depth, and label the meter depth (1-6).
4. Make sure the ruler, color chart and label fit into the picture.
5. Turn on the daylight bulbs.
6. Adjust camera against a grayscale card.
7. Take a picture and slide the core 20-25 cm. Adjust the ruler and make sure there is overlap between pictures. Repeat for entire length.
8. Turn off the daylight bulbs, remove camera.
9. For video log, place the video camera on the stand and repeat the above steps, leaving the camera on while the core is moved.

Graphic Log

1. Set up graph paper with a stratigraphic column (1 inch = 10 cm), grain size column and leave plenty of room for notes. Note core name, section and date.
2. Make a general description of the dominant sediment facies (gyttja), including grain size, color, sediment type, and texture (density).
3. Working up or down the core, cm by cm, describe
 - a) general changes in, or characteristics of, gyttja.
 - b) distinct layers (gyttja or minerogenic), color, thickness and grain size.
 - c) the boundary between changes in sediment type (sharp, gradational).
 - d) the presence of macrofossils or other particles.

CORE PROCESSING*

Sampling

Materials

plastic or glass 20 ml bottles and caps
permanent markers and/or labels
sampling spatula, semi-circular knives
kimwipes, napkins
DI water
meter sticks

Procedure

1. Prior to sampling, label bottles with core name and depth interval
2. Starting from the top and working down, insert semi-circular knives at 1 cm intervals.
3. Scoop out the sediment between each pair of knives into the prepared bottle and cap.
4. Wash knives and spatula in DI water between samples to avoid contamination.
5. Remove large macrofossils and place in separate, labeled bottle or wrap in aluminum foil and seal in a plastic bag.
6. At thick inorganic horizons, adjust the sampling interval to reflect the location of the boundary.
7. Note any observations, such as the exact location of macrofossils, on the graphic log.
8. Refrigerate all samples at 4°C.

MAGNETIC SUSCEPTIBILITY

Sapphire

Materials

Magnetic coil and power box
IBM compatible computer, software disk
core rack (2 X 4's with dowels, shims, bolts and nuts)
permanent marker, measuring tape

Procedure

1. Allow core to come to room temperature for best results. This apparatus works best for whole cores. If half cores are used they should be unwrapped.
2. Mark core at 3 cm intervals from top down - (3 cm is the width of the coil). If the core is longer than 150 cm, it must be logged in 2 separate runs.
3. Assemble rack, place coil in the center of the rack, shim to hold in place.
4. Load software. Set CMS logging mode to fast, input core segment name and info.
5. Position core on rack, with top of core closest to coil, but about 50 cm away.
6. Begin measurements with a FREE AIR measurement with the core out of the coil, by pressing the coil button.
7. The computer will beep when it has completed each measurement; slide the core through at the intervals marked and depress the button each time.
8. When the segment is complete, or 50 measurements have been taken, remove the core and take a second FREE AIR measurement. Then press 9 to end the segment.
9. Repeat as necessary
10. Run each segment at least twice to calculate statistical error.
11. Download data (text file) to spreadsheet or graphing program.

MAGNETIC SUSCEPTIBILITY

Bartington

Materials

Automatic core logging system with coil and meter
IBM compatible computer and software

Procedure

1. Allow core to come to room temperature for best results.
2. Turn on computer and meter, let warm up for 1 hour.
3. Keep metal or other magnetic things away from the coil during the run.
4. Input core length, resolution (0.01) and interval (1 cm). Make sure to give each file a unique name.
5. Place core in boat, top closest to coil.
6. Initiate run. The computer will move the core at the specified interval and take free air measurements before and after the run that can be used to correct for drift.
7. Download data (text file) to spreadsheet or graphing program.

X-RADIOGRAPHS

Materials

X-ray machine - UVM Radiation Safety Lab
lead labels, film

Procedure

1. Place two core sections on the x-ray table.
2. Use lead to label top of core, core name and depth at 20 cm intervals
3. Set controls to machine to measure cores. Experiment with what will give best exposure. Initially set at kV=63, Mas =20, sec=0.16.
4. Load film into tray in darkroom
5. Place film under table, take x-ray.
6. Reload film in darkroom, slide film into developer
7. Reposition core (move about 30 cm) being careful to keep labels in place

note: the x-rays are "stretched" slightly with no distortion at the center and greater distortion at the edges due to a point source of x-rays.

Image Processing

1. Cut each x-ray at the center of the image.
2. Measure the distance between lead labels (usually 2 cm greater than actual distance).
3. If there is not an adequate scale (1 cm intervals) on the x-ray, tape a plastic, transparent ruler on one side of the x-ray.
4. Scan x-ray with a transparency scanner.
5. In *Photoshop 3.0*, compress each image by the measured difference, from the edge to the center using a linear stretch.
6. Import into canvas and match each image cut image at end. Clip edges to match between x-rays and group images to create 1 image per section of the core.
7. Import each section into *NIH Image* and snap a line down the center of the image, creating and saving XY coordinates on a grayscale graph.
8. Export data to spreadsheet or graphing program.

LOSS-ON-IGNITION

Materials

drying oven, burning oven
balance (record to nearest milligram)
numbered crucibles (in pencil on the bottom), trays
DI water, spatula, napkins, kimwipes

Procedure

1. Clean and dry each crucible. Organize crucibles on tray in numeric order.
2. Record crucible weight.
3. Homogenize each sample. If sample is dry, grind with a mortar and pestle. If sample is wet, mix well in sample bottle.
4. Transfer approximately 2 g of sample to crucible (less if dry), recording sample number and crucible number. Keep samples in numeric order to minimize confusion.
5. Clean and rinse spatula to avoid contamination between samples.
6. Repeat steps 2+3 as desired (usually 50-60 per batch).
7. Weigh each crucible/sample and record.
8. Place crucibles in drying oven at 80°C to dry overnight.
9. Remove from oven, let sit 1 hour, weigh.
10. Place in burning oven @450°C for 2 hours
11. Remove from oven, let sit 1 hour, weigh.

TOTAL CARBON AND NITROGEN

Materials

Elemental Analyzer
silver capsules, spatulas and tweezers
microbalance
drying oven, crucibles, mortar and pestle
1N HCl, pipet

Procedure

1. Dry samples in crucibles at $<80^{\circ}\text{C}$. Grind and homogenize sample with mortar and pestle.
2. Using microbalance, weigh 3-40 mg into a silver capsule, recording weight in computer spreadsheet. For organic samples use <10 mg; for sands use 30-40 mg.
3. Place open capsule in culture tray.
4. Add three drops of HCl with a plastic pipet to remove secondary carbonate
5. Allow to sit for 2 hours. Dry overnight at 60°C .
6. Close sample capsule with tweezers and load into carousel.
7. Begin run with a blank and two standards (peach leaves, 5 mg). Run two standards every 20 samples.

NITRIC ACID DIGESTION / CHARCOAL

Materials

centrifuge, centrifuge tubes (in sets of 9), test tube racks
hot water bath
concentrated nitric acid
DI water
Elemental Analyzer, tin capsules, tweezers, spatula etc
balance, microbalance

Procedure

1. Dry samples overnight at $<80^{\circ}\text{C}$. Grind and homogenize the sample with mortar and pestle.
2. Weigh approximately 2 grams into centrifuge tube.
3. Add 15 ml nitric acid and stir. Let sit in hot water bath for 1 hour, stirring after 30 min.
4. Remove from bath and let cool.
5. Centrifuge at 20 on speed dial for 10 min and decant.
6. Add DI and stir, centrifuge and decant
7. Repeat twice.
8. Place test tubes in drying oven overnight (60°C)
9. Transfer ALL of sample into tin capsule. Close the capsule, record weight.
10. Place sample in carousel.
11. Begin run with a blank and two standards (peach leaves, 5 mg). Run two standards every 20 samples.

STABLE CARBON ISOTOPES

Materials

Vacuum line, liquid nitrogen, alcohol
vials and tubes
dilute HCl
Cu, CuO, quartz wool, spatulas
DI water, mortar and pestle

Procedure

1. Add several ml of dilute HCl to each sample. Allow to react for several hours. Rinse several times with DI water.
2. Dry overnight at 80°C. Grind and homogenize sample.
3. Label glass tubes with sample number (use white-out)
4. Weigh out 600 mg CuO, mix with 10-40 mg of sample and funnel into tube.
5. Add 500 mg Cu and plug with quartz wool.
6. Place on vacuum line and seal.
7. Burn 1 hour at 900°C. Allow to cool.
8. Wipe glass clean of white out and relabel with permanent marker.
9. Score glass with razor blade.
10. Set up vacuum line, prepare liquid nitrogen, alcohol mixtures for traps.
11. Break tube, isolate CO₂ and water in liquid nitrogen trap, pump away remaining gases.
12. Isolate water (releasing CO₂) in alcohol trap. Transfer CO₂ into sample container using a liquid nitrogen trap.
13. Analyze sample on the mass spectrometer.

GRAIN SIZE ANALYSIS PREPARATION

Materials

15% HCl
concentrated H₂O₂ (30%)
1M NaOH (40 g of NaOH dissolved in 1L DI water)
Dispersant (25g of sodium metaphosphate dissolved in 500 ml DI water)
Centrifuge and test tubes, test tube racks
hot water bath
glass stir rods, 5 ml pipette

Procedure (all chemicals should be handled under hood)

1. dry samples at 50°C and remove any large pieces of organic matter.
2. place between 0.4-0.6 g of sample in a centrifuge tube (use more if sample lacks fines).
3. To remove secondary carbonate, add 20 ml of HCl, stir and rinse rod into tube with as little DI as possible.
4. Place sample in a hot water bath (50°C) for 2 hours
5. Stir well, centrifuge, decant. If necessary, repeat steps 3-5.
6. Fill tubes 3/4 with DI water, mix well, centrifuge and decant. Repeat twice.
7. To remove organic matter, add 5 ml H₂O₂, stir and rinse rod.
8. After intial reaction wanes, place sample in a hot water bath (50°C) for at least 2 hours. Let sample react overnight (but do not leave hot plate on).
9. Centrifuge decant and rinse as detailed above (steps 5+6).
10. To remove biogenic silica, add 10ml NaOH, stir and rinse rod.
11. Let samples sit in hot water bath at least 4 hours.
12. Centifuge, decant and rinse as detailed above (steps 5+6).
13. Add 5 ml of dispersant to samples; stir vigorously until all clods are broken up.
14. If possible, place on reciprocating shaker for 2 hours prior to analysis.

BULK DENSITY

Materials

semicircular knives, spatula, sharp knife
DI water, ruler
1.2 ml measuring spoon
crucibles, balance

Procedure

1. Insert two semicircular knives into core about 1.5 cm apart. Remove one knife.
2. Make two cuts with regular knife about 3 cm apart perpendicular to the first cuts.
3. Lift the resulting rectangular block of sediment out of the core by lightly pressing a spatula to the open side and lifting the spatula and the remaining semicircular knife.
4. Dissect the block using an exacto knife. Carve out two 1cm^2 cubes.
5. If sediment is too wet to keep its shape, scoop it out directly from the core using a measuring spoon, being sure to level the spoon and clean it well.
6. Place the samples in crucibles, weigh.
7. Dry overnight at 60°C .
8. Allow to sit 1 hour, weigh samples.

APPENDIX C: FIELD DATA

FIELD DATA and NOTES for RITTERBUSH POND - Eden VT
All data is in meters, as recorded by total station, tapes and rods.

Field Crews

1/12 - 1/13/1997: Sarah Brown, Paul Bierman, Dave Shaw
1/19/97: Sarah, Paul, Dave and Tom Davis
1/26/97: Sarah, Paul, Dave, Mike Abbot, Christine Massey, Andrea Lini
3/4/97: Sarah, Paul, Char Mehrtens and Stephen Wright
3/7/98: Sarah, Paul, Christine, Barry and Sandy Doolan, Kris Bryan, Stephen and Rebecca Wright

Benchmark

Total station tripod centered over a steel fence post 2m right of dock, 1-2m on shore. Set to coordinate (1000,1000)
North set at left corner of cabin across pond to the northwest. Approximate coordinates (1240, 1000)

Bathymetry and Sediment Probe Data

DATE	LOCATION	NORTHING	EASTING	WATER DEPTH	ROD LENGTH	SEDIMENT THICKNESS	NOTES
1/12/97	Transect 1						line @ 27.59.50 across pond to snag. 15m intervals
	1	1013.65	1007.25	1.7	5.5	3.8	
	2	1026.77	1014.45	6.4	9.7	3.3	top of hard layer?
	3	1040.25	1021.67	10.2	14.2	4	
	4	1053.38	1029.00	12.8	17.1	4.3	
	5	1066.37	1036.00	13.5	18	4.5	
	6	1079.41	1042.92	13.5	18.6	5.1	
	7	1092.28	1049.86	13.5	17.7	4.2	
	8	1105.11	1056.76	12.7	16.4	3.7	
	9	1118.31	1064.06	11.3	14.5	3.2	
	10	1131.31	1070.96	10.1	13.2	3.1	hard to push
	11	1144.48	1078.14	9	12.4	3.4	hard to push
	12	1158.01	1084.88	8.5	11.8	3.3	
	13	1171.32	1092.30	8	11.2	3.2	
	14	1184.81	1099.46	7.3	10.4	3.1	hard layer @9.5
	15	1197.84	1106.31	5.3	8.3	3	hard layer @7.7
	16	1211.15	1113.42	2.5	6.1	3.6	4.75, pushed hard
	17	1224.54	1120.27			0	not taken - thin ice
18	1238.04	1127.05			0	not taken	
1/13/97	Transect 2						long axis from mid-delta to outlet. 22.5m intervals
	1	1177.99	902.76			0	not taken
	2	1164.35	920.21	4.2	8.4	4.2	hard out
	3	1149.84	937.35	7.4	11.6	4.2	halfway from above
	4	1135.54	955.10	10.4	14.2	3.8	6m water
	5	1121.32	972.99	12.1	16	3.9	
	6	1107.56	990.57	12.6	16.7	4.1	
	7	1093.10	1008.87	13.4	17.5	4.1	
	8	1079.36	1026.43	13.4	17.8	4.4	
	9	1064.26	1044.06	13.5	17.8	4.3	
	10	1050.60	1063.40	13.6	19.3	5.7	
	11	1036.30	1081.89	12.9	17.2	4.3	
	12	1022.76	1100.27	7.7	10.9	3.2	gravel bottom?
	13	1009.30	1119.22	2.2	5.6	3.4	gravel bottom?
	14	995.25	1137.33			0	not taken
15	981.52	1155.87			0	not taken	
	Perimeter						clockwise from benchmark estimation of shoreline
	1	1019.74	982.06				
	2	1025.79	957.60				
	3	1058.37	930.12				
	4	1083.40	913.79				
	5	1108.26	902.28				
	6	1127.32	889.75				
	7	1163.20	894.46				
	8	1203.60	918.67				
	9	1226.32	958.51				

DATE	LOCATION	NORTHING	EASTING	WATER DEPTH	ROD LENGTH	SEDIMENT THICKNESS	NOTES	
1/13/97	Perimeter							
	10	1220.68	997.10					
	11	1215.81	1053.39					
	12	1231.30	1098.80					
	13	1238.28	1126.92					
	14	1219.27	1139.04					
	15	1151.88	1141.93					
	16	1104.76	1145.64					
	17	1070.42	1145.95					
	18	1010.09	1155.70					
	19	1000.13	1145.24					
	20	971.07	1115.59				outlet	
	21	970.33	1092.44				outlet	
	22	958.85	1075.08				rods (snag)	
	23	949.16	1056.71					
	24	967.86	1033.06				2m from shore	
	25	988.90	1014.53					
		Additional Points						
		NW shore	1195.34	1004.52	7.8	10.8	3	easy out
		NW mid	1134.28	1022.11	12.9	16.6	3.7	
		SE mid	999.18	1072.08	9.4	13.7	4.3	
	1/19/97	A	1030.34	1059.42	13.6	17.5	3.9	easy out
		B	1067.33	1058.27	13.4	18.5	5.1	
		C	1063.61	1088.93	12.9	17.65	4.75	
		D	1105.02	1090.28	9	12.1	3.1	hard refusal
E		1134.34	1105.16	4.1	7.8	3.7	refusal	
F		1172.68	1055.42	9.9	12.6	2.7	layer @ 11.4	
G		1193.09	1075.60	7.7	10.25	2.55	layer @ 10 (10cm)	
H		1192.86	981.35	8.1	11	2.9	layer @ 10.45	
I		1185.50	959.00	8.7	12.45	3.75		
J		1130.01	928.68	5.2	9.7	4.5		
K		1074.08	961.71	6.5	11.05	4.55		
L		1052.38	1047.79	13.4	18	4.6		
M		1069.04	1046.49	13.5	18.65	5.15		
1/26/97	1	1073.71	1004.77	12.4	17.05	4.65		
	2	1174.60	959.61	9.55	13.95	4.4		
	3	1076.51	1115.77	6.55	10.4	3.85	refusal (rock)	
	check zero	1239.84	1000.10				corner of cabin	
3/4/97	Core RT-2	1059.84	1061.88				approx from pic.	
	check zero	1239.78	1000.05				corner of cabin	
3/7/98	check zero	12.39.72	1000.04				corner of cabin	

Cores - Reasoner Coring Device

DATE	CORE	NORTHING	EASTING	WATER DEPTH	NOTES
1/19/97	practice			8.7	10 ft practice core taken approx 40m along transect 1 from dock. Piston and corecatcher - easy to drive, difficult to retrieve
1/26/97	1	1056.25	1063.77	13.5	6m barrel with piston and corecatcher. Retrieval with 5 pulleys easy pull out, upper section slashes. - water in barrel
	2	1057.34	1063.62	13.5	6m barrel with piston and corecatcher. Retrieval with 5 pulleys heavy - solid core!
3/4/97	3	1177.06	1096.73	7.8	6m barrel with piston and corecatcher. Retrieval with 6 pulleys bottom in gyttja, could have driven further
	4	1130.34	966.93	12	6m barrel with piston and corecatcher. Retrieval with 6 pulleys driven to refusal, gray sediment at bottom
3/7/98	5	1060.64	1061.58	13.5	6m barrel (sched 40) with piston (set tight!) no corecatcher. Pushed through first meter of sediment THEN set piston. Retrieval with 4 pulleys. Gray liquified sand at bottom.

APPENDIX D: Lab Data

<u>Data Set</u>	<u>Page</u>
Magnetic Susceptibility	138
Paleomagnetism	142
Loss-on-Ignition (LOI)	145
Elemental Analysis (TOC, C/N)	148
Bulk Density	149
Stable Carbon Isotopes	149
Charcoal (Nitric Digestion)	149
Grayscale Density	150
Grain Size	151

Sapphire Susceptibility Data - CORE 2				Sapphire Susceptibility Data - CORE 3				Sapphire Susceptibility Data - CORE 4			
Depth (cm)	Suscept(SI)	Depth (cm)	Suscept(SI)	Depth (cm)	Suscept(SI)	Depth (cm)	Suscept(SI)	Depth (cm)	Suscept(SI)	Depth (cm)	Suscept(SI)
3	6.4E-06	303	1.7E-05	3	2.6E-06	303	9.6E-06	3	3.1E-06	303	1.0E-05
6	9.6E-06	306	1.9E-05	6	5.4E-06	306	1.5E-05	6	5.5E-06	306	1.6E-05
9	1.1E-05	309	1.8E-05	9	7.0E-06	309	2.3E-05	9	6.4E-06	309	3.4E-05
12	1.2E-05	312	1.5E-05	12	8.5E-06	312	3.8E-05	12	6.7E-06	312	2.7E-05
15	1.2E-05	315	1.3E-05	15	9.5E-06	315	4.9E-05	15	6.7E-06	315	9.0E-06
18	1.1E-05	318	1.3E-05	18	9.5E-06	318	3.1E-05	18	7.1E-06	318	4.4E-06
21	1.1E-05	321	1.3E-05	21	9.6E-06	321	1.2E-05	21	6.9E-06	321	2.2E-06
24	1.1E-05	324	1.3E-05	24	9.6E-06	324	7.6E-06	24	6.6E-06	324	3.2E-06
27	1.1E-05	327	1.1E-05	27	9.3E-06	327	6.6E-06	27	6.5E-06	327	5.3E-06
30	1.1E-05	330	1.1E-05	30	9.0E-06	330	6.4E-06	30	6.5E-06	330	6.9E-06
33	1.2E-05	333	1.2E-05	33	8.5E-06	333	6.6E-06	33	6.6E-06	333	8.0E-06
36	1.2E-05	336	1.1E-05	36	8.0E-06	336	8.8E-06	36	6.3E-06	336	9.8E-06
39	1.2E-05	339	1.1E-05	39	7.5E-06	339	1.9E-05	39	5.8E-06	339	1.8E-05
42	1.1E-05	342	1.1E-05	42	5.5E-06	342	2.5E-05	42	5.7E-06	342	2.9E-05
45	9.4E-06	345	1.2E-05	45	4.5E-06	345	1.9E-05	45	5.4E-06	345	4.1E-05
48	9.0E-06	348	1.3E-05	48	3.9E-06	348	1.8E-05	48	5.0E-06	348	5.1E-05
51	8.9E-06	351	1.3E-05	51	4.9E-06	351	3.9E-05	51	5.0E-06	351	5.5E-05
54	9.1E-06	354	1.3E-05	54	6.3E-06	354	5.2E-05	54	5.7E-06	354	5.1E-05
57	9.3E-06	357	1.3E-05	57	7.5E-06	357	2.5E-05	57	5.0E-06	357	5.0E-05
60	9.8E-06	360	1.2E-05	60	1.5E-05	360	1.3E-05	60	4.0E-06	360	8.0E-05
63	1.0E-05	363	1.2E-05	63	2.6E-05	363	1.9E-05	63	3.8E-06	363	1.0E-04
66	1.1E-05	366	1.1E-05	66	3.1E-05	366	3.4E-05	66	3.7E-06	366	1.1E-04
69	1.1E-05	369	1.1E-05	69	3.5E-05	369	3.6E-05	69	3.8E-06	369	1.1E-04
72	1.1E-05	372	1.3E-05	72	3.2E-05	372	2.5E-05	72	3.5E-06	372	1.1E-04
75	1.2E-05	375	1.6E-05	75	2.7E-05	375	2.6E-05	75	3.3E-06	375	1.1E-04
78	1.3E-05	378	1.4E-05	78	3.5E-05	378	3.1E-05	78	3.4E-06	378	1.0E-04
81	1.3E-05	381	1.2E-05	81	4.6E-05	381	6.7E-05	81	4.6E-06	381	7.7E-05
84	1.3E-05	384	1.2E-05	84	2.8E-05	384	7.1E-05	84	8.7E-06	384	5.8E-05
87	1.3E-05	387	1.1E-05	87	1.9E-05	387	4.8E-05	87	1.2E-05	387	5.5E-05
90	1.4E-05	390	1.0E-05	90	3.1E-05	390	4.0E-05	90	1.6E-05	390	5.7E-05
93	1.4E-05	393	1.1E-05	93	4.1E-05	393	5.6E-05	93	1.6E-05	393	5.5E-05
96	1.6E-05	396	1.0E-05	96	4.7E-05	396	6.1E-05	96	1.1E-05	396	8.2E-05
99	1.6E-05	399	1.2E-05	99	5.8E-05	399	5.7E-05	99	1.3E-05	399	1.0E-04
102	1.6E-05	402	1.3E-05	102	5.6E-05	402	4.4E-05	102	2.1E-05	402	9.5E-05
105	1.7E-05	405	1.2E-05	105	3.8E-05	405	3.3E-05	105	2.0E-05	405	8.9E-05
108	1.8E-05	408	1.3E-05	108	3.4E-05	408	3.0E-05	108	1.2E-05	408	7.0E-05
111	1.8E-05	411	1.5E-05	111	3.9E-05	411	2.6E-05	111	8.6E-06	411	5.0E-05
114	1.6E-05	414	1.4E-05	114	3.5E-05	414	2.4E-05	114	8.1E-06	414	7.0E-05
117	1.6E-05	417	1.7E-05	117	3.6E-05	417	2.9E-05	117	8.5E-06	417	0.000116
120	1.6E-05	420	1.7E-05	120	3.3E-05	420	3.1E-05	120	1.1E-05	420	0.000158
123	1.6E-05	423	1.5E-05	123	3.2E-05	423	2.6E-05	123	1.7E-05	423	0.000172
126	1.6E-05	426	3.2E-05	126	3.5E-05	426	3.0E-05	126	2.0E-05	426	0.000175
129	1.5E-05	429	3.1E-05	129	4.0E-05	429	6.0E-05	129	2.7E-05	429	0.000198
132	1.5E-05	432	2.1E-05	132	5.3E-05	432	7.6E-05	132	2.6E-05	432	0.000208
135	8.2E-06	435	1.9E-05	135	1.2E-04	435	7.3E-05	135	1.5E-05	435	0.000201
138	1.2E-05	438	2.0E-05	138	1.7E-04	438	7.5E-05	138	8.1E-06	438	0.000201
141	1.3E-05	441	2.6E-05	141	1.6E-04	441	8.1E-05	141	6.6E-06	441	0.000214
144	1.4E-05	444	4.8E-05	144	1.2E-04	444	7.4E-05	144	6.5E-06	444	0.000222
147	1.5E-05	447	5.9E-05	147	8.0E-05	447	8.3E-05	147	5.8E-06	447	0.000208
150	1.5E-05	450	5.5E-05	150	4.2E-05	450	9.6E-05	150	4.5E-06	450	0.000179
153	1.5E-05	453	3.5E-05	153	2.4E-05	453	8.3E-05	153	4.2E-06	453	0.000185
156	1.5E-05	456	1.9E-05	156	2.6E-05	456	8.5E-05	156	3.7E-06	456	0.000215
159	1.6E-05	459	1.6E-05	159	3.8E-05	459	8.8E-05	159	3.1E-06	459	0.000248
162	1.8E-05	462	1.7E-05	162	3.6E-05	462	8.0E-05	162	3.6E-06	462	0.000323
165	2.4E-05	465	1.6E-05	165	3.5E-05	465	7.9E-05	165	5.8E-06	465	0.000435
168	3.3E-05	468	1.2E-05	168	3.5E-05	468	8.9E-05	168	7.2E-06	468	0.000444
171	2.3E-05	471	1.1E-05	171	2.6E-05	471	1.0E-04	171	7.8E-06	471	0.000497
174	2.4E-05	474	1.3E-05	174	1.7E-05	474	9.4E-05	174	7.1E-06	474	0.00074
177	3.5E-05	477	1.6E-05	177	1.8E-05	477	7.4E-05	177	7.1E-06	477	0.000958
180	2.4E-05	480	1.8E-05	180	2.5E-05	480	7.0E-05	180	6.7E-06	480	0.000949
183	1.6E-05	483	1.9E-05	183	2.1E-05	483	6.3E-05	183	6.9E-06	483	0.000789
186	1.5E-05	486	1.8E-05	186	1.4E-05	486	5.2E-05	186	6.5E-06		
189	2.2E-05	489	1.8E-05	189	1.4E-05	489	4.1E-05	189	5.5E-06		
192	3.4E-05	492	1.9E-05	192	1.0E-05	492	4.3E-05	192	5.8E-06		
195	2.4E-05	495	2.1E-05	195	5.8E-06	495	5.5E-05	195	5.4E-06		
198	1.6E-05	498	2.3E-05	198	5.6E-06	498	7.3E-05	198	4.6E-06		
201	1.5E-05	501	3.0E-05	201	5.4E-06	501	1.9E-04	201	4.2E-06		
204	1.8E-05	504	3.6E-05	204	5.4E-06	504	6.1E-04	204	3.2E-06		
207	1.9E-05	507	3.4E-05	207	5.6E-06	507	1.5E-03	207	2.5E-06		
210	1.6E-05	510	3.0E-05	210	6.4E-06	510	2.7E-03	210	1.8E-06		
213	1.6E-05	513	2.6E-05	213	8.8E-06	513	4.0E-03	213	1.5E-06		
216	1.7E-05	516	2.6E-05	216	1.3E-05			216	1.3E-06		
219	2.3E-05	519	3.0E-05	219	1.5E-05			219	1.1E-06		
222	2.4E-05	522	4.4E-05	222	1.4E-05			222	9.5E-07		
225	2.2E-05	525	5.5E-05	225	9.8E-06			225	8.2E-07		
228	2.5E-05	528	6.8E-05	228	9.4E-06			228	8.0E-07		
231	4.4E-05	531	6.3E-05	231	1.4E-05			231	8.9E-07		
234	5.1E-05	534	7.0E-05	234	1.8E-05			234	1.1E-06		
237	4.1E-05	537	8.1E-05	237	1.3E-05			237	1.1E-06		
240	2.3E-05	540	8.6E-05	240	7.9E-06			240	5.5E-07		
243	1.6E-05	543	1.0E-04	243	6.5E-06			243	7.0E-07		
246	1.4E-05	546	1.0E-04	246	5.1E-06			246	2.4E-06		
249	1.4E-05	549	8.1E-05	249	4.6E-06			249	2.4E-06		
252	1.5E-05	552	4.7E-05	252	4.6E-06			252	8.4E-07		
255	1.5E-05	555	4.1E-05	255	5.1E-06			255	4.0E-07		
258	1.5E-05	558	4.4E-05	258	6.2E-06			258	2.4E-07		
261	1.5E-05	561	4.4E-05	261	7.0E-06			261	3.05E-06		
264	1.2E-05	564	8.5E-05	264	7.6E-06			264	4.28E-06		
267	1.2E-05	567	3.1E-04	267	8.9E-06			267	6.17E-06		
270	1.6E-05			270	9.8E-06			270	9.07E-06		
273	1.8E-05			273	1.0E-05			273	7.56E-06		
276	1.8E-05			276	1.0E-05			276	6.71E-06		
279	1.6E-05			279	1.1E-05			279	6.89E-06		
282	1.6E-05			282	1.2E-05			282	9.03E-06		
285	1.7E-05			285	1.3E-05			285	1.4E-05		
288	1.6E-05			288	1.5E-05			288	1.46E-05		
291	1.6E-05			291	1.7E-05			291	2.5E-05		
294	1.7E-05			294	1.3E-05			294	4.59E-05		
297	1.8E-05			297	1.0E-05			297	3.26E-05		
300	1.8E-05			300	8.7E-06			300	1.28E-05		

Bartington Magnetic Susceptibility Data - CORE 2											
Depth (cm)	Suscept(SI)	Depth (cm)	Suscept(SI)	Depth (cm)	Suscept(SI)	Depth (cm)	Suscept(SI)	Depth (cm)	Suscept(SI)	Depth (cm)	Suscept(SI)
2	1.1	101	3.2	201	4.7	301	4.7	401	3.8	501	15.2
3	1.5	102	3.4	202	5.1	302	4.2	402	3.6	502	16.8
4	1.8	103	3.6	203	5.7	303	4.5	403	3.7	503	18.9
5	2.0	104	3.9	204	6.7	304	5.1	404	4.0	504	19.8
6	2.1	105	4.0	205	7.8	305	5.8	405	4.6	505	18.0
7	2.4	106	4.1	206	8.0	306	6.3	406	5.1	506	15.2
8	2.4	107	4.2	207	7.2	307	5.9	407	5.6	507	13.9
9	2.5	108	4.5	208	6.4	308	5.1	408	5.8	508	13.7
10	2.5	109	4.5	209	6.0	309	4.4	409	5.7	509	13.9
11	2.3	110	4.4	210	5.8	310	4.2	410	5.5	510	13.0
12	2.3	111	4.2	211	5.8	311	4.0	411	5.4	511	11.0
13	2.0	112	3.9	212	5.9	312	3.7	412	5.7	512	10.1
14	1.8	113	3.6	213	5.8	313	3.5	413	6.3	513	10.1
15	1.6	114	3.3	214	5.6	314	3.2	414	6.9	514	11.1
16	1.5	115	3.3	215	5.7	315	3.1	415	7.7	515	12.0
17	1.4	116	3.3	216	6.0	316	3.1	416	8.5	516	12.8
18	1.4	117	3.2	217	6.8	317	3.2	417	8.5	517	13.1
19	1.4	118	3.3	218	8.0	318	3.4	418	7.4	518	14.1
20	1.4	119	3.2	219	9.7	319	3.7	420	6.2	519	17.3
21	1.4	120	3.1	220	10.8	320	3.7	421	9.0	520	21.9
22	1.4	121	3.1	221	10.6	321	3.7	422	12.8	521	25.8
23	1.5	122	3.0	222	9.5	322	3.5	423	17.0	522	26.6
24	1.6	123	3.0	223	8.9	323	3.2	424	19.6	523	27.1
25	1.7	124	2.8	224	8.6	324	3.0	425	19.2	524	30.0
26	1.9	125	2.7	225	8.1	325	2.8	426	16.1	525	33.9
27	2.3	126	2.6	226	7.7	326	2.7	427	12.5	526	35.9
28	2.3	127	2.5	227	8.2	327	2.8	428	9.7	527	36.0
29	2.3	128	2.4	228	9.8	328	3.0	429	7.5	528	34.1
30	2.2	129	2.4	229	13.1	329	3.1	430	6.2	529	33.2
31	2.3	130	2.6	230	17.7	330	3.2	431	5.6	530	33.8
32	2.1	131	2.8	231	22.3	331	3.1	432	5.8	531	35.0
33	1.9	132	2.8	232	25.5	332	3.2	433	6.2	532	37.4
34	1.8	133	2.6	233	26.7	333	3.2	434	6.2	533	40.0
35	1.7	135	2.6	234	26.6	334	3.0	435	6.1	534	41.6
36	1.6	136	3.1	235	25.5	335	2.8	436	6.4	535	42.8
37	1.7	137	3.5	236	23.4	336	2.6	437	7.0	536	44.0
38	1.7	138	3.7	237	20.2	337	2.7	438	8.7	537	44.4
39	1.7	139	3.8	238	16.5	338	2.9	439	11.7	538	45.6
40	1.7	140	3.7	239	12.9	339	2.9	440	16.4	539	49.7
41	1.7	141	3.6	240	10.0	340	2.9	441	21.6	540	54.6
42	1.7	142	3.6	241	8.0	341	3.1	442	25.9	541	57.9
43	1.8	143	3.6	242	6.4	342	3.4	443	28.4	542	59.5
44	1.8	144	3.7	243	5.6	343	3.7	444	29.7	543	60.1
45	1.9	145	3.6	244	5.2	344	4.0	445	29.8	544	59.3
46	2.0	146	3.7	245	5.2	345	4.3	446	28.4	545	57.2
47	2.1	147	3.8	246	5.4	346	4.4	447	26.0	546	53.8
48	2.2	148	3.8	247	5.5	347	4.3	448	22.7	547	48.9
49	2.1	149	3.9	248	5.7	348	4.2	449	18.8	548	41.9
50	2.1	150	3.8	249	5.7	349	4.2	450	14.2	549	33.4
51	2.3	151	3.7	250	6.1	350	4.4	451	9.8	550	25.8
52	2.4	152	3.5	251	6.3	351	4.6	452	6.8	551	21.2
53	2.4	153	3.5	252	6.4	352	4.9	453	4.9	552	19.9
54	2.4	154	3.4	253	6.4	353	5.2	454	4.1	553	20.7
55	2.4	155	3.4	254	6.6	354	5.3	455	3.6	554	21.7
56	2.5	156	3.2	255	6.6	355	5.1	456	3.4	555	21.8
57	2.6	157	3.4	256	6.7	356	5.1	457	3.2	556	22.0
58	2.6	158	3.6	257	6.8	357	4.9	458	3.1	557	22.6
59	2.6	159	3.9	258	6.6	358	4.9	459	3.5	558	21.3
60	2.7	160	4.6	259	6.4	359	4.9	460	4.1	559	17.8
61	2.6	161	4.9	260	6.1	360	4.9	461	4.9	560	14.3
62	2.6	162	5.3	261	5.7	361	4.7	462	5.3	561	12.0
63	2.5	163	5.7	262	5.2	362	4.4	463	4.8		
64	2.5	164	6.8	263	4.4	363	4.2	464	3.9		
65	2.5	165	8.6	265	3.0	364	4.0	465	3.3		
66	2.5	166	11.2	266	4.2	365	3.9	466	2.8		
67	2.6	167	13.8	267	5.2	366	3.9	467	2.7		
68	2.6	168	14.9	268	6.0	367	4.1	468	2.7		
69	2.7	169	13.5	269	6.3	368	4.4	469	2.8		
70	2.6	170	11.0	270	6.5	369	4.9	470	3.0		
71	2.7	171	8.7	271	6.8	370	5.5	471	3.2		
72	2.7	172	7.8	272	6.9	371	6.2	472	3.6		
73	2.9	173	8.0	273	6.6	372	6.7	473	3.9		
74	3.0	174	9.5	274	5.9	373	7.3	474	4.1		
75	3.2	175	12.0	275	5.5	374	7.5	475	4.1		
76	3.0	176	15.1	276	5.1	375	7.0	476	4.3		
77	2.9	177	16.7	277	4.8	376	6.0	477	4.8		
78	2.8	178	16.1	278	4.6	377	5.3	478	5.1		
79	2.8	179	13.6	279	4.3	378	5.0	479	5.4		
80	2.9	180	10.6	280	4.3	379	4.8	480	5.5		
81	2.8	181	8.1	281	4.3	380	4.7	481	5.5		
82	2.9	182	6.4	282	4.2	381	4.7	482	5.4		
83	3.0	183	5.4	283	3.8	382	4.5	483	4.9		
84	2.9	184	5.0	284	3.5	383	4.2	484	4.5		
85	2.9	185	4.8	285	3.2	384	3.6	485	4.4		
86	2.9	186	4.8	286	3.2	385	2.9	486	4.5		
87	2.8	187	5.4	287	3.3	386	2.4	487	4.9		
88	2.7	188	6.5	288	3.5	387	2.3	488	5.2		
89	2.9	189	8.5	289	3.7	388	2.2	489	5.6		
90	3.1	190	11.4	290	3.9	389	2.2	490	6.2		
91	3.2	191	14.7	291	4.2	390	2.3	491	6.8		
92	3.3	192	17.1	292	4.2	391	2.3	492	7.5		
93	3.3	193	17.4	293	4.7	392	2.1	493	8.0		
94	3.4	194	15.3	294	5.0	393	2.2	494	8.4		
95	3.4	195	12.1	295	5.4	394	2.4	495	8.8		
96	3.4	196	9.2	296	5.4	395	2.6	496	9.7		
97	3.4	197	7.0	297	5.2	396	3.0	497	11.2		
98	3.2	198	5.9	298	5.0	397	3.5	498	13.0		
99	3.2	199	5.1	299	4.8	398	3.8	499	14.3		
100	3.1	200	4.7	300	4.4	400	3.9	500	15.2		

Bartlington Magnetic Susceptibility Data - CORE 3

Depth (cm)	Suscept(SI)	Depth (cm)	Suscept(SI)	Depth (cm)	Suscept(SI)	Depth (cm)	Suscept(SI)	Depth (cm)	Suscept(SI)	Depth (cm)	Suscept(SI)
2	-0.1	101	27.1	201	2.4	301	1.6	401	26.1	501	3.4
3	-0.1	102	24.7	202	2.2	302	1.7	402	20.7	502	-1.1
4	0.0	103	21.3	203	2.1	303	2.0	403	15.1	503	-3.5
5	-0.1	104	18.3	204	2.0	304	2.4	404	10.5	504	-2.3
6	0.0	105	16.2	205	1.8	305	3.0	405	7.1	505	2.9
7	-0.1	106	15.3	206	1.6	306	3.8	406	5.4	506	6.2
8	0.0	107	15.5	207	1.6	307	4.6	407	4.9		
9	0.0	108	16.9	208	1.7	308	5.2	408	5.1		
10	-0.1	109	18.5	209	1.8	309	5.7	409	5.5		
11	-0.1	110	19.8	210	2.1	310	6.4	410	5.6		
12	-0.1	111	19.8	211	2.5	311	8.0	411	5.7		
13	-0.1	112	18.9	212	2.9	312	10.7	412	6.6		
14	-0.1	113	17.8	213	3.4	313	15.1	413	7.5		
15	-0.1	114	17.6	214	4.0	314	20.7	414	8.4		
16	0.0	115	17.8	215	4.7	315	26.2	415	9.6		
17	-0.1	116	18.0	216	5.4	316	28.6	416	11.1		
18	-0.1	117	17.6	217	6.0	317	26.5	417	12.9		
19	-0.1	118	17.0	218	6.2	318	21.0	418	14.9		
20	-0.1	119	16.5	219	6.1	319	14.6	419	15.9		
21	0.0	120	17.0	220	5.7	320	9.4	420	15.4		
22	0.0	121	18.1	221	5.1	321	5.9	421	13.5		
23	0.0	122	18.9	222	4.3	322	3.8	422	11.9		
24	0.0	123	18.7	223	3.6	323	2.5	423	11.4		
25	0.0	124	16.4	224	2.9	324	1.7	424	12.1		
26	0.1	126	23.2	225	2.4	325	1.4	425	13.6		
27	0.3	127	26.4	226	2.4	326	1.1	426	16.1		
28	0.3	128	26.2	227	3.0	327	0.9	427	20.6		
29	0.2	129	24.2	228	3.7	328	0.8	428	27.4		
30	0.1	130	22.7	229	4.7	329	0.8	429	35.8		
31	0.2	131	23.4	230	6.1	330	0.7	430	43.4		
32	0.1	132	27.0	231	7.7	331	0.8	431	48.0		
33	0.0	133	34.6	232	8.7	332	0.8	432	49.7		
34	0.1	134	47.2	233	8.6	333	0.9	433	49.6		
35	0.0	135	62.9	234	7.8	334	1.0	434	48.5		
36	-0.1	136	77.1	235	6.8	335	1.2	435	47.6		
37	0.0	137	86.2	236	5.5	336	1.7	436	47.3		
38	0.1	138	90.7	237	4.3	337	2.5	437	48.3		
39	0.2	139	92.1	238	3.3	338	3.6	438	50.9		
40	0.1	140	91.1	239	2.5	339	5.4	439	53.9		
41	0.0	141	87.7	240	2.0	340	7.6	440	55.7		
42	0.1	142	82.3	241	2.0	341	9.5	441	55.0		
43	0.2	143	74.7	242	2.1	342	10.4	442	51.9		
44	0.1	144	66.4	243	2.0	343	10.3	443	48.3		
45	0.2	145	57.7	244	1.8	344	9.4	444	47.5		
46	0.3	146	49.2	245	1.6	345	8.2	445	50.0		
47	0.4	147	40.8	246	1.4	346	6.6	446	53.5		
48	0.6	148	33.1	247	1.6	347	5.4	447	56.8		
49	0.8	149	25.4	248	1.4	348	5.0	448	59.9		
50	1.1	150	20.7	249	1.4	349	5.8	449	63.4		
51	1.4	151	16.1	250	1.4	350	8.2	450	65.7		
52	1.8	152	11.9	251	1.5	351	12.4	451	63.5		
53	2.1	153	9.4	252	1.5	352	18.6	452	56.7		
54	2.2	154	8.5	253	1.5	353	25.5	453	51.2		
55	2.2	155	9.1	255	1.7	354	30.2	454	50.2		
56	2.4	156	10.7	256	1.7	355	30.0	455	52.6		
57	2.7	157	13.6	257	1.5	356	24.6	456	55.8		
58	3.5	158	17.4	258	1.2	357	17.1	457	57.4		
59	4.7	159	20.3	259	0.9	358	10.8	458	56.4		
60	6.6	160	20.8	260	0.8	359	7.1	459	53.6		
61	9.1	161	19.5	261	0.7	360	5.1	460	50.6		
62	12.0	162	18.0	262	0.6	361	4.4	461	47.8		
63	14.4	163	17.5	263	0.5	362	4.4	462	45.8		
64	15.5	164	17.5	264	0.5	363	5.4	463	45.2		
65	15.5	165	17.3	265	0.5	364	7.3	464	45.6		
66	16.1	166	17.4	266	0.4	365	10.2	465	47.2		
67	16.7	167	18.0	267	0.4	366	13.3	466	50.1		
68	16.8	168	18.4	268	0.5	367	16.0	467	53.8		
69	17.5	169	17.3	269	0.4	368	17.2	468	58.0		
70	18.5	170	15.0	270	0.5	369	17.6	469	61.9		
71	17.9	171	12.4	271	0.5	370	17.2	470	65.1		
72	15.5	172	10.4	272	0.4	371	15.4	471	66.3		
73	13.2	173	9.0	273	0.5	372	12.8	472	65.0		
74	11.7	174	8.4	274	0.5	373	10.9	473	61.1		
75	11.5	175	8.5	275	0.5	374	10.6	474	55.2		
76	12.6	176	9.2	276	0.6	375	11.7	475	49.0		
77	14.9	177	10.6	277	0.6	376	12.9	476	44.0		
78	18.2	178	12.4	278	0.7	377	13.3	477	41.1		
79	22.1	179	14.2	279	0.9	378	13.3	478	39.8		
80	24.8	180	14.6	280	1.2	379	14.3	479	39.4		
81	24.4	181	13.9	281	1.4	380	18.0	480	39.1		
82	20.8	182	12.4	282	1.7	381	24.1	481	38.0		
83	15.5	183	10.8	283	1.8	382	30.8	482	36.2		
84	10.6	184	9.3	284	2.2	384	39.5	483	33.9		
85	7.7	185	8.0	285	2.5	385	41.8	484	31.5		
86	6.6	186	7.2	286	2.8	386	36.5	485	28.8		
87	6.7	187	7.0	287	2.9	387	28.8	486	25.9		
88	8.0	188	7.4	288	3.1	388	22.0	487	23.2		
89	10.4	189	7.9	289	3.6	389	17.8	488	21.4		
90	13.2	190	7.7	290	4.1	390	16.9	489	20.6		
91	15.6	191	6.3	291	4.6	391	18.6	490	20.6		
92	17.3	192	4.7	292	4.5	392	22.4	491	21.5		
93	18.4	193	3.5	293	3.7	393	26.8	492	23.3		
94	19.4	194	3.0	294	2.7	394	29.6	493	25.7		
95	20.2	195	2.9	295	2.0	395	30.6	494	27.2		
96	21.2	196	2.9	296	1.6	396	30.9	495	26.4		
97	23.0	197	2.9	297	1.4	397	30.8	496	23.8		
98	25.4	198	2.8	298	1.3	398	30.5	497	20.5		
99	27.1	199	2.6	299	1.4	399	30.1	498	16.6		
100	27.9	200	2.5	300	1.5	400	29.4	499	12.4		
								500	8.0		

Bartlington Magnetic Susceptibility Data - CORE 4									
Depth (cm)	Suscept(SI)	Depth (cm)	Suscept(SI)	Depth (cm)	Suscept(SI)	Depth (cm)	Suscept(SI)	Depth (cm)	Suscept(SI)
1	0.2	101	6.7	201	0.9	301	4.4	401	49.7
2	0.4	102	6.8	202	0.8	302	4.7	402	50.8
3	0.5	103	6.3	203	0.7	303	5.3	403	51.7
4	0.5	104	5.2	204	0.7	304	6.5	404	49.0
5	0.5	105	4.0	205	0.7	305	8.5	405	42.1
6	0.6	106	3.0	206	0.7	306	11.5	406	34.1
7	0.5	107	2.2	207	0.7	307	15.9	407	28.5
8	0.6	108	1.7	208	0.7	308	20.2	408	26.4
9	0.7	109	1.4	209	0.7	309	21.8	409	27.3
10	0.7	110	1.3	210	0.6	310	18.9	410	30.7
11	0.6	111	1.3	211	0.6	311	13.5	411	35.7
12	0.6	112	1.3	212	0.6	312	8.7	412	41.9
13	0.5	113	1.5	213	0.6	313	5.6	413	50.1
14	0.4	114	1.5	214	0.6	314	3.7	414	60.3
15	0.4	115	1.6	215	0.7	315	2.7	415	71.5
16	0.4	116	1.9	216	0.6	316	2.1	416	82.2
17	0.4	117	2.3	217	0.6	317	1.8	417	89.9
18	0.4	118	3.0	218	0.6	318	1.5	418	94.4
19	0.4	119	3.7	219	0.6	319	1.3	419	97.3
20	0.4	120	4.7	220	0.5	320	1.1	420	98.0
21	0.4	121	5.7	221	0.6	321	0.8	421	98.0
22	0.4	122	6.6	222	0.6	322	0.4	422	99.2
23	0.4	123	7.3	223	0.7	323	0.8	423	101.2
24	0.4	124	8.0	224	0.6	324	0.9	424	105.0
25	0.6	125	9.3	225	0.6	325	1.0	425	109.3
26	0.9	126	11.4	226	0.6	326	1.1	426	113.5
27	0.8	127	13.7	227	0.7	327	1.2	427	117.6
28	0.6	128	15.4	228	0.6	328	1.3	428	120.5
29	0.6	129	16.0	229	0.7	329	1.5	429	121.5
30	0.6	130	14.5	230	0.7	330	1.6	430	120.6
31	0.5	131	11.3	231	0.7	331	1.7	431	119.1
32	0.5	132	7.9	232	0.8	332	1.8	432	118.0
33	0.3	133	5.3	233	0.9	333	2.0	433	117.9
34	0.3	134	3.6	234	0.9	334	2.3	434	118.6
35	0.4	135	2.0	235	1.0	335	3.1	435	120.3
36	0.4	136	1.4	236	1.0	336	4.0	436	122.9
37	0.4	137	1.0	237	0.9	337	6.4	437	126.0
38	0.4	138	0.8	238	0.8	338	8.9	438	129.1
39	0.5	139	0.7	239	0.7	339	11.2	439	131.7
40	0.6	140	0.7	240	0.7	340	12.9	440	133.1
41	0.6	141	0.8	241	0.6	341	14.4	441	133.6
42	0.8	142	1.0	242	0.6	342	16.6	442	132.9
43	0.8	143	1.1	243	0.8	343	19.0	443	131.0
44	0.8	144	1.1	244	1.0	344	20.7	444	127.6
45	0.9	145	1.0	245	1.6	345	22.0	445	123.1
46	1.0	146	0.8	246	2.0	346	23.8	446	118.2
47	1.2	147	0.6	247	2.1	347	25.9	447	113.8
48	1.4	148	0.7	248	1.8	348	26.8	448	111.6
49	1.7	149	0.6	249	1.4	349	26.7	449	113.6
50	1.8	150	0.7	250	1.1	350	26.7	450	119.6
51	1.8	151	0.8	251	0.9	351	26.4	451	126.7
52	1.5	152	0.8	252	0.8	352	24.9	452	134.3
53	1.4	153	0.9	253	0.7	353	23.0	453	142.4
54	1.2	154	1.0	254	0.7	354	22.9	454	151.9
55	0.9	155	1.1	255	0.6	355	24.8	455	161.6
56	0.8	156	1.1	256	0.6	356	28.7	456	170.6
57	0.8	157	1.0	257	0.4	357	34.8	457	179.6
58	0.6	158	0.8	258	0.5	358	41.7	458	187.3
59	0.6	159	0.6	259	0.4	359	47.4	459	194.1
60	0.6	161	0.8	260	0.3	360	52.1	460	200.0
61	0.6	162	0.8	261	0.4	361	56.7	461	205.4
62	0.6	163	1.0	262	0.4	362	60.6	462	211.7
63	0.6	164	1.1	263	0.5	363	63.3	463	216.9
64	0.7	165	1.3	264	0.5	364	64.6	464	223.9
65	0.8	166	1.4	265	1.0	365	64.9	465	234.0
66	0.7	167	1.5	266	1.2	366	64.7	466	240.3
67	0.8	168	1.7	267	1.6	367	63.9	467	254.1
68	0.6	169	1.7	268	2.4	368	62.6	468	284.3
69	0.5	170	1.8	269	2.9	369	60.8	469	319.6
70	0.5	171	1.5	270	2.7	370	59.1	470	337.8
71	0.6	172	1.2	271	2.0	371	58.0	471	338.0
72	0.7	173	1.0	272	1.5	372	58.0	472	348.2
73	0.6	174	0.9	273	1.2	373	58.3	473	379.8
74	0.7	175	1.0	274	1.0	374	58.0	474	404.2
75	0.7	176	1.0	275	1.0	375	56.6	475	362.3
76	1.0	177	1.0	276	0.9	376	53.7		
77	1.2	178	1.0	277	1.0	377	49.2		
78	1.8	179	0.9	278	0.9	378	43.1		
79	2.5	180	0.9	279	0.9	379	36.6		
80	3.3	181	1.0	280	1.1	380	31.6		
81	4.1	182	1.2	281	1.6	381	29.0		
82	4.7	183	1.3	282	2.3	382	28.6		
83	5.2	184	1.4	283	3.4	383	28.8		
84	5.6	185	1.4	284	4.4	384	28.8		
85	5.9	186	1.7	285	5.1	385	28.9		
86	6.3	187	1.4	286	5.0	386	29.7		
87	6.9	188	1.1	287	4.9	387	30.7		
88	7.2	189	1.0	288	5.7	388	31.1		
89	7.0	190	1.1	289	8.0	389	30.1		
90	6.3	191	1.2	290	12.4	390	29.0		
91	5.3	192	1.3	291	18.8	391	30.0		
92	4.5	193	1.5	292	25.0	392	34.2		
93	3.7	194	1.5	293	28.4	393	41.3		
94	3.3	195	1.3	294	28.0	394	49.0		
95	3.3	196	1.1	295	24.6	395	54.6		
96	3.6	197	1.0	296	19.2	396	56.9		
97	4.1	198	1.0	297	13.2	397	55.1		
98	4.8	199	1.0	298	8.8	398	52.6		
99	5.5	200	1.0	299	6.0	399	50.4		
100	6.2			300	4.6				

Paleomagnetic Data - CORE 2

Depth	declination	inclination	intensity	Depth	declination	inclination	intensity	Depth	declination	inclination	intensity	Depth	declination	inclination	intensity
0	33.44	-13.067	8.68E-07	151	220.136	59.44	5.92E-05	301	294.053	57.836	4.39E-05	451	65.831	60.104	1.91E-05
2	34.033	-9.318	1.14E-06	153	218.92	60.496	5.51E-05	303	295.47	56.961	4.50E-05	453	57.589	62.243	1.52E-05
4	41.388	-4.422	1.51E-06	155	217.641	61.295	5.12E-05	305	296.481	56.221	4.45E-05	455	49.79	64.951	1.21E-05
6	44.009	-0.78	1.73E-06	157	215.774	62.167	4.74E-05	307	297.251	55.757	4.33E-05	457	40.417	69.615	9.73E-06
8	48.629	3.854	1.89E-06	159	213.887	62.721	4.39E-05	309	297.608	55.965	4.23E-05	459	26.463	77.128	8.12E-06
10	53.917	12.161	2.01E-06	161	212.068	62.649	4.13E-05	311	297.862	56.337	4.13E-05	461	359.98	85.825	7.35E-06
12	59.695	24.53	2.32E-06	163	209.987	62.034	3.95E-05	313	298.683	55.976	4.01E-05	463	196.088	85.004	7.47E-06
14	53.684	40.848	2.63E-06	165	207.767	61.273	3.87E-05	315	299.966	55.167	3.85E-05	465	176.074	77.561	8.57E-06
16	32.201	52.029	3.35E-06	167	206.442	60.559	3.87E-05	317	301.282	55.398	3.64E-05	467	162.117	72.683	1.05E-05
18	4.571	52.877	4.63E-06	169	205.405	60.009	3.91E-05	319	301.465	56.335	3.42E-05	469	143.8	69.929	1.32E-05
20	351.107	48.75	6.36E-06	171	204.698	59.488	3.97E-05	321	300.962	57.325	3.23E-05	471	125.691	68.413	1.65E-05
22	345.999	43.886	8.22E-06	173	204.908	59.196	4.06E-05	323	300.86	58.176	3.08E-05	473	113.049	67.676	2.01E-05
24	343.837	38.496	1.04E-05	175	206.381	59.424	4.16E-05	325	301.416	58.68	2.95E-05	475	106.051	66.097	2.4E-05
26	342.625	34.023	1.25E-05	177	209.205	60.112	4.27E-05	327	302.852	58.965	2.82E-05	477	104.468	64.23	2.76E-05
28	341.868	30.489	1.41E-05	179	212.478	61.22	4.31E-05	329	305.324	59.699	2.67E-05	479	106.318	62.719	3.14E-05
30	342.43	27.283	1.46E-05	181	215.238	62.623	4.24E-05	331	307.429	60.494	2.52E-05	481	107.802	61.376	3.56E-05
32	343.711	24.783	1.42E-05	183	217.134	63.788	4.11E-05	333	309.688	61.389	2.38E-05	483	108.755	60.52	3.98E-05
34	345.8	24.819	1.30E-05	185	217.032	64.065	4.02E-05	335	312.075	61.945	2.29E-05	485	109.469	60.465	4.3E-05
36	350.747	28.391	1.13E-05	187	215.028	62.932	4.03E-05	337	313.861	62.347	2.26E-05	487	110.378	60.56	4.52E-05
38	355.789	35.113	9.77E-06	189	213.86	61.684	4.12E-05	339	312.649	62.991	2.24E-05	489	111.016	60.653	4.7E-05
40	1.667	44.699	9.05E-06	191	214.702	61.6	4.26E-05	341	308.492	64.368	2.21E-05	491	113.564	60.722	4.87E-05
42	5.792	55.018	9.55E-06	193	215.24	62.318	4.43E-05	343	301.966	65.976	2.22E-05	493	122.336	60.664	5.04E-05
44	7.608	61.946	1.11E-05	195	214.467	62.1	4.59E-05	345	294.5	67.17	2.35E-05	495	126.457	60.681	5.21E-05
46	5.27	64.697	1.31E-05	197	212.943	60.281	4.79E-05	347	287.741	66.654	2.60E-05	497	129.484	60.929	5.33E-05
48	0.066	64.7	1.51E-05	199	211.973	58.034	5.14E-05	349	284.186	65.236	2.93E-05	499	131.538	60.869	5.4E-05
50	354.758	63.285	1.67E-05	201	212.063	56.924	5.61E-05	351	282.915	63.168	3.29E-05	501	132.557	60.84	5.41E-05
52	349.344	60.955	1.79E-05	203	213.231	56.848	6.02E-05	353	283.39	61.457	3.68E-05	503	132.744	61.326	5.41E-05
54	345.576	57.788	1.90E-05	205	215.4	57.265	6.21E-05	355	284.426	60.458	4.08E-05	505	132.089	62.003	5.38E-05
56	343.017	54.421	2.00E-05	207	217.374	57.839	6.18E-05	357	285.675	60.056	4.45E-05	507	131.532	62.893	5.31E-05
58	340.945	51.299	2.03E-05	209	218.678	57.807	6.11E-05	359	287.621	59.421	4.73E-05	509	131.078	63.818	0.000052
60	338.515	49.391	1.98E-05	211	218.48	57.19	6.15E-05	361	290.368	58.766	4.92E-05	511	131.424	64.66	5.14E-05
62	335.289	50.943	1.85E-05	213	218.383	55.867	6.33E-05	363	292.994	58.18	5.07E-05	513	132.349	65.267	5.17E-05
64	329.183	57.235	1.73E-05	215	218.934	54.681	6.53E-05	365	295.151	57.892	5.15E-05	515	133.808	66.21	5.26E-05
66	321.5	65.999	1.75E-05	217	220.871	54.87	6.64E-05	367	296.706	57.603	5.15E-05	517	134.711	67.752	5.38E-05
68	320.755	72.719	1.96E-05	219	225.774	57.498	6.62E-05	369	297.384	57.55	5.05E-05	519	134.712	69.654	5.53E-05
70	337.072	75.463	2.34E-05	221	235.56	62.916	6.46E-05	371	297.253	58.079	4.88E-05	521	132.049	70.846	5.71E-05
72	354.646	74.159	2.80E-05	223	254.529	69.234	6.22E-05	373	296.394	58.756	4.69E-05	523	122.756	70.106	5.93E-05
74	3.821	71.781	3.26E-05	225	280.71	72.368	5.97E-05	375	295.644	59.202	4.55E-05	525	107.427	65.484	6.3E-05
76	9.885	70.049	3.69E-05	227	303.855	71.818	5.61E-05	377	295.666	59.322	4.41E-05	527	93.961	56.076	6.93E-05
78	12.759	69.742	4.09E-05	229	318.358	70.032	5.24E-05	379	295.957	59.25	4.20E-05	529	85.123	43.257	8.06E-05
80	14.234	70.593	4.44E-05	231	327.372	69.12	4.98E-05	381	296.284	59.327	3.85E-05	531	80.609	29.981	0.088E-05
82	13.407	71.353	4.69E-05	233	332.204	68.713	4.76E-05	383	296.68	59.99	3.48E-05	533	79.489	19.626	0.000119
84	10.952	71.263	4.89E-05	235	332.779	68.791	4.48E-05	385	296.753	62.226	3.13E-05	535	80.139	12.095	0.000135
86	6.721	70.628	5.03E-05	237	323.064	70.538	4.17E-05	387	295.729	65.145	2.82E-05	537	81.275	6.979	0.000143
88	1.594	70.157	5.05E-05	239	288.842	72.256	4.11E-05	389	294.481	67.28	2.57E-05	539	82.123	4.381	0.000142
90	357.364	70.407	4.89E-05	241	248.634	66.177	4.56E-05	391	293.824	68.63	2.39E-05	541	82.737	3.521	0.000136
92	354.499	71.902	4.60E-05	243	230.227	56.858	5.53E-05	393	292.37	70.384	2.32E-05	543	83.559	2.895	0.000124
94	356.587	74.263	4.33E-05	245	224.018	50.913	6.63E-05	395	286.577	71.921	2.35E-05	545	85.197	2.157	0.000107
96	9.821	75.61	4.19E-05	247	222.413	48.141	7.67E-05	397	279.102	72.249	2.44E-05	547	88.641	3.774	8.55E-05
98	27.373	73.564	4.19E-05	249	223.047	47.377	8.57E-05	399	275.295	71.216	2.60E-05	549	95.583	11.678	6.2E-05
100	39.871	68.558	4.22E-05	251	224.459	47.815	9.18E-05	401	275.23	68.612	2.87E-05	551	109.175	30.117	4.34E-05
102	47.79	63.06	4.22E-05	253	226.242	48.795	9.37E-05	403	276.627	66.49	3.19E-05	553	131.568	53.321	3.63E-05
104	54.204	58.793	4.27E-05	255	228.203	50.13	9.13E-05	405	278.267	63.754	3.49E-05	555	153.31	67.762	3.5E-05
106	60.227	56.596	4.46E-05	257	229.703	51.922	8.55E-05	407	280.448	60.406	3.79E-05	557	157.497	75.634	3.32E-05
108	65.124	55.764	4.76E-05	259	230.678	53.888	7.74E-05	409	283.035	57.394	4.14E-05	559	139.378	79.694	3.03E-05
110	66.999	55.493	5.01E-05	261	231.403	55.651	6.79E-05	411	284.608	55.96	0.000045	561	110.208	79.971	2.68E-05
112	65.752	55.565	5.16E-05	263	232.438	57.992	5.72E-05	413	283.462	56.965	4.71E-05	563	89.504	77.763	2.29E-05
114	63.31	56.332	5.23E-05	265	296.862	72.003	2.45E-05	415	279.301	61.125	4.66E-05				
116	61.01	58.036	5.24E-05	267	302.459	65.427	3.34E-05	417	272.593	68.632	4.52E-05				
118	59.219	59.532	5.22E-05	269	304.621	61.092	4.17E-05	419	262.704	78.579	4.59E-05				
120	57.112	60.023	5.18E-05	271	306.428	58.505	4.90E-05	421	220.34	86.96	4.87E-05				
122	53.993	59.692	5.10E-05	273	307.731	56.592	5.59E-05	423	113.866	83.656	5.04E-05				
124	50.76	59.68	4.97E-05	275	309.375	55.215	6.11E-05	425	104.935	76.186	5.03E-05				
126	49.368	61.381	4.76E-05	277	311.215	53.787	6.36E-05	427	106.407	68.406	5.07E-05				
128	49.929	66.645	4.46E-05	279	312.816	52.508	6.31E-05	429	108.79	61.361	5.33E-05				
130	55.022	75.322	4.19E-05	281	313.925	52.023	5.98E-05	431	110.693	56.86	5.59E-05				
131	84.769	85.254	4.19E-05	283	314.187	52.929	5.44E-05	433	110.326	54.844	5.59E-05				
133	201.724	82.642	4.49E-05	285	314.175	54.752	4.90E-05	435	107.628	54.413	5.33E-05				
135	215.906	74.443	4.92E-05	287	312.969	57.052	4.44E-05	437	104.174	55.075	4.93E-05				
137	220.286	67.303	5.35E-05	289	310.46	59.114	4.10E-05	439	101.734	56.213	4.57E-05				
139	221.246	61.949	5.84E-05	291	306.134	60.									

Paleomagnetic Data - CORE 3

Depth	declination	inclination	intensity	Depth	declination	inclination	intensity	Depth	declination	inclination	intensity	Depth	declination	inclination	intensity
0	353.382	4.588	9.05E-08	150	16.966	52.198	1.26E-05	301	96.479	64	4.22E-07	450	36.911	59.449	2.73E-05
2	356.875	4.765	1.02E-07	152	350.758	65.551	7.81E-06	303	105.336	64.377	4.12E-07	452	36.587	59.723	2.57E-05
4	0.246	8.527	1.13E-07	154	288.099	68.742	5.62E-06	305	147.019	48.29	5.5E-07	454	35.495	62.262	2.39E-05
6	4.371	14.981	1.19E-07	156	254.625	61.37	4.54E-06	307	161.209	29.942	1.05E-06	456	32.895	65.781	2.25E-05
8	9.285	23.083	1.22E-07	158	241.156	56.477	3.78E-06	309	163.246	26.337	1.71E-06	458	32.107	70.557	2.18E-05
10	15.454	34.12	1.25E-07	160	233.225	56.317	3.28E-06	311	161.563	30.269	2.23E-06	460	35.534	75.917	2.23E-05
12	24.813	47.877	1.32E-07	162	227.933	59.498	3E-06	313	158.342	36.68	2.56E-06	462	46.995	79.015	2.44E-05
14	40.222	60.079	1.46E-07	164	226.992	64.989	2.81E-06	315	155.655	40.874	2.71E-06	464	53.569	78.059	2.82E-05
16	59.92	67.366	1.63E-07	166	224.666	75.114	2.64E-06	317	154.316	41.551	2.67E-06	466	48.302	74.667	3.34E-05
18	75.532	70.133	1.81E-07	168	249.653	82.787	2.65E-06	319	154.148	42.132	2.58E-06	468	40.183	71.455	3.83E-05
20	85.298	71.119	1.97E-07	170	333.387	84.074	2.85E-06	321	154.045	45.573	2.51E-06	470	35.1	69.077	4.15E-05
22	94.909	61.792	1.41E-07	172	21.359	76.361	3.26E-06	323	152.349	51.546	2.31E-06	472	32.752	67.758	4.21E-05
24	106.542	62.189	1.5E-07	174	21.986	70.005	3.81E-06	325	144.4	61.224	1.83E-06	474	32.034	67.071	4.17E-05
26	116.928	61.177	1.57E-07	176	21.131	66.341	4.28E-06	327	81.985	75.835	1.28E-06	476	31.742	66.85	4.15E-05
28	123.417	60.193	1.64E-07	178	20.788	63.841	4.54E-06	329	7.289	51.624	1.15E-06	478	31.024	66.067	4.08E-05
30	128.028	60.083	1.7E-07	180	22.042	60.894	4.76E-06	331	353.328	33.014	1.28E-06	480	29.276	63.843	3.88E-05
32	132.147	61.086	1.73E-07	182	28.004	56.52	5.19E-06	333	345.71	25.781	1.4E-06	482	26.917	60.602	3.55E-05
34	136.574	62.333	1.74E-07	184	29.287	53.824	5.6E-06	335	340.789	23.973	1.6E-06	484	26.262	58.756	3.25E-05
36	141.443	64.635	1.77E-07	186	29.718	51.958	5.61E-06	337	338.136	24.739	1.95E-06	486	30.644	58.951	3.05E-05
38	146.54	69.22	1.84E-07	188	29.077	50.174	5.23E-06	339	330.122	28.755	2.34E-06	488	37.537	58.553	3.01E-05
40	152.829	77.45	2E-07	190	27.76	49.832	4.74E-06	341	319.345	43.836	2.27E-06	490	42.863	56.263	3.08E-05
42	199.881	86.781	2.29E-07	192	27.527	52.303	4.31E-06	343	228.082	66.386	2.53E-06	492	43.966	53.871	3.11E-05
44	293.163	81.489	2.8E-07	194	29.293	55.174	3.94E-06	345	174.359	39.82	5.63E-06	494	43.654	51.532	3.03E-05
46	288.638	77.145	3.69E-07	196	30.561	55.24	3.52E-06	347	163.145	32.851	1.06E-05	496	43.173	49.305	2.86E-05
48	254.035	76.838	5.18E-07	198	29.23	54.459	3.08E-06	349	154.056	35.363	1.54E-05	498	42.79	47.552	2.63E-05
50	209.251	71.983	7.83E-07	200	25.712	57.238	2.64E-06	351	148.037	40.907	1.86E-05	500	41.324	46.831	2.3E-05
52	185.896	66.042	1.2E-06	202	22.596	64.341	2.25E-06	353	143.859	44.888	2.02E-05	502	40.602	45.63	1.88E-05
54	171.369	65.19	1.8E-06	204	22.272	70.894	1.96E-06	355	141.827	45.107	2.05E-05	504	37.714	45.054	1.39E-05
56	160.66	66.433	2.63E-06	206	26.859	74.358	1.79E-06	357	143.657	43.257	2.08E-05	506	32.058	47.569	8.92E-06
58	153.906	66.284	3.6E-06	208	37.371	76.618	1.73E-06	359	145.834	42.255	2.18E-05	508	16.944	59.636	4.83E-06
60	142.99	64.513	4.64E-06	210	44.764	76.454	1.79E-06	361	147.133	42.38	2.25E-05				
62	136.245	64.982	5.66E-06	212	40.809	73.577	1.96E-06	363	146.189	43.324	2.09E-05				
64	128.851	64.901	6.82E-06	214	34.152	69.546	2.18E-06	365	143.876	46.917	1.66E-05				
66	130.559	64.813	7.92E-06	216	31.043	66.538	2.34E-06	367	142.401	54.147	1.18E-05				
68	133.183	62.367	8.93E-06	218	30.181	64.809	2.35E-06	369	148.338	59.412	8.68E-06				
70	134.557	61.621	9.82E-06	220	29.791	63.964	2.32E-06	371	161.773	53.977	7.78E-06				
72	128.39	63.012	1.08E-05	222	28.529	63.229	2.37E-06	373	167.381	43.234	8.79E-06				
74	119.097	66.182	1.16E-05	224	25.849	60.906	2.52E-06	375	168.43	36.313	1.06E-05				
76	109.237	68.086	1.16E-05	226	22.76	56.868	2.64E-06	377	167.349	35.445	1.15E-05				
78	101.602	68.719	1.07E-05	228	20.139	52.723	2.61E-06	379	164.878	40.474	1.12E-05				
80	97.44	69.592	9.66E-06	230	18.481	50.569	2.4E-06	381	162.034	48.406	1.05E-05				
82	98.087	71.209	9.12E-06	232	18.2	51.737	2.14E-06	383	160.42	54.064	9.69E-06				
84	100.891	73.571	8.7E-06	234	19.304	55.259	1.99E-06	384	160.131	56.224	9.11E-06				
86	97.705	73.769	7.94E-06	236	21.608	59.015	1.95E-06	386	159.536	57.644	8.91E-06				
88	88.818	75.851	6.74E-06	238	21.925	58.352	1.93E-06	388	156.587	60.977	8.93E-06				
90	72.944	73.577	5.99E-06	240	22.392	55.161	1.81E-06	390	148.235	66.638	8.55E-06				
92	85.033	75.08	5.73E-06	242	24.464	52.346	1.59E-06	392	118.455	75.053	7.55E-06				
94	105.028	75.226	5.96E-06	244	29.373	52.66	1.32E-06	394	46.47	72.562	6.66E-06				
96	117.49	74.059	6.36E-06	246	37.831	55.772	1.09E-06	396	20.954	60.048	6.27E-06				
98	124.911	72.757	6.67E-06	248	55.124	60.241	8.93E-07	398	11.491	54.036	5.8E-06				
100	127.865	72.468	7.02E-06	250	54.449	55.808	7.58E-07	400	10.595	53.182	5.14E-06				
102	127.105	73.673	7.61E-06	252	58.932	53.231	6.08E-07	402	11.909	54.638	4.44E-06				
104	127.927	75.019	8.35E-06	253	137.335	41.629	1.47E-07	404	13.874	57.618	3.78E-06				
106	135.624	74.634	9E-06	255	134.457	42.966	1.68E-07	406	12.248	58.154	3.28E-06				
108	145.305	71.876	9.7E-06	257	135.78	43.548	1.87E-07	408	359.147	60.924	2.73E-06				
110	148.429	69.088	1.09E-05	259	137.884	45.12	2.08E-07	410	346.208	65.908	2.21E-06				
112	141.935	68.195	1.28E-05	261	137.999	47.008	2.26E-07	412	319.319	75.623	1.92E-06				
114	129.088	69.201	1.46E-05	263	135.879	49.403	2.32E-07	414	248.958	81.673	2.07E-06				
116	113.705	69.692	1.58E-05	265	134.501	52.612	2.28E-07	416	195.428	80.904	2.67E-06				
118	104.939	68.581	1.64E-05	267	135.857	56.25	2.16E-07	418	157.293	83.461	3.56E-06				
120	107.278	66.505	1.7E-05	269	141.513	59.261	2.13E-07	420	105.161	84.07	4.66E-06				
122	114.174	64.156	1.87E-05	271	152.54	60.362	2.14E-07	422	80.626	81.204	5.99E-06				
124	115.163	62.704	2.16E-05	273	164.835	60.586	2.15E-07	424	74.981	76.502	7.55E-06				
126	105.568	63.153	2.57E-05	275	174.735	61.151	2.2E-07	426	73.297	73.883	9.4E-06				
128	86.382	62.162	3.11E-05	277	181.218	62.829	2.32E-07	428	73.556	73.147	1.14E-05				
130	70.059	59.344	3.74E-05	279	182.198	61.738	2.53E-07	430	69.325	72.363	1.37E-05				
132	61.516	56.742	4.27E-05	281	174.768	54.534	2.91E-07	432	69.534	71.593	1.61E-05				
134	58.455	55.004	4.55E-05	283	166.722	44.166	3.66E-07	434	62.959	69.621	1.89E-05				
136	57.22	54.131	4.65E-05	285	161.889	37.858	4.65E-07	436	57.747	67.151	2.22E-05				
138	55.183	54	4.67E-05	287	155.248	40.841	5.1E-07	438	54.536	65.442	0.000025				
140	51.43	53.54	4.59E-05	289	151.645	42.956	5.68E-07	440	52.202	63.676	2.69E-05				
142	45.907	51.44	4.25E-05	291	147.29	45.146	5.82E-07	442	49.327	62.31	2.82E-05				
144	40.134	47.457	3.67E-05	293	142.324	46.673	5.61E-07	444	46.291	61.922	2.91E-05				
146	34.051	44.35	2.88E-05	295	136.132	49.319	5.27E-07	446	43.785	61.399	2.94E-05				
148	27.255	45.097	2.02E-05	297	127.496	54.334	4.97E-07	448	41.619	60.352	2.87E-05				
				299	114.24	60.179	4.62E-07								

Paleomagnetic Data - CORE 4															
Depth	declination	inclination	intensity	Depth	declination	inclination	intensity	Depth	declination	inclination	intensity	Depth	declination	inclination	intensity
0	9.235	-54.293	3.48E-07	150	256.617	40.067	2.52E-06	301	233.248	56.609	2.73E-05	451	55.679	56.678	0.000128
2	32.074	-55.04	3.71E-07	152	251.193	49.471	1.8E-06	303	236.577	58.441	2.59E-05	453	59.11	54.534	0.000118
4	47.802	-50.792	4.13E-07	154	252.534	59.387	1.41E-06	305	242.295	64.291	2.29E-05	455	62.787	52.215	0.000106
6	56.216	-45.501	4.65E-07	156	253.23	77.879	1.1E-06	307	249.513	68.211	2.02E-05	457	67.183	50.393	9.21E-05
8	61.328	-38.979	5.19E-07	158	297.419	84.839	9.43E-07	309	243.591	70.551	1.76E-05	459	72.708	48.641	7.94E-05
10	65.12	-31.623	5.7E-07	159	350.509	81.51	7.78E-07	311	230.742	69.079	1.59E-05	461	77.339	47.578	6.68E-05
12	66.631	-24.752	6.13E-07	159	191.006	55.817	4.84E-07	313	223.494	67.449	1.53E-05	463	78.517	46.555	5.31E-05
14	64.427	-18.684	6.47E-07	161	187.892	53.735	6.87E-07	315	224.903	67.656	1.47E-05	465	72.856	45.434	3.69E-05
16	59.147	-13.589	6.85E-07	163	185.588	55.923	8.98E-07	317	234.484	69.61	1.25E-05	467	53.838	42.684	2.15E-05
18	52.48	-9.963	6.71E-07	165	184.738	58.898	1.07E-06	319	262.851	73.479	9.03E-06	469	7.579	26.405	1.12E-05
20	45.161	-7.802	6.75E-07	167	184.928	60.976	1.2E-06	321	322.487	71.728	6.01E-06	471	318.901	-7.657	1.07E-05
22	38.69	-6.578	6.82E-07	169	185.215	61.735	1.27E-06	321	187.36	77.481	4.48E-07	473	291.348	-25.711	1.35E-05
24	34.759	-6.139	6.67E-07	171	184.802	62.68	1.34E-06	323	191.563	82.635	5.62E-07	475	277.872	-33.499	1.6E-05
26	32.319	-6.464	6.3E-07	173	184.194	63.642	1.39E-06	325	202.02	85.409	7.04E-07	477	271.937	-34.537	1.69E-05
28	30.329	-6.958	5.77E-07	175	183.305	64.408	1.42E-06	327	208.662	85.931	8.6E-07				
30	28.361	-6.825	5.19E-07	177	182.439	64.695	1.4E-06	329	200.992	84.973	1.05E-06				
32	26.631	-5.647	4.64E-07	179	181.024	64.414	1.37E-06	331	187.303	82.716	1.3E-06				
34	25.563	-4.721	4.18E-07	181	179.06	62.923	1.41E-06	333	175.94	79.737	1.61E-06				
36	25.069	-2.744	3.91E-07	183	176.711	58.171	1.58E-06	335	166.443	77.656	2.06E-06				
38	24.428	1.585	3.8E-07	185	173.887	52.457	1.8E-06	337	156.071	78.262	2.65E-06				
40	23.357	7.412	3.84E-07	187	170.145	50.327	2.05E-06	339	142.296	80.487	3.4E-06				
42	21.802	12.342	4.08E-07	189	167.338	52.548	2.25E-06	341	127.859	82.251	4.22E-06				
44	19.362	15.655	4.56E-07	191	165.805	55.238	2.38E-06	343	116.148	83.437	5.07E-06				
46	16.793	17.826	5.05E-07	193	165.034	56.447	2.35E-06	345	111.085	84.202	5.96E-06				
48	15.242	18.415	5.37E-07	195	164.622	57.219	2.22E-06	347	122.185	84.133	7.08E-06				
50	14.835	17.155	5.66E-07	197	164.775	59.221	2.1E-06	349	140.443	81.757	8.56E-06				
52	14.812	15.719	5.7E-07	199	165.651	62.276	1.99E-06	351	141.789	77.458	1.07E-05				
54	14.783	15.263	5.79E-07	201	166.901	65.361	1.78E-06	353	137.918	74.694	1.36E-05				
56	15.094	14.954	5.67E-07	203	169.686	70.755	1.45E-06	355	130.862	73.677	1.8E-05				
58	15.81	7.411	9.4E-07	205	184.046	79.914	1.12E-06	357	122.828	74.821	2.37E-05				
60	15.366	6.549	8.94E-07	207	251.016	84.285	9.16E-07	359	107.879	76.096	3.05E-05				
62	14.475	7.036	8.44E-07	209	275.777	81.872	7.78E-07	361	85.633	76.194	3.89E-05				
64	13.161	8.841	7.96E-07	211	272.527	81.064	6.64E-07	363	62.462	74.378	4.84E-05				
66	11.1	11.375	7.56E-07	213	256.415	81.466	5.94E-07	365	43.384	71.16	5.85E-05				
68	8.549	15.541	7.16E-07	215	233.098	81.441	5.49E-07	367	31.759	67.556	6.77E-05				
70	7.271	23.457	6.83E-07	217	213.702	81.246	5.23E-07	369	25.032	64.315	7.46E-05				
72	11.026	36.586	7.04E-07	219	201.938	81.493	5.09E-07	371	21.437	61.254	7.86E-05				
74	23.982	50.582	8.72E-07	221	194.278	81.241	4.99E-07	373	19.672	58.423	8.03E-05				
76	42.055	56.444	1.23E-06	223	186.636	79.211	4.86E-07	375	18.332	56.318	7.95E-05				
78	52.926	55.571	1.84E-06	225	183.63	76.017	4.81E-07	377	16.823	54.492	7.51E-05				
80	59.508	50.24	2.76E-06	227	186.017	73.514	4.95E-07	379	14.736	52.933	6.73E-05				
82	61.331	47.604	3.75E-06	229	189.155	71.979	5.16E-07	381	13.389	52.762	5.8E-05				
84	60.827	47.903	4.51E-06	231	189.646	71.825	5.23E-07	383	14.38	56.498	4.87E-05				
86	62.428	47.024	5.04E-06	233	186.417	72.318	5.18E-07	385	23.345	64.998	4.1E-05				
88	62.706	48.394	5.29E-06	235	181.793	70.52	5.28E-07	387	57.359	74.503	3.71E-05				
90	62.777	50.53	5.52E-06	237	179.821	64.586	5.7E-07	389	103.418	73.625	3.91E-05				
92	62.172	53.015	5.81E-06	239	180.491	59.053	6.43E-07	391	119.341	71.429	4.54E-05				
94	60.378	54.469	6E-06	241	183.528	58.474	7.28E-07	393	119.49	72.154	5.34E-05				
96	57.008	55.051	5.96E-06	243	187.665	60.802	8.25E-07	395	111.315	73.306	6.05E-05				
98	52.88	56.102	5.61E-06	245	190.003	62.009	9.14E-07	397	98.887	73.317	6.56E-05				
100	44.777	59.945	4.98E-06	247	189.755	62.1	9.68E-07	399	84.904	72.594	6.96E-05				
102	30.787	64.6	4.43E-06	249	188.454	63.833	1.02E-06	401	73.6	71.459	7.28E-05				
104	16.954	65.718	4.13E-06	251	187.929	67.182	1.09E-06	403	65.489	70.621	7.29E-05				
106	354.583	63.496	4.01E-06	253	188.349	70.041	1.14E-06	405	56.796	69.718	6.84E-05				
108	336.053	57.722	4.06E-06	255	189.29	72.725	1.09E-06	407	46.465	68.733	6.15E-05				
110	319.24	52.75	4.26E-06	257	190.256	76.544	1.01E-06	409	38.167	68.471	5.49E-05				
112	300.561	56.694	4.58E-06	259	185.768	80.208	9.5E-07	411	34.656	70.171	4.86E-05				
114	254.434	67.653	5.61E-06	261	167.29	81.961	9.2E-07	413	39.847	74.331	4.29E-05				
116	185.064	84.01	8.86E-06	263	126.805	83.201	8.8E-07	415	62.15	79.459	3.99E-05				
118	156.317	55.608	1.52E-05	265	64.687	79.265	8.55E-07	417	108.211	80.431	4.21E-05				
120	137.415	53.198	2.39E-05	267	42.432	69.152	8.75E-07	419	133.179	77.417	4.93E-05				
122	121.267	53.71	3.37E-05	269	36.781	57.563	9.37E-07	421	135.438	75.069	5.95E-05				
124	109.296	54.456	4.2E-05	271	36.31	46.766	1.08E-06	423	130.751	74.539	7.1E-05				
126	102.195	54.167	4.66E-05	273	38.752	40.064	1.33E-06	425	122.75	74.694	8.34E-05				
128	98.576	53.074	4.76E-05	275	44.94	38.171	1.65E-06	427	112.54	75.123	9.76E-05				
130	96.555	52.663	4.71E-05	277	58.294	38.299	2.14E-06	429	100.047	75.462	0.000112				
132	94.288	53.17	4.61E-05	279	74.379	47.952	2.55E-06	431	85.897	75.291	0.000126				
134	89.996	53.93	4.23E-05	281	120.628	59.375	3.35E-06	433	71.839	74.464	0.000137				
136	81.202	53.607	3.47E-05	283	170.864	52.092	5.7E-06	435	59.917	73.074	0.000146				
138	65.721	52.644	2.49E-05	285	195.48	45.607	9.83E-06	437	50.81	71.056	0.000153				
140	43.417	51.97	1.62E-05	287	208.667	46.708	1.48E-05	439	43.886	68.713	0.000157				
142	13.053	53.004	9.59E-06	289	220.816	51.005	1.95E-05	441	39.869	66.097	0.000159				
144	327.38	53.025	5.76E-06	291	230.526	55.154	2.29E-05	443	39.005	63.706	0.000156				
146	287.227	45.568	4.11E-06	293	237.202	56.537	2.45E-05	445	41.328	61.801	0.000151				
148	266.066	39.76	3.24E-06	295	239.173	56.63	2.48E-05	447	45.89	60.21	0.000143				
				297	238.419	55.794	2.57E-05	449	51.247	58.551	0.000135				
				299	234.717	56.217	2.68E-05								

LOSS-ON-IGNITION CORE 2											
Depth (cm)	LOI %	Depth (cm)	LOI %	Depth (cm)	LOI %	Depth (cm)	LOI %	Depth (cm)	LOI %	Depth (cm)	LOI %
1	31.52	101	39.44	201	34.07	301	30.47	401	30.62	501	19.44
2	21.18	102	38.30	202	31.74	302	27.82	402	29.75	502	7.47
3	21.22	103	36.36	203	21.64	303	27.69	403	28.61	503	29.24
4	20.90	104	32.77	204	11.16	304	32.04	404	29.07	504	38.73
5	21.98	105	27.36	205	31.36	305	10.34	405	31.89	505	36.66
6	24.93	106	37.50	206	30.41	306	32.87	406	22.64	506	17.91
7	26.89	107	33.89	207	28.88	307	32.05	407	20.06	507	3.57
8	30.34	108	32.45	208	30.63	308	29.10	408	29.02	508	29.78
9	30.34	109	27.51	209	29.47	309	32.12	409	31.89	509	44.37
10	31.90	110	27.75	210	26.09	310	27.47	410	30.58	510	41.57
11	32.02	111	39.58	211	21.64	311	33.24	411	29.17	511	29.08
12	35.86	112	33.24	212	28.57	312	35.48	412	18.85	512	26.49
13	34.64	113	38.76	213	27.95	313	31.23	413	29.23	513	32.65
14	35.80	114	37.77	214	29.33	314	34.59	414	31.96	514	7.77
15	35.77	115	37.28	215	28.57	315	32.94	415	28.53	515	29.95
16	36.18	116	38.36	216	27.78	316	31.64	415.5	1.69	516	33.89
17	35.51	117	38.76	217	28.38	317	29.91	416	11.36	517.5	23.51
18	35.83	118	32.35	218	5.37	318	32.99	417	30.60	518	2.78
19	35.12	119	37.99	219	5.15	319	30.25	418	29.15	519	4.41
20	34.76	120	35.25	220	26.83	320	28.49	419	28.66	520	12.90
21	35.37	121	38.10	221	26.17	321	32.12	420	30.79	521	23.67
22	35.14	122	36.33	222	4.74	322	33.91	421	28.86	522	2.91
23	36.04	123	33.82	223	11.07	323	34.38	422	2.48	523	20.68
24	36.36	124	34.12	224	35.09	324	34.04	423	8.59	524	1.98
25	35.69	125	35.16	225	16.74	325	34.29	424	11.86	525	3.25
26	34.63	126	31.81	226	36.46	326	30.39	425	11.62	526	20.14
27	35.25	127	34.47	227	37.61	327	32.02	426	21.74	527	3.19
28	36.02	128	36.76	228	28.98	328	31.10	427	16.73	528	12.15
29	35.98	129	35.88	229	3.43	329	33.02	428	19.27	529	11.83
30	31.91	130	36.79	230	5.78	330	31.56	429	28.86	530	5.49
31	25.09	131	35.75	231	5.95	331	31.62	430	29.18	531	1.96
32	23.98	132	31.52	232	5.65	332	35.61	431	32.12	532	14.48
33	27.71	133	28.86	233	6.45	333	36.62	432	27.15	533	12.89
34	33.69	134	31.42	234	6.65	334	35.61	433	31.85	534	1.96
35	35.47	135	33.43	235	6.67	335	36.20	434	31.96	535	2.76
36	37.10	136	36.45	236	9.26	336	38.35	435	26.90	536	17.61
37	40.34	137	35.40	237	16.80	337	33.22	436	29.26	537	15.80
38	37.80	138	34.83	238	21.79	338	32.16	437	33.76	538	2.40
39	38.60	139	38.11	239	30.75	339	35.31	438	32.51	539	4.06
40	36.64	140	34.81	240	30.72	340	36.63	439.5	28.08	540	4.29
41	37.50	141	36.25	241	36.59	341	34.04	440	3.68	541	3.41
42	38.42	142	38.88	242	37.38	342	31.08	441	7.77	542	4.57
43	38.19	143	26.99	243	39.11	343	32.74	442	7.23	543	5.32
44	37.86	144	37.10	244	37.66	344	24.22	443	6.69	544	5.10
45	37.64	145	36.86	245	34.01	345	31.85	444	8.05	545	4.98
46	38.66	146	36.86	246	33.21	346	30.05	445	8.09	546	10.74
47	40.31	147	36.92	247	33.57	347	29.16	446	9.28	547	5.18
48	38.16	148	34.24	248	33.91	348	30.67	447	10.12	548	34.66
49	37.50	149	35.86	249	27.89	349	33.67	448	11.74	549	38.28
50	37.25	150	32.09	250	23.58	350	32.16	449	7.04	550	37.15
51	36.39	151	41.37	251	30.84	351	28.76	450	34.41	551	26.54
52	37.58	152	35.31	252	29.87	352	28.57	451	29.62	552	5.59
53	39.12	153	37.68	253	29.26	353	31.50	452	30.88	553	29.34
54	37.88	154	36.69	254	28.45	354	29.66	453	31.01	554.5	22.92
55	37.86	155	34.02	255	18.56	355	28.00	454	32.55	556	7.75
56	35.90	156	38.93	256	36.16	356	36.12	455	29.96	557	28.31
57	34.98	157	35.09	257	35.96	357	35.19	456	28.26	558	35.39
58	34.08	158	34.20	258	28.53	358	33.23	457	29.41	559	29.24
59	32.82	159	27.78	259	35.17	359	25.44	458	30.30	560	38.77
60	33.09	160	30.32	260	33.33	360	32.13	459	33.96		
61	31.58	161	32.04	261	32.68	361	34.54	460	24.10		
62	29.09	162	31.27	262	37.71	362	31.38	461	14.36		
63	30.53	163	35.14	263	30.99	363	29.92	462	19.35		
64	33.82	164	28.24	264	38.68	364	32.69	463	27.25		
65	36.54	165	8.29	265	36.25	365	34.83	464	31.77		
66	35.19	166	10.11	266	30.34	366	33.66	465	33.97		
67	34.17	167	10.51	267	31.63	367	30.79	466	34.86		
68	34.44	168	15.76	268	34.36	368	28.16	467	32.69		
69	34.78	169	29.93	269	32.27	369	26.32	468	31.30		
70	33.80	170	32.82	269.6	21.99	370	32.65	469	30.83		
71	34.33	171	33.33	270.2	29.98	371	32.04	470	37.22		
72	34.20	172	27.37	271	30.84	372	15.45	471	37.05		
73	31.53	173	25.64	272	32.58	373	20.78	472	30.32		
74	28.98	174	4.62	273	34.67	374	16.19	473	32.64		
75	24.62	175	6.91	274	29.97	375	29.90	474	34.02		
76	39.26	176	8.49	275	32.85	376	31.58	475	42.59		
77	40.59	177	11.12	276	32.70	377	29.79	476	40.70		
78	41.20	178	14.30	277	31.58	378	23.56	477	37.12		
79	40.34	179	28.33	278	36.03	379	32.82	478	29.38		
80	38.16	180	35.73	279	33.46	380	30.28	479	43.22		
81	36.62	181	33.33	280	28.40	381	16.58	480	34.53		
82	39.34	182	32.71	281	33.72	382	30.31	481	32.17		
83	39.67	183	32.56	282	34.49	383	31.44	482	42.65		
84	39.09	184	33.55	283	33.58	384	30.37	483	45.19		
85	40.23	185	31.78	284	31.92	385	30.99	484	45.78		
86	38.80	186	32.14	285	30.23	386	31.86	485	42.77		
87	34.29	187	34.45	286	31.52	387	31.06	486	36.09		
88	37.05	188	29.11	287	29.13	388	30.51	487	40.32		
89	38.71	189	4.95	288	33.46	389	29.65	488	44.66		
90	35.48	190	6.16	289	34.18	390	27.27	489	42.96		
91	33.89	191	6.57	290	33.70	391	28.91	490	38.46		
92	36.08	192	9.30	291	32.87	392	29.90	491	37.50		
93	37.50	193	14.78	292	22.45	393	29.23	492	29.55		
94	38.54	194	21.74	293	30.59	394	29.69	493	27.03		
95	35.37	195	36.07	294	19.82	395	29.96	494	39.39		
96	27.87	196	35.36	295	33.02	396	31.54	495	29.41		
97	33.12	197	30.57	296	35.19	397	30.31	496	26.85		
98	38.34	198	32.99	297	22.39	398	17.80	497	14.51		
99	39.03	199	35.38	298	30.60	399	23.95	498	13.94		
100	39.92	200	34.65	299	32.45	400	30.26	499	26.58		
				300	31.92			500	22.50		

LOSS-ON-IGNITION CORE 3											
Depth (cm)	%LOI	Depth (cm)	%LOI	Depth (cm)	%LOI	Depth (cm)	%LOI	Depth (cm)	%LOI	Depth (cm)	%LOI
1	30.52	101	4.95	201	25.62	301	21.21	401	18.42	501	31.3059
2	30.12	101.5	9.53	202	24.06	302	23.96	402	37.18	502	30.06993
3	29.03	102	11.84	203	24.26	303	26.94	403	34.28	503	31.13924
4	30.34	103	10.94	204	24.36	304	22.66	404	35.78	504	27.04762
5	30.29	104	10.53	205	24.41	305	18.28	405	36.49	505	18.9729
6	30.53	105	10.68	206	26.12	306	16.16	406	34.36	506	12.5498
7	31.21	106	13.26	207	25.00	307	18.05	407	31.23		
8	30.72	107	13.63	208	28.20	308	14.98	408	30.33		
9	32.93	108	8.07	209	27.83	309	27.38	409	27.30		
10	32.00	109	13.38	210	24.92	310	3.87	410	29.46		
11	31.94	110	3.19	211	21.21	311	2.85	410.5	28.57		
12	29.50	111	26.64	212	17.87	312	3.66	411.5	20.67		
13	29.95	112	21.70	213	16.44	313	4.33	412.5	27.52		
14	29.82	113	15.05	214	18.23	314	7.38	413	25.89		
15	29.29	114	10.02	215	21.75	315	8.26	414	25.05		
16	29.96	115.5	10.17	216	18.68	316	22.89	415	19.61		
17	30.29	116	8.03	217	9.00	317	31.54	416	22.75		
18	30.45	117	4.82	218	16.74	318	34.39	417	25.08		
19	30.17	117.5	5.11	219	19.90	319	36.28	418	10.93		
20	31.27	118	15.56	220	17.09	320	35.65	419	10.25		
21	31.34	119	11.03	221	20.79	321	33.67	420	32.72		
22	30.48	120	5.98	222	27.82	322	31.53	421	24.27		
23	30.29	121	7.52	223	26.35	323	30.68	422	24.82		
24	30.53	122	11.19	224	27.84	324	30.91	423	35.01		
25	31.65	123	11.16	225	26.20	325	29.72	424	32.73		
26	32.00	124	3.17	226	27.15	326	27.12	425	31.54		
27	31.47	125	1.76	227	24.13	327	30.00	426	34.47		
28	30.56	126	12.93	228	20.65	328	30.94	427	33.60		
29	30.83	127	12.31	229	19.96	329	26.00	428	3.54		
30	29.74	128	14.21	230	15.83	330	27.27	429	2.92		
31	29.15	129	18.50	231	11.94	331	26.24	430	9.81		
32	29.15	130	15.15	232	9.90	332	26.46	430.5	11.82		
33	29.37	131	9.70	233	18.13	333	27.36	431	4.22		
34	30.43	132	12.03	234	23.73	334	27.98	432	8.39		
35	31.40	133	12.30	235	25.82	335	28.73	433	8.67		
36	30.42	133.5	12.28	236	24.04	336	27.09	434	12.66		
37	29.73	134	2.17	237	28.29	337	25.17	435	10.80		
38	27.89	135	0.93	238	28.11	338	16.51	436	13.29		
39	26.91	136	0.70	239	24.11	339	8.03	437	5.72		
40	26.77	137	1.39	240	20.82	340	6.58	438	3.24		
41	27.78	138	0.45	241	15.27	341	13.28	439	3.98		
42	27.89	139	0.67	242	11.76	342	7.67	440	4.56		
43	26.89	140	0.48	243	24.32	343	17.73	441	4.85		
44	26.58	141	0.55	244	28.77	344	11.36	442	17.88		
45	26.52	142	0.77	245	30.77	345	17.91	443	17.88		
46	25.28	143	3.81	246	33.99	346	33.96	444	16.88		
47	25.55	144	23.16	247	30.00	347	34.06	445	13.89		
48	26.75	145	24.67	248	24.69	348	28.21	446	15.01		
49	23.46	146	21.67	249	26.91	349	25.17	446.5	13.53		
50	21.16	147	22.22	250	30.29	350	21.32	447	9.06		
51	23.60	148	26.00	251	24.29	350.5	15.23	448	8.87		
52	20.49	149	25.82	252	22.72	351.5	1.65	449	1.98		
53	20.57	150	33.33	253	20.26	352.5	1.47	450	7.88		
54	20.84	151	31.88	254	20.96	353	2.49	451	10.33		
55	21.26	152	37.19	255	28.00	354	24.23	452	12.31		
56	24.39	153	38.33	256	24.08	355	26.02	453	12.85		
57	23.86	154	40.76	257	21.93	356	23.34	454	12.62		
58	22.74	155	27.18	258	25.19	357	26.20	455	8.36		
59	16.50	156	36.74	259	27.93	358	26.40	456	5.34		
60	16.31	157	29.26	260	27.41	359	28.12	457	2.18		
61	13.19	158	26.21	261	25.00	360	28.31	458	5.57		
61.5	4.42	158.5	5.58	262	25.81	361	25.72	459	12.35		
62	8.24	159	17.86	263	26.80	362	21.15	460	15.42		
63	18.49	160	23.79	264	28.96	363	15.88	461	9.43		
64	6.09	161	20.82	265	31.34	364	9.02	462	7.93		
65	6.61	162	23.21	266	33.13	365	2.75	463	10.96		
66	21.77	163	10.79	267	30.41	366	13.30	464	9.33		
67	21.05	164	15.41	268	30.34	367	9.42	465	6.08		
68	5.75	165	12.81	269	38.39	368	4.71	466	5.54		
69	3.56	166	11.92	270	30.75	369	3.47	467	3.06		
70	4.66	167	13.54	271	32.44	370	18.15	468	3.01		
71	19.86	168	11.41	272	31.35	371	16.96	469	4.32		
72	13.72	169	13.80	273	32.31	372	19.96	470	1.90		
73	15.29	170	15.71	274	30.75	373	14.99	471	2.52		
74	12.41	171	15.30	275	28.22	373.5	11.18	472	3.86		
75	8.33	172	20.00	276	27.29	374.5	4.95	473	6.65		
76	23.18	173	19.36	277	27.31	375	11.32	474	10.57		
77	14.61	174	13.92	278	25.18	376	18.26	475	13.47		
78	6.47	175	15.55	279	25.86	377	19.44	476	15.49		
79	3.62	176	13.45	280	24.80	378	16.26	477	6.70		
80.5	9.90	177	10.12	281	19.34	379	13.39	478	12.39		
81	12.06	178	8.83	282	19.85	380	7.99	479	15.33		
82	25.38	179	8.67	283	22.43	381	1.88	480	6.20		
83	22.10	180	10.21	284	23.40	382	0.79	481	18.94		
84	22.83	181	14.43	285	19.35	383	26.63	482	15.17		
85	20.50	182	23.16	286	18.07	384	19.83	483	17.48		
86	18.55	183	23.60	287	22.00	385	18.89	484	16.41		
87	13.17	184	16.95	288	16.37	386	24.72	485	16.23		
88	8.92	185	15.75	289	12.78	387	28.60	486	26.07		
89	10.26	186	20.58	290	11.33	388	22.46	487	22.16		
89.9	7.80	187	19.06	291	18.77	389	22.33	488	26.24		
90.4	14.16	188	8.49	292	22.05	390	20.34	489	24.16		
91	15.11	189	5.35	293	24.80	391	12.65	490	27.19		
92	9.33	190	17.32	294	24.73	392	11.16	491	26.88		
93	7.57	191	26.74	295	24.80	392.5	3.81	492	19.76		
94	11.95	192	26.67	296	24.28	393	10.76	492.5	3.52		
95	9.99	193	26.18	297	23.80	394	9.36	493	2.58		
95.2	9.92	194	26.22	298	23.29	395	10.71	494	7.22		
96	7.15	195	25.17	299	23.32	396	9.99	495	19.45		
97	5.26	196	22.14	300	21.67	397	13.87	496	19.67		
98	5.41	197	23.68			398	15.96	497	17.71		
99	5.64	198	23.78			399	8.41	498	19.98		
100	5.23	199	24.36			400	20.03	499	30.05		
		200	24.22					500	28.08		

LOSS-ON-IGNITION CORE 4									
Depth (cm)	%LOI	Depth (cm)	%LOI	Depth (cm)	%LOI	Depth (cm)	%LOI	Depth (cm)	%LOI
1	33.33	101	5.83	201	32.14	301.5	10.45	401	7.95
2	32.61	102	3.52	202	31.33	302	19.82	402	5.93
3	30.82	103	8.37	203	30.79	303	23.74	403	4.83
4	29.91	104	23.21	204	29.74	304	10.83	404	0.96
5	31.17	105	30.79	205	30.69	305	23.43	405	0.86
6	30.61	106	27.51	206	30.43	306.5	10.53	406	21.11
7	32.95	107	26.59	207	30.28	307	2.92	407	20.95
8	34.35	108	24.93	208	31.00	308	3.55	408	20.82
9.5	34.29	109	27.82	209	32.00	309	3.49	409	24.26
10.5	25.41	110	28.72	210	33.22	310	5.44	410	21.51
11	21.46	111	24.74	211	33.44	311	32.49	411	18.54
12	28.65	112	19.38	212	33.19	312	32.42	412	5.47
13	31.55	113	23.81	213	31.60	313	27.88	413	7.61
14	31.03	114	25.98	214	31.99	314	31.33	414	6.76
15	32.88	115	25.77	215	30.89	315	29.17	415	4.50
16	32.83	116	22.04	216	29.14	316	27.43	416	4.97
17	32.71	117	20.27	217	34.28	317	17.39	417	3.64
18	33.69	118	19.08	218	36.47	318	26.32	418	3.28
19	30.80	119.5	8.61	219	36.33	319	28.37	419	3.20
20	29.21	120.5	14.61	220	35.36	320	33.03	420	2.75
21	31.56	121.5	7.59	221	34.28	321	32.14	421	2.39
22	31.90	122	6.72	222	34.69	322	31.48	422	2.30
23	32.11	123	16.20	223	33.82	323	30.74	423	2.74
24	31.52	124	26.24	224	32.23	324	33.05	424	2.41
25	31.48	125	23.47	225	32.00	325	29.25	425	1.41
26	28.92	126	2.91	226	30.67	326	31.33	426	1.31
27	29.38	127	3.84	227	30.71	327	29.57	427	1.28
28	24.41	128	2.62	228	31.83	328	30.40	428	1.20
29	20.58	129	5.89	229	32.51	329	30.15	429	0.83
30	17.52	130	7.15	230	28.82	330	35.71	430	0.82
31	22.94	131	11.01	231	24.83	331	37.66	431	0.97
32	39.18	132	14.89	232	23.40	332	28.75	432	1.28
33	40.24	133	31.74	233	23.57	333	24.94	433	1.23
34	36.77	134	31.97	234	26.79	334	42.19	434	1.66
35	33.33	135	33.45	235	22.04	335	38.55	435	1.15
36	34.52	136	32.14	236	20.45	336	35.12	436	1.25
37	34.11	137	32.33	237	29.13	337	30.61	437	1.72
38	38.92	138	29.90	238	29.07	338	20.64	438	1.77
39	37.23	139	26.98	239	27.09	339	15.52	439	1.56
40	35.39	140	28.57	240	28.12	340	11.25	440	1.11
41	28.29	141	27.46	241	30.77	341	20.31	441	0.98
42	25.84	142	24.13	242	28.57	342	19.91	442	0.95
43	25.76	143	18.97	243	27.21	343	12.92	443	0.93
44	27.71	144	17.33	244	25.67	344	8.95	444	0.89
45	23.51	145	30.56	245	16.60	345	13.47	445	0.99
46	16.42	146	29.12	246	15.93	346	15.90	446	0.91
47	24.92	147	31.48	247	12.85	347	11.72	447	1.08
48	27.70	148	26.28	248	22.46	348	5.97	448	2.90
49	26.48	149	28.57	249	28.04	349	7.68	449	2.01
50	20.65	150	28.21	250	26.20	350	14.04	450	1.28
51	14.23	151	20.35	251	23.41	351	9.17	451	1.36
52	16.15	152	24.94	252	25.78	352	6.46	452	0.98
53	22.26	153	27.32	253	25.64	353	15.02	453	1.54
54	20.75	154	30.11	254	18.91	354	20.77	454	1.01
55	23.32	155	28.33	255	29.63	355	15.47	455	1.00
56	25.42	156	16.67	256	32.21	356	10.34	456	1.07
57	26.45	157	17.91	257	32.35	357	15.31	457	1.17
58	25.31	158	27.56	258	30.73	358	4.03	458	0.92
59	24.89	159	22.42	259	29.89	359	6.82	459	0.81
60	27.70	160	20.31	260	29.41	360	4.76	460	0.68
61	23.53	161	24.19	261	26.69	361	3.15	461	0.69
62	22.93	162	28.88	262	29.19	362	5.27	462	0.43
63	25.14	163	23.76	263	29.05	363	3.03	475	0.93
64	27.38	164	24.60	264	30.71	364	2.95		
65	25.82	165	15.83	265	30.74	365	4.60		
66	21.43	166	26.33	266	29.64	366	3.85		
67	18.71	167	28.13	267	30.65	367	1.59		
68	24.74	168	12.95	268	25.16	368	3.00		
69	28.52	169	6.68	269	3.68	369	2.72		
70	27.66	170	12.39	270	20.80	370	3.58		
71	27.68	171	29.07	271	27.94	371	4.18		
72	27.80	172	29.46	272	28.41	372	2.65		
73	27.31	173	27.30	273	27.38	373	1.83		
74	26.74	174	24.24	274	25.63	374	2.25		
75	27.97	175	25.59	275	25.61	375	2.86		
76	29.07	176	13.64	276	18.61	376	3.17		
77	29.02	177	23.08	277	22.01	377	3.52		
78	29.52	178	30.09	278	30.38	378	2.77		
79	28.33	179	29.41	279	29.63	379	5.95		
80	23.31	180	29.30	280	30.38	380	13.97		
81	13.86	181	23.39	281	30.12	381	21.40		
82	19.31	182	19.03	282	27.81	382	13.52		
83	4.04	183	17.97	283	8.94	383	9.47		
84	21.12	184	28.45	284	8.31	384	10.62		
85	20.16	185	23.04	285	13.04	385	12.44		
86	13.87	185.5	12.66	286	20.09	386	14.74		
87	5.97	186	27.87	287	31.23	387	15.49		
88	7.01	187	31.95	288	29.93	388	14.59		
89	6.51	188	30.58	289	24.93	389	5.84		
90	7.83	189	29.33	290	19.74	390	22.25		
91	20.51	190	26.95	291	3.16	391	19.18		
92	18.22	191	25.08	292	4.11	392	19.57		
93	24.32	191.5	23.16	293	3.84	393	22.64		
94	24.69	192	7.67	294	3.49	394	1.17		
95	25.13	193	14.49	295	5.10	395	2.80		
96	22.73	194	30.37	296	13.87	396	4.32		
97	20.58	195	31.73	297	14.01	397	4.36		
98	5.60	196	30.16	298	21.80	398	1.33		
99	5.54	197	30.47	299	26.55	399	12.32		
100	4.52	198	26.04	300	24.94	400	12.54		
		199	26.33	300.5	20.71				
		200	33.33						

Total Carbon, Total Nitrogen Data - CORE 2														
Depth (cm)	% nitrogen	% carbon	Depth (cm)	% nitrogen	% carbon	Depth (cm)	% nitrogen	% carbon	Depth (cm)	% nitrogen	% carbon	Depth (cm)	% nitrogen	% carbon
1	1.26	16.75	101	1.44	18.69	201	1.11	16.47	301	1.05	14.88	401	1.08	15.22
2	0.68	10.70	102	1.29	17.99	202	1.10	14.96	302	1.00	13.36	402	1.03	14.69
3	0.59	10.30	103	1.17	17.02	203	0.65	9.54	303	1.01	14.51	403	1.20	14.50
4	0.55	10.00	104	1.12	16.23	204	0.28	4.11	304	1.05	15.68	404	1.28	14.70
5	0.76	11.55	105	1.04	14.87	205	0.99	14.40	305	0.20	3.97	405	1.29	15.97
6	0.81	12.10	106	1.28	17.88	206	1.01	14.15	306	1.13	16.27	406	0.85	10.41
7	0.78	11.81	107	0.91	13.53	207	1.03	14.78	307	1.17	15.75	407	0.78	10.68
8	1.05	15.15	108	0.91	13.53	208	1.08	15.12	308	1.04	14.63	408	1.08	12.62
9	1.17	16.51	109	0.87	12.81	209	0.87	13.20	309	1.01	14.43	409	1.31	16.05
10	1.20	16.65	110	1.10	15.86	210	0.77	11.30	310	0.74	10.77	410	1.04	12.75
11	1.12	15.70	111	1.34	18.68	211	0.64	10.04	311	1.11	15.63	411	1.29	15.32
12	1.24	16.39	112	1.12	16.31	212	0.75	10.76	312	1.17	16.69	412	1.31	14.05
13	1.20	16.57	113	1.27	19.12	213	0.74	10.28	313	1.04	14.67	413	1.26	16.30
14	1.27	18.05	114	1.11	17.24	214	0.81	11.07	314	1.16	16.45	414	1.28	15.02
15	1.31	17.89	115	1.23	17.50	215	0.95	12.78	315	1.15	16.36	415	1.11	13.48
16	1.30	18.05	116	1.35	18.36	216	1.06	13.10	316	1.07	14.63	416	0.67	8.14
17	1.18	16.24	117	1.25	18.33	217	0.97	13.12	317	1.05	14.92	417	1.39	15.50
18	1.14	15.66	118	0.99	14.47	218	0.15	1.98	318	1.13	16.05	418	1.33	14.76
19	1.22	17.28	119	1.26	18.43	219	0.22	2.91	319	0.89	13.25	419	1.11	14.00
20	1.18	17.47	120	1.07	16.43	220	0.84	10.95	320	1.04	14.53	420	1.33	15.95
21	1.24	17.70	121	1.17	16.66	221	1.02	12.94	321	1.00	14.79	421	1.17	14.12
22	1.26	17.74	122	1.20	17.21	222	0.22	2.94	322	1.19	16.51	422	0.12	1.22
23	1.24	17.46	123	1.12	16.99	223	0.83	10.01	323	1.21	16.78	423	0.24	3.70
24	1.27	18.04	124	1.11	16.56	224	1.49	16.95	324	1.11	15.45	424	0.38	5.88
25	1.30	18.05	125	1.06	16.34	225	0.60	7.23	325	1.19	17.00	425	0.63	7.85
26	1.21	16.88	126	1.04	16.82	226	1.23	17.19	326	0.99	15.16	426	1.23	13.67
27	1.25	16.93	127	0.92	14.60	227	1.00	16.57	327	1.00	15.28	427	0.59	6.81
28	1.39	18.23	128	1.23	18.02	228	0.91	13.27	328	1.05	15.32	428	1.24	14.26
29	1.20	15.82	129	1.20	17.87	229	0.14	2.15	329	1.03	15.92	429	1.33	15.02
30	1.16	16.73	130	1.39	18.22	230	0.12	2.20	330	0.90	14.67	430	1.17	13.78
31	0.78	12.26	131	1.17	15.31	231	0.15	2.78	331	0.90	13.77	431	1.26	14.48
32	0.88	13.63	132	1.10	14.42	232	0.15	2.71	332	1.19	17.15	432	0.58	7.29
33	1.01	15.11	133	1.00	13.46	233	0.17	3.05	333	1.18	17.98	433	1.33	15.57
34	0.78	12.23	134	1.18	15.35	234	0.19	3.70	334	1.21	18.47	434	0.96	13.36
35	1.11	18.06	135	1.08	15.26	235	0.23	4.35	335	1.18	17.84	435	0.72	8.15
36	1.10	16.56	136	1.58	17.61	236	0.27	4.54	336	1.21	18.92	436	1.26	14.29
37	1.13	17.54	137	1.19	16.04	237	0.38	6.44	337	1.04	19.04	437	1.00	14.38
38	1.15	17.50	138	1.34	17.01	238	0.67	10.89	338	0.90	15.66	438	0.96	14.44
39	1.10	17.79	139	1.27	17.01	239	0.98	14.21	339	1.15	17.11	439	0.57	9.83
40	1.12	17.22	140	1.16	15.76	240	1.06	15.17	340	1.24	17.80	440	0.11	1.66
41	1.16	16.71	141	1.25	16.69	241	1.34	17.42	341	1.10	16.81	441	0.20	3.50
42	1.25	17.95	142	1.19	15.54	242	1.51	17.22	342	0.80	14.05	442	0.18	2.63
43	1.12	16.61	143	1.06	14.44	243	1.56	17.80	343	1.00	15.23	443	0.18	3.22
44	1.17	16.60	144	1.25	17.10	244	1.52	18.33	344	0.64	8.14	444	0.21	3.59
45	1.18	17.76	145	1.36	17.55	245	1.27	15.70	345	0.94	15.56	445	0.21	3.92
46	1.24	18.08	146	1.33	17.11	246	1.14	16.23	346	0.73	13.48	446	0.24	4.43
47	1.24	17.25	147	1.27	16.51	247	1.25	17.20	347	0.93	14.80	447	0.23	4.16
48	1.20	17.55	148	1.25	16.30	248	1.27	17.91	348	0.95	14.89	448	0.25	4.92
49	1.17	17.47	149	1.25	16.64	249	1.02	15.06	349	1.04	15.88	449	0.15	2.69
50	1.20	16.88	150	0.92	13.15	250	0.54	11.16	350	1.02	15.53	450	1.26	16.39
51	1.14	16.98	151	1.09	15.77	251	0.91	13.56	351	0.93	13.36	451	1.16	16.03
52	1.27	17.76	152	1.20	16.79	252	0.96	14.28	352	0.76	13.58	452	1.10	16.23
53	1.27	17.75	153	1.16	17.02	253	1.04	13.60	353	1.04	15.61	453	1.17	14.31
54	1.14	16.44	154	1.02	15.49	254	0.90	13.17	354	1.01	14.72	454	1.40	16.10
55	1.23	16.88	155	1.09	14.84	255	0.42	6.45	355	1.05	14.84	455	1.21	15.12
56	1.15	16.16	156	1.19	16.35	256	1.31	17.88	356	1.29	17.75	456	1.32	17.34
57	1.04	14.68	157	1.07	15.42	257	1.10	16.31	357	1.14	16.81	457	1.26	15.82
58	1.11	16.38	158	1.06	14.50	258	0.96	14.41	358	1.18	16.07	458	1.27	15.49
59	1.12	15.74	159	0.87	11.73	259	1.12	17.53	359	0.97	12.80	459	1.37	16.47
60	1.02	15.70	160	0.64	8.44	260	1.15	15.16	360	1.15	15.80	460	1.04	12.67
61	0.89	13.93	161	1.10	14.62	261	1.17	16.83	361	1.04	15.28	461	0.64	7.36
62	0.88	10.76	162	1.19	16.54	262	1.33	17.60	362	0.98	14.97	462	0.78	9.46
63	0.92	14.68	163	1.15	17.18	263	0.91	12.63	363	0.96	14.17	463	1.08	13.39
64	1.07	16.75	164	0.69	10.24	264	1.24	17.35	364	1.07	15.42	464	1.21	15.34
65	1.17	17.43	165	0.23	4.12	265	1.38	17.88	365	1.16	16.29	465	1.35	15.40
66	1.14	16.77	166	0.21	4.14	266	1.21	16.25	366	1.08	15.93	466	1.30	16.38
67	1.07	15.68	167	0.27	5.06	267	1.32	17.09	367	0.95	14.56	467	1.26	15.55
68	1.14	16.35	168	0.59	8.73	268	1.18	15.91	368	0.82	12.51	468	1.23	15.57
69	1.05	15.34	169	1.00	13.78	269	1.14	15.43	369	0.87	13.04	469	1.11	14.50
70	1.08	15.92	170	0.74	11.77	269.5	0.82	11.20	370	0.97	15.54	470	1.31	18.33
71	0.98	15.82	171	0.93	13.66	270	0.13	2.34	371	1.12	15.28	471	1.37	18.33
72	1.02	15.53	172	0.74	11.00	271	1.14	16.48	372	0.49	7.30	472	1.25	15.37
73	1.07	15.95	173	0.62	8.91	272	1.13	15.85	373	0.78	11.09	473	1.22	15.48
74	0.82	13.49	174	0.13	1.82	273	1.21	16.59	374	0.64	9.18	474	1.26	16.90
75	0.51	8.35	175	0.16	2.78	274	1.18	15.52	375	0.97	14.72	475	1.47	20.80
76	1.33	19.05	176	0.24	3.93	275	1.17	16.14	376	1.11	15.19	476	1.45	21.11
77	1.23	17.53	177	0.27	4.52	276	1.16	16.24	377	1.04	14.11	477	1.58	20.90
78	1.43	16.87	178	0.38	6.42	277	1.17	16.41	378	0.84	12.59	478	1.14	15.54
79	1.15	23.66	179	0.93	13.37	278	1.19	17.08	379	0.89	14.07	479	1.57	21.57
80	1.18	16.71	180	0.96	14.05	279	1.02	15.16	380	0.96	14.72	480	1.17	16.39
81	1.45	18.98	181	0.98	14.22	280	1.04	15.93	381	0.65	9.26	481	1.08	14.98
82	1.15	17.84	182	0.85	12.43	281	1.05	16.18	382	1.20	16.01	482	1.47	21.12
83	1.45	19.67	183	1.00	13.90	282	1.15	16.41	383	1.15	16.20	483	1.63	23.81
84	1.25	17.52	184	0.98	14.09	283	1.09	16.12	384	1.04	15.56	484	1.61	22.28
85	1.42	19.27	185	0.85	13.35	284	1.09	15.28	385	1.06	15.90	485	1.44	20.30
86	1.40	19.52	186	0.84	13.81	285	1.12	16.25	386	1.00	16.13	486	1.28	17.18
87	1.23	16.49	187	0.81	13.44	286	0.83	12.13	387	1.04	14.79	487	1.54	21.55
88	1.18	16.59	188	0.60	9.32	287	0.86	13.43	388	0.87	13.53	488	1.57	21.39
89	1.26													

BULK DENSITY - CORE 2

depth (cm)	Volume (cc)	wet density	% water	original %water (LOI)	dry density	average dry density
5	1.2	1.225	73.33	83.6	0.327	0.327
45	1.2	1.031	89.25	89.2	0.111	0.114
45	1.2	1.076	89.16	89.2	0.117	
93	1.2	1.155	88.02	88.6	0.138	0.126
93	1.2	1.032	89.01	88.6	0.113	
145	1.0	1.267	86.58	87.4	0.170	0.170
195	1.0	1.115	85.11	85.4	0.166	0.169
195	1.0	1.223	86.02	85.4	0.171	
272	1.0	1.452	83.54	83.0	0.239	0.241
272	1.0	1.471	83.55	83.0	0.242	
307	1.0	1.307	84.01	83.3	0.209	0.194
307	1.0	1.094	83.73	83.3	0.178	
344	1.0	1.453	77.91	75.2	0.321	0.295
344	1.0	1.274	78.89	75.2	0.269	
391	1.0	1.136	83.27	81.2	0.190	0.205
391	1.0	1.258	82.75	81.2	0.217	
391	1.0	1.183	82.33	81.2	0.209	
428	1.0	1.217	84.22	86.0	0.192	0.187
428	1.0	1.167	84.40	86.0	0.182	
457	1.0	1.486	81.36	80.8	0.277	0.277
483	1.0	1.284	82.87	82.9	0.220	0.223
483	1.0	1.161	80.53	82.9	0.226	
510	1.0	1.214	81.71	82.4	0.222	0.222
551	1.2	1.128	80.95	80.8	0.215	0.215
558	1.0	1.012	82.41	82.5	0.178	0.183
558	1.0	1.104	83.06	82.5	0.187	

Stable Carbon Isotopes - CORE 2

Depth (cm)	Delta 13-C
188	-30.43
189	-26.82
190	-26.56
191	-26.61
194	-27.85
195	-31.72
228	-31.39
229	-27.58
230	-26.65
232	-26.58
233	-26.64
234	-26.73
235	-27.09
237	-28.01
238	-28.10
239	-29.80

Nitric Digestion DATA - CORE 2

Depth (cm)	% carbon	Depth (cm)	% carbon	Depth (cm)	% carbon	Depth (cm)	% carbon	Depth (cm)	% carbon
40	1.23	179	1.25	232	0.22	290	2.06	445	0.31
41	1.40	180	1.29	233	0.24	335	2.39	446	0.32
42	1.48	181	1.32	234	0.21	336	2.16	447	0.34
43	1.86	182	1.37	235	0.26	337	1.36	448	0.36
44	1.48	183	1.48	236	0.26	338	1.33	449	0.26
45	1.81	184	1.42	237	0.34	339	1.31	450	2.15
46	1.98	185	1.12	238	0.67	340	1.45	451	2.14
47	1.82	186	1.24	239	1.02	341	1.33	452	2.04
48	1.93	187	1.17	240	1.15	342	0.73	536	0.90
49	1.45	188	0.81	241	1.55	343	1.23	537	0.96
50	1.75	189	0.29	275	2.12	344	0.70	538	0.04
51	1.08	190	0.20	276	1.90	345	0.77	539	0.16
52	1.45	191	0.20	277	2.08	346	0.74	540	0.17
53	1.29	192	0.26	278	2.01	347	1.04	541	0.15
54	0.99	193	0.31	279	1.81	348	0.91	542	0.16
55	1.13	194	0.46	280	1.68	349	0.75	543	0.17
56	1.18	195	1.88	281	1.91	350	0.88	544	0.19
171	1.03	196	1.69	282	1.84	437	1.87	545	0.19
172	0.83	197	1.06	283	1.77	438	1.77	546	0.24
173	0.65	226	1.61	284	1.65	439	1.05	547	0.16
174	0.29	227	1.47	285	1.88	440	0.30	548	2.26
175	0.25	228	1.14	286	1.20	441	0.29	549	2.83
176	0.28	229	0.21	287	1.28	442	0.24	550	3.29
177	0.28	230	0.37	288	2.25	443	0.27		
178	0.37	231	0.23	289	2.03	444	0.26		

GRAYSCALE DENSITY - CORE 2									
Depth (cm)	Density	Depth (cm)	Density	Depth (cm)	Density	Depth (cm)	Density	Depth (cm)	Density
1	177.17	101	159	201	134.03	301	139.31	401	149.53
2	179.79	102	159.03	202	130	302	142.65	402	140.71
3	185.53	103	157.63	203	121.38	303	83.484	403	152.29
4	186.87	104	152.92	204	112.78	304	136.41	404	123.7
5	187.1	105	155.72	205	59.548	305	154.53	405	113.72
6	187.01	106	151.84	206	123.16	306	154.65	406	120.71
7	187.15	107	154.3	207	140.73	307	153.67	407	140.17
8	187.06	108	160.82	208	126.58	308	155.74	408	141.35
9	187.14	109	172	209	142.76	309	140.83	409	140.59
10	187.13	110	175.08	210	124.92	310	158.24	410	148.5
11	187.06	111	157.31	211	115.24	311	161.83	411	118.25
12	187.11	112	163.91	212	116.62	312	157.95	412	144.75
13	187.09	113	164.93	213	127.33	313	157.72	413	145.43
14	187.04	114	172.37	214	133.37	314	154.65	414	124.74
15	187.08	115	169.1	215	126.18	315	152.04	415	41.049
16	187.02	116	168.11	216	128.31	316	149.89	416	125.13
17	187	117	168.53	217	122.79	317	145.75	417	136.14
18	186.99	118	168.71	218	116.18	318	138.85	418	110.92
19	187	119	161.87	219	33.383	319	140.04	419	105.98
20	186.99	120	170.17	220	51.945	320	149.43	420	61.201
21	187	121	168.9	221	98.035	321	123.87	421	20.078
22	187	122	159.9	222	111.79	322	132.3	422	36.991
23	187	123	159.41	223	79.151	323	140.69	423	82.872
24	187	124	161.08	224	65.525	324	133	424	119.77
25	187	125	160.78	225	118.26	325	136.96	425	108.92
26	187	126	158.2	226	94.557	326	144.83	426	129.18
27	187	127	168.29	227	103.85	327	141.83	427	147.5
28	186.94	128	166.6	228	110.57	328	145.13	428	150.09
29	186.21	129	189	229	155.74	329	138.04	429	146
30	183.13	130	180.56	230	116.96	330	150.14	430	135.79
31	175.79	131	166.54	231	26.842	331	151.86	431	113.88
32	175.49	132	160.96	232	23.537	332	156	432	136.47
33	176.11	133	162.67	233	27.759	333	156.15	433	132.01
34	177.75	134	114.33	234	28.489	334	154.87	434	133.78
35	174.13	135	126.21	235	31.503	335	153.23	435	143.96
36	168.66	136	131.97	236	51.982	336	160.56	436	131.86
37	175.96	137	135.07	237	49.825	337	159.64	437	130.07
38	178.35	138	141.44	238	104.59	338	157.64	438	75.162
39	189.71	139	144.94	239	135.39	339	149.48	439	20.236
40	199.24	140	147.81	240	150.69	340	152.28	440	20.486
41	202.37	141	150.89	241	147.56	341	138.47	441	19.68
42	203.57	142	142.82	242	162.67	342	141.07	442	19.327
43	203.92	143	151.82	243	162.35	343	147.44	443	18.387
44	203.97	144	157.53	244	173.76	344	144.32	444	19.693
45	203.77	145	154.49	245	176.06	345	145.26	445	19.711
46	203.6	146	155.47	246	156.7	346	142.68	446	24.266
47	202.96	147	149.4	247	149.35	347	150.82	447	28.35
48	193.35	148	150.85	248	153.37	348	140.85	448	54.34
49	175.41	149	147.83	249	157.97	349	119.28	449	115.75
50	179.23	150	143.86	250	155.4	350	104.52	450	128.83
51	166.27	151	144.03	251	152.99	351	100.67	451	136.53
52	162.53	152	148.79	252	138.51	352	105.41	452	142.18
53	155.84	153	147.44	253	119.95	353	128.72	453	140.57
54	153.22	154	140.17	254	118.19	354	131.18	454	142.07
55	155.23	155	142.85	255	115.21	355	132.9	455	141.94
56	153.69	156	139.1	256	130.66	356	114.35	456	143
57	151.86	157	136.44	257	130.39	357	134.05	457	144.83
58	153.39	158	134.3	258	114.26	358	150.07	458	141.9
59	149.66	159	121.97	259	135.86	359	149.85	459	125.06
60	143.18	160	102.54	260	136.27	360	151.82	460	101.49
61	139.28	161	125.1	261	136.56	361	151.63	461	119.9
62	134.66	162	124.57	262	144.15	362	157.48	462	142.32
63	131.13	163	120.7	263	130.71	363	159.28	463	153.29
64	121.71	164	120.03	264	118.71	364	157.02	464	147.71
65	125.19	165	26.111	265	130.06	365	153.97	465	152.06
66	129.95	166	18.811	266	143.6	366	148.42	466	148.53
67	134.14	167	21.946	267	144.38	367	150.07	467	143.99
68	134.17	168	65.646	268	107.1	368	154.59	468	139.83
69	136.02	169	106.54	269	93.644	369	125.76	469	139.74
70	141.45	170	119.02	270	149.37	370	113.68	470	137.64
71	154.27	171	127.27	271	156.19	371	97.373	471	123.09
72	159.19	172	120.4	272	160.23	372	149.57	472	126.34
73	153.45	173	122.85	273	166.01	373	154.37	473	122.82
74	137.25	174	86.896	274	157.87	374	149.71	474	136.78
75	140.52	175	24.325	275	157.17	375	140.39	475	132.38
76	165.26	176	19.37	276	171.01	376	152.62	476	129.51
77	166.99	177	28.375	277	163.68	377	148.73	477	105.4
78	170.65	178	55.01	278	165.64	378	147.56	478	123.46
79	174.51	179	116.82	279	151.79	379	106.03	479	110.42
80	171.83	180	127.31	280	159.78	380	138.34	480	100.77
81	168.11	181	130.53	281	160.75	381	116.99	481	115.59
82	169.57	182	135.22	282	159.86	382	132.06	482	130.44
83	170.11	183	134.15	283	158.52	383	133.72	483	138.8
84	167.81	184	130.95	284	163.78	384	136.17	484	136.95
85	173.53	185	139.19	285	155.3	385	145.53	485	129.08
86	186.84	186	132.76	286	146.99	386	147.18	486	126.42
87	193.61	187	132.25	287	157.69	387	124.7	487	134.63
88	182.93	188	136.59	288	161.65	388	145.61	488	142.8
89	168.26	189	144.09	289	158.19	389	150.23	489	133.25
90	147.9	190	55.644	290	152.75	390	154.7	490	126.05
91	147.3	191	19.281	291	97.964	391	149.36	491	122.79
92	147.18	192	25.329	292	92.233	392	146.02	492	105.76
93	138.71	193	40.056	293	115.4	393	152.78	493	110.74
94	137.1	194	52.421	294	129.6	394	152.2	494	108.51
95	131.47	195	91.741	295	115.32	395	147.86	495	67.239
96	141.62	196	119.25	296	127.68	396	120.55	496	55.2
97	146.68	197	124	297	146.47	397	139.46	497	98.223
98	168	198	149.78	298	147.05	398	152.27	498	86.006
99	156.06	199	138.82	299	147.67	399	156.62	499	63.88
100	154.27	200	132.5	300	148.74	400	154.11	500	17.215

GRAIN SIZE DATA

CORE 2 - Layer i

Sample #	229	230	231	232	233	234	235	236	237	238
Mean:	26.49	41.02	46.67	45.78	47.71	48.64	41.87	44.05	47.82	50.22
Median:	13.99	30.1	35.09	34.51	35.42	36.42	32.1	31.56	34.85	36.9
D(3,2):	4.08	6.919	7.534	7.386	7.357	7.538	6.9	6.708	7.228	11.03
Mode:	14.94	37.96	50.23	50.23	50.23	55.14	50.23	50.23	55.14	60.52
S.D.:	40.96	39.82	42.84	41.84	44.49	44.6	35.67	42.43	45.47	44.13
C.V.:	154.7	97.08	91.79	91.4	93.24	91.68	85.2	96.32	95.09	87.87
Skewness:	4.195	2.756	2.134	2.125	2.115	1.982	1.302	2.112	2.131	1.247
Kurtosis:	22.79	13.81	8.207	8.294	7.778	6.925	1.614	7.324	7.844	1.106
% <										
10	2.864	6.453	6.882	6.774	6.708	6.735	6.052	5.842	6.336	6.781
25	6.641	14.75	16.38	16.14	16.15	16.31	14.61	14.07	15.38	16.25
50	13.99	30.1	35.09	34.51	35.42	36.42	32.1	31.56	34.85	36.9
75	28.55	54.77	64	62.89	65.84	67.96	59.57	60.94	66.59	71.71
90	56.37	87.76	101.4	99.39	104.8	107	92.31	98.57	106.5	115.9

Particle Diameter(μm)	Volume %	Volume %	Volume %	Volume %	Volume %	Volume %	Volume %	Volume %	Volume %	Volume %
1	3.03	1.21	1.16	1.19	1.19	1.2	1.34	1.37	1.29	1.22
2	11.29	4.2	3.97	4.02	4.08	4.1	4.64	4.85	4.4	4.35
5	45.1	26.78	23.34	23.66	23.41	23.06	25.54	26.23	24.19	23.36
20	24.58	37.05	34.27	34.53	33.11	32.13	34.15	32.77	31.76	30.46
50	8.35	24.68	29.63	29.29	29.99	31.09	28.48	27.28	29.85	31.12
125	2.91	3.5	5.26	4.93	5.72	6.02	3.66	4.87	5.92	7.88
250	0.69	0.409	0.37	0.321	0.446	0.401	0.0017	0.376	0.506	0
500	0.0031	0.0026	9.90E-05	0.0018	0.0018	0.0015	0	0	0.0016	0
1000	0	0	0	0	0	0	0	0	0	0
2000	0	0	0	0	0	0	0	0	0	0

CORE 2 - layer q

Sample#	440	441	442	443	444	445	447	448	449
Mean:	27.93	45.7	46.48	46.76	47	48.37	48.74	50.92	68.03
Median:	16.23	33.63	34.47	34.36	34.59	35.76	35.43	37.28	55.92
D(3,2):	4.379	7.264	7.353	7.501	7.358	7.471	7.341	7.552	9.364
Mode:	16.4	50.23	50.23	50.23	50.23	55.14	55.14	55.14	87.9
S.D.:	36.39	43.58	43.77	44.58	44.08	45.15	46.3	47.59	56.29
C.V.:	130.3	95.36	94.17	95.34	93.78	93.33	94.98	93.47	82.74
Skewness:	3.629	2.344	2.24	2.28	2.063	2.054	2.1	1.919	1.34
Kurtosis:	19.48	9.813	8.705	8.568	6.972	7.203	7.453	5.947	2.75
% <									
10	3.325	6.418	6.617	6.773	6.54	6.627	6.549	6.702	8.778
25	7.552	15.38	15.88	16.01	15.74	16.07	15.85	16.4	23.24
50	16.23	33.63	34.47	34.36	34.59	35.76	35.43	37.28	55.92
75	33.53	62.59	63.59	63.4	64.82	67.11	67.45	71.25	98.99
90	63.28	99.84	101.1	101.6	103.5	107	108.9	113.9	143.5

Particle Diameter (μm)	Volume %	Volume %	Volume %	Volume %	Volume %	Volume %	Volume %	Volume %	Volume %
1	2.48	1.26	1.22	1.17	1.24	1.23	1.23	1.22	0.999
2	9.88	4.35	4.18	4.07	4.24	4.18	4.22	4.13	3.08
5	41.86	24.54	23.86	23.95	23.96	23.35	23.65	22.77	16.21
20	27.61	33.72	33.85	34.16	33.13	32.43	32.11	30.99	23.98
50	11.74	28.63	29.21	28.85	29.4	30.29	29.79	31.13	39.15
125	2.52	4.97	5.16	5.24	5.52	6.03	6.41	7.21	13.97
250	0.392	0.472	0.481	0.579	0.458	0.478	0.516	0.544	0.951
500	0	0.0026	0.0012	4.60E-05	0	6.90E-05	0.0021	0.0013	0.0024
1000	0	0	0	0	0	0	0	0	0
2000	0	0	0	0	0	0	0	0	0

CORE 2 layer t

Sample #	538	539	540	541	542	543	544	545	546	547
Mean:	32.27	44.22	49.52	50.77	49.79	46.92	49.23	62.7	60.98	72.91
Median:	19.14	33.29	37.77	39.39	38.11	35.01	36.7	49.36	47.45	63.02
D(3,2):	4.68	7.119	7.588	7.716	7.524	7.118	7.19	8.483	8.275	9.746
Mode:	18	45.75	55.14	60.52	55.14	55.14	55.14	80.08	72.95	96.49
S.D.:	40.23	40.24	44.65	44.45	43.79	42.96	45.11	53.98	53.79	57.06
C.V.:	124.6	91.01	90.17	87.55	87.94	91.56	91.63	86.1	88.22	78.26
Skewness:	3.436	2.07	1.992	1.755	1.631	1.925	1.856	1.459	1.566	1.211
Kurtosis:	17.57	7.552	7.081	5.173	4.057	6.374	5.536	3.117	3.737	2.423
% <										
10	3.95	6.619	7.068	7.272	6.995	6.487	6.676	8.068	7.494	9.554
25	8.861	15.66	17.24	17.85	17.11	15.7	16.36	20.75	19.54	27.11
50	19.14	33.29	37.77	39.39	38.11	35.01	36.7	49.36	47.45	63.02
75	40.35	60.99	68.9	71.45	70.14	65.63	68.77	90.65	87.78	105.4
90	73.47	95.79	107.6	109.3	109.1	103.5	108.9	135.4	132.8	148.7

Particle Diameter(μm)	Volume %	Volume %	Volume %	Volume %	Volume %	Volume %	Volume %	Volume %	Volume %	Volume %
1	1.9	1.22	1.18	1.15	1.18	1.24	1.22	1.05	1.15	0.965
2	7.98	4.08	3.8	3.67	3.85	4.22	4.05	3.31	3.65	2.84
5	38.47	24.45	21.85	21.08	21.94	23.84	22.8	18	18.86	14.04
20	29.59	34.96	32.63	31.81	31.86	32.57	31.9	26.31	26.43	21.53
50	15.33	28.58	32.05	33.61	32.42	30.16	31.08	36.93	36.18	42.14
125	2.92	4.26	6	6.27	6.43	5.48	6.37	11.74	11.02	15.88
250	0.578	0.309	0.455	0.404	0.272	0.338	0.416	0.819	0.84	0.972
500	7.60E-05	0	6.90E-05	0	0	0	2.30E-05	8.40E-05	0.0017	0.0038
1000	0	0	0	0	0	0	0	0	0	0
2000	0	0	0	0	0	0	0	0	0	0

GRAIN SIZE DATA

CORE 3 layer i

sample #	134	135	136	137	138	139	140	141	142
Mean:	91	124.2	157.4	142.5	173.5	183	161.4	189.8	196.3
Median:	68.52	106.5	133.4	121.2	148.3	156.6	132	152.7	158.3
D(3,2):	10.86	14.72	17.22	15.6	17.09	18.2	15.87	16.76	17.34
Mode:	127.6	140.1	153.8	153.8	185.3	185.3	168.8	223.4	223.4
S.D.:	80.67	109.5	138.5	128.8	151.1	156.4	146.8	182.2	188.8
C.V.:	88.65	88.15	87.99	90.39	87.11	85.47	90.95	96.02	96.19
Skewness:	1.344	3.151	2.644	2.851	2.376	2.137	2.184	2.202	2.02
Kurtosis:	1.865	21.07	12.47	15.12	10.06	8.149	8.455	7.707	6.397
% <									
10	10.93	16.84	20.39	17.28	20.36	20.93	16.82	16.29	15.64
25	28.13	50.22	67.07	55.75	71.28	74.75	56.01	54.82	51.25
50	68.52	106.5	133.4	121.2	148.3	156.6	132	152.7	158.3
75	132.3	168.7	206.9	190.2	230.2	245.3	219.9	264.2	276
90	202.9	241.3	303.9	277.5	336.4	359.7	334.2	392	413.2

Particle Diameter(μm)	Volume %	Volume %	Volume %	Volume %	Volume %	Volume %	Volume %	Volume %	Volume %
1	0.843	0.642	0.529	0.591	0.49	0.479	0.579	0.544	0.581
2	2.38	1.66	1.42	1.62	1.39	1.36	1.67	1.67	1.81
5	13.56	8.24	6.96	8.11	7.04	6.92	8.37	8.88	9.26
20	21.6	13.28	9.98	11.66	9.66	9.29	11.46	11.57	12.13
50	32.88	33.53	26.71	28.62	21.92	20.32	24.5	19.11	17.47
125	21.98	32.58	37.03	35.18	37.61	36.78	32.86	29.82	28.4
250	5.28	8.08	14.06	11.49	17.68	20.21	16.6	22.46	23.51
500	0.01	0.716	2.07	1.45	2.88	3.39	2.72	4.2	5.17
1000	0	0.165	0.298	0.256	0.391	0.388	0.248	0.829	0.822
2000	0	0	0	0	0	0	0	0	0

Core 4 layer i

Sample #	126	127	128	129	130	131
Mean:	34.63	39.07	55.3	51.93	49.01	47.27
Median:	23.72	28.66	45.6	42.02	37.65	34.93
D(3,2):	5.692	6.457	8.568	7.984	7.697	7.353
Mode:	28.69	37.96	60.52	60.52	55.14	55.14
S.D.:	36.95	37.56	46.76	44.13	44.35	44.84
C.V.:	106.7	96.13	84.55	84.99	90.49	94.86
Skewness:	2.947	2.591	2.008	1.801	2.05	2.267
Kurtosis:	14.5	12.48	7.686	5.918	7.307	9.019
% <						
10	4.684	5.846	8.37	7.62	7.068	6.519
25	11.12	13.61	21.5	19.18	17.17	15.71
50	23.72	28.66	45.6	42.02	37.65	34.93
75	45.41	53.21	76.05	72.68	67.83	65.28
90	75.65	83.89	112.8	108.4	104.9	103.3

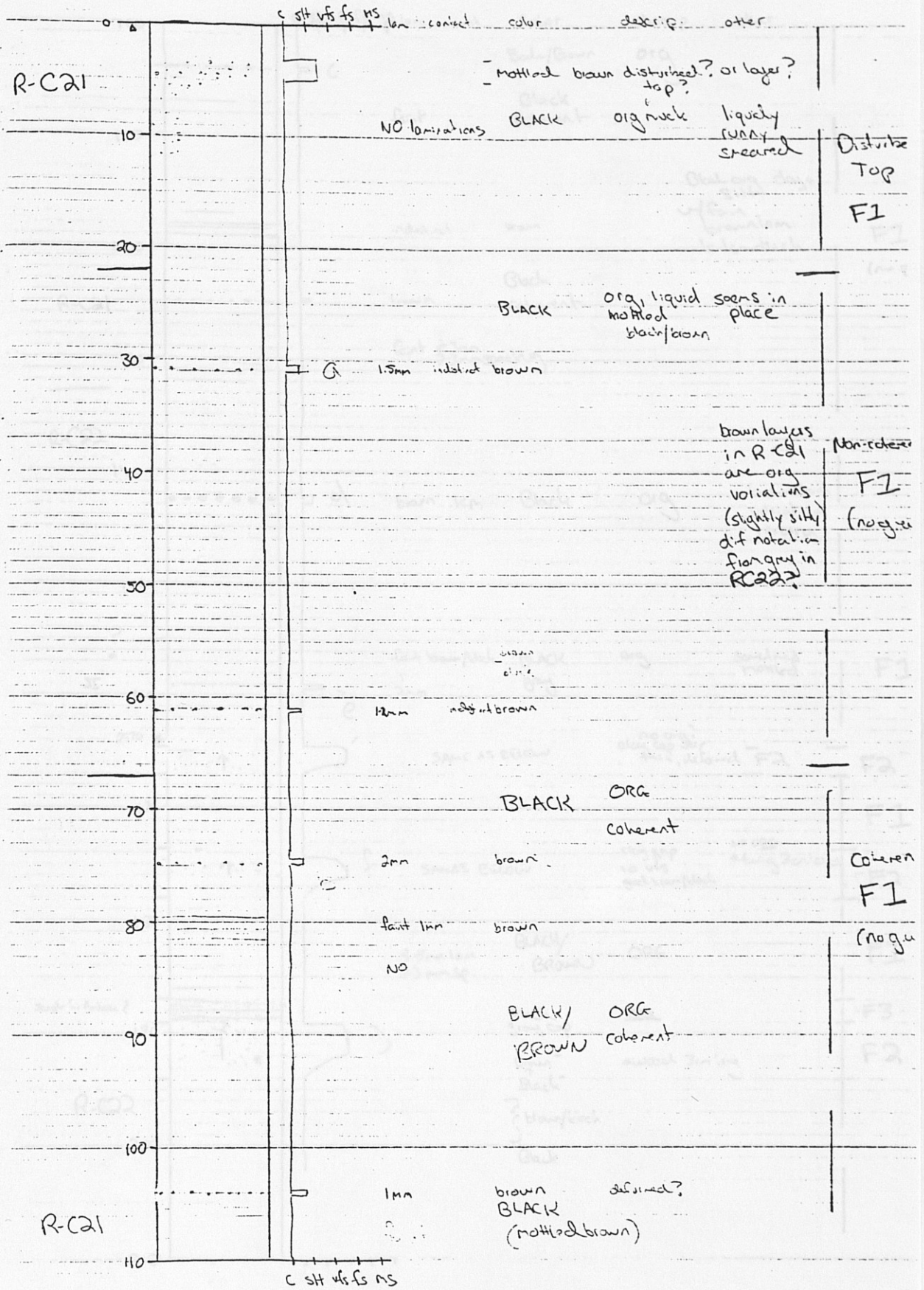
Particle Diameter(μm)	Volume %	Volume %	Volume %	Volume %	Volume %	Volume %
1	1.79	1.39	1.07	1.12	1.16	1.24
2	6.23	4.71	3.19	3.51	3.85	4.25
5	32.83	28.22	17.27	19.46	22.01	23.9
20	34.82	35.87	30.93	31.55	32.81	32.73
50	18.49	24.19	38.36	36	32.15	29.93
125	2.81	2.91	6.72	5.97	5.56	5.34
250	0.324	0.332	0.63	0.439	0.49	0.554
500	2.30E-05	0	0.004	0	8.40E-05	0.0021
1000	0	0	0	0	0	0
2000	0	0	0	0	0	0

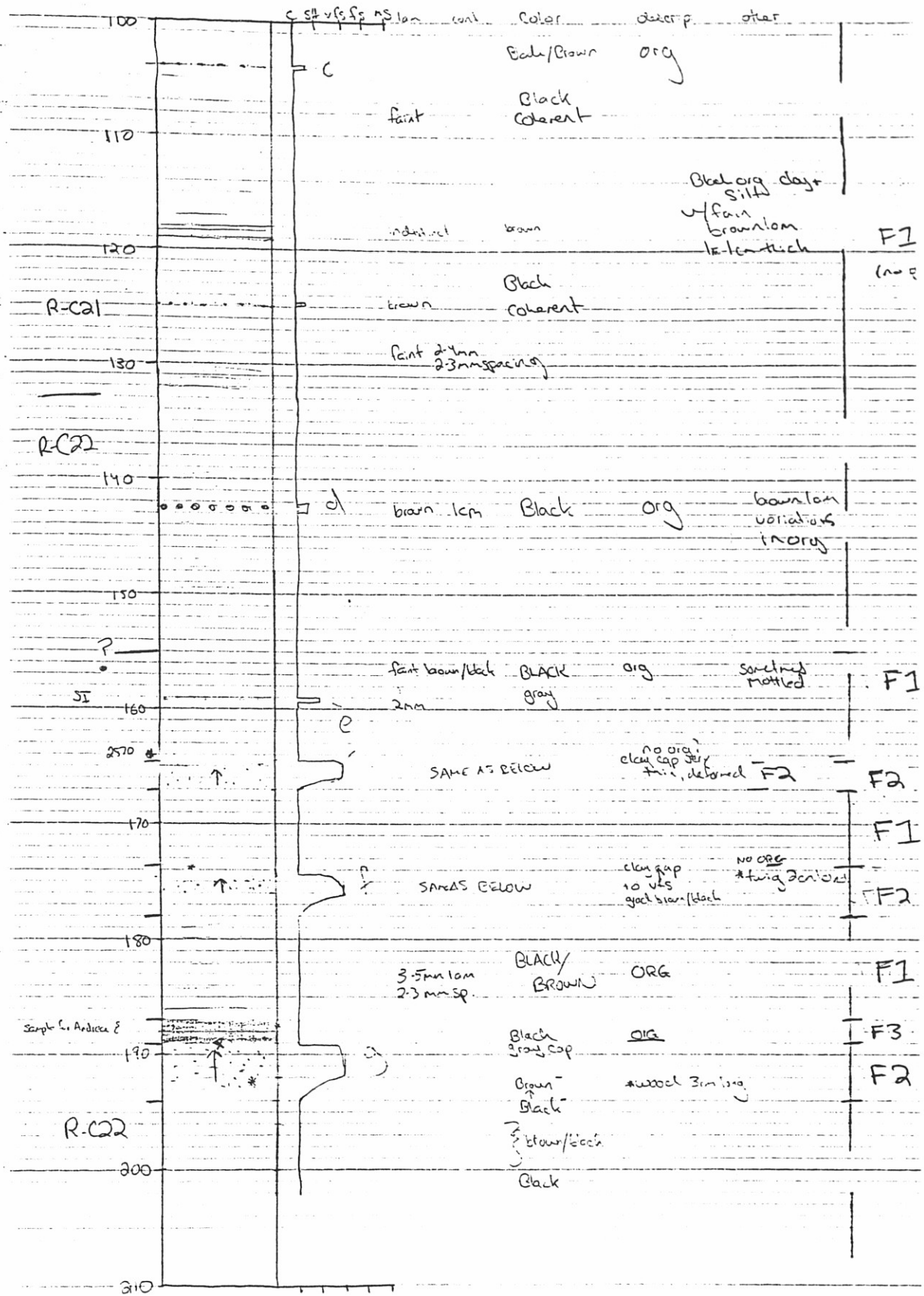
APPENDIX E: Age Model

AGE MODEL - 14C and calendar years BP

Depth (cm)	model depth	14C years	calendar years	Depth (cm)	model depth	14C years	calendar years	Depth (cm)	model depth	14C years	calendar years	Depth (cm)	model depth	14C years	calendar years
1	1	13	12	76	76	958	935	151	151	1903	1857	226	210	2513	2574
2	2	25	25	77	77	970	947	152	152	1915	1870	227	211	2523	2586
3	3	38	37	78	78	983	959	153	153	1928	1882	228	212	2532	2598
4	4	50	49	79	79	995	972	154	154	1940	1894	229			
5	5	63	62	80	80	1008	984	155	155	1953	1907	230			
6	6	76	74	81	81	1021	996	156	156	1966	1919	231			
7	7	88	86	82	82	1033	1009	157	157	1978	1931	232			
8	8	101	98	83	83	1046	1021	158	158	1991	1943	233			
9	9	113	111	84	84	1058	1033	159	159	2003	1956	234			
10	10	126	123	85	85	1071	1046	160	160	2016	1968	235			
11	11	139	135	86	86	1084	1058	161	161	2029	1980	236			
12	12	151	148	87	87	1096	1070	162	162	2041	1993	237			
13	13	164	160	88	88	1109	1082	163	163	2054	2005	238	213	2535	2612
14	14	176	172	89	89	1121	1095	164	164	2066	2017	239	214	2550	2632
15	15	189	185	90	90	1134	1107	165				240	215	2566	2652
16	16	202	197	91	91	1147	1119	166				241	216	2582	2672
17	17	214	209	92	92	1159	1132	167				242	217	2597	2692
18	18	227	221	93	93	1172	1144	168	165	2081	2025	243	218	2613	2712
19	19	239	234	94	94	1184	1156	169	166	2091	2037	244	219	2628	2732
20	20	252	246	95	95	1197	1169	170	167	2100	2049	245	220	2644	2752
21	21	265	258	96	96	1210	1181	171	168	2110	2061	246	221	2660	2773
22	22	277	271	97	97	1222	1193	172	169	2119	2074	247	222	2675	2793
23	23	290	283	98	98	1235	1205	173	170	2129	2086	248	223	2691	2813
24	24	302	295	99	99	1247	1218	174				249	224	2706	2833
25	25	315	308	100	100	1260	1230	175				250	225	2722	2853
26	26	328	320	101	101	1273	1242	176				251	226	2738	2873
27	27	340	332	102	102	1285	1255	177				252	227	2753	2893
28	28	353	344	103	103	1298	1267	178	171	2139	2098	253	228	2769	2913
29	29	365	357	104	104	1310	1279	179	172	2148	2110	254	229	2784	2933
30	30	378	369	105	105	1323	1292	180	173	2158	2122	255	230	2800	2953
31	31	391	381	106	106	1336	1304	181	174	2167	2135	256	231	2816	2974
32	32	403	394	107	107	1348	1316	182	175	2177	2147	257	232	2831	2994
33	33	416	406	108	108	1361	1328	183	176	2187	2159	258	233	2847	3014
34	34	428	418	109	109	1373	1341	184	177	2196	2171	259	234	2862	3034
35	35	441	431	110	110	1386	1353	185	178	2206	2183	260	235	2878	3054
36	36	454	443	111	111	1399	1365	186	179	2215	2196	261	236	2894	3074
37	37	466	455	112	112	1411	1378	187	180	2225	2208	262	237	2909	3094
38	38	479	467	113	113	1424	1390	188	181	2235	2220	263	238	2925	3114
39	39	491	480	114	114	1436	1402	189				264	239	2940	3134
40	40	504	492	115	115	1449	1415	190				265	240	2956	3154
41	41	517	504	116	116	1462	1427	191				266	241	2972	3175
42	42	529	517	117	117	1474	1439	192				267	242	2987	3195
43	43	542	529	118	118	1487	1451	193				268	243	3003	3215
44	44	554	541	119	119	1499	1464	194	182	2244	2232	269	244	3018	3235
45	45	567	554	120	120	1512	1476	195	183	2254	2244	270	245	3034	3255
46	46	580	566	121	121	1525	1488	196	184	2263	2257	270			
47	47	592	578	122	122	1537	1501	197	185	2273	2269	271	246	3050	3275
48	48	605	590	123	123	1550	1513	198	186	2283	2281	272	247	3065	3295
49	49	617	603	124	124	1562	1525	199	187	2292	2293	273	248	3081	3315
50	50	630	615	125	125	1575	1538	200	188	2302	2305	274	249	3096	3335
51	51	643	627	126	126	1588	1550	201	189	2311	2318	275	250	3112	3355
52	52	655	640	127	127	1600	1562	202	190	2321	2330	276	251	3128	3376
53	53	668	652	128	128	1613	1574	203	191	2331	2342	277	252	3143	3396
54	54	680	664	129	129	1625	1587	204				278	253	3159	3416
55	55	693	677	130	130	1638	1599	205	192	2340	2354	279	254	3174	3436
56	56	706	689	131	131	1651	1611	206	193	2350	2366	280	255	3190	3456
57	57	718	701	132	132	1663	1624	207	194	2359	2379	281	256	3206	3476
58	58	731	713	133	133	1676	1636	208	195	2369	2391	282	257	3221	3496
59	59	743	726	134	134	1688	1648	209	196	2379	2403	283	258	3237	3516
60	60	756	738	135	135	1701	1661	210	197	2388	2415	284	259	3252	3536
61	61	769	750	136	136	1714	1673	211	198	2398	2427	285	260	3268	3556
62	62	781	763	137	137	1726	1685	212	199	2407	2440	286	261	3284	3577
63	63	794	775	138	138	1739	1697	213	200	2417	2452	287	262	3299	3597
64	64	806	787	139	139	1751	1710	214	201	2427	2464	288	263	3315	3617
65	65	819	800	140	140	1764	1722	215	202	2436	2476	289	264	3330	3637
66	66	832	812	141	141	1777	1734	216	203	2446	2488	290	265	3346	3657
67	67	844	824	142	142	1789	1747	217	204	2455	2501	291	266	3362	3677
68	68	857	836	143	143	1802	1759	218				292	267	3377	3697
69	69	869	849	144	144	1814	1771	219				293	268	3393	3717
70	70	882	861	145	145	1827	1784	220	205	2465	2513	294	269	3408	3737
71	71	895	873	146	146	1840	1796	221	206	2475	2525	295	270	3424	3757
72	72	907	886	147	147	1852	1808	222				296	271	3440	3778
73	73	920	898	148	148	1865	1820	223	207	2484	2537	297	272	3455	3798
74	74	932	910	149	149	1877	1833	224	208	2494	2549	298	273	3471	3818
75	75	945	923	150	150	1890	1845	225	209	2503	2562	299	274	3486	3838
												300	275	3502	3858

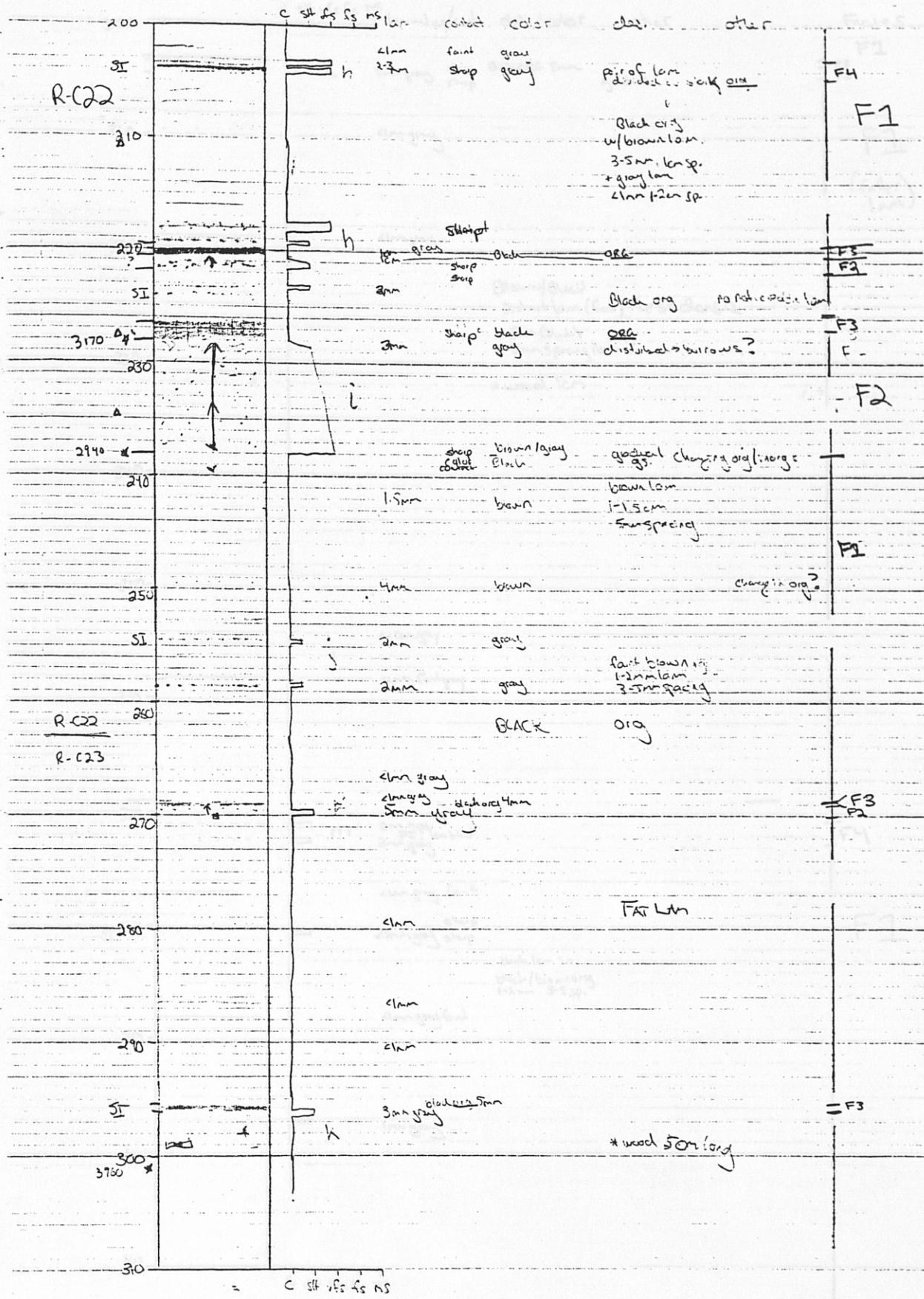
Depth (cm)	model depth	14C years	calendar years	Depth (cm)	model depth	14C years	calendar years	Depth (cm)	model depth	14C years	calendar years	Depth (cm)	model depth	14C years	calendar years
301	276	3518	3878	376	350	4672	5365	451	413	6065	6920	527			
302	277	3533	3898	377	351	4688	5386	452	414	6097	6950	528			
303	278	3549	3918	378	352	4703	5406	453	415	6130	6980	529			
304	279	3564	3938	379	353	4719	5426	454	416	6162	7010	530			
305				380	354	4734	5446	455	417	6194	7039	531			
306	280	3580	3958	381	355	4750	5466	456	418	6227	7069	532			
307	281	3596	3979	382	356	4766	5486	457	419	6259	7099	533	478	8316	9299
308	282	3611	3999	383	357	4777	5506	458	420	6291	7129	534			
309	283	3627	4019	384	358	4799	5529	459	421	6324	7159	535			
310	284	3642	4039	385	359	4821	5553	460	422	6356	7188	536	479	8355	9346
311	285	3658	4059	386	360	4843	5577	461	423	6388	7218	537	480	8395	9393
312	286	3674	4079	387	361	4865	5602	462	424	6420	7248	538			
313	287	3689	4099	388	362	4887	5626	463	425	6453	7278	539			
314	288	3705	4119	389	363	4909	5651	464	426	6485	7308	540			
315	289	3720	4139	390	364	4931	5675	465	427	6517	7337	541			
316	290	3736	4159	391	365	4953	5699	466	428	6550	7367	542			
317	291	3752	4180	392	366	4975	5724	467	429	6582	7397	543			
318	292	3767	4200	393	367	4997	5748	468	430	6614	7427	544			
319	293	3783	4220	394	368	5019	5773	469	431	6647	7457	545			
320	294	3798	4240	395	369	5041	5797	470	432	6679	7486	546			
321	295	3814	4260	396	370	5063	5821	471	433	6711	7516	547			
322	296	3830	4280	397	371	5085	5846	472	434	6743	7546	548	481	8434	9440
323	297	3845	4300	398	372	5107	5870	473	435	6776	7576	549	482		
324	298	3861	4320	399	373	5129	5895	474	436	6808	7606	550	483		
325	299	3876	4340	400	374	5151	5919	475	437	6840	7635	551	484		
326	300	3892	4360	401	375	5173	5943	476	438	6873	7665	552			
327	301	3908	4381	402	376	5195	5968	477	439	6905	7695	553	485		
328	302	3923	4401	403	377	5217	5992	478	440	6937	7725	554	486		
329	303	3939	4421	404	378	5239	6017	479	441	6970	7755	555			
330	304	3954	4441	405	379	5261	6041	480	442	7002	7784	556			
331	305	3970	4461	406	380	5283	6065	481	443	7034	7814	557	487		
332	306	3986	4481	407	381	5305	6090	482	444	7066	7844	558	488		
333	307	4001	4501	408	382	5327	6114	483	445	7099	7874	559	489		
334	308	4017	4521	409	383	5349	6139	484	446	7131	7904	560	490		
335	309	4032	4541	410	384	5371	6163	485	447	7163	7933				
336	310	4048	4561	411	385	5393	6187	486	448	7196	7963				
337	311	4064	4582	412	386	5415	6212	487	449	7228	7993				
338	312	4079	4602	413	387	5437	6236	488	450	7260	8023				
339	313	4095	4622	414	388	5459	6261	489	451	7293	8053				
340	314	4110	4642	415	389	5481	6285	490	452	7294	8077				
341	315	4126	4662	416	390	5503	6309	491	453	7334	8124				
342	316	4142	4682	416				492	454	7373	8171				
343	317	4157	4702	417	391	5525	6334	493	455	7412	8218				
344	318	4173	4722	418	392	5547	6358	494	456	7452	8265				
345	319	4188	4742	419	393	5569	6383	495	457	7491	8312				
346	320	4204	4762	420	394	5591	6407	496	458	7530	8359				
347	321	4220	4783	421				497	459	7569	8406				
348	322	4235	4803	422				498							
349	323	4251	4823	423				499	460	7609	8453				
350	324	4266	4843	424	395	5613	6431	500	461	7648	8500				
351	325	4282	4863	425	396	5635	6456	501	462	7687	8547				
352	326	4298	4883	426	397	5657	6480	502							
353	327	4313	4903	427	398	5679	6505	503	463	7727	8594				
354	328	4329	4923	428	399	5701	6529	504	464	7766	8641				
355	329	4344	4943	429	400	5723	6553	505	465	7805	8688				
356	330	4360	4963	430	401	5745	6578	506	466	7845	8735				
357	331	4376	4984	431	402	5767	6602	507							
358	332	4391	5004	432	403	5789	6627	508							
359	333	4407	5024	433	404	5811	6651	509	467	7884	8782				
360	334	4422	5044	434	405	5833	6675	510	468	7923	8829				
361	335	4438	5064	435	406	5855	6700	511	469	7962	8876				
362	336	4454	5084	436	407	5877	6724	512	470	8002	8923				
363	337	4469	5104	437	408	5899	6749	513	471	8041	8970				
364	338	4485	5124	438	409	5921	6773	514							
365	339	4500	5144	439	410	5943	6797	515	472	8080	9017				
366	340	4516	5164	440				516	473	8120	9064				
367	341	4532	5185	441				518	474	8159	9111				
368	342	4547	5205	442				518							
369	343	4563	5225	443				519							
370	344	4578	5245	444				520							
371	345	4594	5265	445				521	475	8198	9158				
372	346	4610	5285	446				522							
373	347	4625	5305	447				523	476	8238	9205				
374	348	4641	5325	448				524							
375	349	4656	5345	449	411	6001	6861	525							
				450	412	6033	6890	526	477	8277	9252				

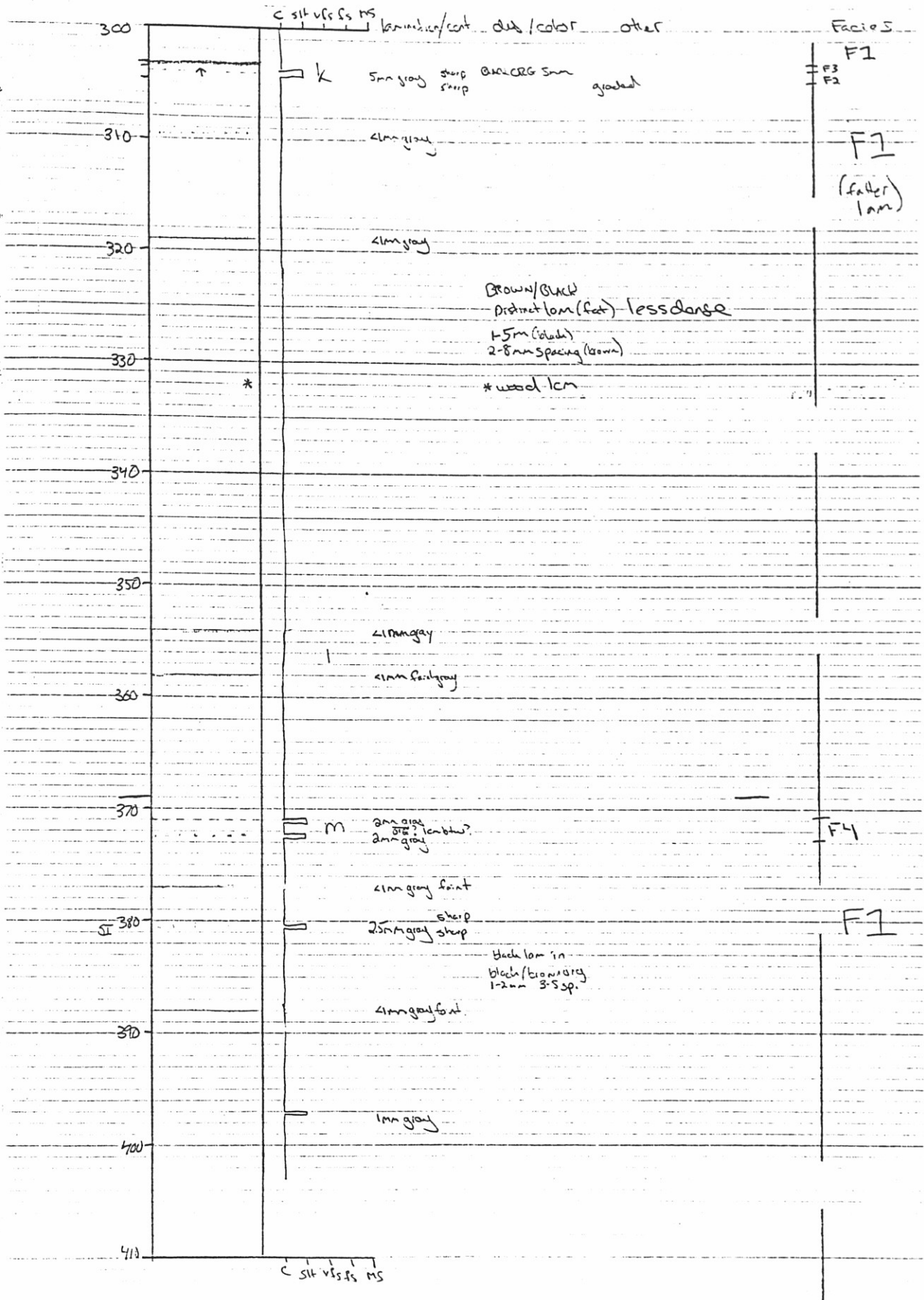


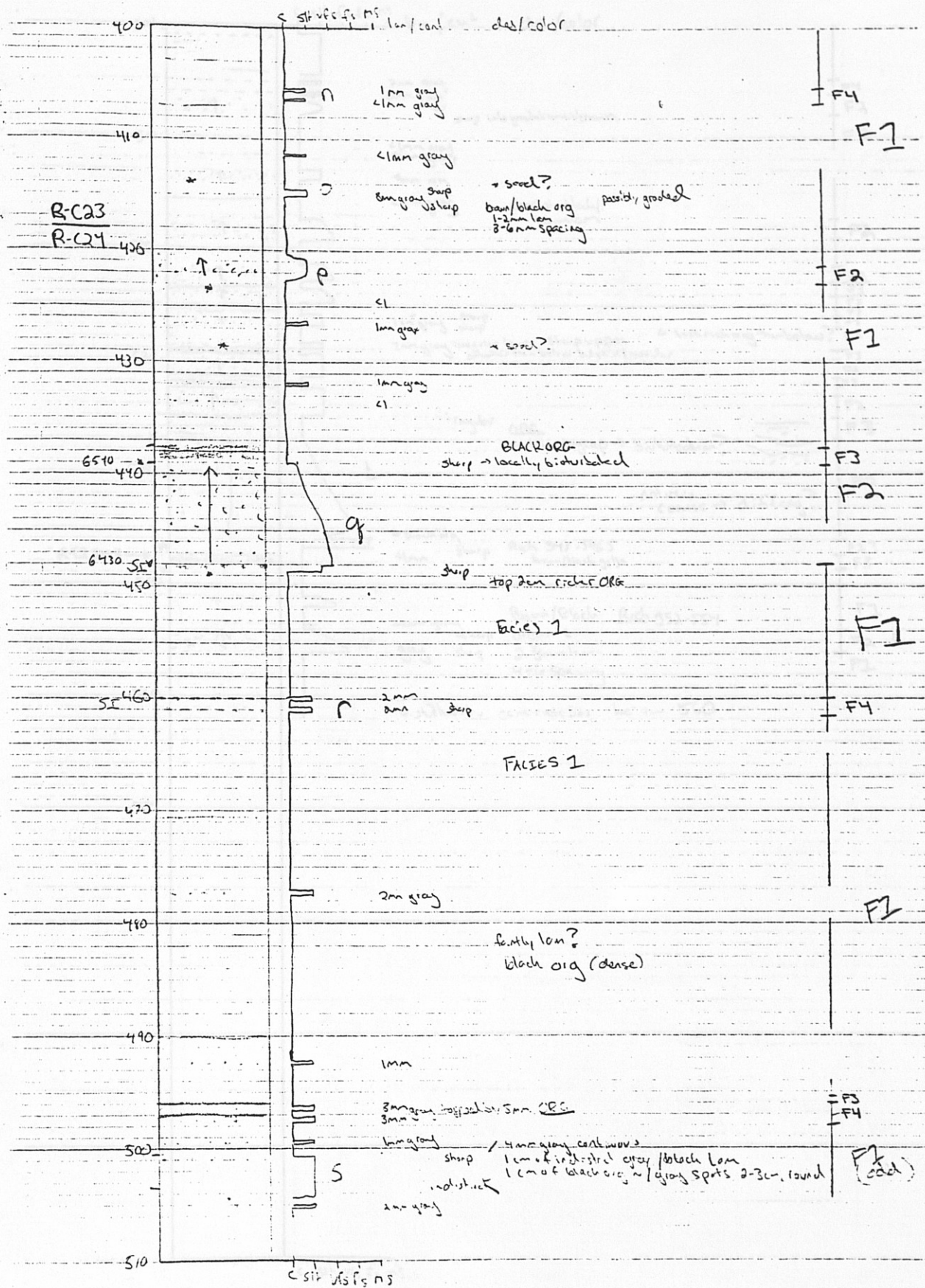


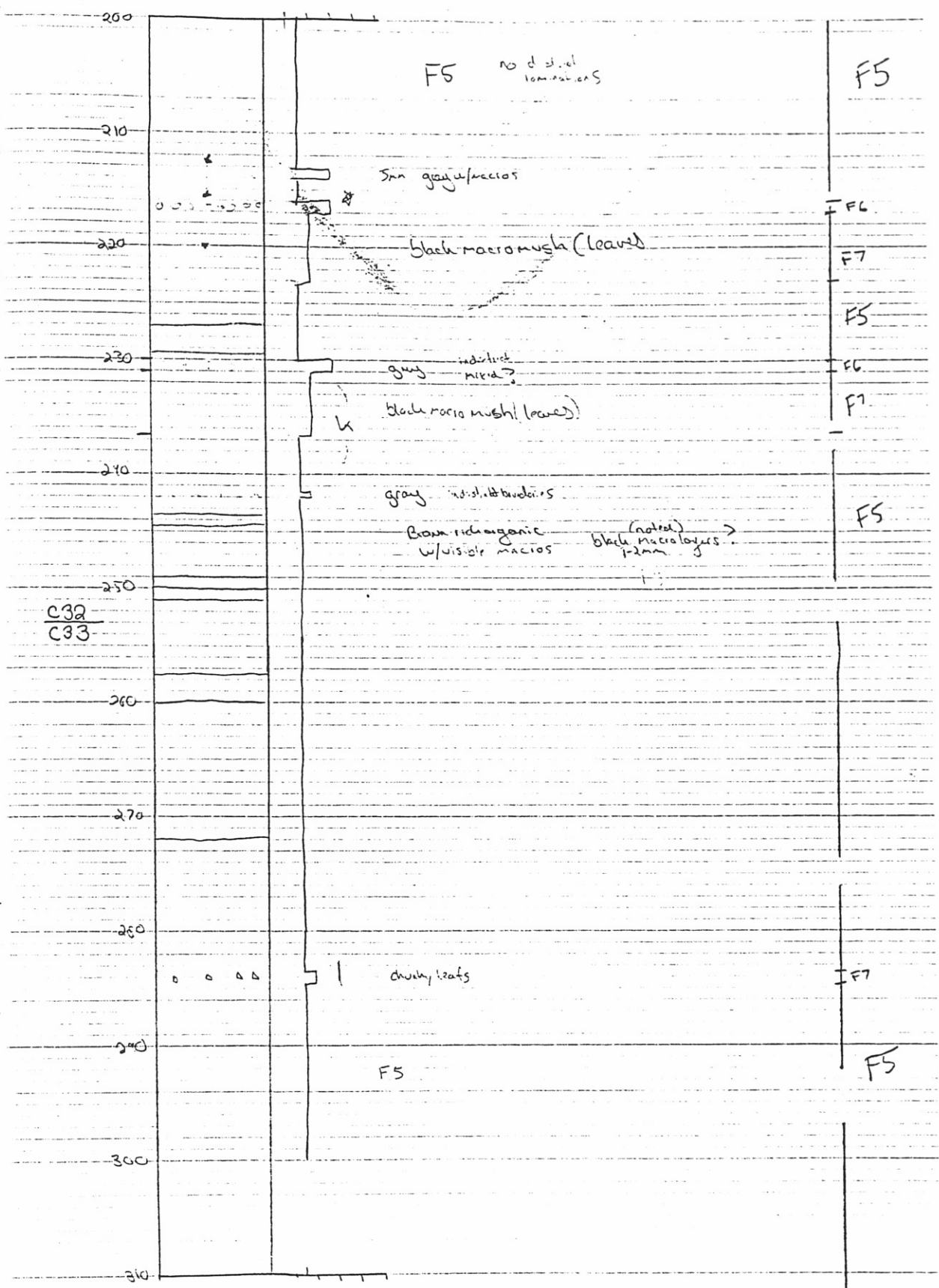
Facies 2 → org black ← locally biohermatized
 clay silt cap
 vts 156
 red brown org
 org black

Facies 3 → extremely black
 spongy org
 (low density)









F4 black macris horizons → leaf or wood
 F5 brown rich org w/ macris (sometimes visible)
 F6 gray layers w/ leaf not on top or bottom

